PB 210 256

FINAL REPORT

EXPERIMENTAL INVESTIGATION OF THE PENETRATION AND DISPERSION PHENOMENA IN THE LIMESTONE INJECTION METHOD

Prepared by

S. H. Schwartz and R. N. Salzman

Under Contract With:
National Air Pollution Control Administration
Contract No. CPA-22-69-149
June 30, 1969 to April 29, 1971

Reproduced by
NATIONAL TECHNICAL
INFORMATION SERVICE
U S Department of Commerce
Springfield VA 22151

210

BIBLIOGRAPHIC DATA SHEET

1. Report No. APTD-1134

2. 106

3. Recipient's Accession No. PB-210 256

4. Title and Subtitle

Experimental Investigation of the Penetration and Dispersion Phenomena in the Limestone Injection Method

5. Report Date April 1971

6.

7. Author(s)

S. H. Schwartz and R. N. Salzman

8. Performing Organization Rept. No.

9. Performing Organization Name and Address

Engineering Experiment Station
West Virginia University
Morgantown, West Virginia

10. Project/Task/Work Unit No.

11. Contract/Grant No. CPA-22-69-149

12. Sponsoring Organization Name and Address

Department of Health, Education, and Welfare
National Air Pollution Control Administration

13. Type of Report & Period Covered Final

14.

15. Supplementary Notes

16. Abstracts

The aim was to model the geometry and flow conditions of the Shawnee Unit 10 Boiler during the dry limestone injection process. The basic goal was to determine the penetration and dispersion characteristics of the limestone injection. A cold-gas model was selected with a geometric scale factor of 12.5 to 1. The combustion gases and the solid-gas injection flow conditions in the boiler were simulated by keeping the values of the relevant dimensionless parameters for the model as close as possible to those of the full scale Shawnee unit. Since full scale limestone distribution results were available, a comparison of these data with those of the model was made. The degree of dispersion of the limestone was characterized by a percent coverage value which in effect is the fraction of complete mixing of the limestone and SO_2. Percent coverage values were calculated for the Shawnee boiler for each of the three injection levels. The same was done for the model at one turbulence level and then additional tests were conducted at a fixed injection level under various turbulence conditions. The variation in dispersion with injection level followed the same pattern for both the model and full scale system with the lower rear injection providing the largest percent coverage and the front, the smallest. At each injection level the model and full scale system fractional coverage values deviated by approximately ten to twenty percent. A qualitative comparison of the distribution of the limestone for each system was also made. The low and high limestone concentration locations generally tended to be similar which is consistent with the relatively good agreement in overall percent coverage values.

17. Key Words and Document Analysis. 17a. Descriptors

Air pollution
Limestone
Additives
Simulation
Flow rates
Combustion products
Boilers
Sulfur dioxide
Concentration (composition)

17b. Identifiers/Open-Ended Terms

17c. COSATI Field/Group 13B

18. Availability Statement Unlimited

19. Security Class (This Report) UNCLASSIFIED

20. Security Class (This Page) UNCLASSIFIED

21. No. of Pages 211

22. Price $3.00/$0.95

FORM NTIS-35 (10-70)

USCOMM-DC 40329-P71

FOREWARD

This is the final report on the "Experimental Investigation of the Penetration and Dispersion Phenomena in the Limestone Injection Study." This work was accomplished for the National Air Pollution Control Administration of the Department of Health, Education and Welfare under Contract No. CPA-22-69-149 dated June 30, 1969.

Dr. S. H. Schwartz, Project Director, and Mr. R. N. Salzman, Research Assistant, both members of the Mechanical Engineering Department of West Virginia University, performed the work for this study.

The authors wish to express their appreciation to Dr. H. W. Butler, Department Chairman, for his support during this study and to Drs. R. A. Bajura and D. E. McKee for their technical advice and assistance. Thanks is also given to Messrs. D. Garletts and H. Martin for their roles in building the Shawnee Model System and to Mrs. Mary Ann Vecchio for her assistance in preparing this report.

As is often the case, all of those who have in one way or another assisted in this study cannot be named here but our thanks go to those individuals at NAPCA and TVA. However, Messrs. D. Clay, R. Stern and M. Hooper are singled out for their cooperation and assistance in their capacities relating to the technical management of this project.

TABLE OF CONTENTS

Page

FOREWARD i

LIST OF TABLES iv

LIST OF FIGURES v

NOMENCLATURE viii

ABSTRACT x

CHAPTER

1.0 INTRODUCTION 1-1

2.0 SUMMARY 2-1

- 2.1 Introduction 2-1
- 2.2 Literature Review 2-1
- 2.3 Fractional Analysis 2-2
- 2.4 Initial Experimentation 2-8
- 2.5 Square Duct Experiments 2-8
- 2.6 Shawnee Model Experiments 2-11
- 2.7 Comparison of Model and Full Scale Results 2-13

3.0 EXPERIMENTAL EQUIPMENT AND INSTRUMENTATION 3-1

- 3.1 Introduction 3-1
- 3.2 The Blower 3-1
- 3.3 Test Sections 3-3
- 3.4 Filter 3-10
- 3.5 Solid-Gas Feed System 3-13
- 3.6 Pitot Tube 3-16
- 3.7 Isokinetic Sampling Probe 3-17
- 3.8 Hot Wire Probe 3-17
- 3.9 Optical Probe 3-20
- 3.10 Laser Velocimeter 3-22

4.0 TEST PROCEDURES 4-1

- 4.1 Introduction 4-1
- 4.2 Feed System 4-1
- 4.3 Isokinetic Probe 4-3
- 4.4 Hot Wire Probe 4-4
- 4.5 Straight Test Section 4-5
- 4.6 Shawnee Test Section 4-8

TABLE OF CONTENTS (Continued)

Page

CHAPTER

5.0 EXPERIMENTAL RESULTS AND DISCUSSION 5-1

5.1 Introduction 5-1
5.2 Penetration and Concentration Results for Twelve-Inch Duct 5-2
5.3 Shawnee Model Experiments 5-6
5.4 Comparison with Shawnee Results 5-45

6.0 RECOMMENDATIONS FOR FUTURE WORK 6-1

6.1 Recommendations to Improve Technological Understanding of Injection and Dispersion . . . 6-1
6.2 Recommendations -- Related Directly to Shawnee System 6-2

REFERENCES R-1

APPENDIX A - LITERATURE REVIEW A-1

A.1 Introduction A-1
A.2 Jet Injection Studies A-1
A.3 Transport of Particles in Turbulent Flow Field A-8
A.4 References A-12

APPENDIX B - BIBLIOGRAPHY B-1

APPENDIX C - FRACTIONAL ANALYSIS C-1

C.1 Introduction C-1
C.2 Previous Work C-1
C.3 Fractional Analysis of Solid-Gas Injection C-4
C.4 Shawnee Model C-29
C.5 Summary C-32
C.6 References C-36

APPENDIX D - DATA D-1

LIST OF TABLES

Table		Page
2.1	Various Correlation Relations for Jet Trajectory Data .	2-3
2.2	Independent Dimensionless Parameters	2-6
2.3	Range of Parameters	2-7
2.4	Overall Percent Coverage	2-14
5.1	Turbulence Scale	5-13
5.2	Overall Density Distribution at Plane A-A	5-34
5.3	Data from Shawnee Boiler	5-46
5.4	Example of Shawnee Data Supplied by O.A.P.	5-47
5.5	Overall Percent Coverage	5-50
A.1	Various Correlation Relations for Jet Trajectory Data .	A-4
C.1	Dimensionless Parameters Obtained in Solid-Gas Suspension Studies	C-3
C.2	A Comparison of Scaling Techniques	C-5
C.3	Summary of Dimensionless Groups Obtained by Two Techniques	C-28
C.4	Independent Dimensionless Parameters	C-31
C.5	Independent Variables	C-34
C.6	Range of Parameters	C-35

LIST OF FIGURES

Figure Page

2.1 Trajectory Data 12" x 12" Duct 2-10

2.2 Concentration Profile Along Centerline of 12" x 12" Duct 2-12

3.1 Centrifugal Fan Output 3-2

3.2 Lead-in Duct 3-4

3.3 Square Duct 3-6

3.4a Shawnee Model 3-7

3.4b Shawnee System 3-7

3.4c Location of Data Acquisition Points in Plane A-A 3-8

3.4d Photograph of Shawnee Model System 3-8

3.4e Photographs of Shawnee Model 3-9

3.5 Turbulence Generators, Screens, etc. 3-11

3.6 Filter System 3-12

3.7 Pitot Tube 3-12

3.8a Solid-Gas Feed System 3-14

3.8b Photograph of Feeder System 3-15

3.9a Isokinetic Probe System 3-18

3.9b Photograph of Isokinetic Sampling Probe System 3-18

3.10 Isokinetic Probe Holder 3-19

3.11 Photograph of Hot Wire Probe System 3-19

3.12 Full Size Representation of Optical Probe 3-21

3.13a Photograph of Optical Concentration Probe 3-23

3.13b Optical Concentration Probe Circuit Diagram 3-23

3.14 Schematic of Laser Velocimeter 3-25

4.1 Photograph of 12 in. x 12 in. Duct with Laser 4-6

4.2 Trajectory Photographs 4-6

LIST OF FIGURES (Continued)

Figure		Page
5.1	Trajectory Data 12" x 12" Duct	5-3
5.2	Trajectory Comparison of a Single Particle with a Homogeneous Jet	5-5
5.3	Concentration Profile Along Centerline of 12" x 12" Duct	5-7
5.4	Velocity and Intensity - Screens - Plane A-A	5-8
5.5	Velocity and Intensity - 2" Grid - Plane A-A	5-9
5.6	Velocity and Intensity - Vortex Generator - Plane A-A .	5-10
5.7	Velocity and Intensity - Open Box - Plane A-A	5-11
5.8	Shawnee Model Plane A-A - 2" Grid (Concentration Profiles)	5-21
5.9	Shawnee Model Plane A-A - Screens (Concentration Profiles)	5-22
5.10	Normalized Density Distribution - Shawnee Model Plane A-A (2" Grid, L-1)	5-23
5.11	Normalized Density Distribution - Shawnee Model Plane A-A (2" Grid, L-2)	5-24
5.12	Normalized Density Distribution - Shawnee Model Plane A-A (2" Grid, L-3)	5-26
5.13	Shawnee Model Plane A-A (Concentration Profiles, L-2) .	5-28
5.14	Shawnee Model Plane A-A (Concentration Profiles, L-2) .	5-30
5.15	Shawnee Model Plane A-A (Concentration Profiles, L-2) .	5-31
5.16	Normalized Density Distribution - Shawnee Model Plane A-A (Vortex Generator, L-2)	5-32
5.17	Normalized Density Distribution - Shawnee Model Plane A-A (Open Box, L-2)	5-33
5.18	Penetration Profiles - Shawnee Model Plane A-A	5-37
5.19	Shawnee Model Position Y-Y Concentration Profiles . . .	5-40
5.20	Shawnee Model Plane Y-Y Data Acquisition Points	5-41
5.21	Velocity Profile and Intensity at Plane Y-Y of Model, Velocity Profile at Plane B-B Shawnee Boiler	5-42

LIST OF FIGURES (Continued)

Figure Page

5.22 Shawnee Model Plane Y-Y Concentration Profiles 5-43

5.23 Shawnee Model Plane Y-Y Concentration Profiles 5-44

5.24 Normalized Mass Flow Rates, $\dot{m}_{p_i}/\bar{\dot{m}}_p = C$, Plane A-A, Injection Level 1 5-52

5.25 Normalized Mass Flow Rates, $\dot{m}_{p_i}/\bar{\dot{m}}_p = C$, Plane A-A, Injection Level 2 5-53

5.26 Normalized Mass Flow Rates, $\dot{m}_{p_i}/\bar{\dot{m}}_p = C$, Plane A-A, Injection Level 3 5-54

A.1 Effects of Plume Temperature on Trajectory for Two Velocity Ratios A-9

C.1 Coordinate System - Fractional Analysis C-7

C.2 System Definition for Integral Approach C-15

NOMENCLATURE

a	particle radius
A	area
C_1, C_2	constants
d	nozzle diameter
D	duct width
D_p	eddy diffusivity of gas in gas/solids fluid
$\hat{D}_p$	turbulent diffusivity of particles
Dpw	diffusivity of particles at wall
F	time constant for momentum transfer between particles and gas
f, f_o	total friction factors (with solids/gas alone)
g	gravitational constant
I	intensity, v'/U_o
K_m	effectiveness parameter
L	duct length
m	mass of particle
$\dot{m}_{p_i}$	local particulate mass flow rate
$\dot{m}_{s_i}$	local theoretical particulate mass flow rate to satisfy stoichiometry
$\bar{\dot{m}}_p$	mean particulate mass flow rate averaged over all $\dot{m}_{p_i}$'s
$\dot{M}_T$	total particulate mass flow rate through cross section
P	pressure
q	electric charge per particle
r	vector representing spatial location in duct
Re	Reynolds number
S	surface area of control volume

t	time
u	gas turbulence velocity in x direction
U	gas velocity in x direction
U_p	particle velocity in x direction
$\overline{U}$	time averaged gas velocity in x direction
V, W	gas velocities in y and z directions, respectively
V_p, W_p	particle velocities in y and z directions, respectively
v'	RMS turbulence velocity at x = 0
$\mathcal{V}$	volume
x, y, z	spatial coordinates
x'	distance downstream from injection point
y'	penetration distance of jet
ϵ_o	permittivity of free space
Λ	scale of turbulence at x = 0
μ	viscosity
ν	kinematic viscosity
ρ	density
ρ_o	gas density in duct
ρ_j	jet mixture density
ρ_p	density of particulate phase
$\hat{\rho}_p$	material density of particles
ρ_{Po}	particulate cloud density at x = 0
τ	shear stress

ABSTRACT

This study was undertaken to model the geometry and flow conditions of the Shawnee Unit 10 Boiler during the dry limestone injection process. The basic goal was to determine the penetration and dispersion characteristics of the limestone injection into the Shawnee boiler with the aid of a model. A cold-gas model was selected to simplify the instrumentation and measurement problems.

The model was scaled geometrically with a scale factor of 12.5 to 1. The combustion gases and the solid-gas injection flow conditions in the boiler were simulated by keeping the values of the relevant dimensionless parameters for the model as close as possible to those of the full scale Shawnee unit. The dimensionless parameters were identified by nondimensionalizing the governing conservation equations and boundary conditions associated with solid-gas flow. However, a lack of information on the turbulence characteristics in the full scale boiler prevented a matching of the turbulence intensity and dimensionless turbulence scale. As a result model experiments were repeated over a range of values for those two parameters to yield information on the effect of turbulence on dispersion in the model. At present it is not known if this range of values bracketed the operating conditions of the full scale system.

Since full scale limestone distribution results were available, a comparison of these data with those of the model was made. The degree of dispersion of the limestone was characterized by a percent coverage value which in effect is the fraction of complete mixing of the limestone and SO_2 at Plane A-A.

Percent coverage values were calculated for the Shawnee boiler for each of the three injection levels. The same was done for the model at

one turbulence level and then additional tests were conducted at a fixed injection level under various turbulence conditions. The variation in dispersion with injection level followed the same pattern for both the model and full scale system with the lower rear injection providing the largest percent coverage and the front, the smallest. At each injection level the model and full scale system fractional coverage values deviated by approximately ten to twenty percent. A qualitative comparison of the distribution of the limestone ~~across Plane A-A~~ for each system was also made. Here, as might be expected, point by point agreement between the model and full scale system was not as close as were the overall coverage values. Nevertheless, the low and high limestone concentration locations generally tended to be similar which is consistent with the relatively good agreement in overall percent coverage values. This suggests that the Shawnee model used in this study was an adequate representation of the full scale unit.

1.0 INTRODUCTION

This study was undertaken to better understand the penetration and dispersion characteristics associated with the limestone injection technique for removing sulfur oxides from the combustion gases of a coal-fired power plant boiler. The fundamental assumption underlying this investigation was that a necessary condition for removal of the sulfur oxides is a uniform distribution of the limestone with respect to the SO_2 in the combustion gases in the region where the temperature range for chemical reaction between the SO_2 and the limestone occurs. The main objective of this study was to develop a scale model which would simulate the limestone dispersion characteristics of the full scale Shawnee system.

The original plan for achieving the goal of scaling the limestone dispersion was essentially composed of two parts. The first was to identify, through analysis, the important flow parameters associated with the injection technique. This was to be coupled with single and multiple nozzle experiments to provide a more basic understanding of the relationships among the flow variables as they affect the penetration and dispersion phenomenon. The plan was to use the results from this portion of the program to aid in effecting the second half of the program. The second half consisted of the design, fabrication, and operation of an experimental program which utilized a scale model of the No. 10 Shawnee steam plant boiler section located in Paducah, Kentucky. Both the geometry and flow conditions were to be modeled as closely as possible so that the results would be useful in evaluating the full scale Shawnee system. The following discussion summarizes the major tasks required to complete this study.

2.0 SUMMARY

2.1 Introduction

The following discussion lists the major steps that were taken during this study to determine the dispersion characteristics in the Shawnee system. These include the literature survey, the fractional analysis to identify the experimental parameters, the experimental program and the conclusions. In general, the original scope of work proposed for this investigation was met although additions and deletions to this plan were made during the course of the study.

2.2 Literature Review

The literature review initiated prior to the start of the contract continued throughout the duration of the study. A variety of injection studies have been reported in the literature and range from the deflection of liquid jets injected normal to an air stream to the spreading of a free solid-gas jet.

The literature survey was broken into several categories for convenience. The following is a list of these categories which were covered in the study and were felt to be related to the limestone injection problem:

1. Injection of a gas jet into a transverse gas stream
2. Injection of a liquid jet into a transverse gas stream
3. Free and coflowing jets (single and two phase)
4. Stack emissions
5. Transport of particles in a turbulent flow field

Appendix B is a bibliography including the five above categories.

However, it was found that none of the reported studies have considered either of the following aspects related to limestone injection:

1. Solid-gas jet injected into a transverse stream
2. The effects of ambient turbulence conditions on the dispersion of the jet

Nevertheless, all of the five listed categories do provide some overlap with the limestone injection problem. In particular, category (1), the gas jet into a transverse stream most closely resembles the present problem. Jet trajectories have been determined experimentally both by monitoring a tracer gas mixed with the injectant gas and by measuring the temperature profile along the plume of a heated injectant gas. The penetration equations resulting from these experimental studies are shown on the accompanying chart, Table 2.1.

The last four equations in Table 2.1 strongly suggest that the dynamic pressure ratio ($\rho_j V_j^2 / \rho_o U_o^2$) may be an important dimensionless parameter for jet injection problems. However, results from the literature do not indicate whether these relationships hold for a solid-gas jet. If it is shown that the solid-gas jet can be treated as a homogeneous mixture then these relationships should be valid. Conversely, if it were experimentally demonstrated that these relationships are valid for the jet then it would be assumed that the jet behaves as a homogeneous mixture and that the dynamic pressure ratio (with the mixture density represented by ρ_j) is a jet trajectory parameter for scaling purposes.

2.3 Fractional Analysis

In the beginning of this study the experimental work and the analysis for identifying the dimensionless parameters were carried out in a somewhat parallel effort. However, early in the program first priority was assigned to the fractional analysis or the nondimensionalization of the governing

AUTHOR (S)	PENETRATION EQUATION
Callaghan and Ruggeri (4)	$\frac{y'}{d} = C^{37}\left(\frac{\rho_j}{\rho_o}\right)^{.57}\left(\frac{V_j}{U_o}\right)^{.64}\left(\frac{x'}{d}\right)^{.26}$ C = dimensionless coefficient Author notes that powers vary with changes in d
Weiland and Trass (5)	$\frac{y'}{d} = K_1\left(\frac{\rho_j}{\rho_o}\right)^{\alpha}\left(\frac{V_j}{U_o}\right)^{\beta} x^{\gamma} d^{\delta-1}$ Blowing air into duct: $\alpha = .5$ $\gamma = .25$ $\beta = .66$ $\delta = .70$ Sucking air through duct: $\alpha = .64$ $\gamma = .22$ $\beta = .71$ $\delta = .56$ Note: The units of this equation do not check.
Patrick (3)	$\frac{y}{d} = \left(\frac{\rho_j V_j^2}{\rho_o U_o^2}\right)^{.425}\left(\frac{x'}{d}\right)^{n}$ $.33 \le n \le .38$
Shandorov*	$\frac{y'}{d} = \left(\frac{\rho_j V_j^2}{\rho_o U_o^2}\right)^{.392}\left(\frac{x'}{d}\right)^{.392}$
Ivanov*	$\frac{y'}{d} = \left(\frac{\rho_j V_j^2}{\rho_o U_o^2}\right)^{.434}\left(\frac{x'}{d}\right)^{.333}$
Norgren and Humenik (8)	$\frac{y'}{d} = .87\left(\frac{\rho_j}{\rho_o}\right)^{.47}\left(\frac{V_j}{U_o}\right)^{.85}\left(\frac{x'}{d}\right)^{.32}$

*Referenced in Abromovich (9)
All of the above references are listed in Appendix A.

Table 2.1. Various Correlation Relations for Jet Trajectory Data

flow equations. This was necessary since a well planned experimental effort requires prior knowledge of the relevant dimensionless parameters.

Prior to the initiation of this program it was decided that an entirely analytical approach to the limestone dispersion problem would not be a good one. As a result a combined experimental and analytical approach was selected. Here the conservation of mass and momentum equations along with the boundary conditions were nondimensionalized with the characteristic values of the system. This partial analysis with the resulting dimensionless parameters or pi groups was then used as the starting point for an experimental program. The departure from further analytical effort at this point was due to the complex interactions between the particles and the turbulent stream. This makes a solution to the governing equations impossible to conceive of at this time.

The identification of the dimensionless parameters served the two basic aims of this study. First, the parameters were needed to plan experiments related to the penetration and dispersion of a single jet. Here the parameters were varied to determine the relative effect of each on the penetration and dispersion. These parameters were also used in designing a scale model of the Shawnee system. In modeling, the values of the parameters for both the full size system and the model are kept the same or as close as possible in order to preserve the similarity between the two systems. Ideally, with this arrangement, the governing equations for both the full sized Shawnee system and the model are identical. In effect then the experimental results for the model will be equally valid for the full scale system in that the results are a form of solution of the governing equations in a physical rather than mathematical form.

The significant groups obtained by a fractional analysis of the Shawnee boiler are shown in the first column of the dimensionless parameter chart, Table 2.2. In scaling the Shawnee boiler it is desirable to satisfy as many of these dimensionless terms as is possible. Prior to constructing the model, the terms which could be scaled were identified. Before this was done the dimensionless parameters were rewritten since several of the groups were included within each other. It was desirable to break these groups into a set of independent dimensionless parameters. This is shown in column 2 of the same chart.

A linear geometric scaling was used, so that the first dimensionless term is automatically satisfied. The injection nozzle size was also scaled linearly, preserving the ratio (d/D) in a number of terms. The next chart (Table 2.3) provides the actual ranges for these independent dimensionless parameters for both the Shawnee boiler and the model. These numerical results demonstrate that Π_1 and Π_4 are scaled within the limits indicated by the Shawnee operating conditions. The effect of not satisfying Π_5 exactly cannot be ascertained without further experimentation. However, since there is only a factor of three difference (rather than several orders of magnitude difference) between the scaling parameter the effect is not expected to be large.

For Π_2 and Π_3 it was known in advance that the turbulence data for the Shawnee would be difficult to obtain. Therefore, the operational conditions of the model included a wide range of turbulence conditions. In this manner it was hoped that it would be possible to bracket the values for the actual boiler conditions.

From Equation (19)	Independent Dimensionless Terms		Descriptive Term
$\frac{L}{D}$ & $\frac{d}{D}$	same:	$\Pi_o = \frac{L}{D}$ & $\Pi_o' = \frac{d}{D}$	Geometric Scale
$\frac{\rho_o U_o D}{\mu}$	same:	$\Pi_1 = \frac{\rho_o U_o D}{\mu}$	Reynolds Number
$\frac{\upsilon'}{U_o}$	same:	$\Pi_2 = \frac{\upsilon'}{U_o}$	Turbulence Parameter
$\frac{\Delta}{D}$	same:	$\Pi_3 = \frac{\Delta}{D}$	Turbulence Parameter
$\frac{\rho_j V_j^2 d^2}{\rho_o U_o^2 D^2}$	rewritten:	$\Pi_4 \times (\Pi_o')^2$ $\Pi_4 = \frac{\rho_j V_j^2}{\rho_o U_o^2}$	Dynamic Pressure Ratio
$\frac{FD}{U_c} \sim \left[\frac{\nu}{aU_o}\right]\left(\frac{\rho_o}{\rho_p}\right)\left(\frac{D}{a}\right)$	rewritten:	Π_5/Π_1 $\Pi_5 = \frac{\rho_o}{\rho_p}\left(\frac{D}{a}\right)^2$	Particle Interaction Parameter
$\frac{\rho_j V_j d^2}{\rho_o U_o D^2}$	(not scaled)	$\Pi_6 = \frac{\rho_j V_j}{\rho_o U_o}$	Mass Flux Ratio

Table 2-2. Independent Dimensionless Parameters

Shawnee	Group	Model
$4.1 \times 10^5 \leq \Pi_1 \leq 6.5 \times 10^5$	$\Pi_1 = R_e = \frac{U_0 D}{\nu}$	$5.21 \times 10^5 \leq \Pi_1 \leq 5.69 \times 10^5$
$135 \leq \Pi_4 \leq 465$	$\Pi_4 = \frac{\rho_i V_i^2}{\rho_0 U_0^2}$	$209 \leq \Pi_4 \leq 331$
$\Pi_5 = 2.18 \times 10^7$	$\Pi_5 = \frac{\rho_0}{\rho_p}\left(\frac{D}{a}\right)^2$	$\Pi_5 = 6.7 \times 10^6$

Table 2.3. Range of Parameters

2.4 Initial Experimentation

The initial small scale experiments were designed to ascertain whether or not the dynamic pressure ratio was a valid pi group. Two small scale ducts (2" x 3" and 6" x 1") were used to investigate this relationship. In addition to the experiments a digital program was written to calculate the trajectory of individual particles injected into a transverse stream. The preliminary results of the small duct experiments indicated that the injection path was much closer to the trajectory predictions of the homogeneous jet studies outlined on the chart than the computerized predictions for individual particles.

The small scale experiments were also useful in determining the requirements necessary for the injection feed system. In addition, some experimentation with illuminating the jet plume for photographic purposes was accomplished with these apparatus.

2.5 Square Duct Experiments

The larger 12" x 12" duct was designed and built as the smaller experiments were being phased out. Incorporated into this design were the bag filter system to handle the heavier dust loading and the improved closed feed system. This pressurized feed system enabled the mass flow rates of the air and solids as well as the mean injection velocity to be measured. The duct was designed to provide more carefully controlled conditions with which to study single nozzle injection experiments. In addition, it was utilized to make final modifications and checks of the auxiliary equipment and instrumentation that were to be incorporated into the Shawnee model tests.

During the course of checking out these subsystems, the feed system was modified until a reliable, steady feed rate of solids was achieved. In addition the capabilities of the blower were determined and both pitot tube and hot wire measurements of the duct velocities were obtained. Some effort was also put into developing the optical concentration probe with this duct system. Dust deposition on the optical surfaces proved to be a problem and due to time limitations its development was terminated although the prognosis for its successful completion was good. Finally, the substitute isokinetic probe technique for obtaining concentration measurements was checked out with the same duct. Because of the substantial improvements in the injection system, the trajectory studies were repeated for comparison with the preliminary data obtained using the small ducts. The experiments performed using this improved hardware substantiated the trends indicated by the small scale ducts (Figure 2.1). Therefore, further design considerations for the Shawnee model included the dynamic pressure ratio ($\rho_j V_j^2 / \rho_o U_o^2$) to scale the injection trajectory phenomena.

These trajectory tests were run in a horizontal duct, hence, the question arose as to the applicability of these results to the case of injection into a vertical boiler. The relative importance of the gravitational to the inertial terms for the injection process is indicated by the Froude number (gL/U_o^2). This dimensionless group was calculated and the value was in a range indicating that the orientation of the gravitational field is not significant to the injection process.

Experiments were also run with this test section in order to determine the effects of the ambient turbulence on the jet trajectory and dispersion. Unfortunately, there was insufficient time for any extensive experimentation on this aspect of the study since the 12" x 12" duct had to be

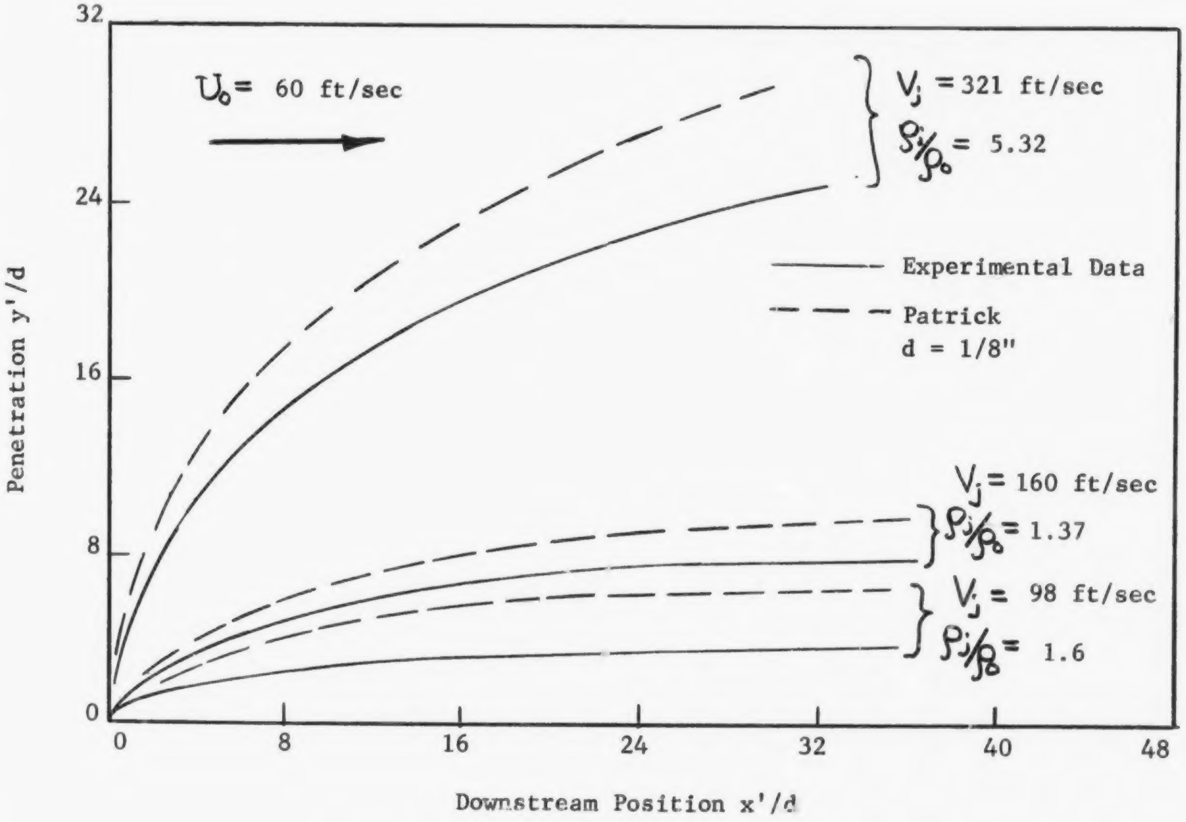

Figure 2.1. Trajectory Data 12" x 12" Duct

dismantled and replaced by the Shawnee model. The only results parameterizing turbulence obtained are shown in Figure 2.2. These results have not been substantiated by further testing and at this time can only be considered as preliminary data.

2.6 Shawnee Model Results

Upon completion of the fabrication of the Shawnee model, it replaced the 12" x 12" duct. All three injection levels were studied with the improved feeder system allowing all of the nozzles at any given level to be used. The turbulence parameters obtained from the fractional analysis were a dimensionless turbulence scale and intensity. These were systematically varied by using several different turbulence producing devices. These devices were selected to cover a wide range of eddy sizes as well as turbulence intensities. The concentration profiles were then compared for the various turbulence conditions.

The results indicated that the most significant effect on the concentration profile at Plane A-A was the distance from the injection plane to Plane A-A. Hence, it was found that the lower rear injection plane produced a significantly higher degree of dispersion than the other two injection planes. The turbulence intensity was also found to play some part in the dispersion phenomenon. It appears from the present data that an increase in dispersion occurs with an increase in turbulence intensity. However, increasing the intensity from three to ten percent (a factor of three) only resulted in an improvement in the dispersion of the order of ten percent.

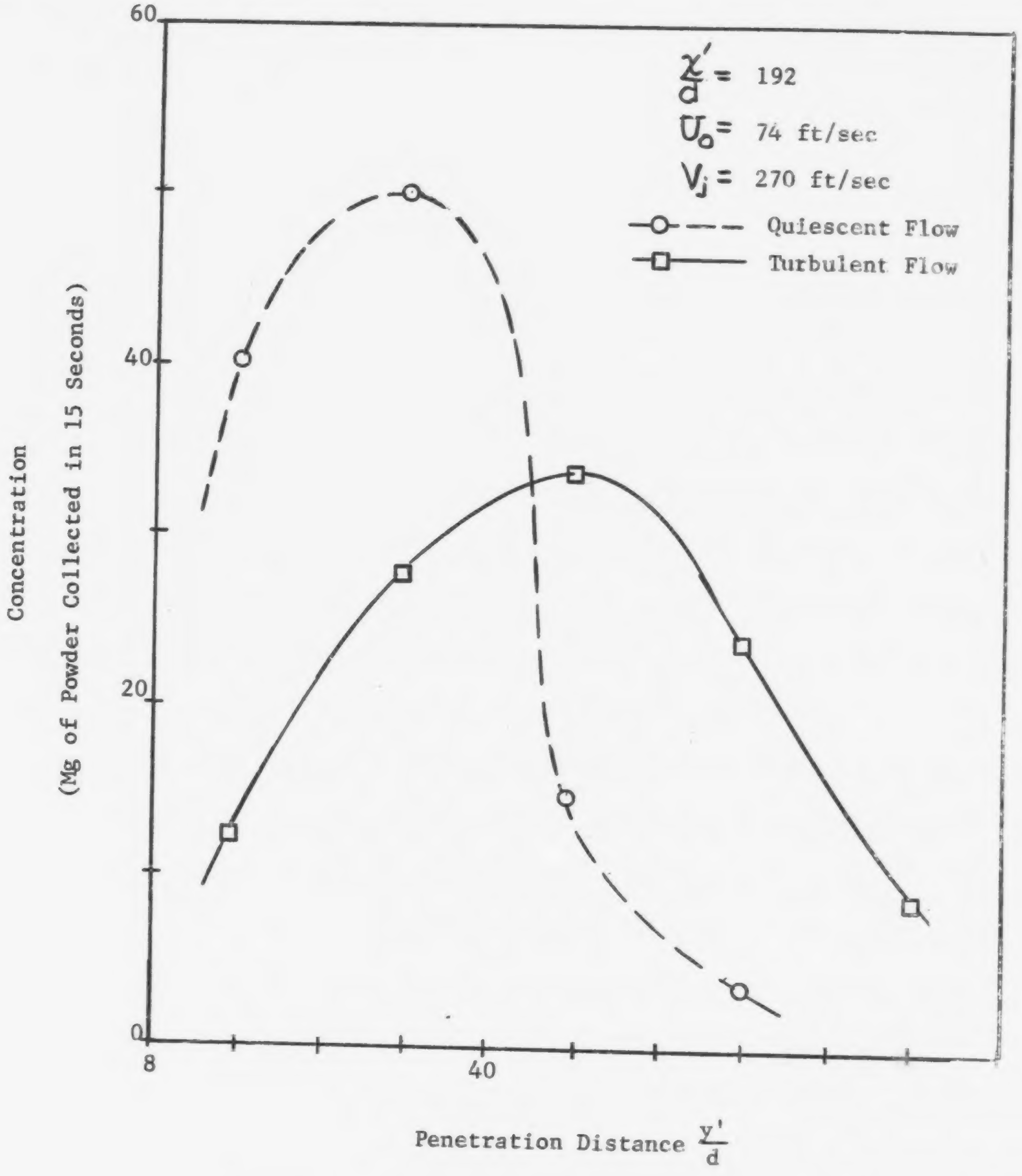

Figure 2.2. Concentration Profile Along Centerline of 12" x 12" Duct

2.7 Comparison of Model and Full Scale Results

The data in this model study are compared with the data provided by the O.A.P. and the specific tests used for comparison are listed in Table 5.3. The data from both studies were used to calculate the fraction (or percent) of uniform coverage for each of the three injection levels. Unfortunately, it will not be possible to compare these data on an equivalent basis since exact modeling was not maintained. Several types of deviations from exact modeling occurred. First the turbulence level in the Shawnee boiler is unknown and hence could not be matched with any model turbulence. Furthermore, the dynamic pressure ratio for the front injection in the Shawnee boiler was approximately 50 percent greater than this ratio at the other two levels while the dynamic pressure ratio was kept constant for all three levels in the model experiments. Also the excess air was varied in the Shawnee boiler experiments whereas the duct mass flow rate was kept the same throughout the testing in the model. Finally, no specific information was made available on the variations, if any, between the injection mass flow rates for each of the nozzles at Shawnee. Any significant variations of this type would also influence the dispersion characteristics.

Table 2.4 gives the average percent coverage for each of the three injection levels based on the experiments listed in Table 5.3. The model coverage for the two-inch grid are presented along with the Shawnee calculations for all three levels. The most general observation that can be made is that the results from the model are consistent with those from the full scale system. In particular both systems found the same relative standing for the three injection levels with regard to fractional coverage. Furthermore, the magnitudes of the coverage values at each level for each system were reasonably close together. However, it should be noted that

Table 2.4. Overall Percent Coverage

	Model (2" Grid)	Shawnee*
Level 1	66	70.9
Level 2	85	74
Level 3	49.1	63.2

*These values averaged over all experiments listed in Table 5.3.

the variations between levels in the model were not as great as those in the Shawnee boiler. However, the dynamic pressure ratios for the model and full scale system differed by 50 percent for the front injection level which may have contributed to this discrepancy.

Thus, in summary it is felt that the agreement between the model and full scale coverage values is due to the modeling efforts. In particular, the values of the dimensionless parameters for the model were kept as close as possible to those of the full scale boiler as was indicated in Table 2.3. At the same time it is recognized that modeling was not complete and the above stated deviations from exact modeling are the likely causes of differences in the percent coverage values.

3.0 EXPERIMENTAL EQUIPMENT AND INSTRUMENTATION

3.1 Introduction

The experimental program was performed using a system designed specifically for this study. The total apparatus requirements include the main air flow system, the solid-gas feed system, and the instrumentation necessary for monitoring the process and obtaining the concentration data.

The main air flow system contains three components, which are: (1) the blower, (2) the two test sections, and (3) the filter. The solid-gas feed system, which performs the function of mixing the solid phase with the air and injecting it into the test sections, completes the list of equipment necessary to obtain the flow and injection process.

There are five major instrumentation components. These are: (1) a pitot tube, (2) an isokinetic sampling system, (3) a hot wire probe, (4) an optical concentration probe, and (5) a laser velocimeter. At the termination of data acquisition, development of the last two instruments was not complete and they were not used. Each of the flow system components and the instrumentation components are described separately below.

3.2 The Blower

The blower system is composed of three parts; a fan, a D.C. motor, and a D.C. generator. The fan is a centrifugal type made by American Blower Inc. and is connected in line to a General Electric D.C. motor. The power for this motor is supplied by a General Electric speed variator unit which is used to regulate the output of the fan. The operational envelope of this blower system is shown in Figure 3.1.

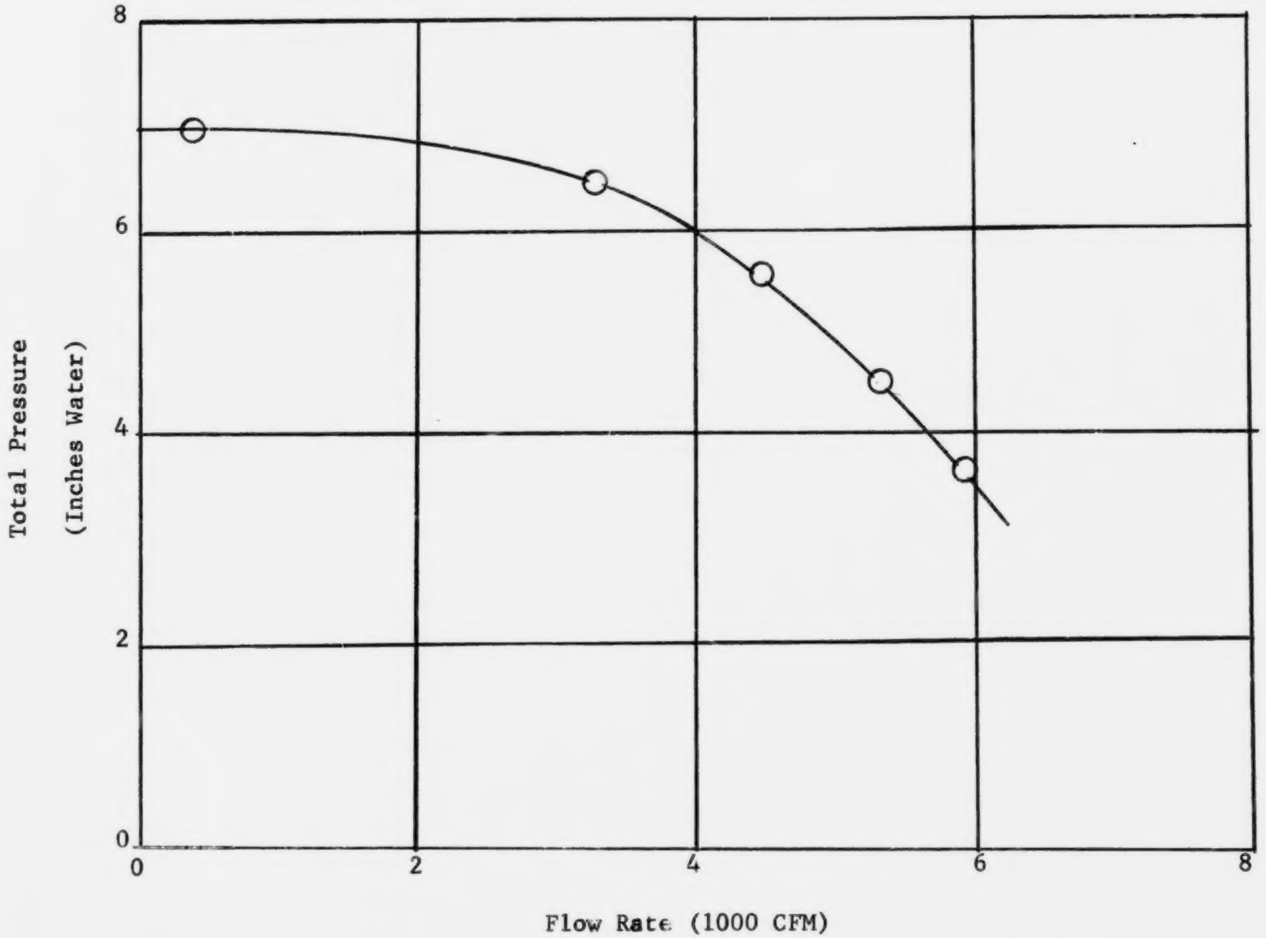

Figure 3.1. Centrifugal Fan Output

3.3 Test Sections

3.3.A Straight Test Section

The straight test section used for this experiment has a square cross section twelve inches to a side and is made with transparent materials. The top and bottom portions are one and one-half inch thick pieces of plexiglass, respectively. The sides are one-quarter inch thick white plate glass. These transparent materials were selected for observing and photographing the process.

The lead-in duct upstream of the test section is constructed of galvanized sheet metal. This conduit contains a convergent transition section (to match the blower outlet to the 12-inch square duct) and a straight 12-inch square section which is six feet long. A flow straightener has been placed in the duct immediately behind the convergent section. This flow straightener is made of a number of one inch I.D. by six inch long seamless steel tubes which were fastened together forming a square packing of parallel tubes which fill the entire cross section. This was done to eliminate the flow angulation induced by the fan. A turbulence generating grid is placed a short distance upstream of the test section when increased duct turbulence is desired. The turbulence generating device is a grid of one inch rods placed on two inch centers and mounted in a wooden frame. Figure 3.2 shows the dimensions of this lead-in duct as well as the locations of the flow straightener and turbulence generating grid.

This test section contains a single injection port. The solid-gas jet is injected through a 1/8 inch nozzle placed in the top section of the duct with the axis normal to it. The isokinetic concentration measurements are

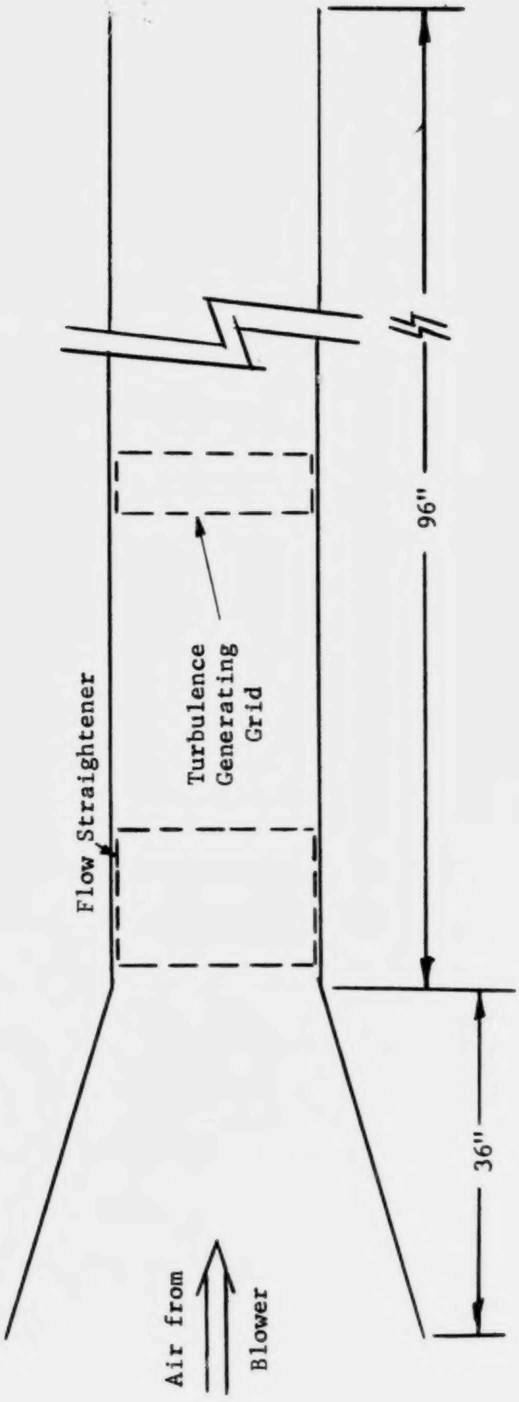
Flow Straightener
Turbulence Generating Grid
96"
36"
Air from Blower

Figure 3.2. Lead-in Duct

made at a test plane two feet downstream of the nozzle as is shown in Figure 3.3. The test section terminates inside the filter system box eliminating the need for a special exhaust duct.

3.3.B Shawnee Test Section

The Shawnee model test section is a scaled down version of one side of boiler number ten at the Shawnee Power Station near Paducah, Kentucky. A ratio of 12.5:1 has been used in scaling the model to the boiler. The model is constructed of wood with glass sides (1/4 inch thick white plate glass). This makes visual observation and photography of the plume possible. The wood section is made of plywood with two inch by four inch framing to stiffen the structure. Figure 3.4 shows the details of this test section.

For the Shawnee model, a flexible plastic duct connects the fan to a "stagnation" box immediately under the test section. The air proceeds upwards through a series of screens or turbulence generating devices which are used to control flow conditions in the test section. Two types of fine mesh screens are used to smooth the flow and reduce the turbulence intensity. Both a large grid and cylindrical vortex generators are used to promote turbulence. These turbulence conditions were produced by removing the stagnation box face plate and sliding the appropriate turbulence frames into or out of the box. The entire set of frames included four frames with fine mesh (window type) screens, one frame with one inch wooden dowels on two inch centers, and one with vortex generating cans. The four turbulence conditions created in this study were obtained in the following manner.

1. Turbulence reduction screens -- all four screen frames in place.

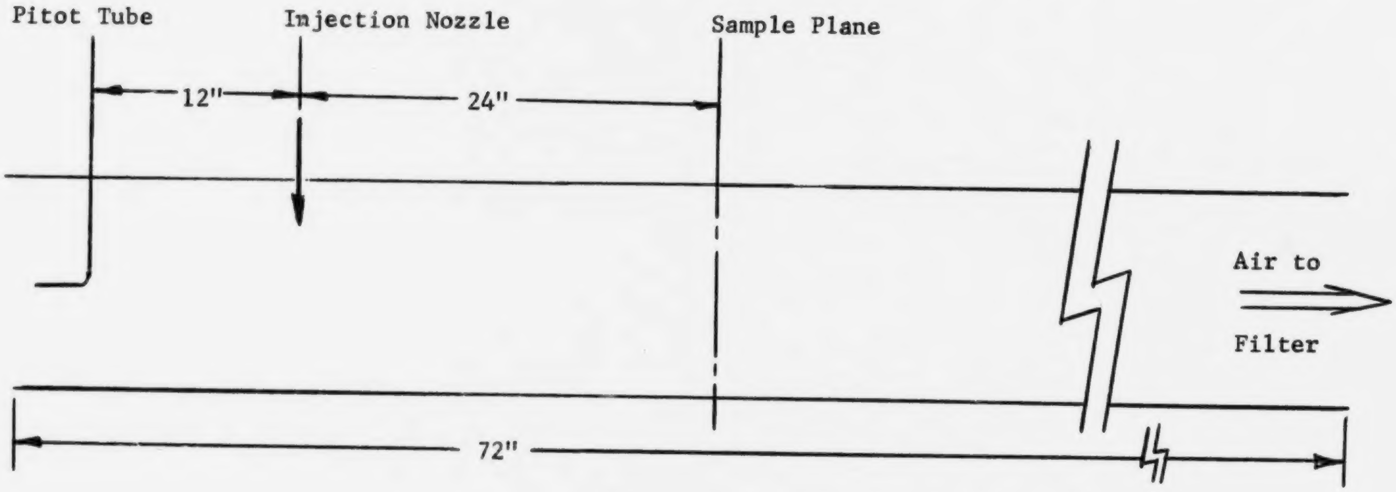
Pitot Tube
Injection Nozzle
Sample Plane
12"
24"
72"
Air to
Filter

Figure 3.3. Square Duct

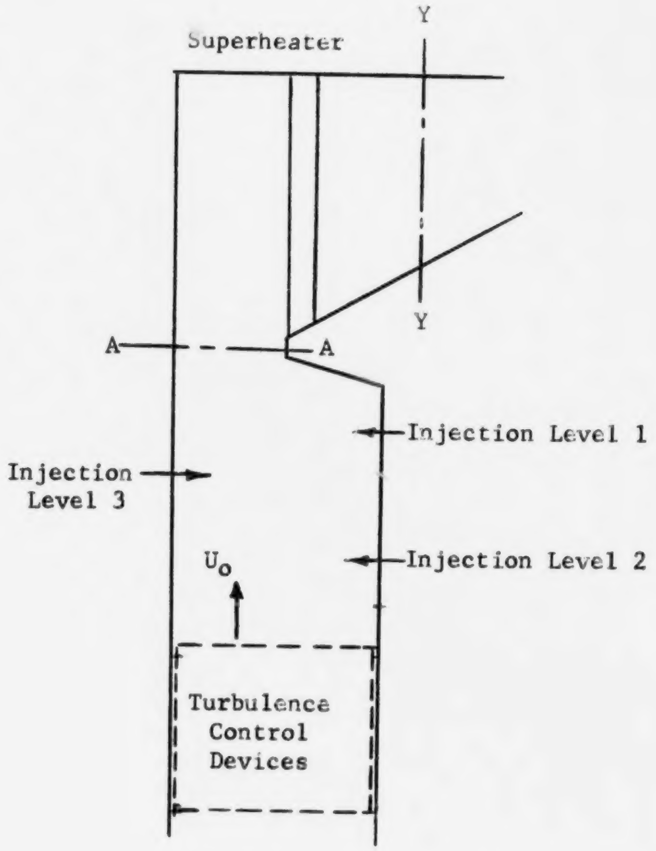
Superheater
Y
Y
A
A
Injection Level 1
Injection Level 3
Injection Level 2
U_o
Turbulence Control Devices

Figure 3.4a. Shawnee Model

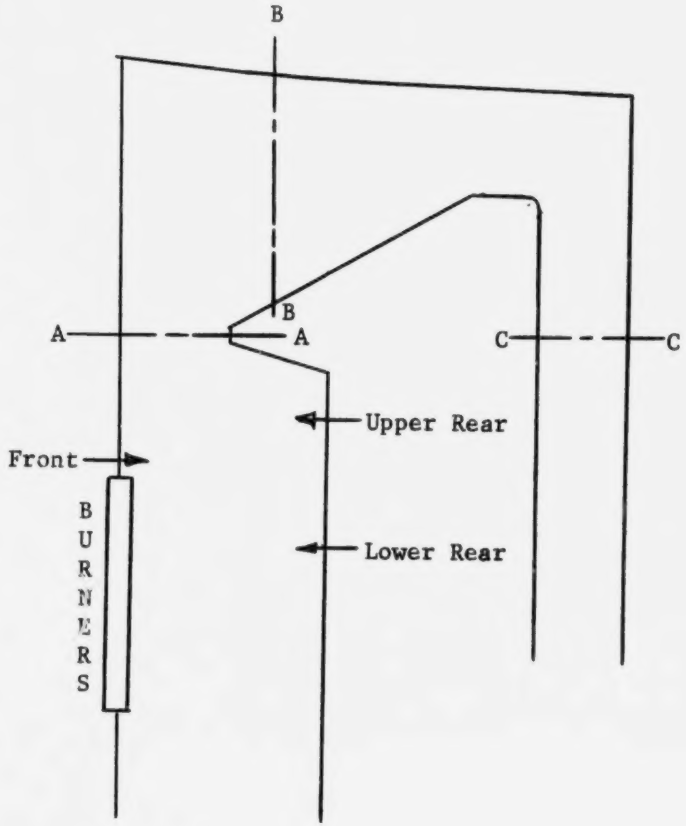
B
B
A
A
C
C
Upper Rear
Front
Lower Rear
BURNERS

Figure 3.4b. Shawnee System

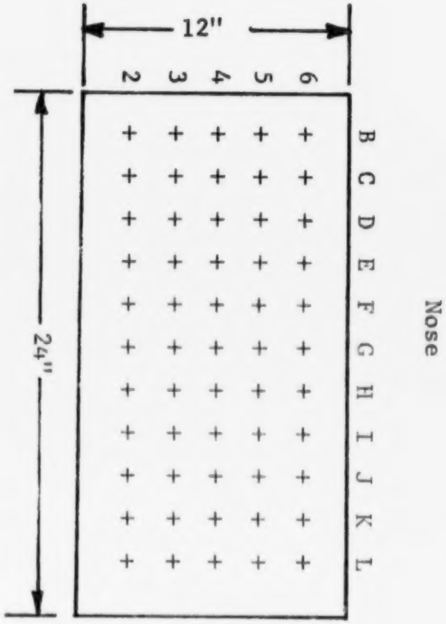
Nose
B
C
D
E
F
G
H
I
J
K
L
2
3
4
5
6
12"
24"

Figure 3.4c. Location of Data Acquisition Points in Plane A-A

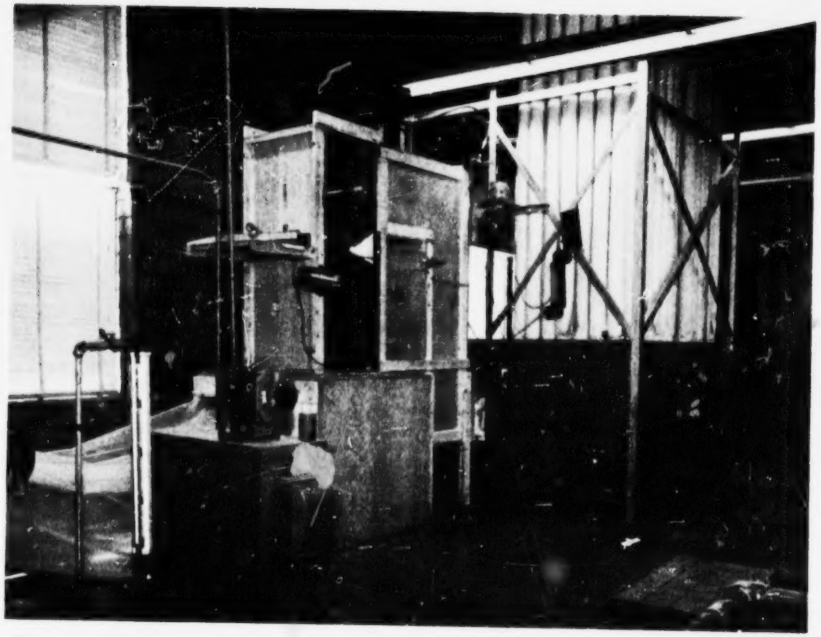

Figure 3.4d. Photograph of Shawnee Model System

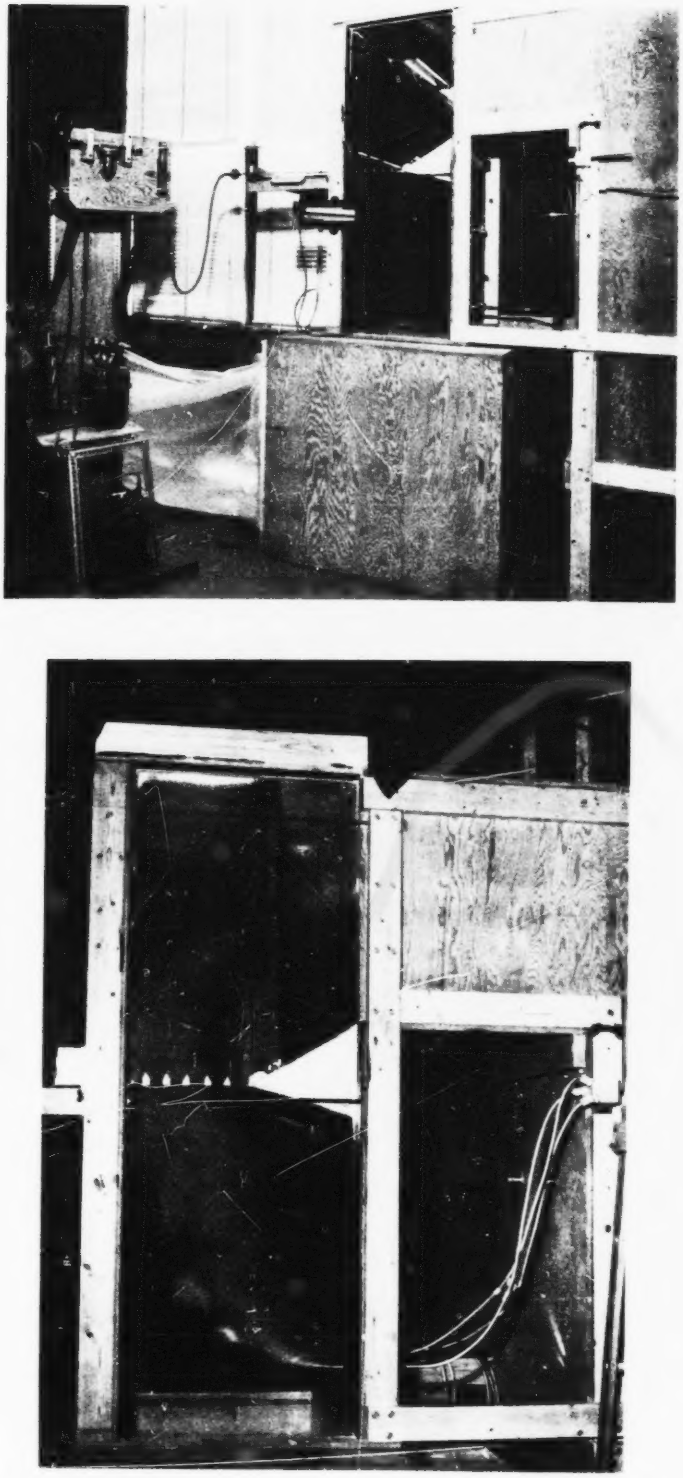

Figure 3.4e. Photographs of Shawnee Model

2. Two inch grid -- three screen frames and the two inch grid, with the grid in the top slot.
3. Vortex generator -- one screen and the vortex generating frame in the higher position.
4. Open box -- all devices removed.

These devices are shown in Figure 3.5. The air then passes through the test section where it makes a sweeping turn and proceeds through a series of rods which are scaled to the first bank of superheater tubes at Shawnee. The air is then ducted back down and into the filter.

As in the Shawnee half boiler, there are a total of eight nozzle locations for the Shawnee model. There are two levels at which there are three nozzles across the duct and a third level with two nozzle locations. The injection nozzles are scaled linearly with the boiler dimensions and correspondingly are 5/32 inch in diameter. Figure 3.4b is a schematic of the Shawnee boiler for comparison with the Shawnee model of Figure 3.4a.

3.4 Filter

The filter system was built at West Virginia University specifically for this project. In house construction was necessary to assure fit into the available lab space and because it cost considerably less than an equivalent commercially available unit.

The filter contains 96 cylindrical cloth filters which are suspended over a large collection box (Figure 3.6). The filter bags and the perforated receiving sheets were purchased from the Pangborn Corporation. Access to the box for purposes of removing dust is provided for by a bolt-on lid.

Reproduced from best available copy.

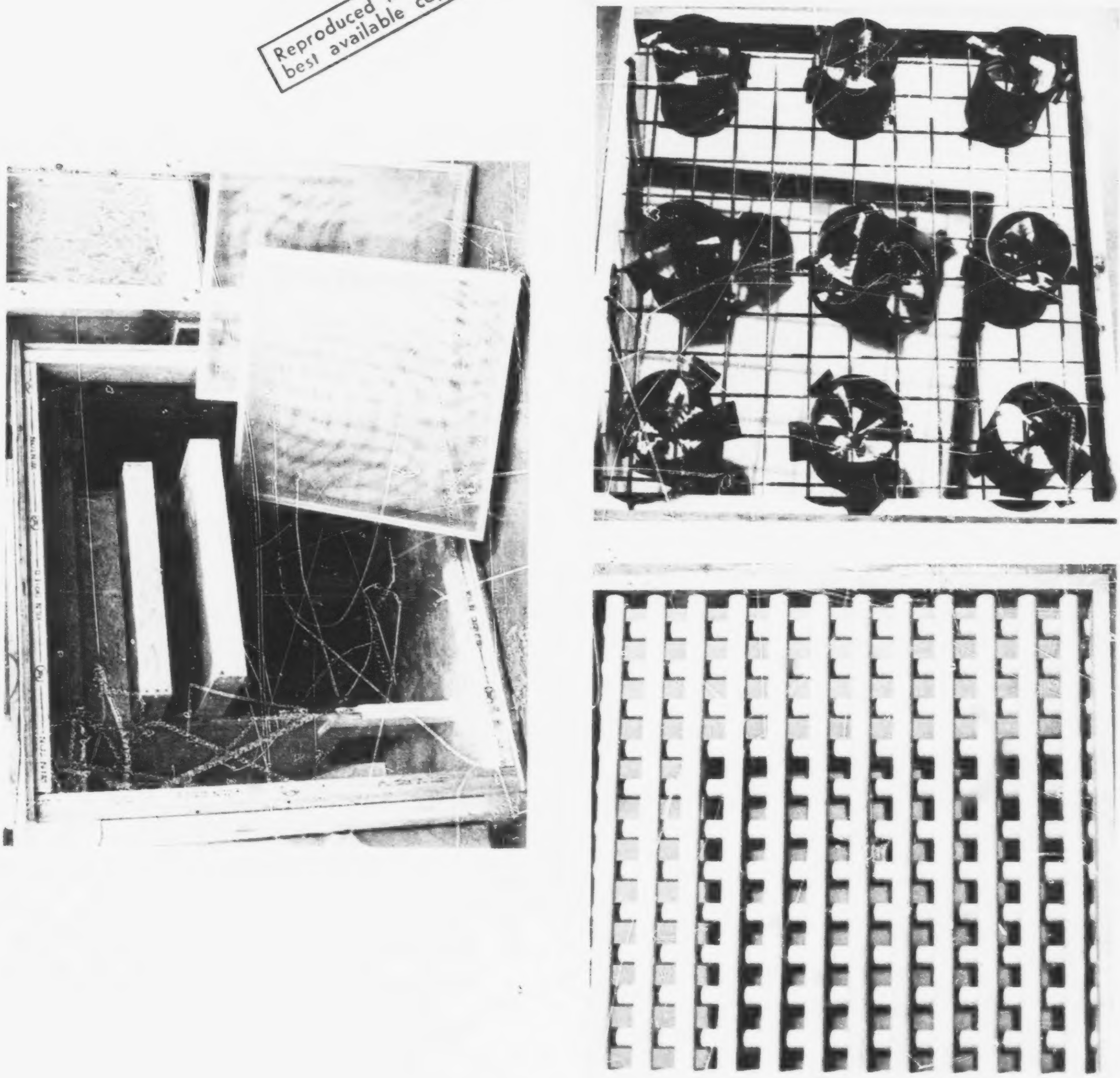

Figure 3.5. Turbulence Generators, Screens, etc.

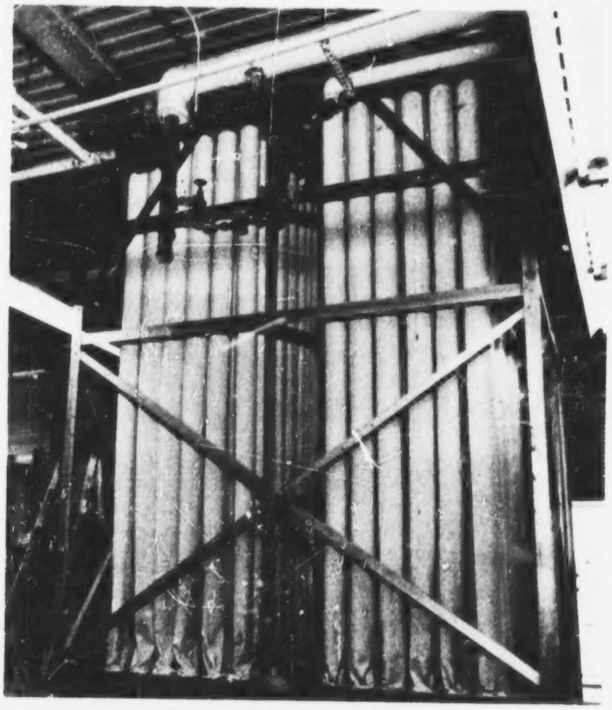

FILTER SYSTEM

Figure 3.6

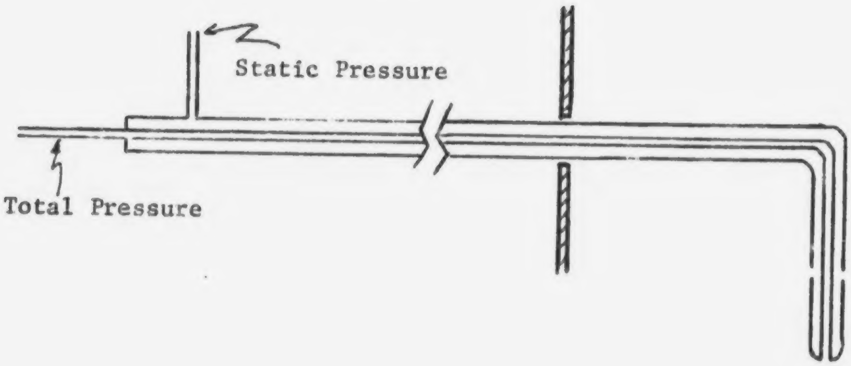
Static Pressure
Total Pressure

PITOT TUBE

Figure 3.7

3.5 Solid-Gas Feed System

For this study, it was necessary to have a steady and consistent jet issuing into the main stream, hence, it was essential that the feeder expel the solid phase at a constant rate. It was also necessary that the system be completely closed so that the air and solid mass flow rates can be monitored and controlled. The feed system designed and built for this project satisfies these requirements.

The essentials of the present feed system are shown in Figure 3.8a. This feed system has a combination vibration and stirring action in the hopper section to assure a smooth flow of the solid phase. At the base of the hopper the air is mixed with the solid phase. This two-phase flow then proceeds through a screw chamber, which further enhances mixing. After the solid-gas flow exits from the screw chamber it is directed into a manifold block. The block divides the flow into two or three streams depending upon the number of nozzles being utilized. A block with three exit ports is used for feeding the three nozzles at injection levels one and two. A manifold block with two exit paths is used for injection at level three as well as for penetration studies.

The hopper was designed to hold approximately five pounds of dry powder. The cylindrical portion of the hopper is constructed of seamless aluminum tubing with five inch I.D. by six inch O.D. and is about seven and one-half inch long. The lower portion, also aluminum, has a short cylindrical section with a truncated conical section below. The apex angle of this conical section is 60 degrees. The exit port at the bottom of the hopper is 1/2 inch I.D.

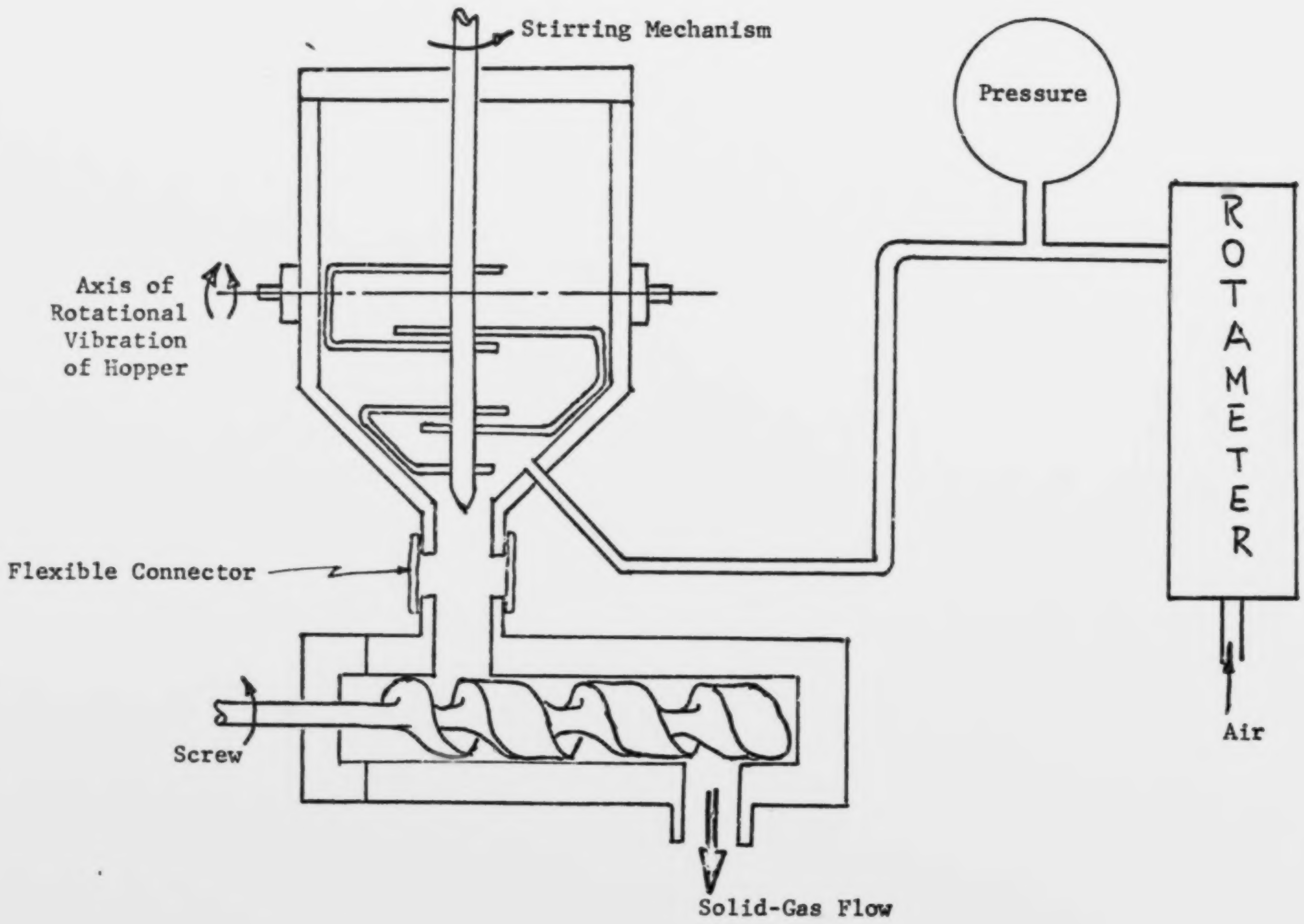
Stirring Mechanism
Pressure
Axis of
Rotational
Vibration
of Hopper
ROTAMETER
Flexible Connector
Screw
Air
Solid-Gas Flow

SOLID-GAS FEED SYSTEM

Figure 3.8a

Reproduced from best available copy.

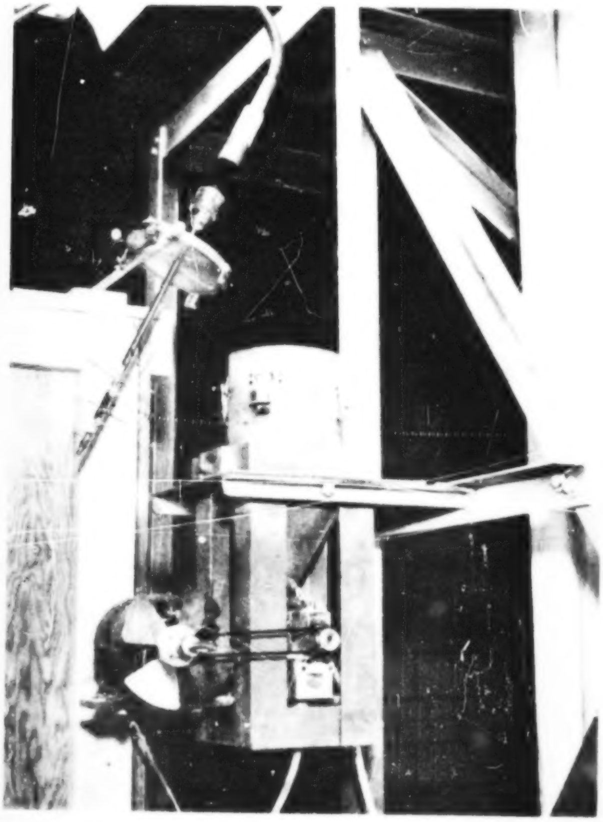

Figure 3.8b. Photograph of Feeder System

The stirring mechanism rotates on a double sealed (pressure sealed) bearing installed in the lid. It is driven through a flexible shaft by a combination motor and reduction gear box (Janette Manufacturing Company Model SU30). The final drive operates at 24 RPM.

In addition to the stirring mechanism, the hopper is also vibrated to facilitate the flow of the solid phase. The axis of vibration passes through the cylindrical portion of the hopper, six and one-half inches from the top. A small crank (1/16 inch throw) and split journal bearing were constructed for the purpose of vibrating the hopper. The connecting rod is attached to the base of the conical section, which moves the full distance of the crank throw. The crank is driven by the same motor which is used to drive the screw. The motor is a Dayton Model 5K-070 (1/10 hp at 1000 RPM).

The hopper is connected to the screw housing by a flexible hose, allowing the hopper to vibrate while the screw remains fixed. The screw is a one inch wood auger bit, which rotates in an aluminum screw housing. The horizontal distance between the inlet (from the hopper) and outlet (to the manifold block) is two inches.

3.6 Pitot Tube

A two-element pitot tube is used in conjunction with an inclined manometer to give direct readings of the dynamic head. The pitot tube is stainless steel with an inner copper tube. There is a stagnation hole at the tip and a series of static pressure pin holes (Figure 3.7) are located 1/2 inch from the tip.

3.7 Isokinetic Sampling Probe

The isokinetic sampling probe is a complete system in itself. It consists of the probe protruding into the flow (probe body), a solids collection filter, a rotameter and a vacuum pump. The schematic, Figure 3.9a, shows the flow path and locations of the various parts of the system.

The vacuum pump used is the Precision Scientific Company Model 75 driven through a V-belt by a General Electric 1/3 hp motor. Air is drawn through the probe body, the filter, the rotameter, the by-pass valve, and finally into the pump.

The probe body is constructed of 1/8 inch copper tubing reinforced over the straight portion with a section of 1/4 inch copper tubing. The probe holder (Figure 3.10) with two degrees of freedom allows the probe to be moved to any location in a given plane. In line with the probe is a two-piece filter made to be quickly taken apart for insertion or removal of the filter paper. The paper filters are 4.7 cm diameter discs.

The by-pass valve is used to control the intake rate of the probe. Hence, it is possible to match the velocity at the probe tip to the duct velocity in the vicinity of the probe.

3.8 Hot Wire Probe

The hot wire probe is used for measuring velocity by relating the velocity of a fluid over the probe wire to the convective heat transfer. Because of the rapid response of the electronic circuitry of the probe to changes in velocity, it is the prime method of measuring turbulence properties. There are two principle types of hot wire probes available; these

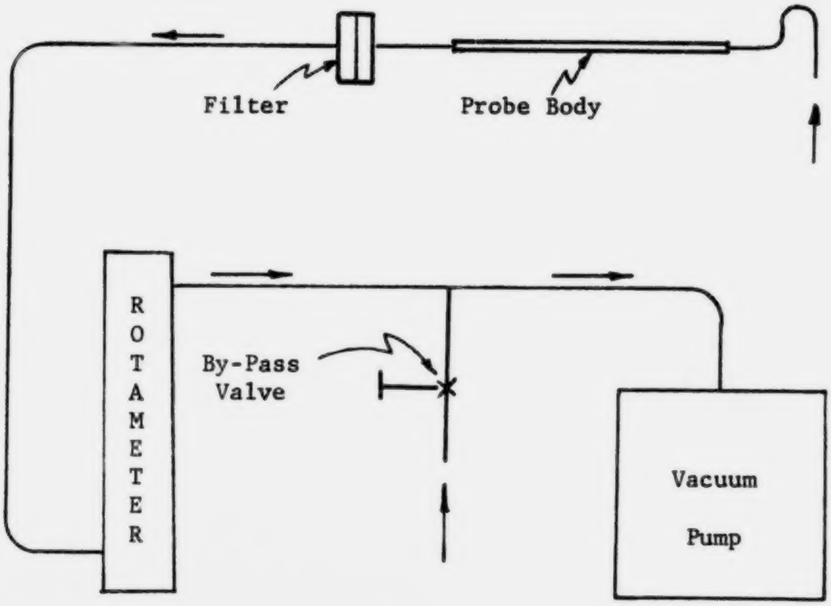
Filter
Probe Body
R O T A M E T E R
By-Pass Valve
Vacuum Pump

Figure 3.9a. Isokinetic Probe System

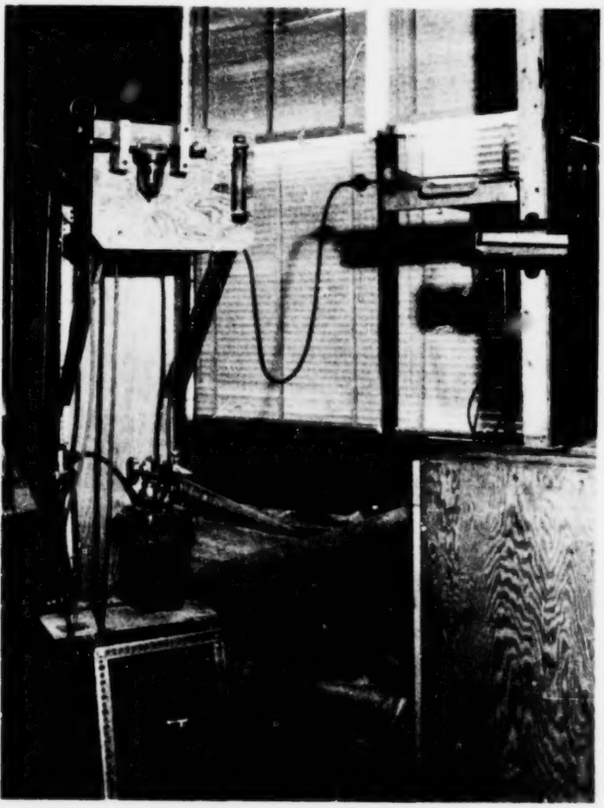

Figure 3.9b. Photograph of Isokinetic Sampling Probe System

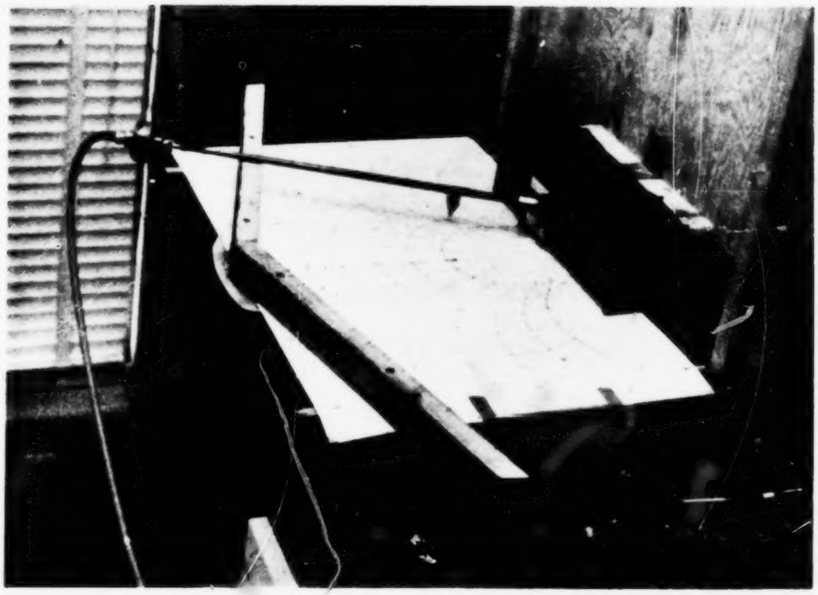

Figure 3.10. Isokinetic Probe Holder

Reproduced from best available copy.

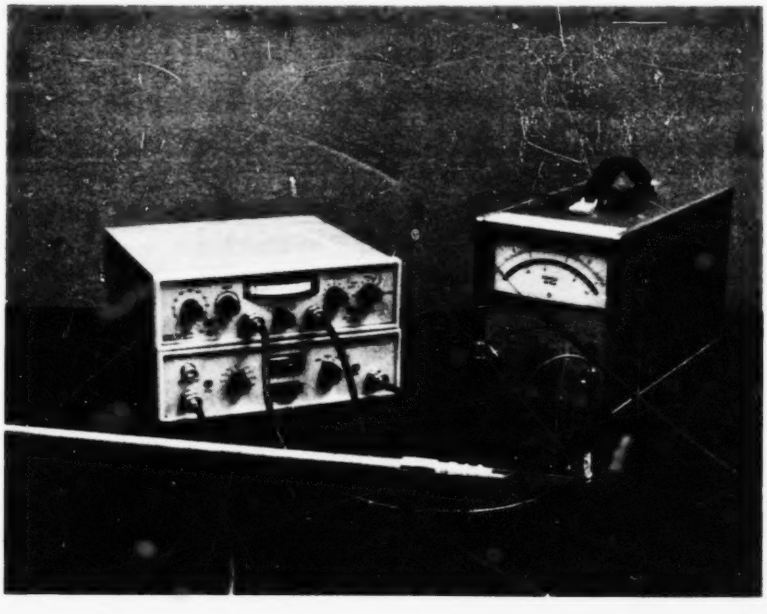

Figure 3.11. Photograph of Hot Wire Probe System

are the constant-current and constant-temperature probes. The constant-temperature type probe has been used for this experiment.

The particular unit used is the DISA 55D05 battery operated CTA (constant temperature amplifier) and the DISA 55D15 linearizer. The linearizer has a small D.C. voltage gauge which indicates mean velocity but it was necessary to use a separate root mean square voltmeter for determining turbulence intensity. The Hewlett-Packard 3400A RMS voltmeter was used to obtain the A.C. component (Figure 3.11). A probe body for the hot wire was constructed to fit the isokinetic probe holder so that the duct cross section would be traversed in the same manner with this probe as with the isokinetic probe.

3.9 Optical Concentration Probe

An optical concentration probe is desirable in order to obtain instantaneous as well as average values of solid concentration at a point. The isokinetic probe reported in Section 3.7 can perform only the latter function. This probe is basically a modification of existing probes reported by Soo (1) and Ehmer (2). This particular design arose over the need for an inplace measurement with a capability for low concentration measurements and a small probe head. The probe described in this section has been built and operated successfully. It has responded to low concentrations of smoke, however, operating in a particulate environment has caused particle deposition on the optical surfaces. It is anticipated that this problem could be overcome yielding an attractive two-phase flow instrument.

In Figure 3.12 a full-sized sketch of the existing probe is shown and gives an indication of the compactness of such a probe. This figure does

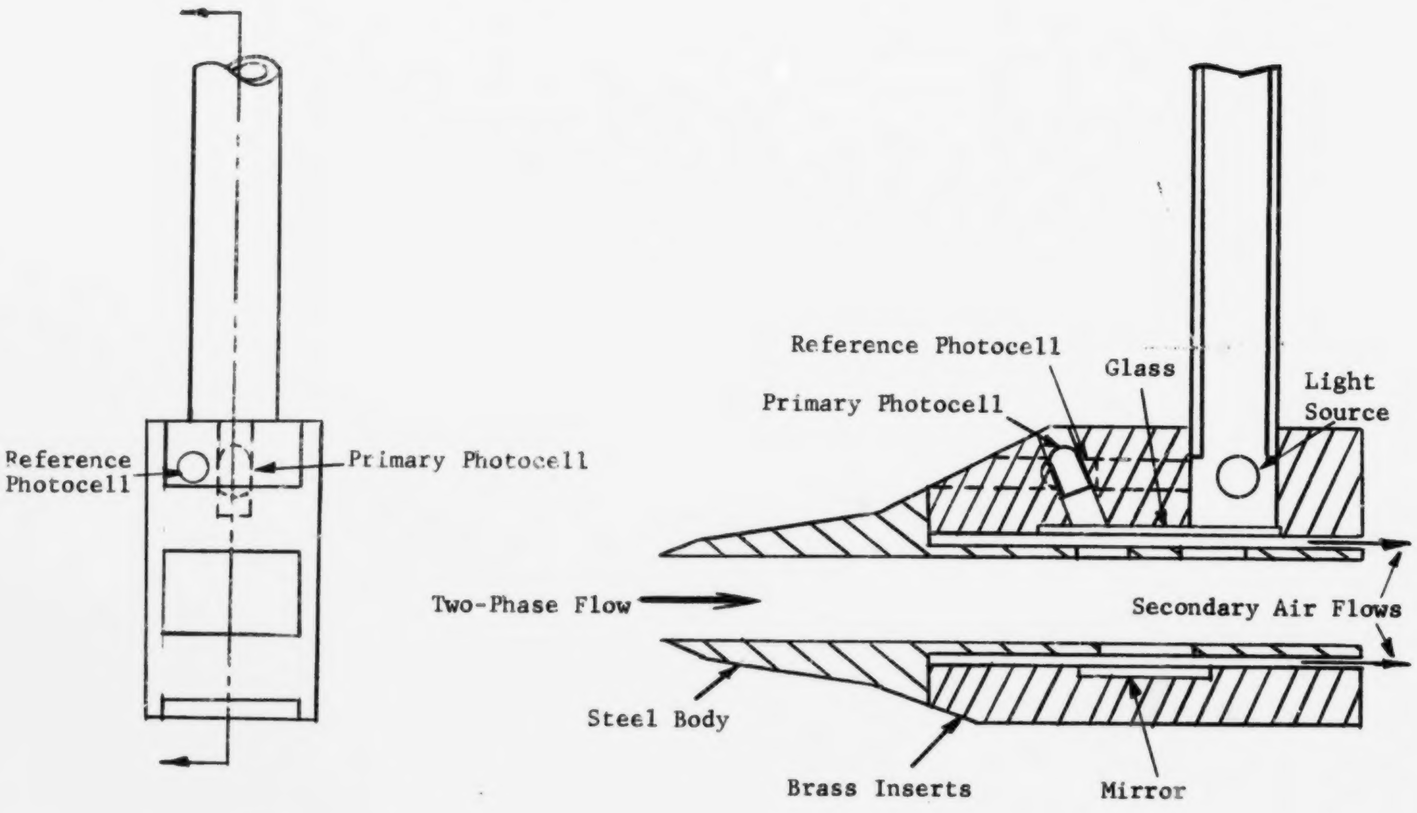
Reference Photocell
Primary Photocell
Reference Photocell
Glass
Light Source
Primary Photocell
Two-Phase Flow
Secondary Air Flows
Steel Body
Brass Inserts
Mirror

Front View

Cutaway Side View

Figure 3.12. Full Size Representation of Optical Probe

not detail the secondary air flow for preventing dust buildup on the optical surfaces or the electrical connections, both of which are conducted down the center of the support rod. The reference photocell is adjacent to the primary (source) photocell and receives light directly from the light source through a channel. The reasons for having two photocells and placing them so close to each other are: (1) variations in light bulb intensity would not effect the zero reference positions since both cells would be reacting to the same change, and (2) photocells are temperature sensitive, hence, the close proximity lessens any significant temperature effects.

The circuit diagram is presented in Figure 3.13b. The power supply is the Kepco ABC 40-0.5N. The differential amplifier is a Tektronix 1A 7-A used in conjunction with a Tektronix 547 scope.

3.10 Laser Velocimeter

The velocity of the gaseous phase of the solid-gas injection can be calculated, knowing the air mass flow rate through the feed system and the pressure at the nozzle exit. There is no correspondingly simple way of calculating the velocity of the solid phase, which very likely has a slip velocity relative to the gaseous phase. The laser velocimeter is an instrument which would directly measure the velocity of the solid phase and yet in no way interfere with the injection process. The velocity of the particles is determined by detecting the Doppler shift of the laser light scattered from the moving stream of particles.

A laser velocimeter has been constructed and operated successfully in a bench arrangement, measuring the velocity of a rotating ground glass

Reproduced from best available copy.

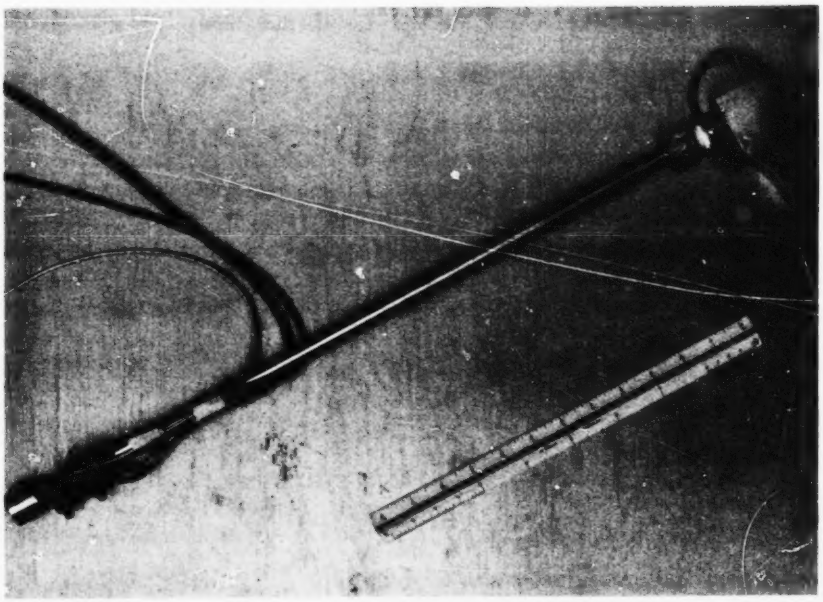

Figure 3.13a. Photograph of Optical Concentration Probe

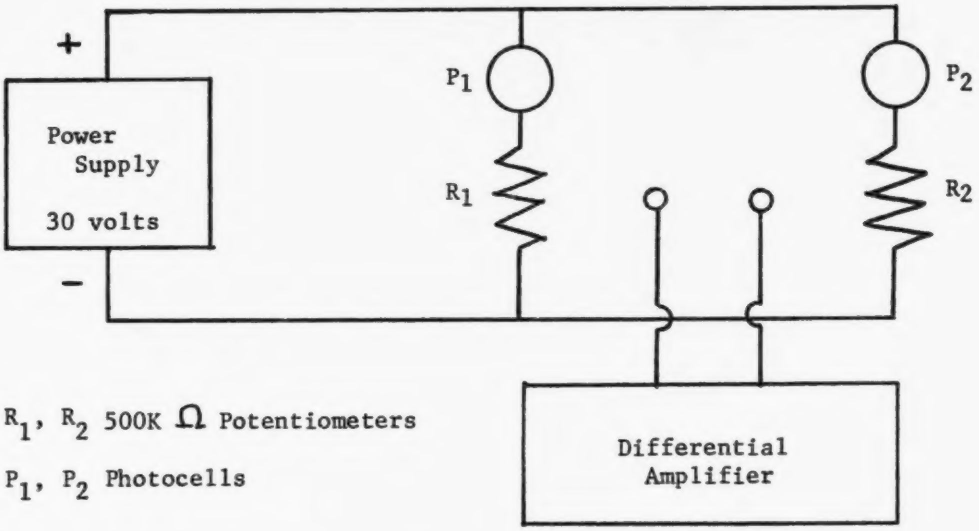
+
-
Power Supply
30 volts
P_1
P_2
R_1
R_2
Differential Amplifier

R_1, R_2 500K Ω Potentiometers

P_1, P_2 Photocells

Figure 3.13b. Circuit Diagram

OPTICAL CONCENTRATION PROBE

disc. Figure 3.14 shows the configuration of the light path for this setup. The laser used is the five mw Spectra Physics stabilite Model 20 with a Spectra Physics 256 exciter. The light is picked up by an RCA 8344 photomultiplier tube with a grid bias supplied by a Fluke 412B high voltage power supply. The output from the tube is processed through a Keithley Instruments 104 wideband amplifier into a Tektronix 3L10 spectrum analyzer used in conjunction with the 561A oscilloscope. The spectrum analyzer indicates the beat frequency which results from combining two waves of different frequency, that is, light directly from laser and light reflected from the particles which experiences a Doppler shift. This beat frequency can then be related to the particulate velocity.

The optical alignment of the necessary mirrors and lenses requires sensitive adjustment capabilities. Time did not permit the fabrication of a portable optical bench for achieving this sensitivity. However, it is felt that such an arrangement is entirely feasible as other somewhat similar applications of the laser velocimeter have been reported as being successful.

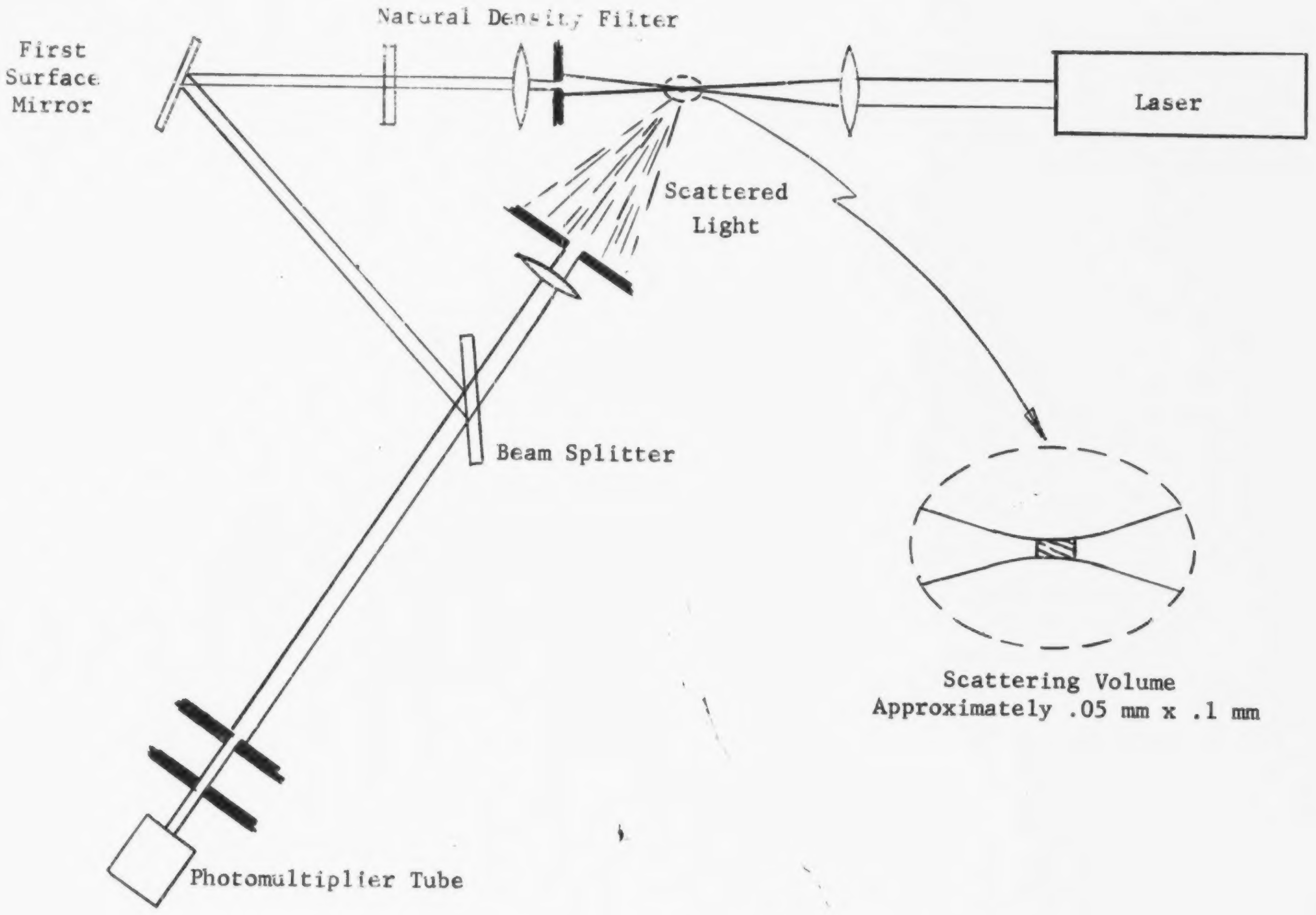
Natural Density Filter
First Surface Mirror
Laser
Scattered Light
Beam Splitter
Scattering Volume
Approximately .05 mm x .1 mm
Photomultiplier Tube

Figure 3.14. Schematic of Laser Velocimeter

4.0 TEST PROCEDURES

4.1 Introduction

In this chapter, the operation of the experimental program will be discussed in detail. Separate sections will be devoted to discussion of the operation of each of the two test sections as well as operation of the feed system, isokinetic probe, and hot wire probe.

During the course of the experimental program, operational techniques improved as expected. Appreciable changes can be noted in certain aspects of the test procedure when comparing early square duct experiments to the final Shawnee model experiments. As an example the problem of bridging of powder in the feeder hopper was not entirely eliminated until the Shawnee model was operational. In addition, since most of the data were taken with the Shawnee model, test procedures discussed will reflect those employed with the model experiments.

For the reasons outlined above, the data obtained from the twelve inch by twelve inch duct are not considered as reliable as those obtained for the Shawnee model.

4.2 Feed System

The hopper is loaded and the feeder is operated until empty for each concentration data measurement obtained and at the end of each run the air flow rate is increased to help remove any particulate deposition which occurs during a run. It has been found that if the feeder was stopped during the injection process or deposition allowed to build, blockages would be formed in the lines.

The hopper lid must be removed before loading. Since the stirring mechanism is driven with a flexible cable, the attachment of the stirring mechanism to the lid does not present any problems for filling the hopper. A predetermined amount of powder is loaded into the hopper then the lid is replaced and secured.

The feeder air line valve is opened at the same time that the motors driving the stirring mechanism, the screw, and the crank for vibrating the hopper are turned on. Pressure adjustments are made at the rotameter to maintain it at a constant value for each run. The value for this pressure is determined by calibrating the feed system to match Shawnee dynamic pressure ratios.

The method of calibration is as follows. A known mass of powder is placed in the hopper. The feed system is turned on, the pressure held constant, and the rotameter value monitored. One observer monitors the injection nozzles and uses a stop watch to observe the length of time necessary to empty the hopper. In this way the flow rate of the powder can be determined. The air mass flow rate and, hence, nozzle velocity is calculated using the rotameter and pressure data. A sample calculation of the dynamic pressure ratio is shown below:

Powder 2.531# Time 38.6 sec. = 0.642 min.

$$\left.\begin{array}{ll}\text{Press} & 29\\ \text{Roto} & 26\end{array}\right\} Q = 5.58 \text{ cu.ft./min.}$$

V_j = 231 ft./sec.

$$\dot{m} = \frac{2.531\#}{.642 \text{ min.}} = 3.93\#/\text{min.}$$

$$\rho_j = .0752\#/\text{cu.ft.} + \frac{3.93\#/\text{min.}}{5.58 \text{ cu.ft./min.}} = .782\#/\text{cu.ft.}$$

$$\text{Dynamic Pressure Ratio} = \left(\frac{\rho_j}{\rho_o}\right)\left(\frac{V_j}{U_o}\right)^2 = \left[\frac{.782}{.0752}\right] \cdot \left[\frac{231}{45}\right]^2 = 274$$

Once the feed system is calibrated, it is necessary only to monitor the pressure for normal operation. Calibration runs made at different times for the same operating conditions indicate a variation on the order of ± seven percent.

4.3 Isokinetic Probe

The operation of the isokinetic probe is relatively simple once the tip velocity can be related to rotameter readings (Figure 3.9). Since calibration curves for rotameters do not give negative pressure correction curves, it was necessary to calibrate the rotameter to the system. A Rockwell 250 dry gas meter was used for this purpose. By adjusting the by-pass valve on the vacuum pump, it is possible to vary the flow through the system (rotameter and dry gas meter). Once the system is calibrated to the rotameter, it is necessary only to choose the correct rotameter setting for a given duct position.

The operation of the probe is as follows. First, the vacuum pump is turned on and remains so for the entire operation. Then the filter paper is placed in the holder and the two halves of the holder are fastened together in the operating position. The probe is adjusted in the holder until the tip is at the proper location in the duct. The probe tip is then rotated 180 degrees from the orientation for data sampling. The by-pass valve is adjusted until the rotameter is at the proper setting. The feed system is turned on and when the injection appears to have reached its steady state operating condition, the probe tip is rotated to the predetermined orientation for sampling. At the end of the sampling time period, the probe is rotated 180 degrees once again. The filter paper is removed, a new one installed and the probe is again ready to operate.

In order to determine the amount of dust injected into the probe when in the nonoperating position (rotated 180 degrees), special tests were run. The probe was positioned in an area of high concentration (about 70 mg/10 sec.) and the procedure outlined in the previous paragraph was followed except that the probe was not rotated into the flow. The results gave an indication of the intake of powder collected prior to and immediately following the sampling period while powder was still being injected into the system. These tests were run for about 20 seconds each. In each case, less than six mg was collected. Hence, it was concluded that the intake of powder prior to and after the test period was a small fraction of that obtained during the sampling period.

4.4 Hot Wire Probe

The procedure for setting up the hot wire probe is standard and outlined step by step in the manuals accompanying the unit. Once the components are assembled and the unit calibrated, the amplifier resistance is adjusted to match that of the hot wire probe. Then the gain is adjusted so that the output voltage corresponding to the maximum duct velocity is within the range of the linearizer (less than three volts). The output voltage from the linearizer is shaped to be directly proportional to the velocity normal to the wire. Therefore, it is only necessary to obtain the voltage corresponding to a single known velocity in order to calibrate the probe over the entire operational range. This was done by using the pitot tube.

The turbulent fluctuations are also picked up with the hot wire probe. These fluctuations are measured with respect to the mean velocity and are put on a root mean square meter. The value read is $\sqrt{\overline{u'^2}}$ or the square root of the mean value of the fluctuating component of velocity squared. The ratio of this value to the mean velocity U_o, u'/U_o, is defined as the intensity. The intensity as well as the mean velocity can be obtained in this manner at any location in the plane of measurement.

4.5 Straight Test Section

Two types of experiments were performed using the straight duct. The first was the acquisition of data for the trajectory in the vicinity of the nozzle exit. The second set of experiments were conducted to ascertain the effects of turbulence for a single injection condition.

The operation of the main duct and the feed system are the same for both experiments. First, the blower system is turned on and the air velocity is monitored using a pitot tube set at the center of the duct one foot upstream of the injection nozzle. The blower is adjusted to the proper velocity as indicated by the pitot tube and maintained at that level throughout the test, where periodic adjustment of the blower was necessary due to dust buildup in the bag filter system. Then the feed system hopper was filled and preparations for operation of the feed system were performed as outlined in Section 4.2.

From this point on the operations were different for the two experiments. In the experiment to obtain the trajectory, a laser beam was used to illuminate about a ten-inch portion of the plume. The laser was placed on the floor, Figure 4.1, since the bottom of the duct is 2.2 feet above the floor level. The light was directed through a cylindrical lens which

Reproduced from best available copy.

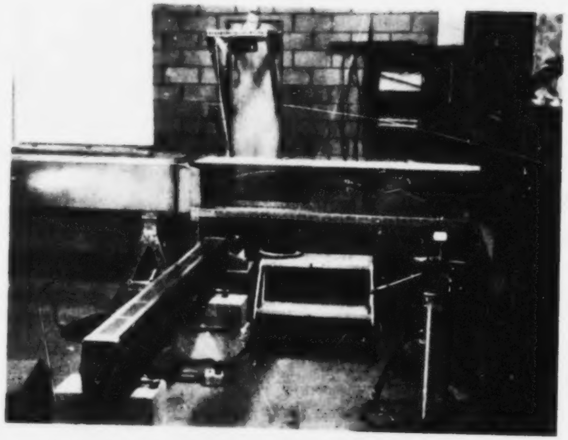

Figure 4.1. Photograph of 12 in x 12 in Duct with Laser

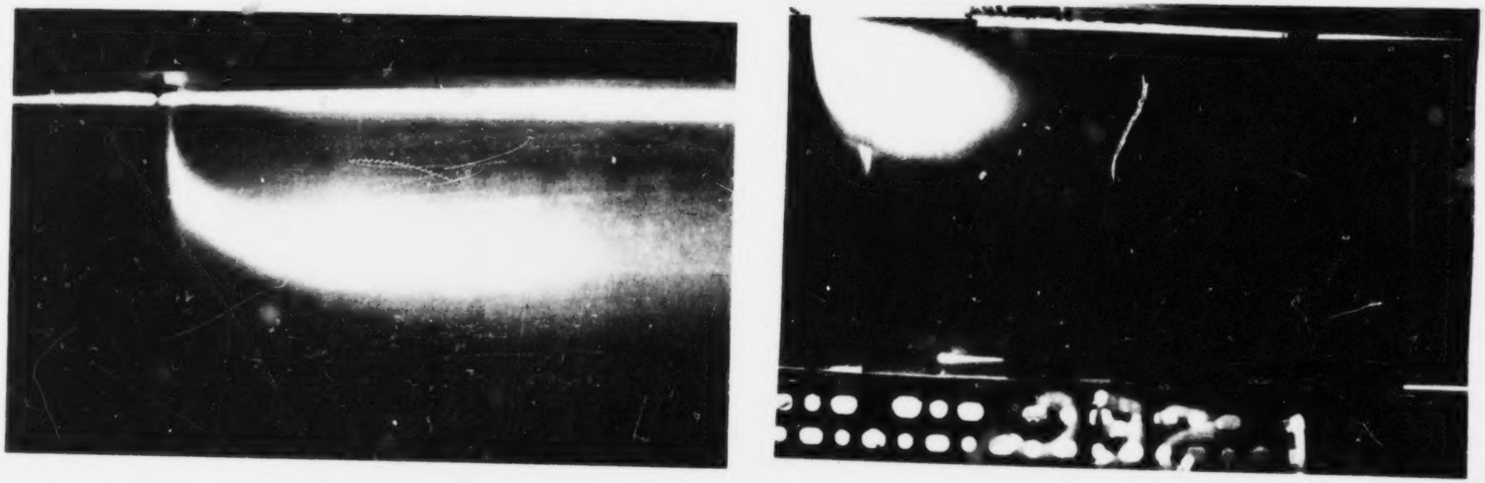

Figure 4.2. Trajectory Photographs

spread the light in a vertical plane (much like an open fan). The light, after passing through the lens, was reflected off a first surface mirror, at an angle of 45 degrees, straight up into the duct such that the plane of the light was coincident with the jet centerline and parallel to the duct walls. In this way, the portion of the duct from the nozzle to a distance of about ten inches downstream was illuminated by a thin sheet of light. Although no measurements were made, visual observations indicated that thickness of this fan of light was on the order of 1/32 inch. Hence, it was possible to observe a thin slice of the jet plume.

A thin sheet of clear plastic was taped to the side of the duct, and the experiment proceeded. One observer traced the shape of the plume on the plastic sheet. This process was repeated for a number of different dynamic pressure ratios. These ratios were obtained by varying the main duct velocity. This was found to be preferable to varying the feed system operating condition.

Because of the concentrated intensity characteristics of the laser light there was sufficient light for photographic work. However, it was necessary to blacken the interior surface of the far side glass wall and to perform a number of other alterations to eliminate reflection and other undesirably illuminated surfaces. The photographic results are shown in Figure 4.2.

The isokinetic probe was used to obtain the profile of the injected plume at a point two feet downstream of injection for the experimental work related to testing the effects of variations in turbulence. For the first flow condition, only the flow straighteners were placed in the duct. This corresponded to the "quiescent" condition. For the second condition, the turbulence generating grid was placed about half a foot downstream of the flow straighteners. The average velocity (as measured by the pitot tube) was kept the same for both cases as was the feed system operating condition. The isokinetic data was taken along the vertical center axis of the duct. That is, at points two inches, four inches, six inches, eight inches, and ten inches from the top of the duct and at a position two feet downstream of the injection point.

The actual operation of the system is a combination of Sections 4.2 and 4.3. The feed system is turned on and monitored. When the mass flow rate out of the injection nozzle reaches the steady state condition, the probe was rotated to the sampling position for 15 seconds and then turned back. This process was repeated for both turbulence conditions at all the required probe locations.

4.6 Shawnee Test Section

The bulk of the Shawnee model experimental program has been devoted to obtaining concentration profiles at Section A-A by injecting at the three different levels corresponding to those used at Shawnee and for four different types of duct turbulence. For all nine test conditions, the duct mean velocity and the dynamic pressure ratio of the injection process were held constant. In addition, experiments were performed to study penetration, injection superposition at Plane A-A, and dispersion at Section B-B. For all of these tests the isokinetic probe was used to obtain the concentration profiles.

The blower was turned on and set at the scaled operating condition. This corresponded to a dynamic head of .430 inches of water (45 ft./sec.)

at Section A-A. It was necessary to check and reset the blower approximately every four runs to maintain this level. The next steps were to prepare the isokinetic probe and the feed system for operation. One observer started the feed system and the other operated the isokinetic probe. This process was repeated from 50 to 90 times to obtain a single concentration profile at Plane A-A for each of the four turbulence conditions and injection positions. There were a possible total of 55 sampling points for each condition although all were not used for any given set of turbulence and injection conditions.

For each of these conditions, the intensity of turbulence was measured using the hot wire probe. It was necessary to do this only once for each condition since the turbulence generated by these devices remains constant so long as the flow velocity is not changed.

For the superposition tests, the nozzles at injection level 2 were utilized along with the turbulence reducing screens. One nozzle was left in place, and the other two were removed and inserted into the exhaust section. In this manner the feeder was operating under identical conditions (i.e., feeding three nozzles) as in the previous tests. Data were obtained for each of the three nozzle positions at level 2.

The penetration tests were performed using the two nozzle-manifold. One nozzle injected into the exhaust portion of the test section, and the other was placed in the center nozzle position of injection level 2. Three different feeder operating conditions were utilized. Duct conditions were maintained with the turbulence reduction screens at the Shawnee model duct velocity (45 ft./sec.). As for the previously mentioned Shawnee model tests, the concentration data were obtained with the isokinetic probe at Plane A-A.

During the final portion of the experimental test program, a limited amount of concentration data were obtained for model Section Y-Y. For these data, all three nozzles at injection level 2 were utilized. Two different duct turbulence conditions were used; one with the turbulence reduction screens and the other with the vortex generator.

This concluded the Shawnee model test program. Over 750 data points were obtained during this program. Each of these required operational procedures outlined at the beginning of the section and detailed in Sections 4.4 and 4.5.

5.0 EXPERIMENTAL RESULTS AND DISCUSSION

5.1 Introduction

This section will present the experimental results and their interpretation. As with previous sections of this study, the data from the twelve-inch duct will be treated separately from those from the Shawnee model. The twelve-inch duct results include single jet trajectory data as well as downstream concentration profiles for two different turbulence conditions. Most of the Shawnee model experiments were conducted to obtain concentration profiles at Plane A-A for each of the three injection levels. These experiments were run with one injection level operating at any given time which corresponds to the limestone distribution study at Shawnee conducted early in 1971. For the model experiments a range of turbulence conditions was studied. In addition, some concentration data were taken at Plane Y-Y (close to B-B) to compare with the data taken at Plane A-A.

5.2 Penetration and Concentration Results for Twelve-Inch Duct

5.2.1 Introduction

The twelve-inch straight duct experiments were planned in order to aid in the design of the Shawnee model experiments. In particular, it was designed to handle the dual roles of providing an experimental arrangement for the study of a single solid-gas jet and to serve as a checkout facility for the various components that were eventually utilized in the Shawnee model system. The twelve-inch straight duct was oriented horizontally even though the real system and the scale model are oriented vertically. But, as is shown in Appendix C, gravitation effects are not significant to the injection and dispersion phenomena. Therefore, the orientation of this duct will not have an effect on the applicability of the data so obtained. Hence, the experiments with this test section supplement those with the Shawnee model.

The original plan was to spend more than half the time allocated to the straight duct experiments for single jet trajectory and dispersion tests. The remaining time was to be used experimenting to determine the effects of multijet injection and injection angle on dispersion. However, during the course of the study it was necessary to devote more time than planned to the feeder and concentration probe development. Consequently, the experimental single solid-gas jet experiments were reduced in number which significantly limited the quantitative conclusions that were drawn. Nevertheless, trajectory data were obtained for a solid-gas jet which were compared with existing gas jet correlations. In addition, qualitative information on the effect of increased turbulence intensity and scale on the downstream concentration profile was obtained. No work was done in the straight duct for multiple injection or for variation in injection angle.

5.2.2 Trajectory Results

The trajectory data were obtained by visual observation. Here, as mentioned earlier, the laser beam was optically transformed into a vertical plane of light which sliced through the solid-gas plume providing good illumination. The plume envelope was then traced onto transparent plastic sheet attached to the face of the duct. The solid curves in Figure 5.1 represent the centerline value of the measured envelope of the

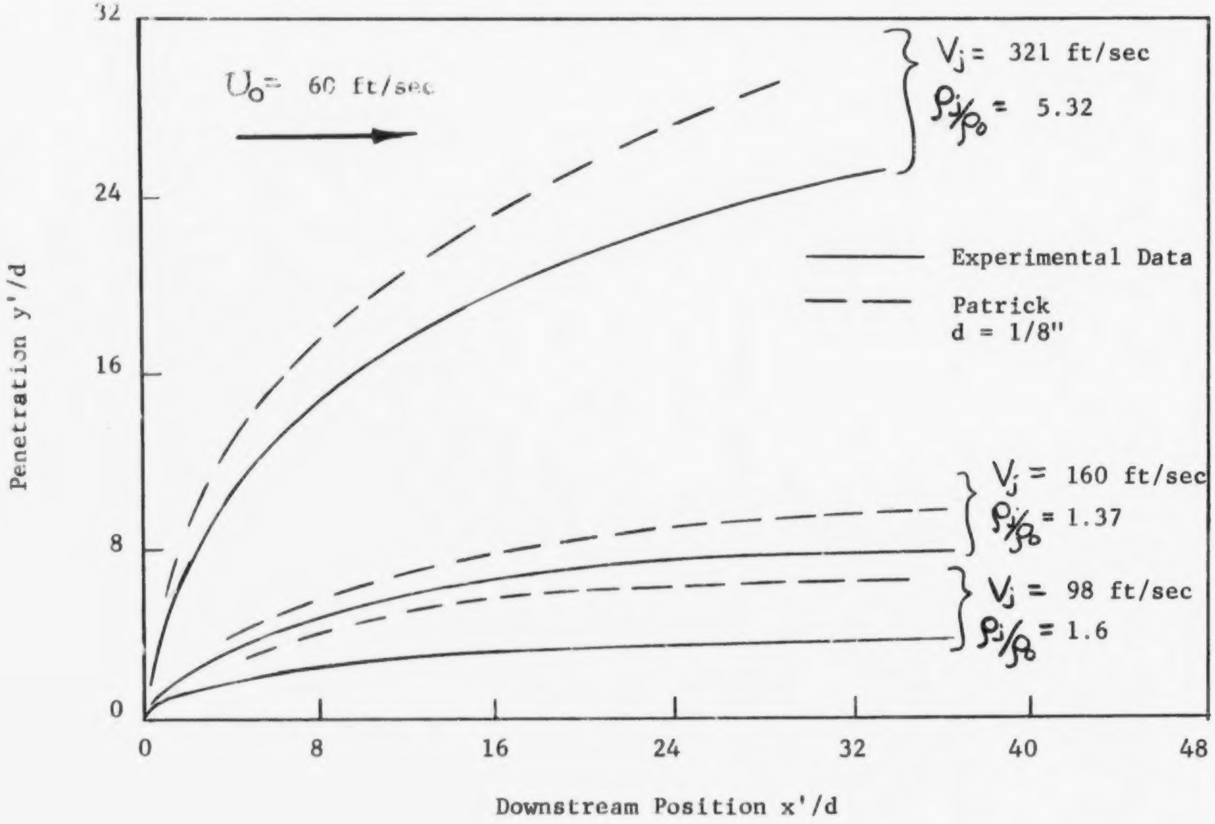

Figure 5.1. Trajectory Data 12" x 12" Duct

plume. The dotted curves represent the correlation obtained by Patrick (3) for a gas jet study. The experimental values of ρ_j from this study treat the solid-gas flow as a homogeneous mixture. The value of ρ_j in Patrick's correlation corresponds to a gas density for the jet which is different from that of the transverse stream. Nevertheless, agreement between Patrick's prediction and the two-phase jet is significantly better than that between single particle trajectories and the same two-phase jet. Figure 5.2 shows the trajectory paths as predicted by Patrick's equation along with the numerical solution for a single particle. Unfortunately, conclusions drawn from such few results would be premature. Independent variables such as particle size, particle density, and free stream turbulence were not parameterized. In addition, the geometrical centerline of the plume may not represent the true centerline of the plume. In fact, the ideal method for determining the jet trajectory would be to take concentration profile measurements at various downstream locations.

In summary, while the limited number of trajectory curves for the solid-gas jet are in fair agreement with Patrick's correlation, the flow regime considered here was too narrow to endorse that correlation for a solid-gas jet. Before doing so, it would be necessary to conduct a systematic study over a range of values for the dimensionless parameters obtained in Section 3.

5.2.3 Concentration Profile Measurements

Several experiments were also conducted to compare the effect of turbulence intensity on the distribution of particulate in the duct. This was done by obtaining concentration data both for the relatively quiet flow in the duct approximately ten feet downstream from the flow

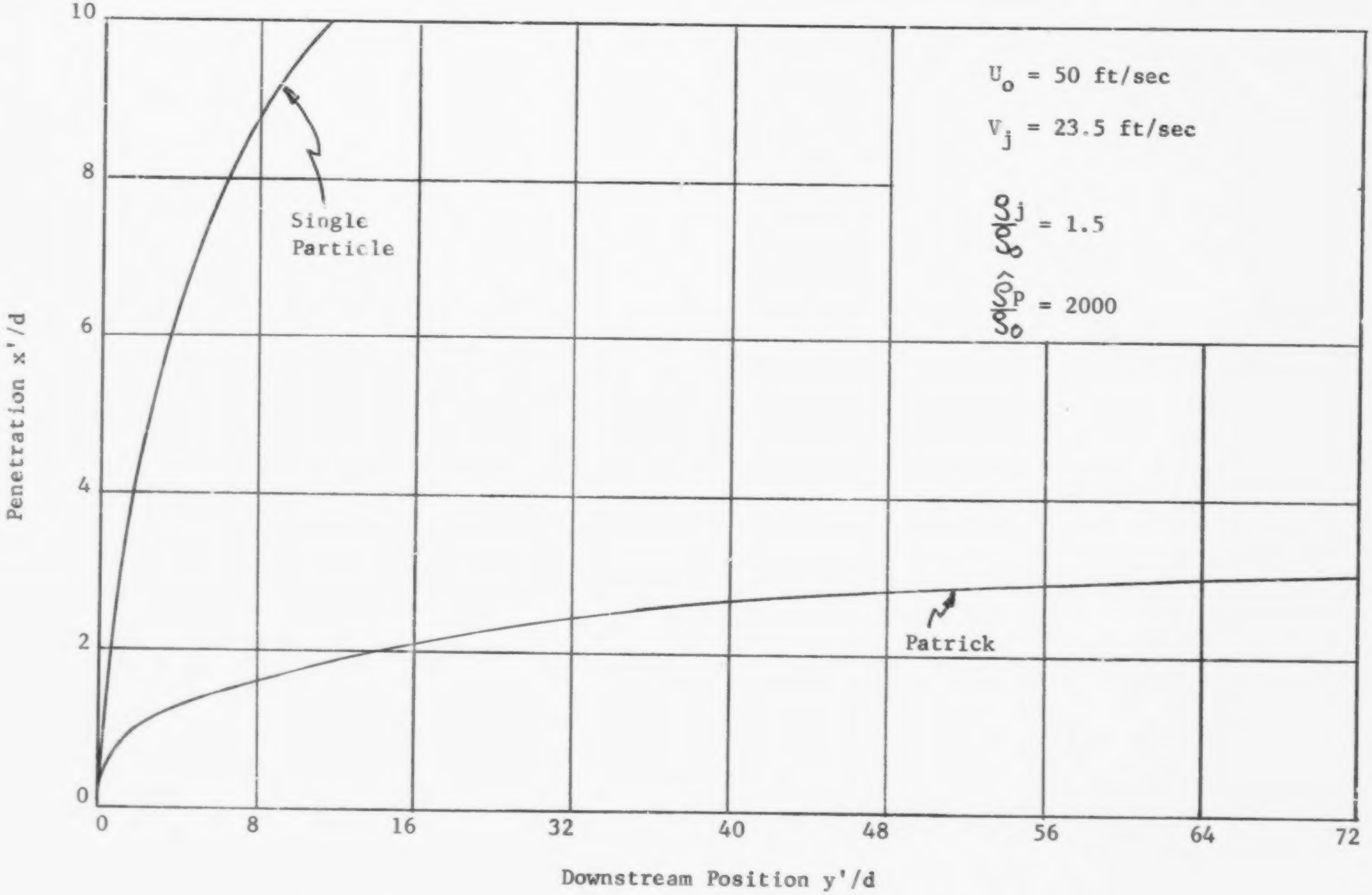

Figure 5.2. Trajectory Comparison of a Single Particle With a Homogeneous Jet

straighteners and for a more turbulent condition produced by a grid. Figure 5.3 shows the two concentration profiles along a vertical axis through the center of the duct two feet downstream of the point of injection. As expected, the more turbulent condition increased the dispersion.

5.3 Shawnee Model Experiments

5.3.1 Introduction

The primary goal of this portion of the experimental program was to operate the model after the full-size Shawnee system. Appendix C discusses the fractional analysis and details the required fluid properties and flow variables necessary to keep the dimensionless pi groups the same for both the full-scale system and the Shawnee model. The experiments were carried out meeting these requirements as nearly as possible. As mentioned earlier, the turbulence parameters were undefined in the Shawnee boiler and as a result it was necessary to experiment over a range of turbulence conditions with the intent of learning what effects these conditions have on dispersion. The resulting concentration profiles at Plane A-A are presented along with comparisons and conclusions as to the effects of the various turbulence conditions and injection levels on the concentration profiles.

5.3.2 Turbulence Conditions in the Shawnee Model

5.3.2.1 Introduction

Various devices for promoting turbulence were tried in this program and are described below. Measurements of the turbulence intensity in Plane A-A were obtained for each device and are presented in Figures 5.4, 5, 6 and 7. The turbulence scale was not measured so that

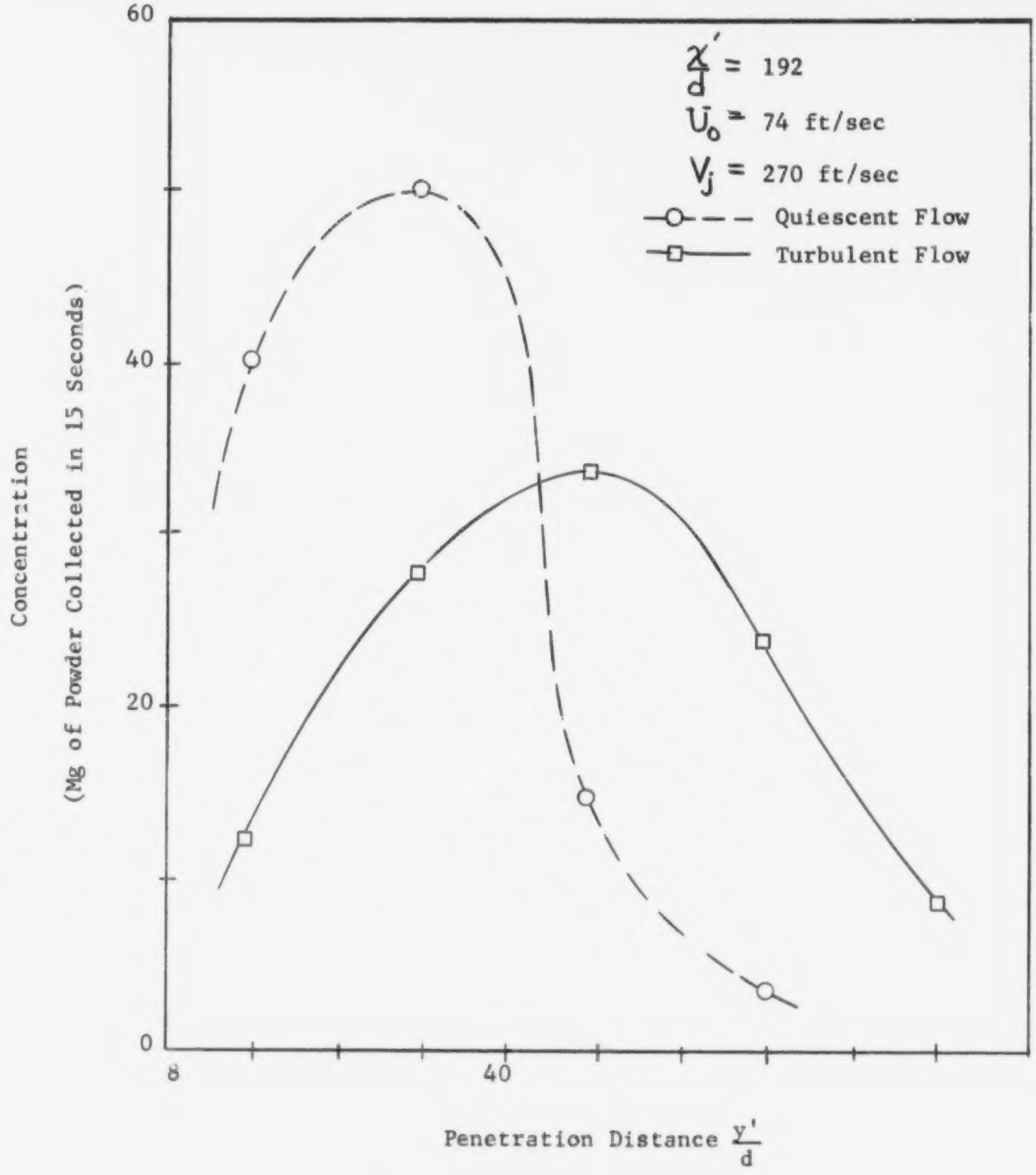

Figure 5.3. Concentration Profile Along Centerline of 12" x 12" Duct

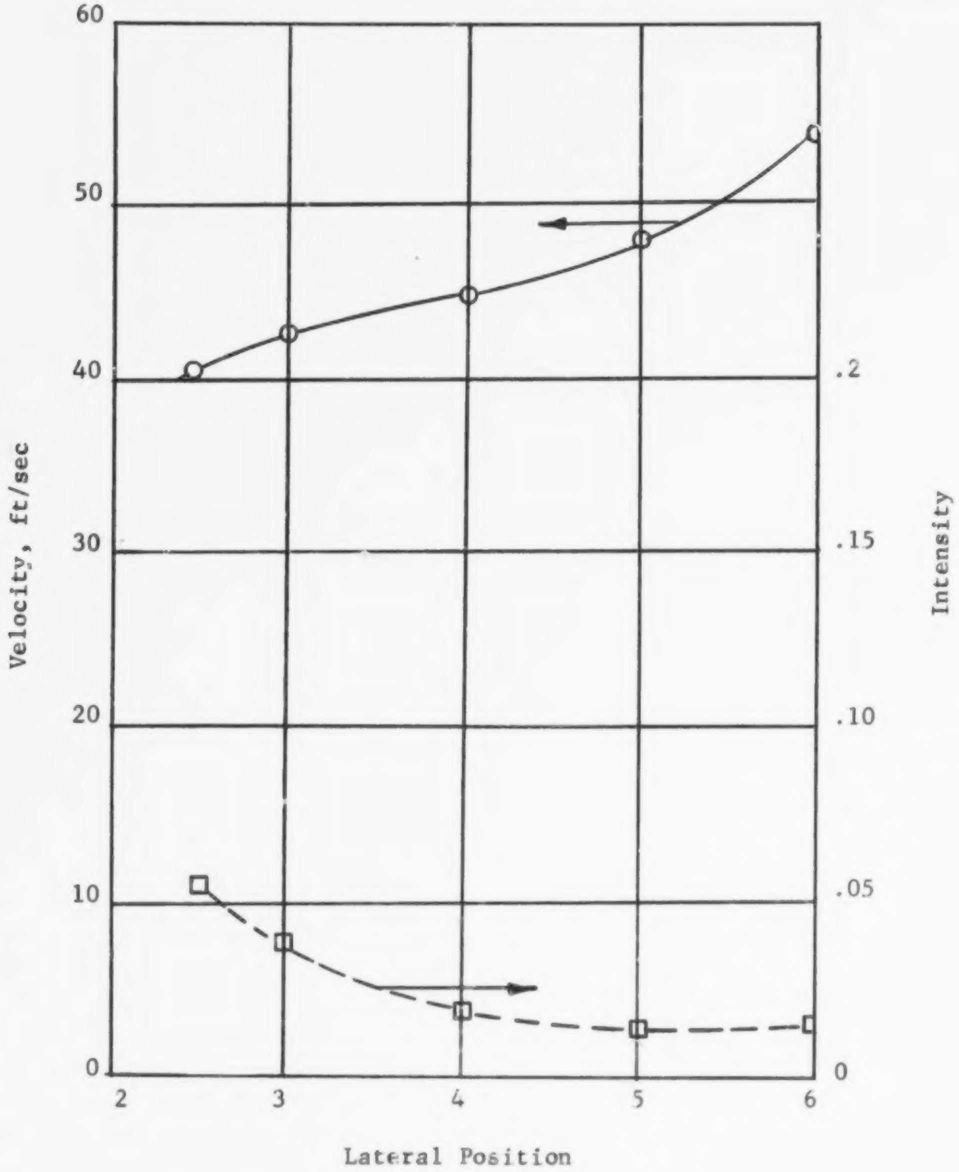

Figure 5.4. Velocity and Intensity - Screens - Plane A-A

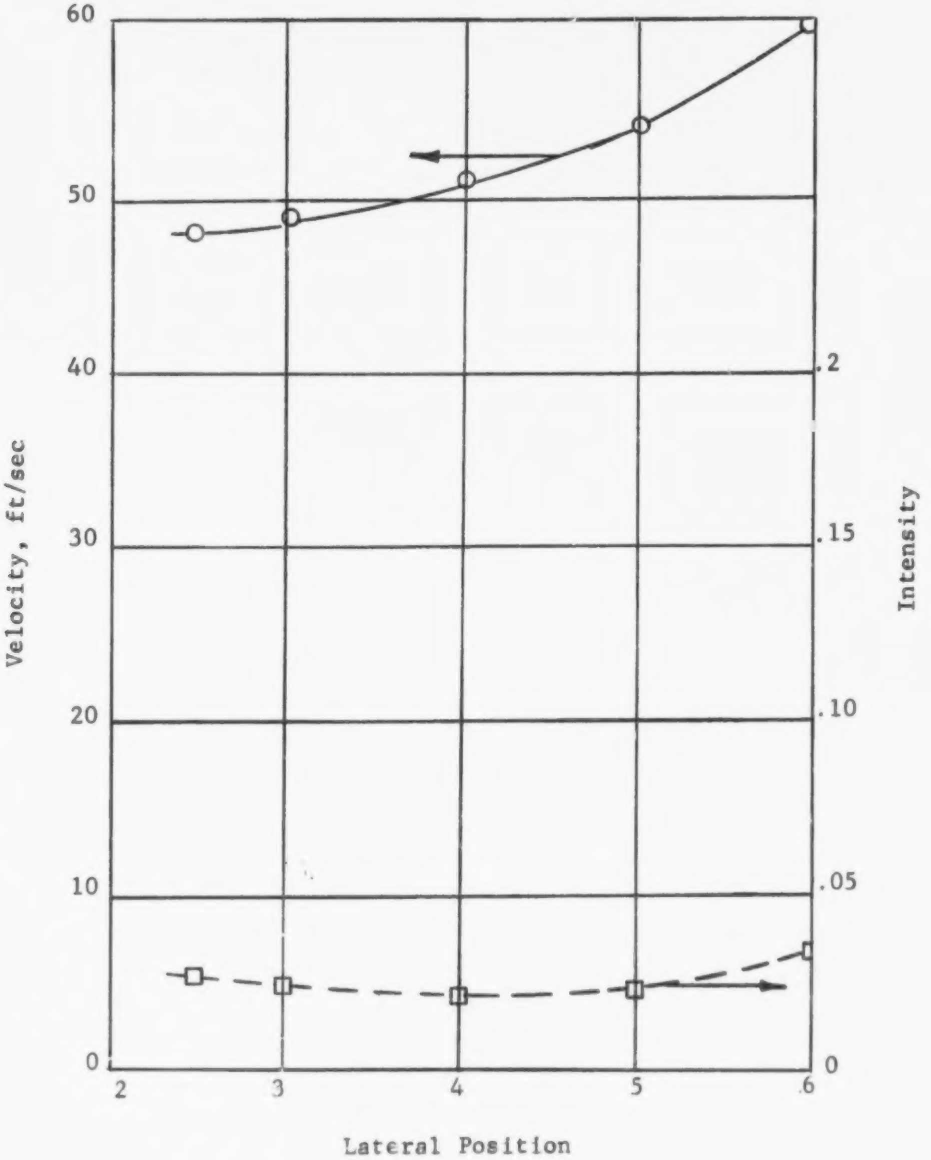

Figure 5.5. Velocity and Intensity - 2" Grid - Plane A-A

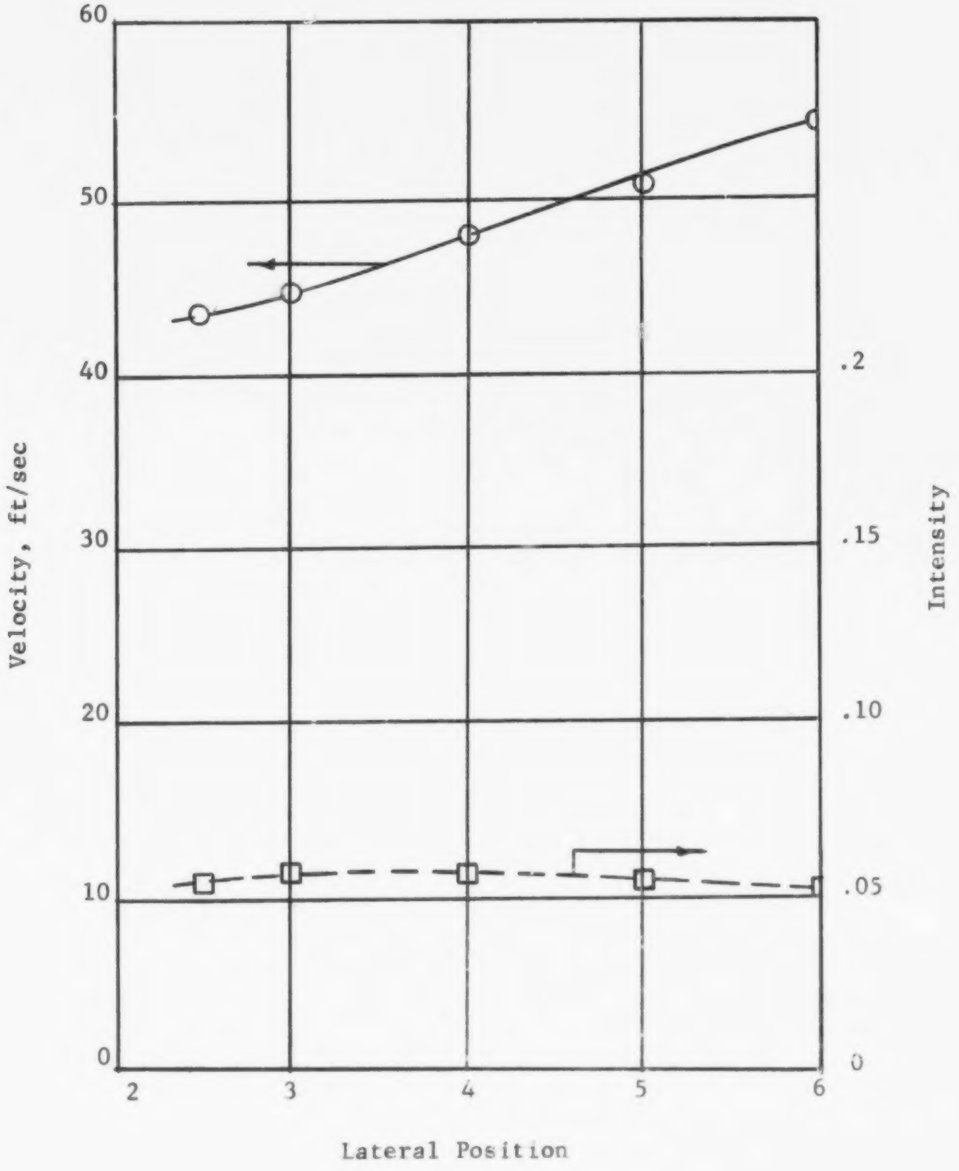

Figure 5.6. Velocity and Intensity - Vortex Generator - Plane A-A

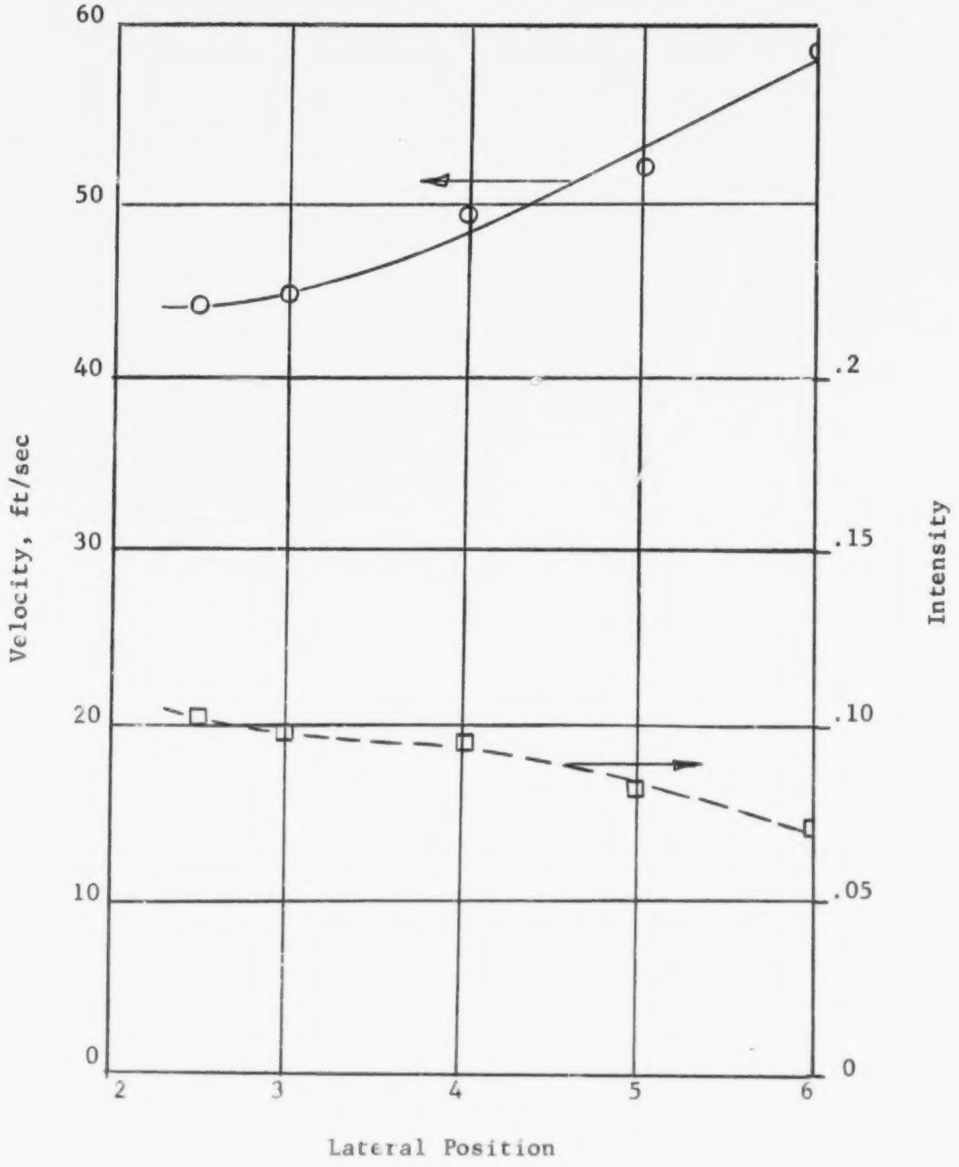

Figure 5.7. Velocity and Intensity - Open Box - Plane A-A

approximate values, as suggested by the literature, were assigned to each condition. The following sections consider each condition separately presenting both the measured values of intensity and a discussion of the resulting turbulence scale.

5.3.2.2 Fine Wire Screens

Eight wire screens placed in series upstream of the injection ports provided the least turbulent condition. As shown by Dryden, et al. (4), the turbulence intensity is reduced as more screens are added. This flow condition was used to obtain a reference condition with which to compare the concentration results from the more turbulent flow situations. Figure 5.4 shows the velocity profile in the north-south direction through the center of the model as well as the turbulence intensity. The velocity measurements were time averaged values at each point. The measurements of the velocity profile in the east-west direction show little variation in velocity in that direction. As can be seen in Figure 5.3 the turbulence intensity did not exceed seven percent with the fine wire screens.

Some indication of the scale of turbulence can be obtained from studies where screens were used to reduce blower turbulence in wind tunnels. Dryden and Batchelor and Townsend (5, 6) present data for the scale of turbulence as a function of the distance downstream of the screens for different mesh screens. The screen solidities for these studies do not match those of this study but should be close enough for making a rough estimate of the scale. Table 5.1 gives the values of the scale at Plane A-A based on both Dryden's and Batchelor and Townsend's results.

Author	Screens	2" Grid
Dryden (4)	-----	0.4 in.
Batchelor & Townsend (5)	-----	0.896 in.
Batchelor & Townsend (6)	.185 in.	-----

Table 5.1. Turbulence Scale

5.3.2.3 Two-Inch Grid

This configuration consisted of six wire screens in series upstream of the two-inch grid. Here the two-inch grid replaced the top set of screens. This grid was used to obtain a significantly larger scale of turbulence. Figure 5.5 shows the mean velocity profile in the north-south direction, as well as the turbulence intensity, in the same direction at Plane A-A.

The scale can be estimated in the same manner as was done for the wire screens and Table 5.1 also includes these values.

5.3.2.4 Vortex Generators

This technique was employed to somewhat resemble the flow conditions in the boiler although the flow direction at the Shawnee burners is at right angles to its direction at Plane A-A whereas the main duct flow is in line with vortex generators in the model. However, the basic reason for using this technique was to produce a swirling motion approximately scaled to the size representative of the swirls in the Shawnee boiler at the secondary air exit. It should be noted that the swirls produced are of an entirely different nature than the near isotropic turbulence produced by the grids. In fact, characterizing the swirls as turbulence could be misleading. Nevertheless, it is expected that the phenomenon of mixing produced by them is somewhat analogous to that produced in a turbulent field.

There is also some question as to whether or not the swirling motion remains intact after combustion takes place. Although a more thorough investigation into this question is required, indications in the literature are that the swirls do remain intact and that cold gas studies of this motion are a reasonably close approximation to the actual combustion conditions. As a result, it is felt that this turbulence promoting technique, of the four techniques used in this study, most closely resembles the actual fluid motion at Shawnee.

Figure 5.6 shows the mean velocity profile in the north-south direction with this configuration and the turbulence intensity in the same direction. As can be seen, the intensity values are greater than either of the two grid generating devices. The burners which produce the swirl in the Shawnee system are approximately 30 inches in diameter. In the scaled down version, this would correspond in a diameter slightly less than three inches. The vortex generators used in this study produce vortices in the neighborhood of two to four inches which is based on the size of the tubes and vanes. Although no measurements of the achieved size of the swirls were made, it is felt that the size of the model vortices are scaled reasonably close to those values determined from the scaling equations.

5.3.2.5 Open Box - No Barriers

A final set of experiments was conducted without any generating devices present. It was felt that intensity produced by the fan should be greater in this case and that effect on distribution would provide additional knowledge. However, no indications of the turbulence scale are readily available with this arrangement. As a result, it remains an unknown since a good estimate could not be made.

Figure 5.7 shows the north-south mean velocity profile and the north-south intensity profile. Here, the intensity level was found to be approximately fifty percent greater than that of the vortex generators.

5.3.3 Measurements of Concentration Profile at Plane A-A

5.3.3.1 Introduction

Concentration profile measurements at Plane A-A were made for all three injection levels with the screens and with the two-inch grid. However, only injection level two was used for the other turbulence generating arrangements. Nevertheless, it is believed that the results do show the comparative effects of a varying turbulence level on the dispersion of the solid phase. The data were analyzed from several viewpoints. First, the effect of the distance from the injection plane to Plane A-A on the degree of dispersion is covered. Then, the change in the dispersion from a fixed injection plane for different turbulence levels is considered. Graphs for each injection level and turbulence condition are provided in Appendix D in place of data tables.

In comparing the concentration data for each level, it should be noted that levels 1 and 2, labeled L-1 and L-2, each have three nozzles and are located on the same side of the boiler whereas L-3 is on the opposite side and has only two nozzles. Thus, a comparison between L-1 and L-2 is more likely to isolate the effect of distance from the injection point to the sampling plane. Nevertheless, all three levels must be considered in the evaluation of the effect of injection location since each has been tested in the Shawnee limestone distribution study.

5.3.3.2 Concentration Profile and Isodensity Plot

5.3.3.2.1 Introduction

The data at Plane A-A will be presented in two different manners, each of which has certain advantages. One method uses the same form as is presented with the raw data and is in the same form as the data TVA has provided from the Shawnee experiments. Here, profiles are either shown in the east-west direction (transverse) for a fixed distance from the nose (lateral position) or in the north-south direction (lateral) for a fixed distance from the east or west wall (transverse position). This technique, more qualitative in nature, tends to emphasize the heavier concentrations in the vicinity of the jets (east-west profiles) as well as the concentration distribution in the direction of the jet axes (north-south profiles). In these cases, the data have been taken directly from Appendix D.

A second technique which is more useful for a quantitative assessment of the degree of uniformity of the solid-phase employs isodensity plots of Section A-A. This is an effective representation for showing the influence of nozzle location and turbulence on the dispersion of the jet. For these charts a normalized density is utilized. A perfect distribution would result in a uniform value of 1.0 for the normalized density values in these charts. For example, if a stoichiometric mass of powder were injected into the model, the normalized density plots would indicate the local fraction of a stoichiometric mixture.

5.3.3.2.2 Definitions

The concentration profiles and the isodensity plots are different representations of the same data which in the raw form are in terms of mass collected or injected per unit time. Although some uniformity may have been achieved by placing all of the data in terms of density, it was felt that this would not aid in data interpretation and hence it was not done.

The concentration profiles are in fact plots of the mass of powder collected in 20 seconds at each isokinetic probe location as a function of the collection location. Sample collection points were located in both Planes A-A and Y-Y.

The isodensity graphs can be thought of as constant density contours. The density values are normalized so that these dimensionless density values are a measure of the degree of dispersion. The normalized density ρ_N is defined as

$$\rho_N = \frac{\rho_{p_i}}{\overline{\rho}_p} \tag{5.1}$$

where ρ_{p_i} = local particle density as measured with the probe at location i

$$\rho_{p_i} = \frac{(\dot{m}_p)_{i\ \text{probe}}}{V_{\text{probe}} A_{\text{probe}}} \tag{5.2}$$

and

$\overline{\rho}_p$ = average particle density in Plane A-A as measured by total feed rate through the nozzles

$$\overline{\rho}_p = \frac{(\dot{m}_p)_{\text{feeder}}}{V_{\text{duct}} A_{\text{duct}}} \tag{5.3}$$

Thus, ρ_N is the ratio of the local density to the theoretically uniform density in Plane A-A. Hence, if complete dispersion were to occur, ρ_N would have the value one at every point in Plane A-A. The isodensity graphs indicate the regions that are heavy in particulate ($\rho_N > 1$) and those with less than the mean value ($\rho_N \angle 1$). The values of ρ_N can be determined directly from the measured mass flow rate collected in the probe and that injected through the nozzle. This can be shown by combining equations (1) and (2) with equation (3) which defines ρ_N. Here

$$\rho_N = \frac{\dfrac{(\dot{m}_P)_{i\,PROBE}}{V_{PROBE}\,A_{PROBE}}}{\dfrac{(\dot{m}_P)_{FEEDER}}{V_{DUCT}\,A_{DUCT}}} = \frac{(\dot{m}_P)_{i\,PROBE}\;A_{DUCT}}{(\dot{m}_P)_{FEEDER}\;A_{PROBE}} \qquad (5.4)$$

where $V_{probe\ tip}$ is matched properly to V_{duct}.

5.3.3.2.3 Data Accuracy

It is necessary to establish the accuracy of both the mass collected per unit time with the probe as used in the concentration profiles and the isodensity contours. This was done by comparing the value of the total solid mass flux determined by measuring the mass flow rate from the feeder injected through the nozzles to the mass flux as obtained by estimating the total mass flux from 55 collection points in Plane A-A. Measuring the total mass flow rate injected through the nozzles and dividing it by the cross-sectional area of the duct gives $(\dot{m}_p)$ feeder/A_{duct}. On the other hand, the average mass flow rate per unit area can also be obtained by averaging the mass flow rate per unit area over a number of samples collected with the isokinetic probe. Here this mean value is obtained by

$$\frac{\overline{\dot{m}_P}}{A_{PROBE}} = \frac{1}{M}\sum_{n=1}^{M}\frac{(\dot{m}_P)_{n\,PROBE}}{A_{PROBE}} \qquad (5.5)$$

The value of M, the number of collection points in Plane A-A, was 55. Thus, if the isokinetic sampling was exact then

$$\frac{(\dot{m}_P)_{FEEDER}}{A_{DUCT}} = \frac{\overline{\dot{m}_P}}{A_{PROBE}} \qquad (5.6)$$

Evaluation of the data for the two-inch grid and the screens showed that the difference between the two mass flux values was approximately six percent. Since this difference could either be due to feed rate inaccuracies or collection errors, it will be assumed that the six percent error is the overall error in the values of both the concentration profiles and the isodensity contours. It is also of interest to note that with this identity in equation (5.4) that ρ_N can be written as

$$\rho_N = \frac{(\dot{m}_p)_i}{\bar{\dot{m}}_p} \qquad (5.7)$$

5.3.3.3 Effect on Distance from Injection to Plane A-A

5.3.3.3.1 Concentration Profile

Figure 5.8 shows the concentration profile in the transverse direction at position 4 for each of the three injection levels. These data were all taken with the two-inch grid configuration. From a qualitative viewpoint, it is found that injection from level 2 which is farthest from Plane A-A resulted in the most uniform distribution in the transverse direction. Figure 5.9 compares the profiles in the lateral direction for each of the levels with screens being used in each case. Again the same general trend results. That is, injection level 2 produces the most uniform dispersion of the three levels. One can observe from both figures that an injection at L-3 results in a slightly more uniform pattern than L-1, but as stated earlier, they are on opposite walls and do not have the same number of nozzles. However, both figures do illustrate that L-2 definitely results in a more uniform profile than L-1 where L-2 is approximately 30 percent further from Plane A-A than is L-1.

5.3.3.3.2 Isodensity Contours

A comparison of injection levels 1, 2 and 3 (Figures 5.10, 5.11 and

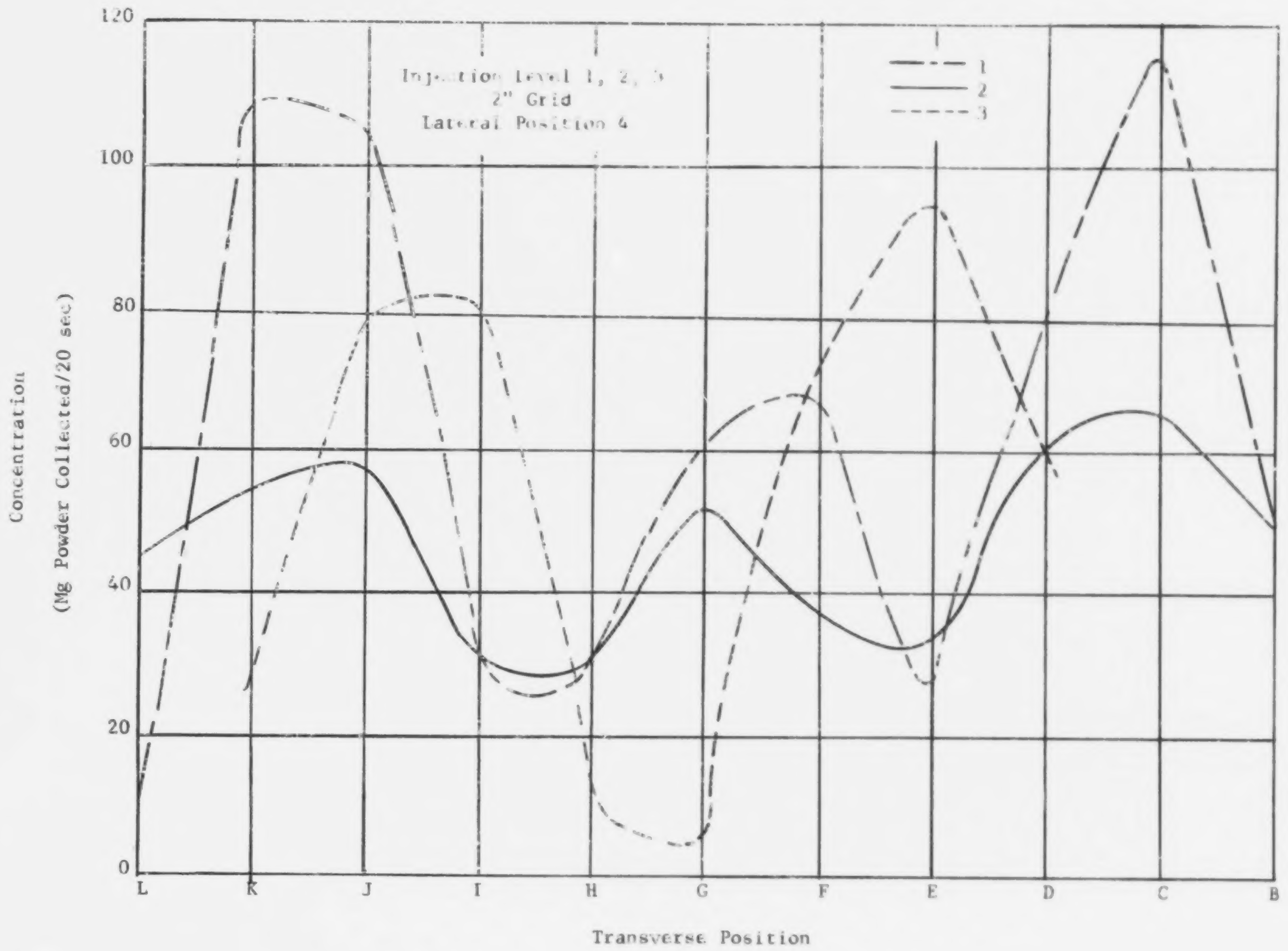

CONCENTRATION PROFILE

Figure 5.8. Shawnee Model Plane A-A - 2" Grid

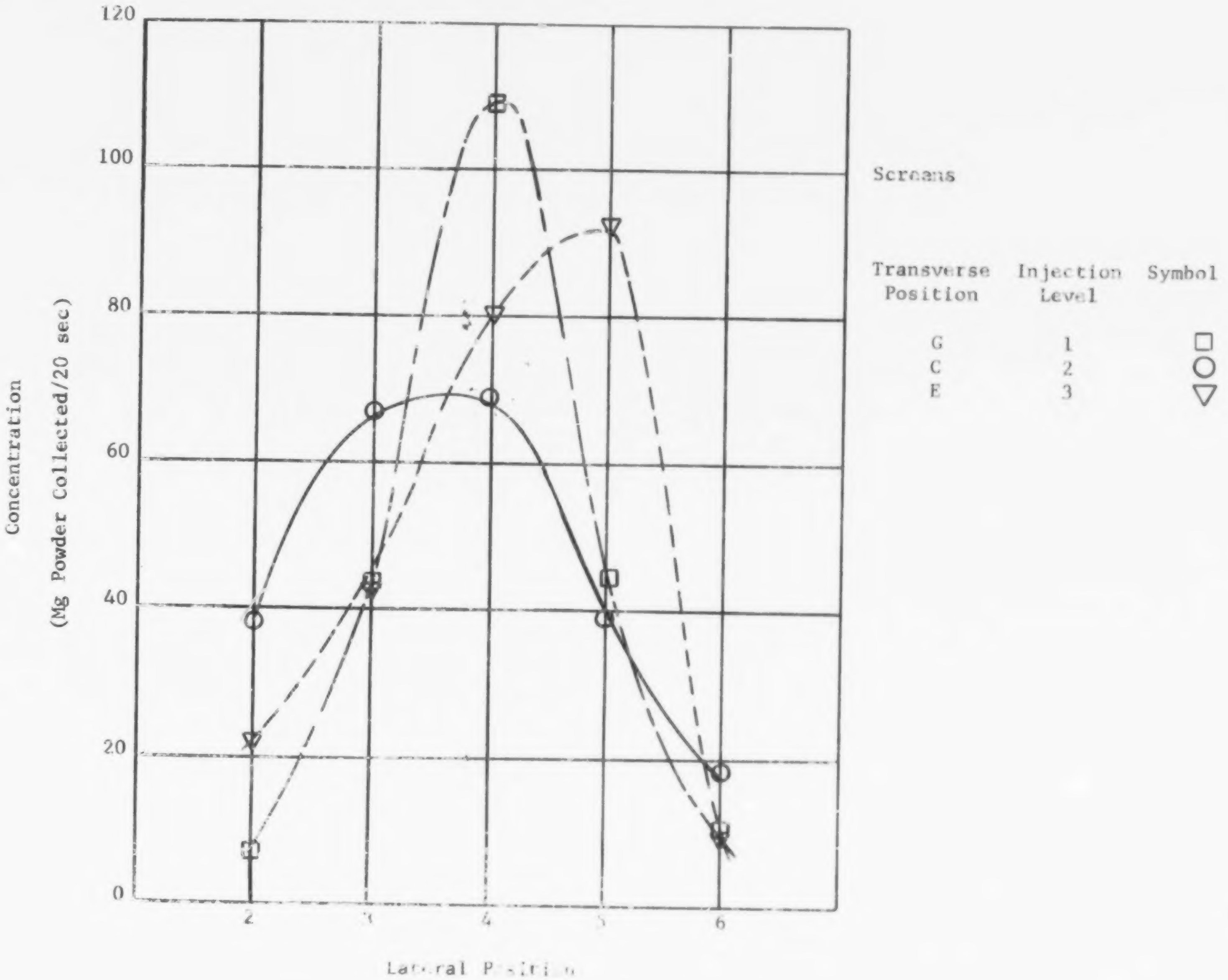

Figure 5.9, Shawnee Model Plane A-A - Screens

Injection Level 1 - 2" Grid

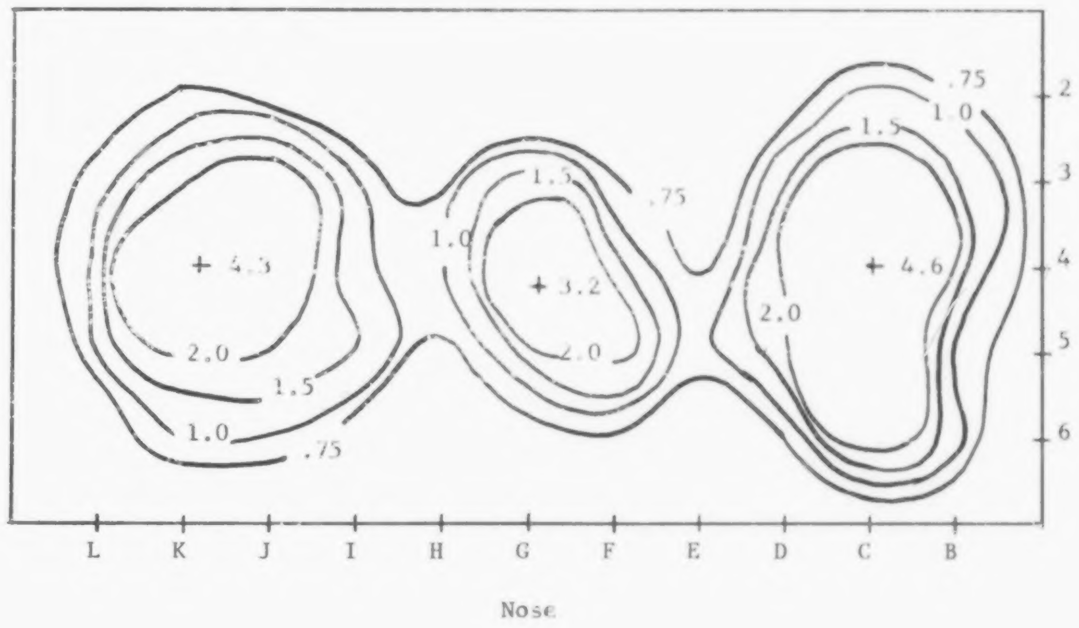

Figure 5.10. Normalized Density Distribution - Shawnee Model Plane A-A

Injection Level 2 - 2" Grid

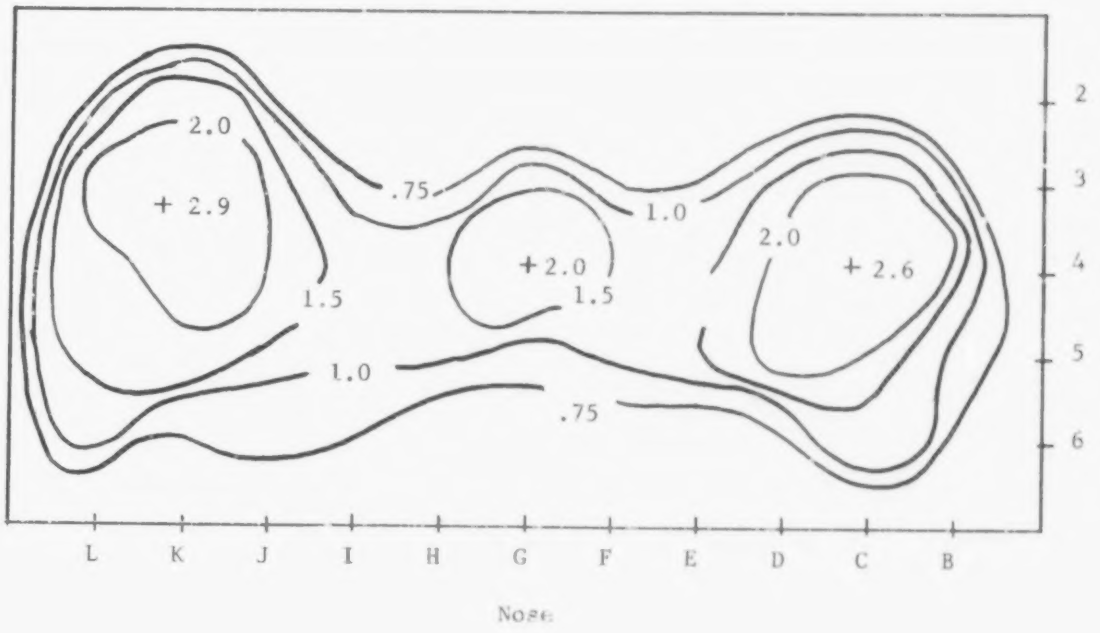

Figure 5.11. Normalized Density Distribution - Shawnee Model Plane A-A

5.12, respectively) for the two-inch grid turbulence generator provides a good indication of the effect of location on dispersion. It was found that with injection level 1 each jet maintains its own identity. The peak values for the normalized density range from 3.2 to 4.6. More than 63 percent of the volumetric flow at A-A has a density of less than 1.0. For 17 percent of the plane, the concentration is greater than 2.0. Simple calculations show that 71 percent of the dust is contained within 37 percent of the fluid passing through Plane A-A. Hence, dispersion is relatively poor in this case.

For injection level 2, there is significant dispersion when compared with that of level 1. Note that the peaks are consistently about 30 percent less. As with injection level 1, more than half, 59 percent, of the two-phase fluid passing Plane A-A has a normalized density of less than 1.0. The major difference between injection levels 1 and 2 is the overall uniformity of solid distribution across the duct. The peak concentrations for level 2 are lower with a correspondingly smaller density gradient across the duct.

Less data were obtained for injection level 3, but it can be seen that this case represents the poorest dispersion of the three. Nearly 80 percent of the solid phase is contained within 30 percent of the fluid. For this injection level, the peaks are well defined and concentration drop-off is quite rapid at the boundary.

5.3.3.3.3 Summary

The differences between the dispersion of the plumes injected at level 1 and 2 can be explained by the increased path length to Plane A-A. The centerline path for injection level 1 is about 25 in., that for 2 is

Injection Level 3 - 2" Grid

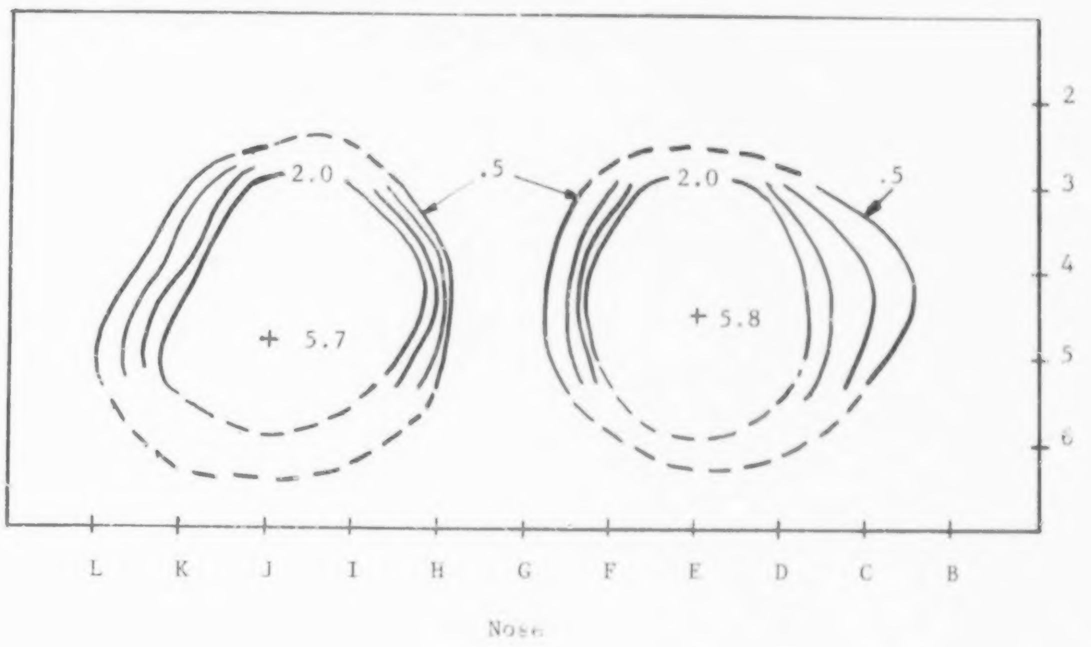

Figure 5.12. Normalized Density Distribution – Shawnee Model Plane A-A

37 in. Hence, significantly greater dispersion could be expected for level 2 as has been the case.

The explanation for the difference in dispersion when comparing levels 2 and 3 is less certain. The path length for injection at level 3 is nearly the same as that for injection level 1, hence, the dispersion is not due to path length alone. One possible explanation is that the difference is a result of the nose impinging on the flow. This would cause a velocity gradient and acceleration of the flow which may induce greater dispersion.

5.3.3.4 Effect of Turbulence on Dispersion at Plane A-A

5.3.3.4.1 Introduction

This discussion will consider the trend of dispersion with increased turbulence intensity. The details of the four levels of turbulence considered here are discussed in Section 5.3.2. The effect of turbulence on dispersion can only be fully discussed with respect to injection level 2 where all four turbulence levels were used. The previous section covered the effect of injection level on dispersion and it is felt that the general trend of improved dispersion with distance from the sampling plane will hold for all turbulence levels in this study. Thus, it is expected that the degree of dispersion at level 2 should be greater than that at levels 1 and 3 for all four turbulence levels. Again, the discussion will be broken into two parts, one with the profiles and the other with the isodensity contours.

5.3.3.4.2 Concentration Profiles

Figure 5.13 illustrates the effect of turbulence on the concentration profile in the transverse direction for injection level 2 at lateral

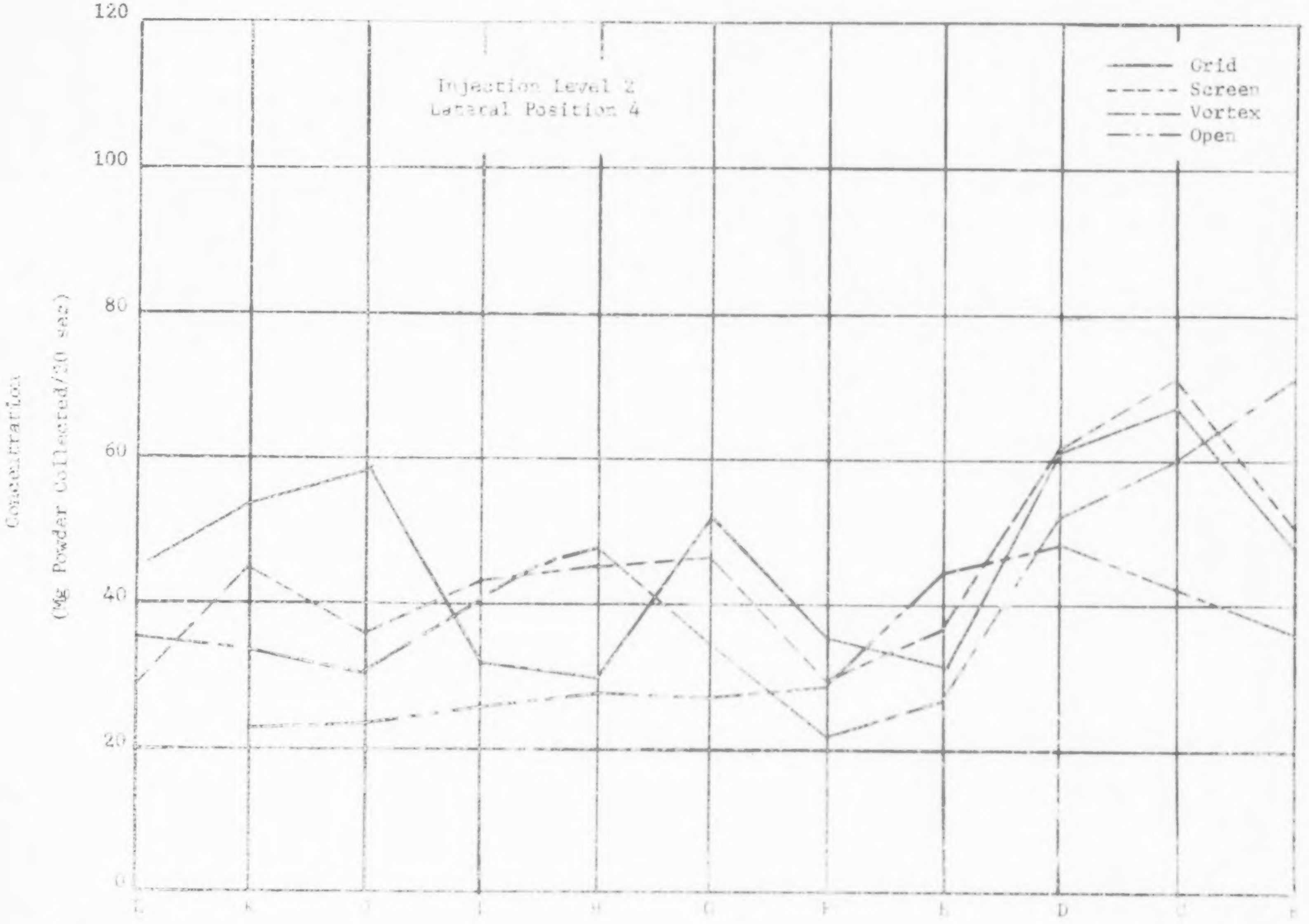

CONCENTRATION PROFILE

Figure [illegible]. Shawnee Model Plane A-A positions 3 and 4. As can be seen, the profiles corresponding to the screens, two-inch grid, and vortex generators are not significantly different. However, the open box profile is flatter than the other three. This trend was observed at all of the lateral positions. The turbulence intensity for the open box is greater than that for the other three turbulence conditions and the results are consistent with the expectation that increased turbulence intensity does promote dispersion. Figures 5.14 and 5.15 indicate that the same trend occurs in the lateral direction. In particular the profiles for the open box appear to be flatter than the others. However, variations among the other three profiles are not as apparent and this is reflected in the more quantitative evaluation below.

5.3.3.4.3 Isodensity Contours

The contour maps for the vortex generators and the open box system are represented by Figures 5.16 and 5.17. Figure 5.11 corresponds to the two-inch grid data. Again all three figures are based on data obtained for injection level 2. Table 5.2 presents this data in a tabulated form for all of the conditions represented with normalized density distribution charts. The cross section of the duct is divided into two parts. The percentage of cross-sectional area which has a solid density greater than the mean density and that which has a density less than the mean. In terms of the normalized density contours this represents the percent area with the normalized distribution greater than unity (column 1) and less than unity (column 4), respectively. These are noted as % G.T. 1.0 and % L.T. 1.0, respectively in Table 5.2. The column immediately following these columns indicates the percent of the entire injected solid

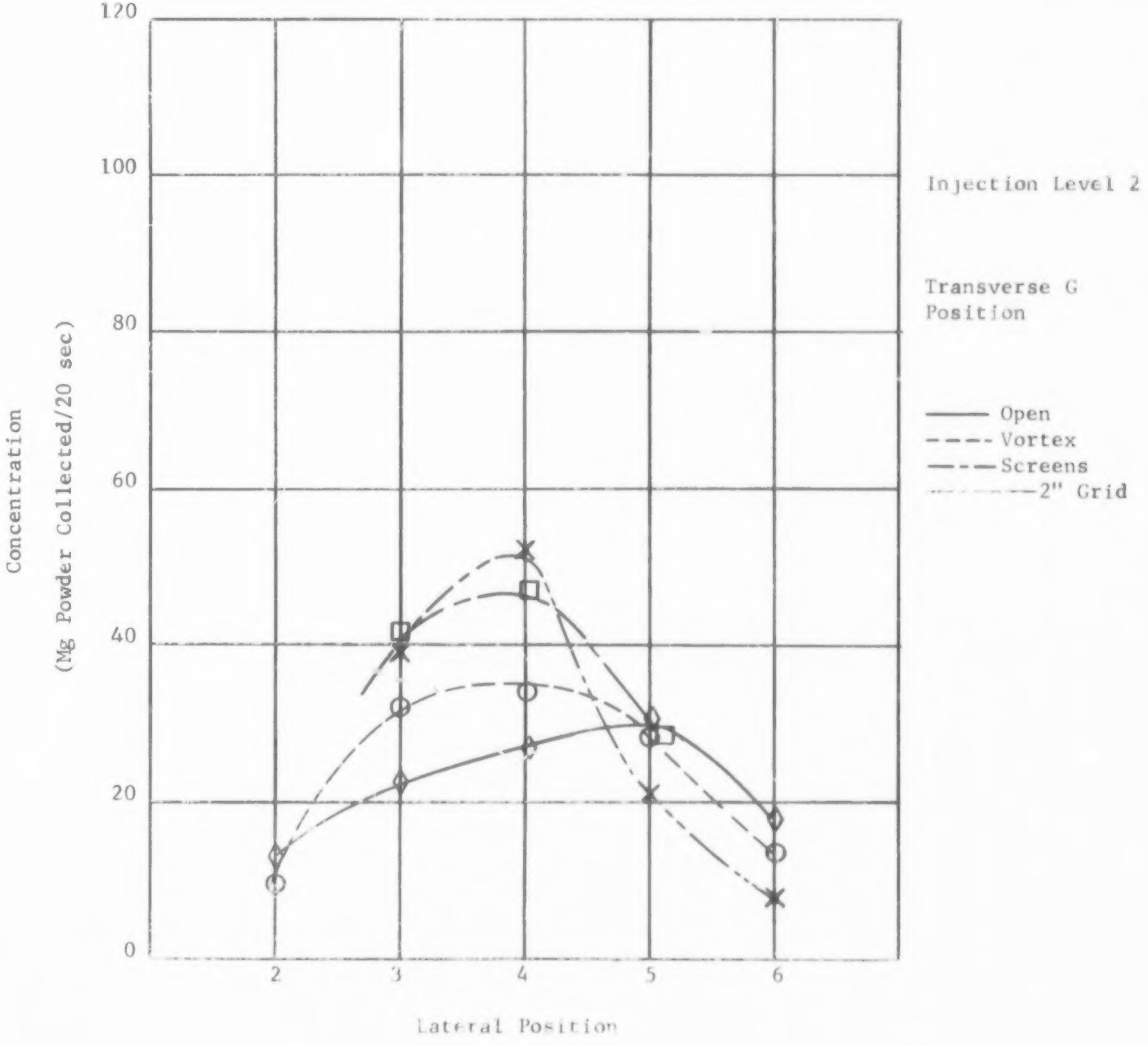

Figure 5.14 Shawnee Model Plane A-A

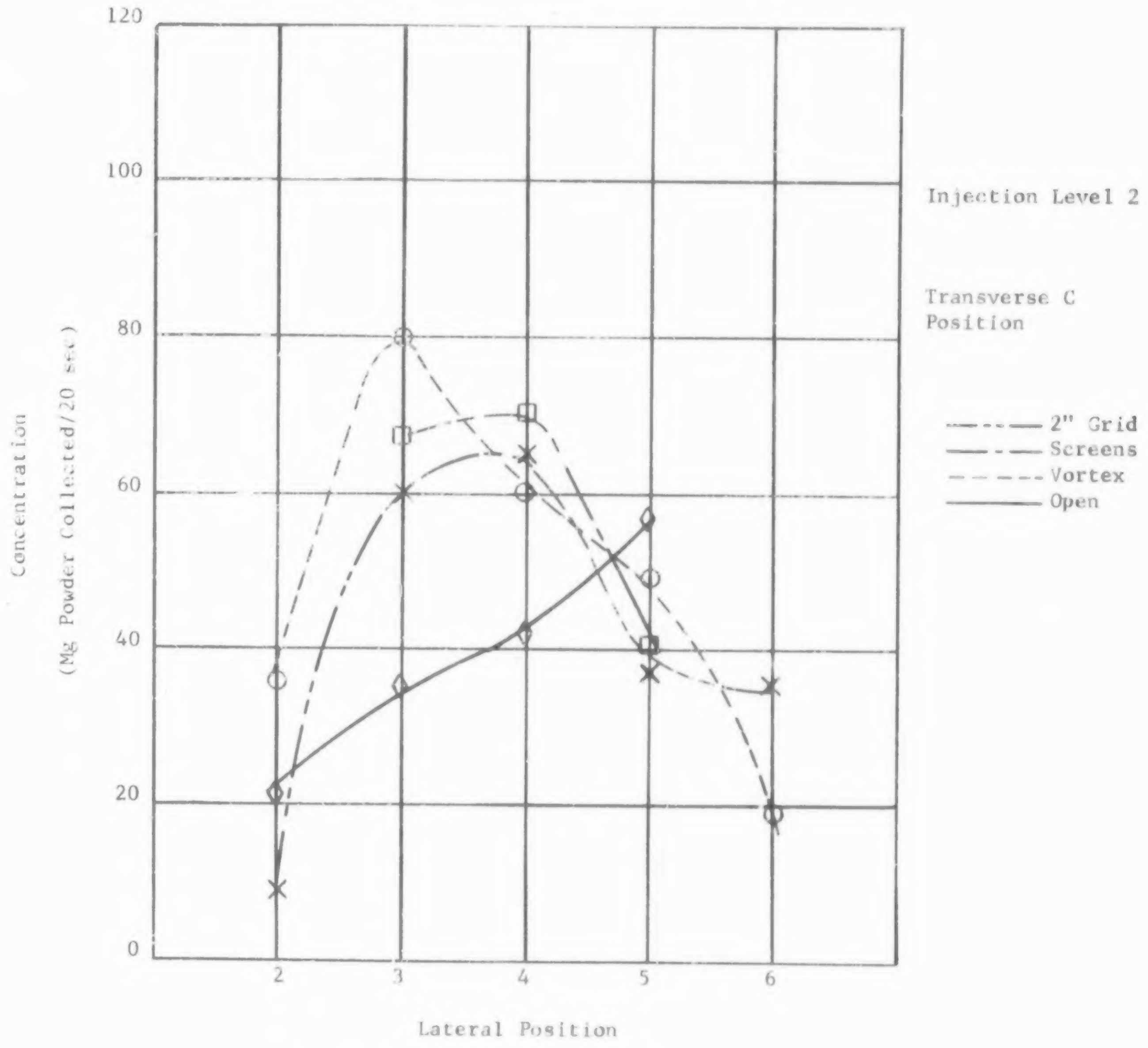

Figure 5.15. Shawnee Model Plane A-A

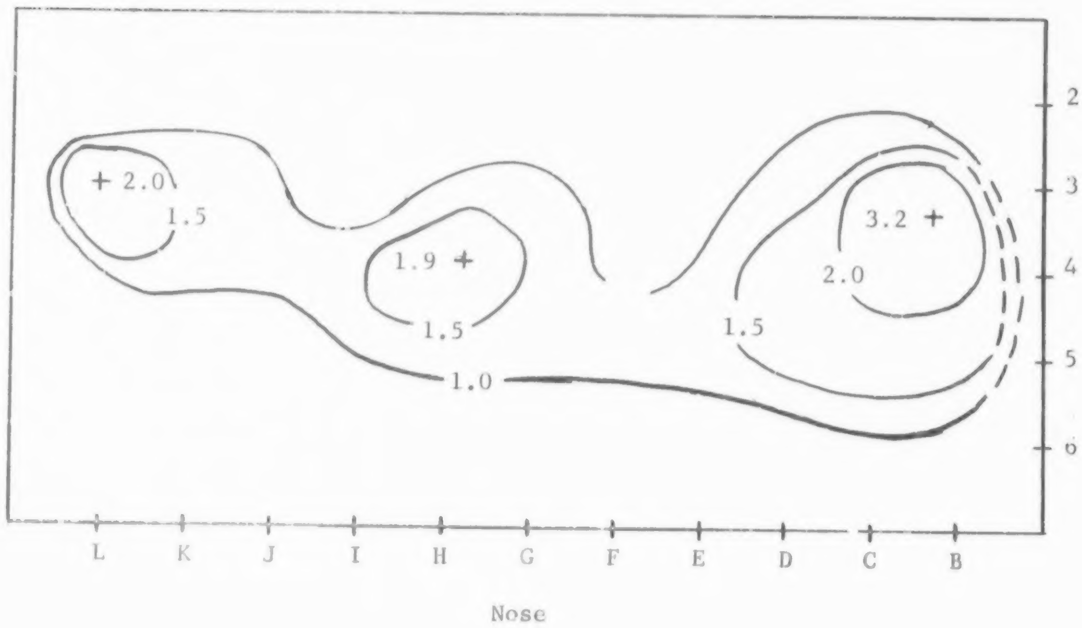

Injection Level 2 - Vortex Generator

Figure 5.16. Normalized Density Distribution - Shawnee Model Plane A-A

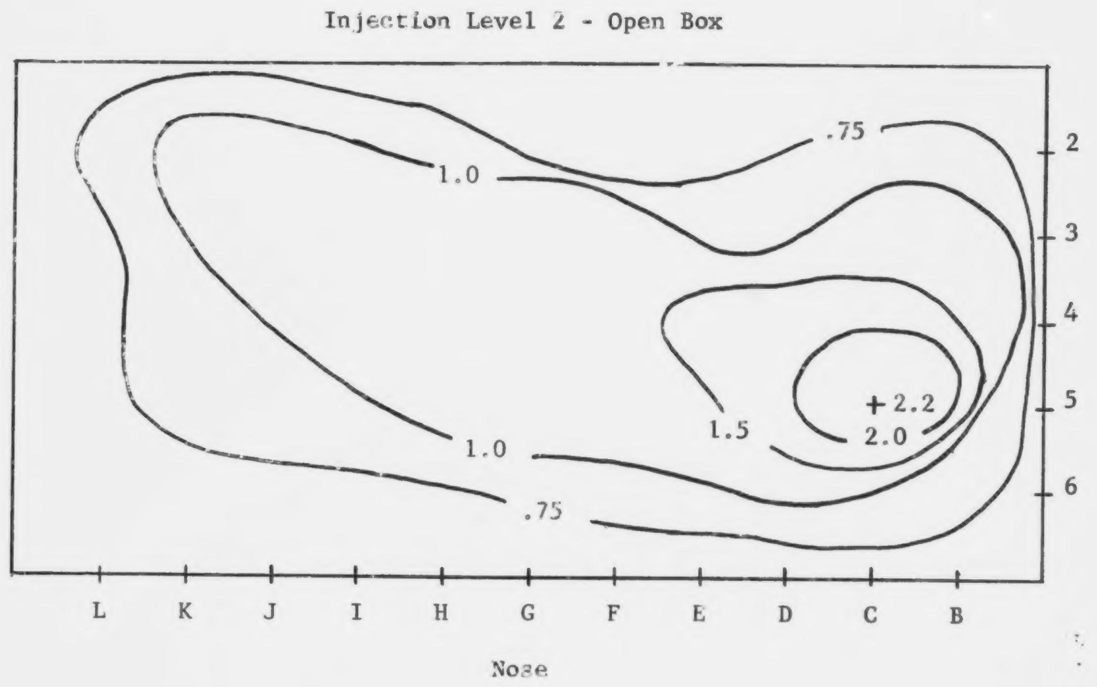

Injection Level 2 - Open Box

Figure 5.17. Normalized Density Distribution - Shawnee Model Plane A-A

	% G.T. 1.0 (A)	% of Solid Within A	Average Density in Area Included by A	% L.T. 1.0 (B)	% of Solid Within B	Average Density in Area Included by B	Overall Percent Coverage
Level 1 2" Grid	37	71	1.92	63	29	.46	66
Level 2 2" Grid	41	56	1.36	59	44	.747	85
Level 3 2" Grid	27.6	78.5	2.84	72.4	21.5	.297	49.1
Level 2 Vortex	34	46.5	1.36	66	53.5	.811	87.5
Level 2 Open	38	46	1.21	62	54	.871	92

Table 5.2. Overall Density Distribution at Plane A-A

mass crossing these respective areas. The sum of these columns (2 and 5) will always be 100 percent. Columns 3 and 6 represent the normalized average density in these two portions of cross section A-A.

The last column of Table 5.2 represents a method of assigning a quantitative value to the density distribution for the various conditions. The rationalization behind this determination is as follows. Assume that a stoichiometric mass of powder is injected into the duct. The regions where the normalized density is greater than one results in a complete reaction eliminating all the SO_2. In the region where the normalized density distribution is less than one there is complete reaction, but of course since there is a deficiency of the solid in this area some of the SO_2 does not react. For example, the open box case has 38 percent of the area with an excess of 100 percent of stoichiometric mixture and the remaining 62 percent has an 87.1 percent average coverage. Thus, the overall percent coverage is calculated as

$$\text{overall percent coverage} = 38 + 87.1\ (.62) = 85 \text{ percent.}$$

Note that this indicates that range of coverage when comparing the two-inch grid to the open box at level 2 is 85 to 92 percent or a 7.6 percent increase when going from the two-inch grid to the open box. However, when comparing level 1 with level 2 for the two-inch grid there is an increase from 66 percent to 85 percent which corresponds to an increase of 22.3 percent. Thus, it appears that within the limits of this particular study that the influence of injection level upon dispersion was greater than the level of turbulence.

This type of calculation appears to be a reasonable one for assigning a quality number to the dispersion characteristics for the various injection levels and turbulence conditions. Nevertheless, it should be emphasized that these figures do not represent the expected percent removal of SO_2 but only the upper limit of what could be removed if no other limiting factors to complete reaction were present.

5.3.3.5 Effect of Dynamic Pressure Ratio

A limited number of tests were run in the Shawnee model to correlate the trajectory dependence upon the dynamic pressure ratio. This was necessary for a number of reasons. The primary reason was that the data obtained from the twelve-inch duct did not establish the dependence of trajectory upon the dynamic pressure ratio with complete assurance. Secondly, the twelve-inch duct trajectory data were obtained by visual inspection of the plume rather than by more exact measurements of the concentration profile. A third reason for this series of runs was that the Shawnee model has a much more complex flow pattern than the straight duct. The projection of the nose in the boiler might be expected to exaggerate the trajectory phenomena and perhaps emphasize some secondary effect not previously noticed. The center nozzle at level 2 was used for these experiments.

Normalized concentration profiles for three different dynamic pressure ratios are shown on Figure 5.18. It is immediately obvious that the penetration does increase with increasing dynamic pressure ratio. Another aspect which can be identified from these limited tests is that dispersion appears to increase with an increase of dynamic pressure ratio. This points to the possibility that dispersion may be dependent upon either the dynamic pressure ratio or the path length of the plume centerline.

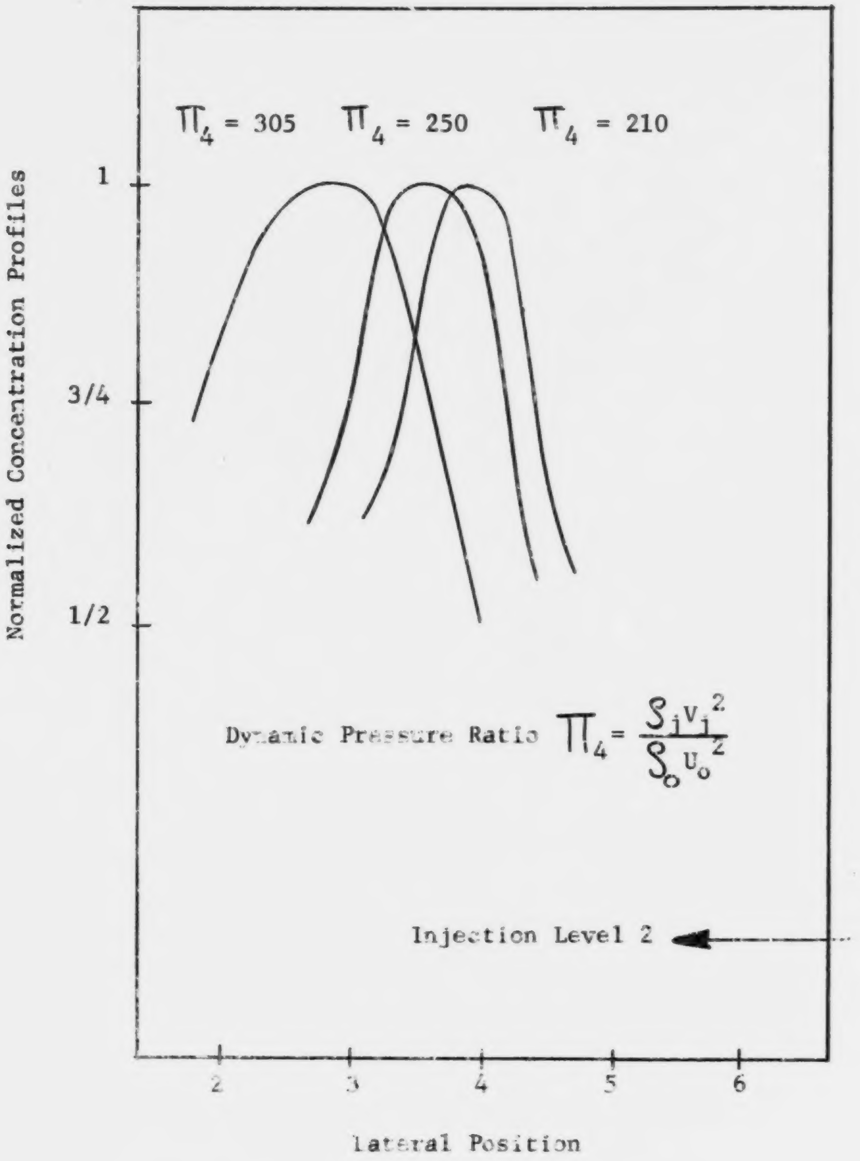

Figure 5.18. Penetration Profiles - Shawnee Model Plane A-A

Interesting results are obtained by assuming that the trajectory equation can be written in the form

$$\frac{y'}{d} = K_1 \left[\frac{\rho_j V_j^2}{\rho_o U_o^2}\right]^{K_2} \left(\frac{x'}{d}\right)^{K_3} \tag{5.8}$$

This form corresponds to the experimentally determined trajectory correlations for a homogeneous jet as shown in the last four equations of Table 2.1. For the three penetration profiles obtained in these model boiler texts x'/d is a constant, so that the penetration equation can be written

$$\frac{y'}{d} = K^* \left[\frac{\rho_j V_j^2}{\rho_o U_o^2}\right]^{K_2} \tag{5.9}$$

Comparing the three trajectories by considering the point of highest concentration to be the jet centerline it is possible to determine K^*, k_2 and check these values. It was found that the data best correlated to

$K^* = 18.6$

and $k_2 = 0.371$.

The dependence of penetration upon the dynamic pressure ratio compares very favorably with the equations of Table 2.1 where the value of k_2 varies between 0.392 and 0.45. This is also consistent with the 12-inch duct results which indicate that the solid-gas jet trajectory may be represented by a homogeneous jet injected into a transverse stream of a different density.

5.3.4 Concentration Profiles at Plane Y-Y

Because of the location of the sampling port on the model, Plane Y-Y was sampled instead of the plane equivalent to B-B. Since both are close together, no significant differences in concentration results would be expected. The basic purpose for this portion of the investigation was to probe for any significant or unexpected results. Figure 5.19 is a plot of the concentration profile along a vertical axis through the center of the duct at Plane Y-Y. The data for screens and the vortex generators indicate an appreciable reduction in solid loading away from the top surface of the model. Figure 5.20 shows the data acquisition points in Plane Y-Y. It should be noted from Figure 5.21 that for nearly eight inches below the top, the velocity profile is nearly flat. This means that mass flow rate of air is nearly uniform over this portion while the particle loading is reduced by a factor of four.

Further, since nearly 80 percent of the total mass flow rate of air passes through the top eight inches of Plane Y-Y, this indicates a somewhat less than uniform dispersion at Plane Y-Y. In addition some data were taken in the transverse direction both two inches and six inches below the top surface. These results are shown in Figures 5.22 and 5.23. Here, only one side of the centerline was probed but indications are that the distribution is of the same order of uniformity in this direction as in Plane A-A.

In summary, the concentration profile measurements in Plane Y-Y show a relatively uniform distribution in the transverse direction but an uneven one in the vertical direction. This distribution would probably yield an overall percent coverage in the range of 50 to 75 percent (although this has not been calculated and demonstrated to be the actual case). It appears that the heavier dust loading near the top is due to the 90 degree turn that fluid makes before entering the superheater section of the model boiler.

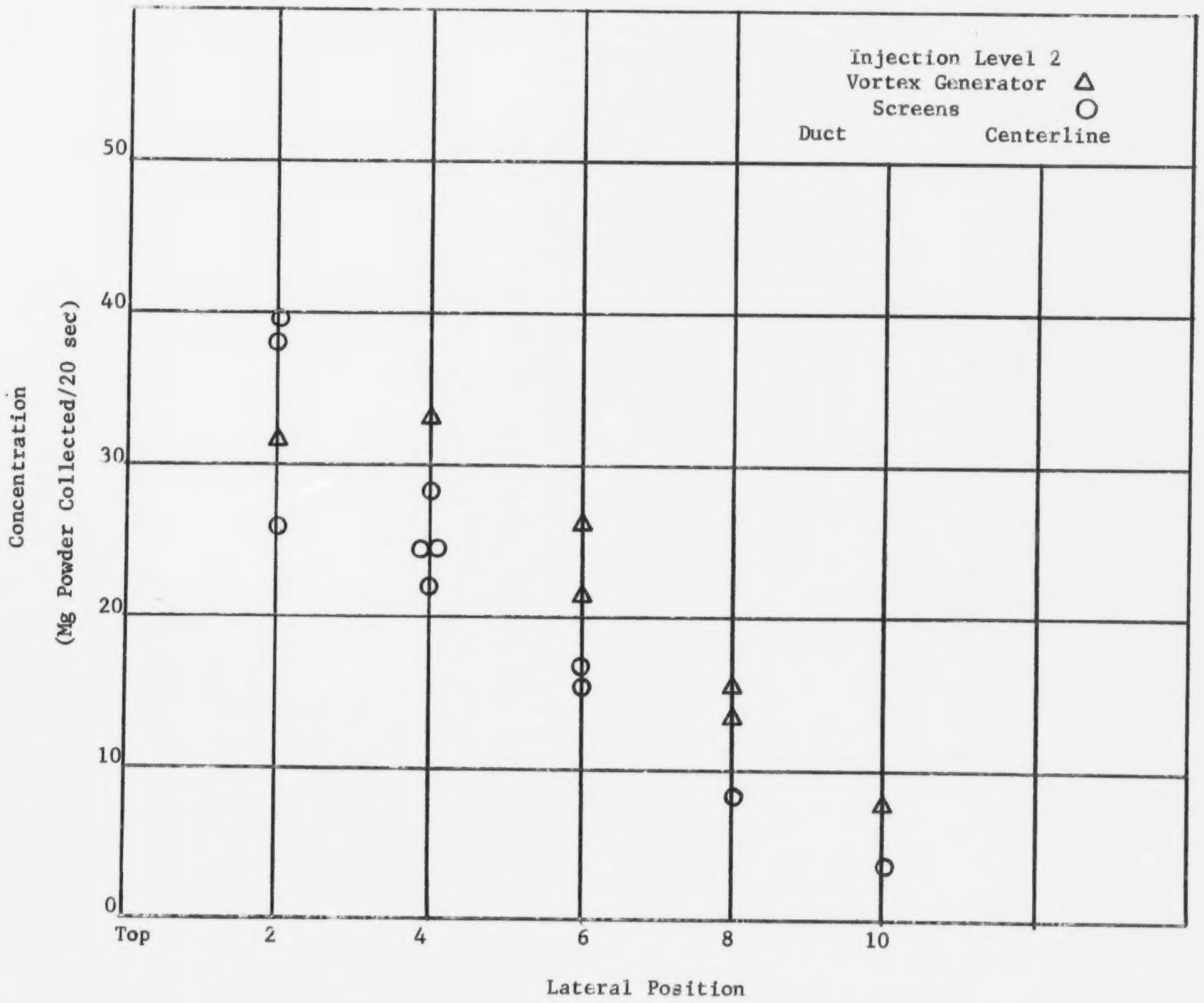

Figure 5.19. Shawnee Model Position Y-Y Concentration Profiles

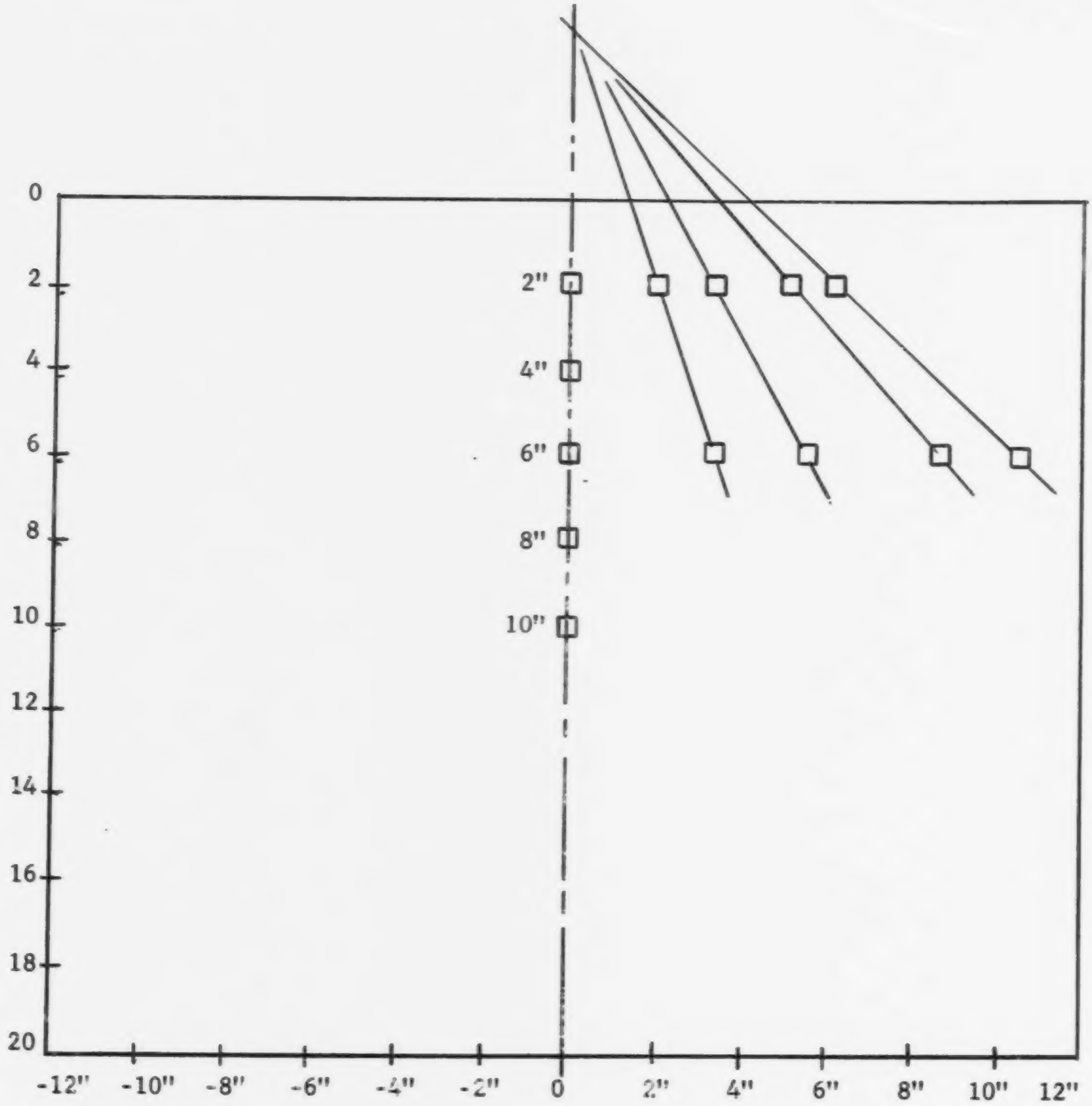
0
2
4
6
8
10
12
14
16
18
20
2"
4"
6"
8"
10"
-12"
-10"
-8"
-6"
-4"
-2"
0
2"
4"
6"
8"
10"
12"
Data Acquisition Points

Figure 5.20. Shawnee Model Plane Y-Y
Data Acquisition Points

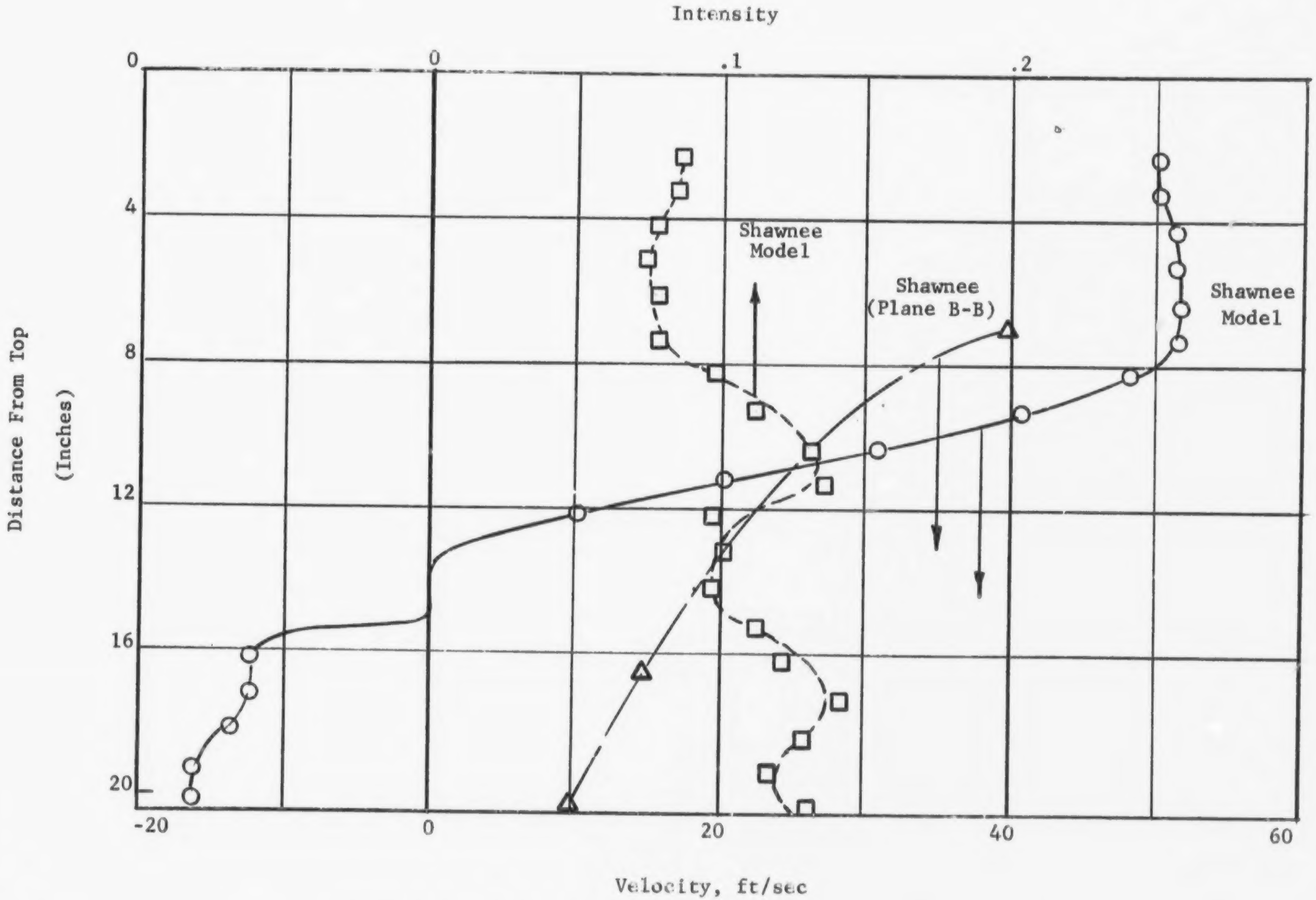

Figure 5.21. Velocity Profile and Intensity at Plane Y-Y of Model, Velocity Profile at Plane B-B Shawnee Boiler

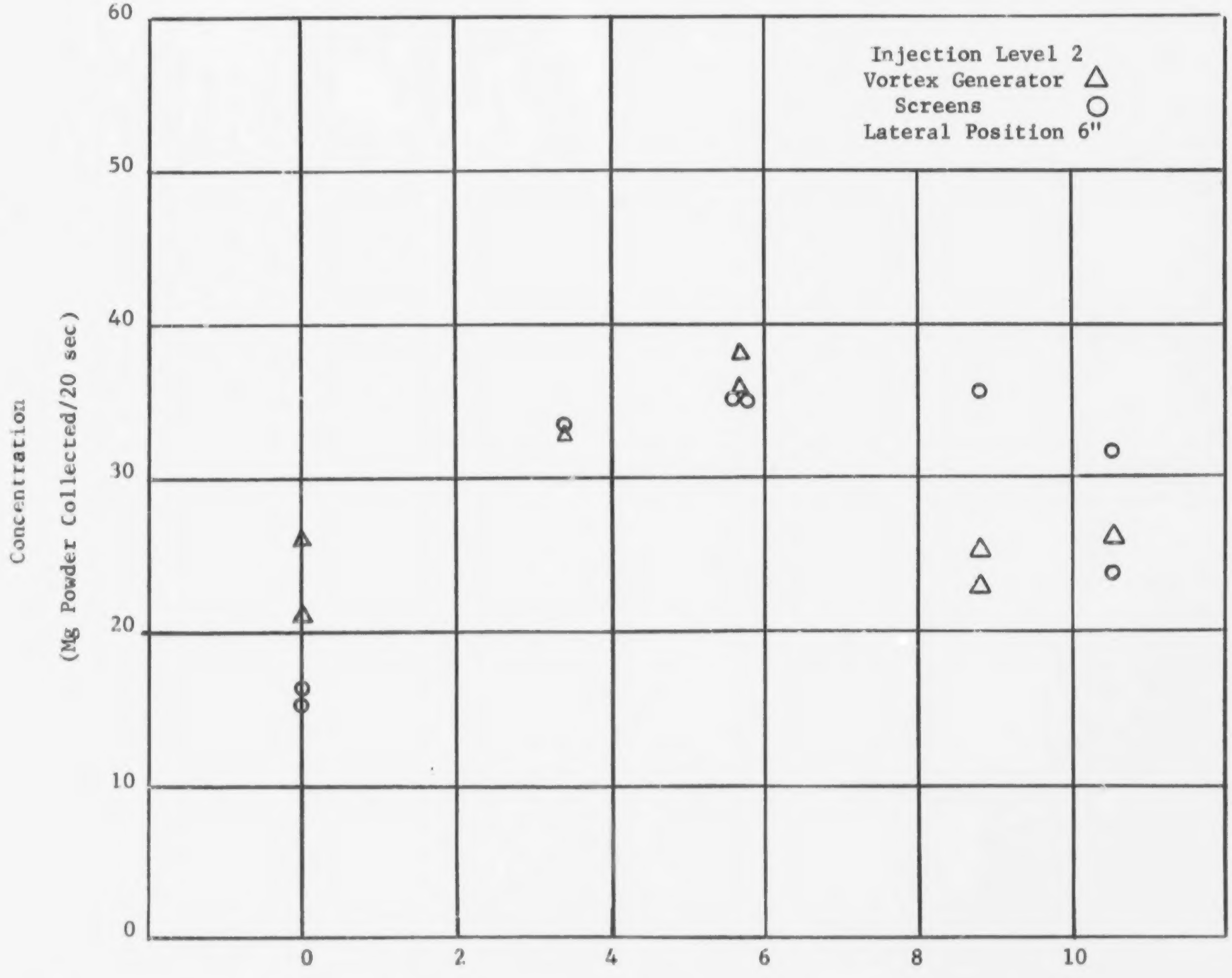

Figure 5.22. Shawnee Model Plane Y-Y

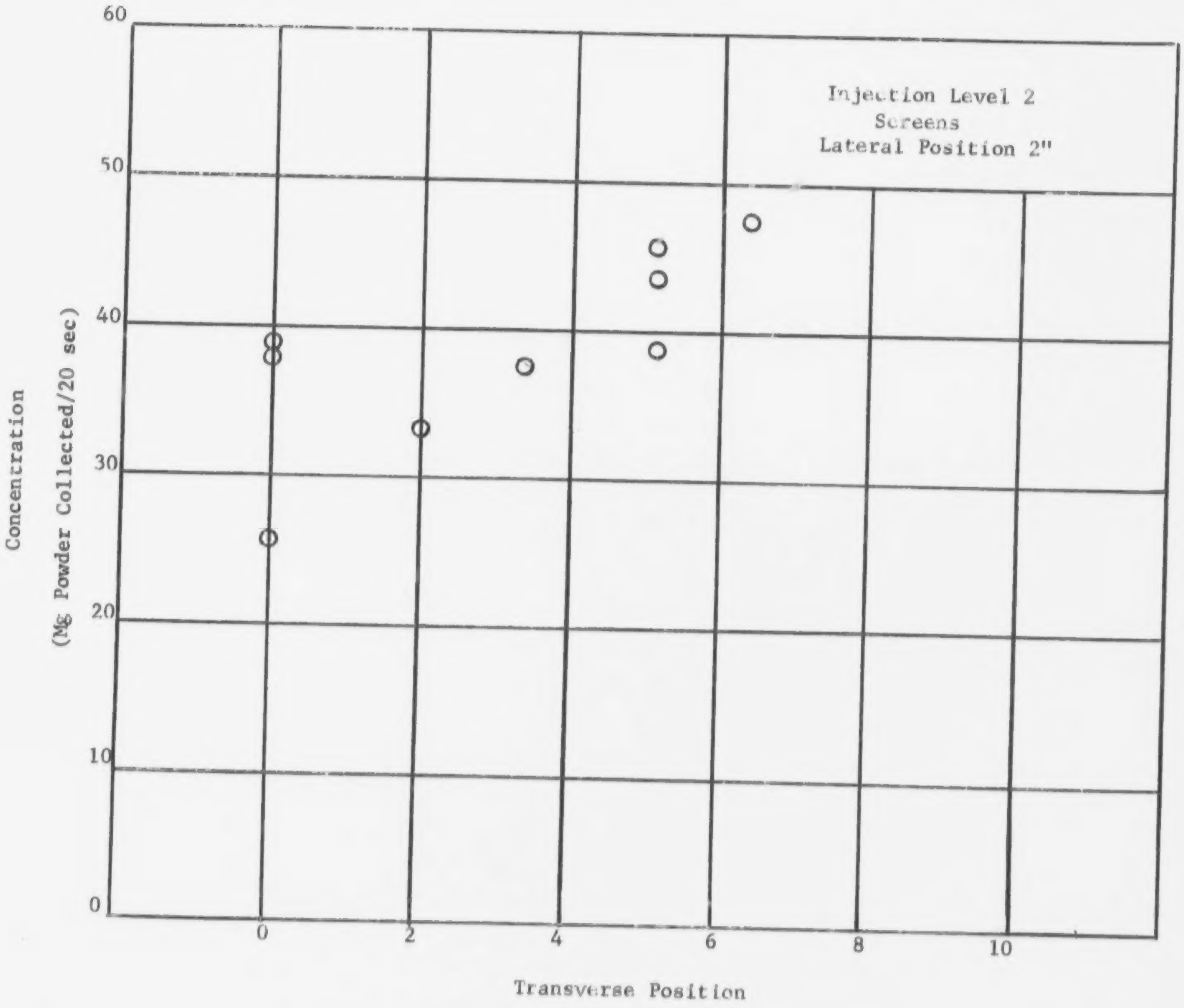

Figure 5.23. Shawnee Model Plane Y-Y

5.4 Comparison with Shawnee Results

This study presents one of those unusual situations where the results of the model experiments are preceded by those for the full scale operation. As it turns out, the model results have proven to be consistent with those from the Shawnee boiler. Here both the magnitude of the degree of dispersion and the trend in these values with injection location for the model compare favorably with those from the full scale system. However, it is necessary to reemphasize that for several reasons exact modeling was not carried out in this study. Thus, some discussion of the effects of the deviations from exact modeling on the comparative results will also follow.

5.4.1 Data from Shawnee Boiler

The O.A.P. has provided dust distribution data from the limestone dispersion studies in the Shawnee boiler. These data were collected during the period from December 1970 through January 1971. The data included east and west side results as well as all three injection locations. Table 5.3 lists the test numbers and dates of those data which were used for comparison with the model data.

5.4.2 Basis for Comparison of Data

Table 5.4 provides an example of the type of data that was given by the O.A.P. As can be seen from this table the velocity profile is not uniform whereas the model velocity profile was nearly uniform (see Figure 5.5). Hence, even though the parts per million values for the SO_2 were listed as uniform for all 24 locations, the mass flow rate at each of these locations varied from point to point. As a result the theoretical values of the mass flow rate of CaO needed for stoichiometry for each location varied proportionately to the SO_2 mass flow rates. In the model study the required CaO

Table 5.3. Data from Shawnee Boiler

Test	Side	Injection Location	Date
S601	E&W	Upper Rear	12/8/70
S603	E	" "	12/10/70
S604	W	" "	"
S602	E&W	" "	"
S604	E&W	" "	
S901	E&W	" "	1/5/71
S902	E&W	" "	"
S601	E&W	Lower Rear	12/3/70
S603	E&W	" "	"
S601	E&W	" "	12/4/70
S607	E&W	" "	"
S901	E&W	" "	"
S902	E	" "	"
S903	W	" "	"
S602	E&W	Front	12/11/70
S601	E&W	"	12/16/70
S604	E&W	"	"

Table 5.4. Example of the Shawnee Data Supplied by the O.A.P.

Tennessee Valley Authority - Division of Power Production
Sulfur Oxide Removal from Power Plant Stack Gas
Full-Scale Limestone Injection Tests at Shawnee Unit 10

Test No. S601   Date: December 16, 1970

(The following is a partial representation of a given test data sheet)

Test Conditions

Unit Load, MW			143	
Boiler Load, MLBS/HR			1000	
Coal Rate, LBS/HR			121600.	
Limestone Rate, LBS/LBCOAL			0.157	
Injection Velocity, FT/SEC			193	
Injection Angle, Degrees			0	
Injection Elevation			FRONT	
Limestone Type, BCR NO.			2061	
Particle Size, Microns			4.7	
Stoichiometry			1.88	
Coal Type, Contract No.			81T10	
Excess Air, Percent -	WEST	19.0	EAST	18.0

Limestone Distribution Index

Sampling Location	SO_2 PPM	CAO GR LDG GRNS/CUFT	VELOCITY FT/SEC	SO_2 CUFT/SEC	CAO GRNS/SEC ($\dot{m}_{p_i}$)	THEORET CAO GRNS/SEC ($\dot{m}_{s_i}$)
1	2120.	0.07	59.9	0.0245	1.	23.
2	2120.	0.15	68.7	0.0277	2.	26.
3	2120.	0.46	64.5	0.0268	6.	26.
4	2120.	0.99	57.7	0.0240	11.	23.
5	2120.	0.29	38.2	0.0181	2.	17.
6	2120.	0.41	74.1	0.0339	7.	32.
7	2120.	0.24	63.6	0.0313	4.	30.
8	2120.	0.42	72.7	0.0274	5.	26.
9	2120.	2.95	77.9	0.0289	40.	28.
10	2120.	7.31	67.0	0.0245	85.	23.
11	2120.	8.14	69.2	0.0250	96.	24.
12	2120.	2.61	74.8	0.0289	36.	28.
13	2120.	3.45	41.4	0.0167	27.	16.
14	2120.	2.55	47.0	0.0184	22.	18.
15	2120.	3.28	44.9	0.0173	27.	17.
16	2120.	3.09	45.2	0.0172	25.	16.
17	2120.	4.02	52.5	0.0198	38.	19.
18	2120.	2.72	54.3	0.0207	27.	20.
19	2120.	0.72	37.6	0.0161	6.	15.
20	2120.	0.91	35.1	0.0148	6.	14.
21	2120.	0.85	28.9	0.0120	5.	11.
22	2120.	2.15	32.5	0.0133	13.	13.
23	2120.	0.29	40.8	0.0170	2.	16.
24	2120.	0.18	27.0	0.0128	1.	12.

mass flow rate was assumed to be uniform across Plane A-A since the velocity profile was nearly uniform.

The calculations of the percent coverage of powder was based on the assumption that the total mass flow rate of CaO was equal to the amount required for complete removal of SO_2 with uniform coverage. The total mass flow rate of particulate is labeled as $\dot{M}_T$. The actual mass flow rate of particulate at any location (i) is termed $\dot{m}_{p_i}$ (see Equation 5.7) and $\dot{m}_{s_i}$ is the theoretical mass flow rate at location (i) for a stoichiometric mixture. In order to determine the percent coverage it is assumed that all of the CaO passing through location (i) will satisfy the local stoichiometry condition with the SO_2 whenever $\dot{m}_{s_i} > \dot{m}_{p_i}$. On the other hand, whenever $\dot{m}_{p_i} > \dot{m}_{s_i}$ it is assumed that the excess $(\dot{m}_{p_i} - \dot{m}_{s_i})$ leaves the boiler without reacting and that only the difference, $\dot{m}_{s_i}$, will be available for combination with the SO_2. Thus, the total fraction of CaO that satisfies the condition for stoichiometry is

$$\text{Friction} = \frac{\sum_i \dot{m}_{p_i}\Big|_{(\dot{m}_{s_i} > \dot{m}_{p_i})} + \sum_i \dot{m}_{s_i}\Big|_{(\dot{m}_{p_i} > \dot{m}_{s_i})}}{\dot{M}_T} \qquad (5.10)$$

The formula was used to determine the degree of coverage for both the model and Shawnee boiler data. The model calculations were somewhat simplified since it was assumed that $\dot{m}_{s_i} = \bar{\dot{m}}_p$ was the same for all locations in Plane A-A. Although this dispersion model does not represent the chemical process it does provide a very acceptable method for comparing dispersion data. The description above is a loose argument to indicate the logic behind this criterion and give a physical meaning to the value of the "overall percent coverage" term.

5.4.3 Quantitative Comparison of Results

The values of $\dot{m}_{p_i}$ and $\dot{m}_{s_i}$ were obtained from the full scale Shawnee data listed in Table 5.3 and Table 5.5 gives the results of the percent coverage calculations for the experiments listed. Note that the tests are categorized according to nozzle location. Table 5.5 compares the average values of the percent coverage for the three nozzle locations of the Shawnee experiments with the model values with the two-inch grid turbulence from Table 5.2. Thus, although the turbulence conditions probably were not matched, the pattern of the highest degree of coverage with the lower rear injection level, followed by the upper rear injection level and last with the front injection level was obtained for both the model and the full scale boiler. In addition the magnitude variation between the model and full scale system at each of the rear injection levels was less than ten percent. The front injection variation was near 25 percent but the dynamic pressure ratio was 50 percent greater for the full scale system than for the model.

5.4.4 Graphical Comparison of Results

While the quantitative results of the model appear to be consistent with the results of the Shawnee boiler, one cannot use overall averages alone as conclusive proof of good modeling. As a result a point by point comparison as well as the overall percent coverage must be considered to help support the validity of the modeling process. Isodensity contour diagrams obtained for the model as well as the Shawnee experiments will be used for this purpose. The Shawnee contour lines represent fixed values of the ratio of the mass flow rate to the mean value of the mass flow rate for the entire duct. The isodensity lines from the model can also be considered the same way since from Equation 5.7

Table 5.5. Overall Percent Coverage

	Model (2" Grid)	Shawnee*
Level 1	66	70.9
Level 2	85	74
Level 3	49.1	63.2

*These values averaged over all experiments listed in Table 5.3.

$$\delta_N = \frac{\dot{m}_{p_i}}{\bar{\dot{m}}_p}$$

Thus, each continuous curve represents a constant value of $\frac{\dot{m}_{p_i}}{\bar{\dot{m}}_p}$ in the contour diagrams.

Figures 5.24, 5.25 and 5.26 show both a model and full scale contour diagram for each of the injection configurations.

It is suggested here that there are similarities even though the individual contour lines are not coincident when comparing the model and full scale diagrams. In fact the well defined high ratio areas in the model located along the nozzle's axis do not appear in the Shawnee boiler diagrams. However, what might be construed as barely discernable traces of such patterns can be found in the Shawnee diagrams. The mass flow ratios are higher in these vicinities whether or not these are in fact traces of such patterns. Furthermore, the outer envelopes with much lower ratios are similar for both the model and full scale figures. Thus, in a gross sense the high and low areas are generally in the same corresponding locations.

5.4.5 Discussion of Comparisons

At this time it does not appear to be possible to pinpoint the reasons for the apparent quantitative and qualitative differences in the two systems. As stated earlier the turbulence level in the full scale boiler is unknown and was probably not similar to the model turbulence. Also the model velocity profile was uniform and the Shawnee profile was not. In addition, the mean velocity varied by as much as 20 percent in the Shawnee experiments listed in Table 5.3 whereas the model mean velocity was kept constant. Furthermore, the dynamic pressure ratio for the front injection

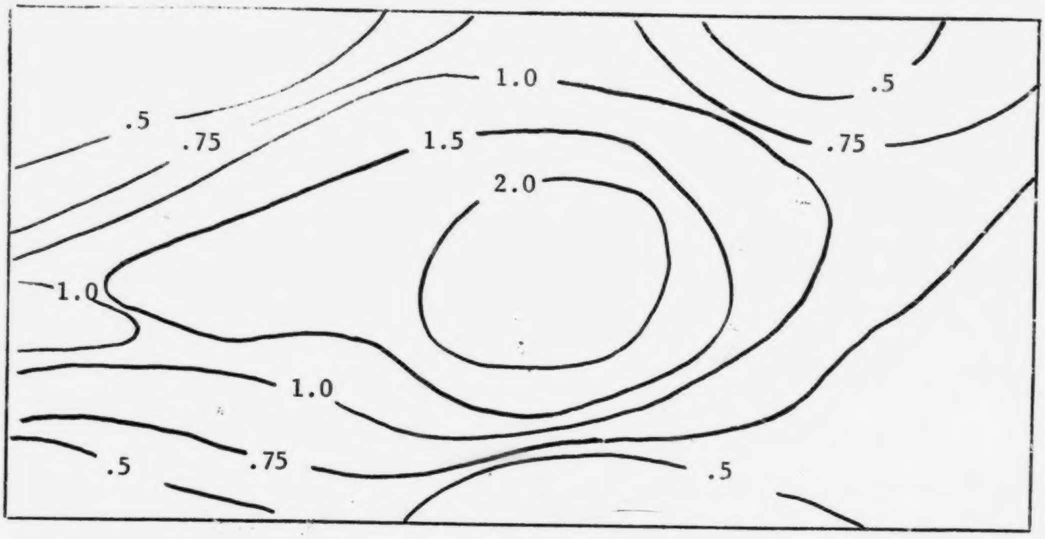

Shawnee Boiler - Test: S602, East, 12-10-70

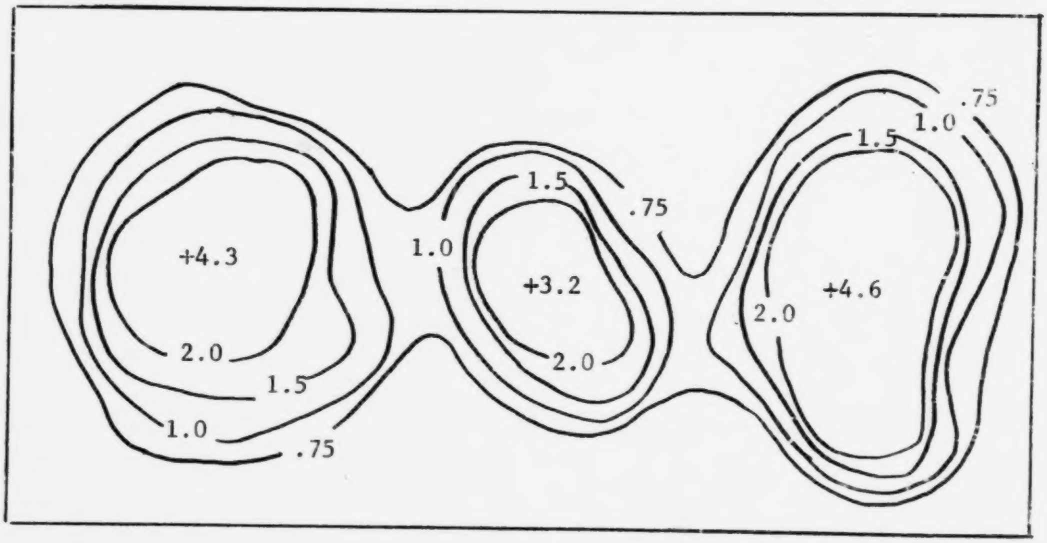

Shawnee Model - 2" Grid

Figure 5.24. Normalized mass flow rates, $\frac{\dot{m}_{p_i}}{\bar{\dot{m}}_p} = C$, Plane A-A, Injection Level 1

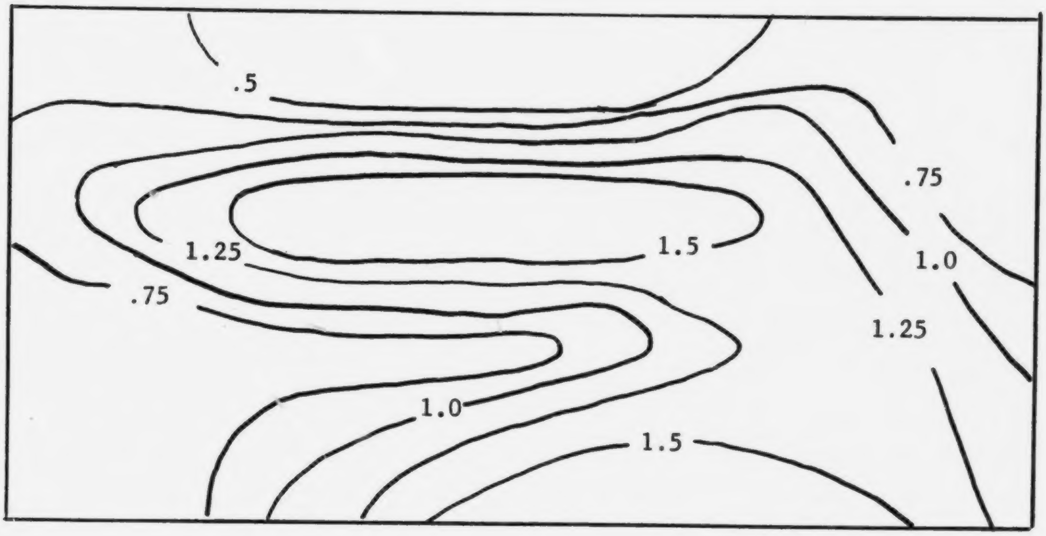

Nose

Shawnee Boiler - Test: S601, West, 12-4-70

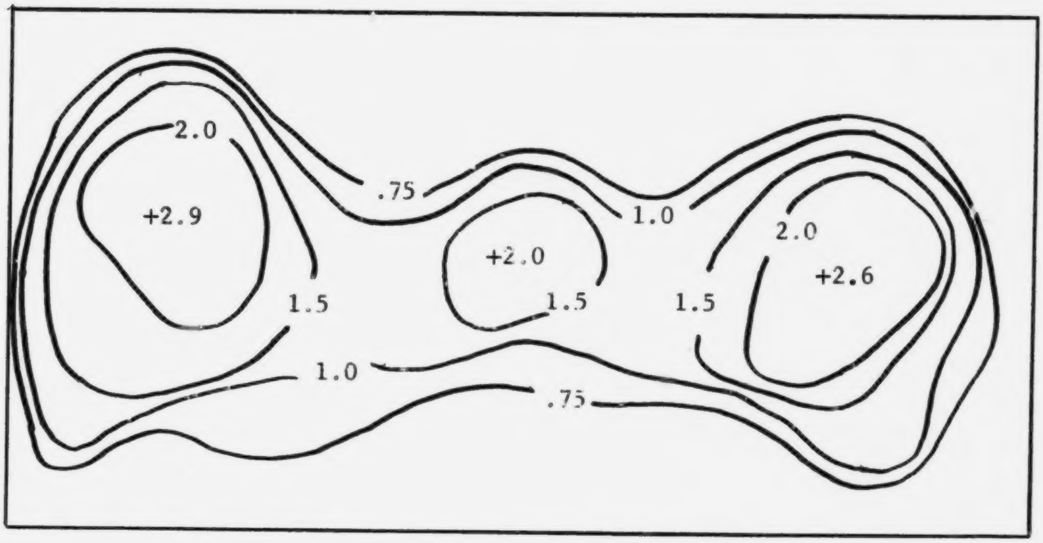

Nose

Shawnee Model - 2" Grid

Figure 5.25. Normalized mass flow rates, $\frac{\dot{m}_{pi}}{\bar{\dot{m}}_p} = C$, Plane A-A, Injection Level 2

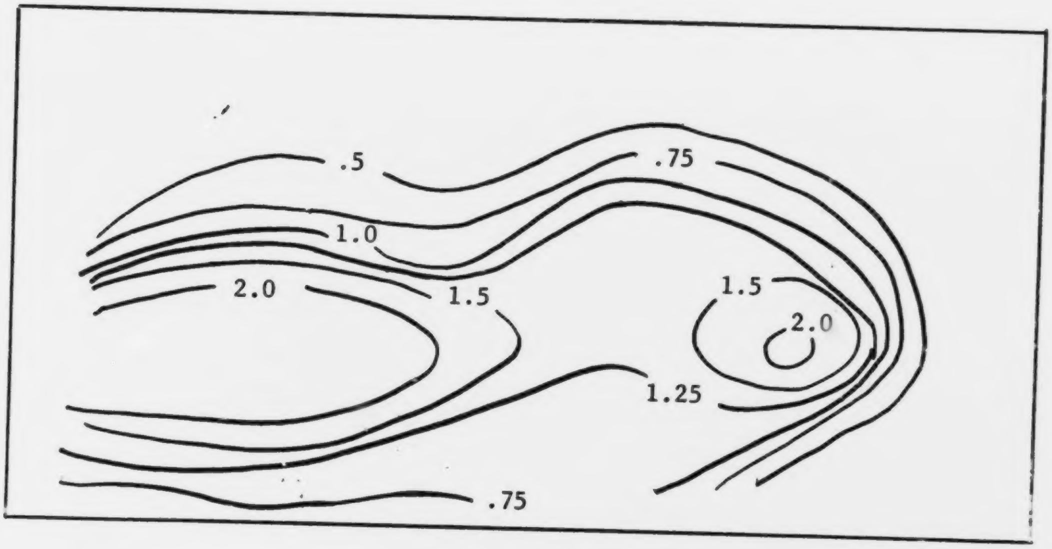

Nose

Shawnee Boiler - Test: S602, East, 12-12-70

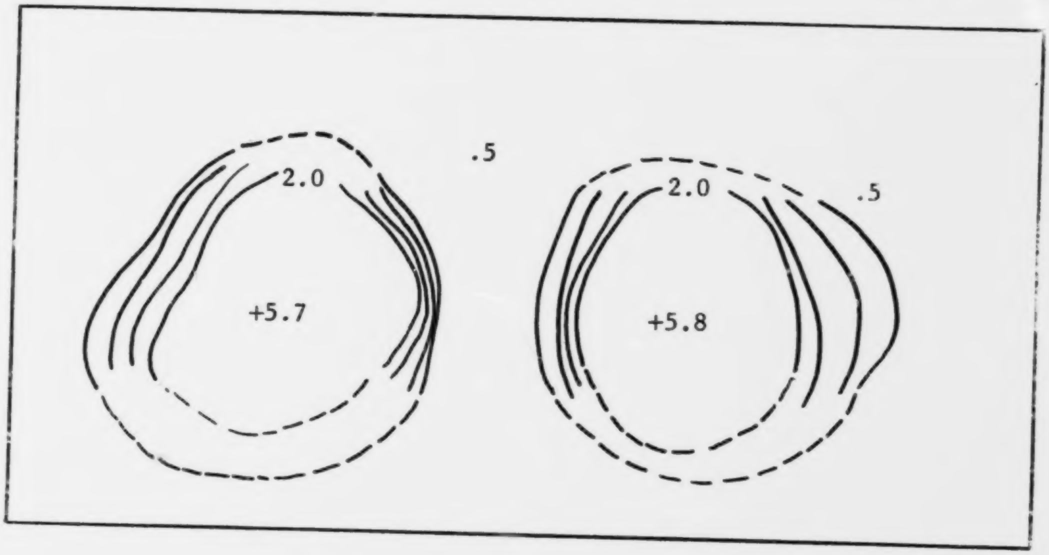

Nose

Shawnee Model - 2" Grid

Figure 5.26. Normalized mass flow rates, $\frac{\dot{m}_{p_i}}{\bar{\dot{m}}_p}$ = C, Plane A-A, Injection Level 3

was 50 percent greater than for the other two Shawnee injection levels. Another possible factor are variations in the nozzle to nozzle injection velocity and mass flow rate. The model experiments indicated that care had to be taken to prevent clogging in the lines as well as in the manifold which distributed the flow from the main feeder. Since no information has been made available on the operational characteristics of the nozzle distribution system at Shawnee, this is only mentioned as a possible source of differences. In summary there were test variations in the flow characteristics in the relatively complex Shawnee system whereas the model conditions were easily held constant from test to test. As a result exact modeling comparisons cannot be made. Nevertheless, results seem to indicate that the model does serve as an experimental approximation to the solid-gas flow phenomenon in the Shawnee boiler.

6.0 RECOMMENDATIONS FOR FUTURE WORK

It should be mentioned that the following recommendations are made in light of the fact that EPA has indicated that no additional effort will be placed into the dry limestone process. As a result any suggestions for study to improve the efficiency of the mixing process in the Shawnee boiler may be somewhat academic. Nevertheless, they will be presented in keeping with the original intent of this dispersion study. However, in addition, recommendations of a more general nature which could broaden the technological base for understanding the dispersion of injected solids will be presented.

6.1 Recommendations to Improve Technological Understanding of Injection and Dispersion

The following recommendations are predicated on the assumptions that the two-phase injection process is common to many engineering applications and that it is not well understood. In particular, the injection of a solid-gas jet perpendicular to or at some angle to a cross stream of a single phase fluid cannot be accurately described at the present time. The dry limestone process is one current example of a situation where lack of injection and dispersion design information was a definite handicap during an ongoing program. In the future similar situations more than likely will arise, some perhaps within the domain of O.A.P., where two-phase injection and dispersion information will be needed. Thus, it is recommended that a parametric study of the injection phenomena be made with a single nozzle in a straight duct. Here an experimental program could be designed with the dimensionless parameters obtained in this study. Such a study would detail the relative importance of the various dimensionless groups to injection and dispersion. By doing so one would have both the individual as well as the composite effect of such variables as turbulence, particle size, and injection velocity on the penetration and distribution. Table 2.2 outlines the dimensionless parameters that would be considered in this recommended program.

A closely related topic to the basic dispersion study is the development of an optical concentration probe where the reading is taken directly in the flow situation (see Section 3.9). The ability to read instantaneous concentration values would provide a much firmer basis for evaluating the distribution of powder in a duct. The readings in this study were time averaged over 20 seconds, those at Shawnee over five minutes so that the possibility remains that pulsations of the order of a second or two could easily go undetected but could have some significance in a meaningful definition of dust distribution. Thus, it is recommended that effort be given to the further development of a probe similar to the one built for this study or to developing a new one with the above stated capability.

6.2 Recommendations -- Related Directly to Shawnee System

1. Acquire additional data with Shawnee Model where needed
    a. Study effects of turbulence at Plane A-A for Levels 1 and 3
    b. Study effects of turbulence at Plane Y-Y
    c. Measure turbulence scale at Plane A-A with dual hot wire system
2. Consider techniques for improving dispersion in Shawnee Model

    At present only straight nozzles, at three or four fixed injection levels have been tried at Shawnee. Also the dynamic pressure ratio was not changed appreciably. A planned model program would be instituted to vary nozzle angle, vary nozzle patterns and number, introduce several types of nozzle swirl and also parameterize the dynamic pressure ratio as well as the other pi groups. Such information would indicate the trends of dispersion with each of the nozzle variables as well as with other variables included in the dimensionless parameters. This information should indicate the optimum injection configuration for dispersion and penetration.

3. Conduct investigation to determine turbulence conditions in Shawnee boiler -- incorporate into model

Perform detailed literature search of swirl flow and flame turbulence in order to arrive at best estimate of turbulence environment in the Shawnee boiler. These conditions would then be simulated with the Shawnee model. Then a comparison with the new dispersion data could be made with the present turbulent data from the model.

REFERENCES

1. Soo, S. L., Trezek, G. J., Dimick, R. C., and Hohnstreither, G. F. "Concentration and Mass Flow Distribution in a Gas-Solid Suspension," Ind. Eng. Chem. Fundamentals, V. 3, 1964, pp. 98-106.

2. Ehmen, E. E. "An Improved Fiber Optic Probe for Low Particulate Concentrations," M. S. Thesis, U. of Illinois, 1969.

3. Patrick, M. A. "Experimental Investigation of the Mixing and Penetration of a Round Turbulent Jet Injected Perpendicularly into a Transverse Stream," Trans. Instn. Chem. Engrs., Vol. 45, 1967, pp. T16-T31.

4. Dryden, H. L., Schubauer, G. B., Mock, W. C., and Skramstad, H. K. "Measurements of Intensity and Scale of Wind-Tunnel Turbulence and Their Relation to the Critical Reynolds Number of Spheres," NBS Report No. 581, 1937, p. 109.

5. Batchelor, G. K., and Townsend, A. A. "Decay of Isotropic Turbulence in the Initial Period," Proc. Roy. Soc. London, Series A, Vol. 193, 1948, p. 539.

6. Batchelor, G. K., and Townsend, A. A. "Decay of Turbulence in the Final Period," Proc. Roy. Soc. London, Series A, Vol. 194, 1949, p. 527.

APPENDIX A

LITERATURE REVIEW

A.1 Introduction

The present problem requires an understanding of two interdependent phenomena; that is, the injection and the dispersion of a two-phase jet. The first portion is the study of the trajectory of the solid-gas jet injected into a transverse stream. The second part of the problem is the dispersion of the solid phase following this injection. The literature review, started early in this study, covered both of these areas. To date, no reports of similar work have been found in the literature with the exception of a preliminary study at Babcock and Wilcox, Pfeifer (1), on limestone injection. For that study, a scale model was built and tested but an orderly scaling procedure was not utilized in designing the model. Because there have been no directly comparable studies, it has been necessary to review the literature of related subjects. These studies include analyses of jet injections for a variety of configurations. In addition to studies of injection phenomena, the area of statistical turbulence as related to the dispersion of particles has also been searched. Hence, the results of the literature search have been categorized into the subjects of jet injections and particle transport in turbulent flow.

A.2 Jet Injection Studies

The variety of injection studies researched have included a range from those concerned with the deflection of liquid jets injected normal to a gas stream to those involving the spreading of a free solid-gas jet. Of these, some have considered the effects of shear induced turbulence at the boundary of the jet with respect to mass and momentum transfer. However, none of the work reviewed have considered either of the two following situations:

1) Solid-gas jet injected into transverse gas stream

2) Effect of ambient turbulent conditions on dispersion of a jet.

For convenience, the jet injection review will be divided into the following subject areas, each of which is related to some facet of the present study.

1. Injection of a gas jet into a transverse gas stream.
2. Injection of a liquid jet into a transverse stream.
3. Free and coflowing jets (single and two-phase).
4. Stack emission.

Appendix B is a bibliography which is divided in a similar manner so that there is a bibliography associated with each topic.

A.2.1 Injection of a Gas Jet Into a Transverse Gas Stream

The topic of jet penetration into a transverse flow has been given a reasonable amount of attention in the literature. Results are usually correlated to the densities and velocities of the jet and transverse flow. This is generally accomplished by forming dimensionless groups and correlating the experimental data (location of the jet centerline) to these groups. The form for these dimensionless groups varies from worker to worker but essentially the injection penetration is expressed in terms of one of the three functional relations listed below

$$\frac{y'}{d} = f\left(\frac{x'}{d}, \frac{\rho_j}{\rho_o}, Re_j, \frac{V_j}{U_o}\right) \tag{A-1}$$

$$\frac{y'}{d} = f\left(\frac{x'}{d}, \frac{\rho_j V_j^2}{\rho_o U_o^2}\right) \tag{A-2}$$

$$\frac{y'}{d} = f\left(\frac{s}{d}, \frac{\rho_j V_j^2}{\rho_o U_o^2}\right) \tag{A-3}$$

Keffer and Baines (2) argue that the jet Reynolds number does not have an appreciable effect in the jet problem and consequently neglect it. The second equation, like the first, is often used to correlate the data and appears to have the advantage of being easier to correlate since the densities and velocities are combined into a single grouping. Patrick (3) used the second approach and demonstrated that the constants and powers in a correlation equation containing these groups are only valid over particular ranges of dynamic pressure ratio, $\rho_j V_j^2/\rho_o U_o^2$. Table 2.1 lists a few of the empirically derived correlation equations as reported in the literature. All neglect jet Reynolds number. Some are correlations along the lines of equation (1), the others equation (2). References (4-8) fall into the group most closely associated with equation (1) and references (3, 9) with equation (2). Keffer and Baines demonstrate a more reduced form for their jet centerline data, equation (3), which closely parallels the form of equation (2). Here the dimensionless penetration is related to the dynamic pressure ratio and distance along the jet centerline rather than along the duct.

A semianalytical approach for gas jets has also been performed by several authors including Abramovich (9), Wooler (10), and Braun and Goldstein (11). In all three, some aspect of the analysis requires experimental information. Abramovich's approach requires the value of a drag coefficient for the crosswind flow normal to the jet. Nevertheless,

AUTHOR(S)	PENETRATION EQUATION
Callaghan and Ruggeri (4)	$\frac{y}{d} = C^{.37}\left(\frac{\rho_j}{\rho_o}\right)^{.57}\left(\frac{V_j}{U_o}\right)^{.64}\left(\frac{x'}{d}\right)^{.26}$ C = dimensionless coefficient Author notes that powers vary with changes in d
Weiland and Trass (5)	$\frac{y'}{d} = K_1\left(\frac{\rho_j}{\rho_o}\right)^{\alpha}\left(\frac{V_j}{U_o}\right)^{\beta} x^{\gamma} d^{\delta-1}$ Note: The units of this equation do not check. Blowing air into duct: $\alpha = .5$ $\gamma = .25$ $\beta = .66$ $\delta = .70$ Sucking air through duct: $\alpha = .64$ $\gamma = .22$ $\beta = .71$ $\delta = .56$
Patrick (3)	$\frac{y'}{d} = \left(\frac{\rho_j V_j^2}{\rho_o U_o^2}\right)^{.425}\left(\frac{x'}{d}\right)^{n}$ $.33 \le n \le .38$
Shandorov*	$\frac{y'}{d} = \left(\frac{\rho_j V_j^2}{\rho_o U_o^2}\right)^{.392}\left(\frac{x'}{d}\right)^{.392}$
Ivanov*	$\frac{y'}{d} = \left(\frac{\rho_j V_j^2}{\rho_o U_o^2}\right)^{.434}\left(\frac{x'}{d}\right)^{.333}$
Norgren and Humenik (8)	$\frac{y'}{d} = .87\left(\frac{\rho_j}{\rho_o}\right)^{.47}\left(\frac{V_j}{U_o}\right)^{.85}\left(\frac{x'}{d}\right)^{.32}$

*Referenced in Abromovich (9)

Table A.1. Various Correlation Relations for Jet Trajectory Data

Abramovich found that his solution compared favorably with the experimental results of Shandorov and Ivanov (see Abramovich). Wooler and Braun and Goldstein also required trajectory information in order to complete their analyses. As with the other experimental results, these studies were based on a gas phase jet and crosswind. Consequently, results may not apply to a solid-gas jet.

To summarize, the relationships described above correspond to gas jets injected into gas crossflows where ρ_j is the homogeneous jet density. Hence, the use of any of these equations to predict the trajectory of a solid-gas jet would be questionable until it was ascertained whether or not the jet behaved like a homogeneous fluid. If this were the case, then the mixture density of the solid-gas flow at the nozzle would be treated as the representative density, ρ_j, of the jet.

A.2.2 Injection of a Liquid Jet Into a Transverse Gas Stream

Only the most general aspects of this phenomena appear to be applicable to the solid-gas jet. The liquid jet is by nature a single phase jet rather than a two-phase one. Breakup into a two-phase jet occurs at some distance (determined by the flow conditions and physical properties) away from the nozzle. As a result, forces on the jet prior to breakup are entirely different from that for a solid-gas jet. Here, dimensionless numbers such as the Weber number and Bond number come into play since surface tension forces must be considered in a liquid jet. Liquid jet studies range from free jets to jets issuing into crosswinds. Most studies have been primarily concerned with the degree of liquid breakup although a few have studied the jet trajectory. Povinelli (12) did develop a correlation equation for the jet trajectory utilizing the concept of the dynamic pressure ratio. However, he replaced the crosswind velocity and distance downstream with the time that the liquid was exposed to the crosswind. This, however, makes the equations difficult to use since time is not as convenient an independent variable as is distance downstream. Clark (13) considers the breakup of a liquid jet but not its penetration distance. However, he also uses the dynamic pressure ratio to correlate data where the relative velocity of the gas with respect to the liquid replaces the normally used crosswind velocity. Other references examined (14, 15) yielded little information with respect to the correlation of trajectory curves.

A.2.3 Free and Coflowing Jets (Single and Two-Phase)

The geometry of these problems makes these the simplest of the two-phase injection problems and although there are no exact solutions, phenomenological mass and momentum transfer relations give quite satisfactory results. Trajectory information cannot be obtained from studies in this category, but the dispersion of particles may have many similarities between these types of injected flows and transversely injected flows. Hence, it may be possible to compare results from the crosswind-jet problem with the coaxial jet at some distance downstream from the injection point.

One study which appears to closely resemble that of the proposed one was made by Goldschmidt and Eskinazi (16). They used a plane jet with a liquid aerosol and measured the turbulent Schmidt eddy diffusivity across the plume. Here the turbulence was generated at the jet-free stream interface. However, the turbulent scale and intensity of the free stream were not considered nor were the drop size and density parameterized.

Csanady (17) investigating the dispersal of effluents in lakes did touch upon the influence of lake turbulence on the effective eddy diffusivity. Indications were that the diffusivity increased as the intensity increased. Although the effect of turbulence scale was discussed, no measurements were made.

Other two-phase jet studies have considered fringe problems which are inherent in two-phase injections. In studies by Soo (18) and Lee and Soo (19) the effects of particulate electrostatic charge was treated. In these papers the charge was induced on the particles to control distribution and collection of the dust. Doughman and Lewis (20) found that the particle plume boundary moved further from the plume axis as the smallest particles in a given distribution were decreased in size. Laats (21) investigated the effect of particle loading on free jet dynamics and found the effect of the solid phase on the transverse mass process. Kusui (22) found that the performance of a water jets was dependent upon the surface roughness of the nozzle's inner wall. These studies are mentioned basically to point out that although many of these fine points were not considered in the present study, such studies may be required at some future date in order to interpret results or improve the design of the present injection equipment.

A.2.4 Stack Emission

Considerable work has been done in this area over a period of more than forty years. This work has included both simple analytic studies and many experimental investigations. Major emphasis has been placed on obtaining equations to predict plume trajectory and particulate deposition from the plume. In a paper by Bryant and Cowdrey (23), model plume trajectories were studied resulting in curves of trajectory showing the effects of various temperature differences between the plume and ambient, Figure 2.1. The interest here is limited to those portions of the curves where the trajectory is indistinguishable from the curve with no temperature difference. This is the portion of the curves where inertial effects predominate and gravity (thermal buoyancy) effects have not yet become significant.

If considerations are included for the natural turbulence associated with wind, then this class of problem and the present study have a great deal in common. Bosanquet (24) noticed that large scale eddies (size of plume diameter or larger) contribute to plume meandering but only the smaller eddies contribute to turbulent dispersion. Qualitatively, this would seem reasonable, unfortunately, no papers have been found in this group which have tried to correlate measured turbulence parameters (intensity and scale) to plume trajectory and dispersion data.

A.3 Transport of Particles in Turbulent Flow Field

Another subject area of direct interest to this experimental program is the dispersion of a solid phase as a result of turbulent motions of the carrier fluid. In particular, the dispersion of the jet plume downstream of the injection point should be similar to that associated with a single particle in a turbulent stream. The literature contains studies of the transport of particles in a turbulent flow field as well as equations of motion utilizing the continuum concept of a gas phase and a particle cloud. Appendix B contains a bibliography associated with this area of the literature review.

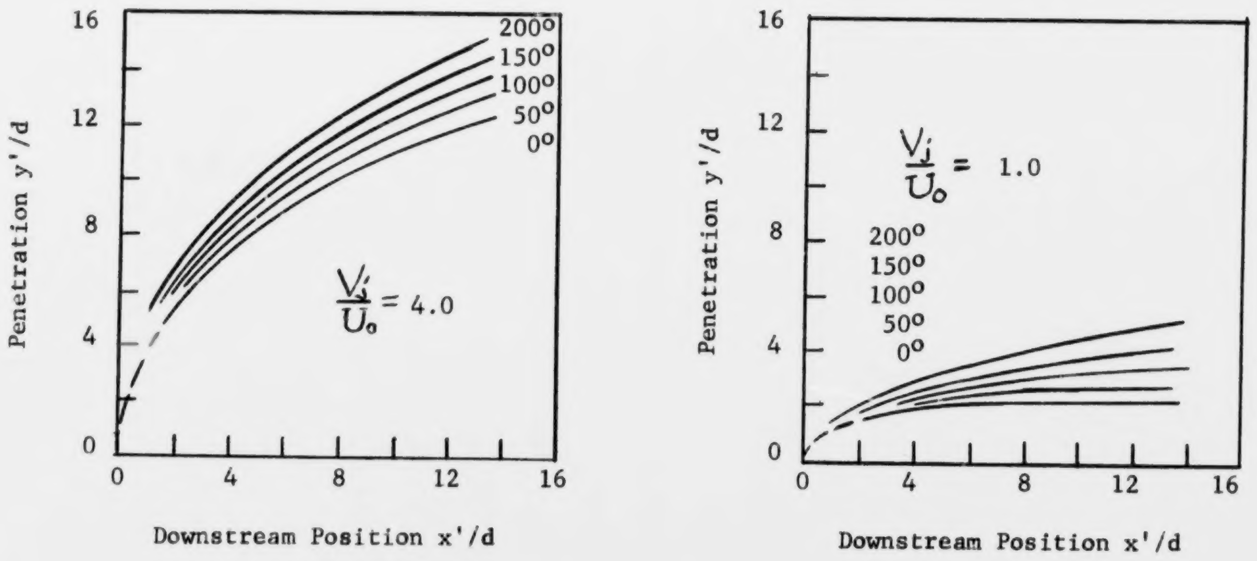

Exit Temperature in C° Above Ambient

Figure A.1. Effects of Plume Temperature on Trajectory for Two Velocity Ratios

One aspect of particular interest is the result obtained by analyzing the equation for an accelerating particle in an accelerating fluid (sometimes referred to as the Oseen, Basset, Boussinesq equation). By nondimensionalizing this equation and sizing the various terms (Appendix C) a dimensionless group is obtained which relates the particle dynamics to those of the fluid (the forcing function)

$$\Pi_D = \left[\frac{\nu}{a v'}\right]\left[\frac{\Delta}{a}\right]\left[\frac{\rho_0}{\hat{\rho}_p}\right] \tag{4}$$

This is a term which appears in papers by Ahmadi (25), Soo (26), and Householder and Goldschmidt (27) and has been used to correlate turbulent dispersion data.

Another aspect of two-phase turbulent motion are the studies in two-phase statistical turbulence. This is essentially an extension of the theories developed by Taylor, Von Karman, Kolmogoroff, etc. (a collection of these papers is contained in reference (28)). The addition of solid particles does require additional rigor in order to account for the interaction between the solid phase and the carrier fluid. Since Tchen's (29) paper on this subject in 1947, a good deal of work has been done both of an analytical and experimental nature. Of the many papers available on this subject, those by Friedlander (30), Liu (31), and Soo, Ihrig, and El Kouh (32) are of particular interest. The first two papers present relationships for the statistical behavior of the solid phase, in particular, statistical relationships for turbulent slip velocity and dispersion of the solid phase. It is worth noting that though their respective approaches to the problem are different, the resulting equations for turbulent dispersion of the particles are essentially the same. In the final paper referred to, the authors experimentally determined the effects of solid particles on the stream turbulence characteristics. They also obtained some information on the turbulent behavior of the particle phase as a result of the stream turbulence where the correlation term used was the Π_D term noted above.

A.4 References

1. Pfeifer, W. A. "Jet Penetration and Distribution Studies - Limestone Injection Model," Babcock and Wilcox Research and Development Division Report, Ref. LR-69-6071-01-1, 1969.

2. Keffer, J. F., and Baines, W. D. "The Round Turbulent Jet in a Crosswind," J. Fluid Mech., 1963, V. 8, p. 481.

3. Patrick, M. A. "Experimental Investigation of the Mixing and Penetration of a Round Turbulent Jet Injected Perpendicularly into a Transverse Stream," Trans. Instn. Chem. Engrs., Vol. 45, 1967, pp. T16-T31.

4. Callaghan, E., and Ruggeri, R. S. "A General Correlation of Temperature Profiles Downstream of a Heated-Air Jet Directed Perpendicularly to an Air Stream," NACA Tech. Note 2466.

5. Weiland, R. H., and Trass, O. "Jet Penetration in Turbulent Streams," Canadian J. of Chem. Engr., V. 47, August 1969, Technical Note, pp. 443-444.

6. Pratte, B. D., and Baines, W. D. "Profiles of the Round Turbulent Jet in a Cross Flow," Journal of the Hydrualics Division, V. 92, 1967, p. 53.

7. Carlson, C. W., Hsu, J. J., and Meyers, C. A. "The Penetration and Mixing of Air Jets Directed Perpendicular to a Stream," ASME Paper 68-WA/GT-6.

8. Norgren, C. T., and Humenik, F. M. "Dilution-Jet Mixing Study for Gas-Turbine Combustors," NASA TN D-4695.

9. Abromovich, G. N. The Theory of Turbulent Jets, MIT Press, 1963.

10. Wooler, P. T. "Flow of a Circular Jet into a Cross Flow," J. of Aircraft, V. 6, N. 3, 1969, pp. 283-284.

11. Braun, W., and Goldstein, M. E. "Analysis of the Mixing Region for a Two Dimensional Jet Injected at an Angle to a Moving Stream," NASA TN D-5531, 1969.

12. Povinelli, F. P. "Displacement of Disintegrating Liquid Jets in Crossflow," NASA TN D-4334.

13. Clark, B. J. "Breakup of a Liquid Jet in a Transverse Flow of Gas," NASA TN D-2424.

14. Adelberg, M. "Breakup Rate and Penetration of a Liquid Jet in a Gas Stream," AIAA J., V. 5, N. 8, August 1967, pp. 1408-1415.

15. Catton, I., Hill, D. E., and McRae, R. P. "Study of Liquid Jet Penetration in a Hypersonic Stream," AIAA Journal, V. 6, 1968, p. 2084.

16. Goldschmidt, V., and Eskinazi, S. "Two Phase Turbulent Flow in a Plane Jet," J. Applied Mech., December 1966, pp. 735-747.

17. Csanady, G. T. "Dispersal of Effluents in the Great Lakes," Water Research, V. 4, 1970, p. 79-114.

18. Soo, S. L. "Electrohydrodynamic Jets," Proceedings of the 11th Midwestern Mechanics Conference, 1969.

19. Lee, Y. N., and Soo, S. L. "Effects of Electrostatic Charges on Dust Particles in a Jet," Presented at Air Pollution Control Association Meeting, 1970.

20. Doughman, E., and Lewis, C. H. "Radial Lag of Solid Particles in Delaval Nozzles," AIAA Journal, V. 3, 1965, p. 169.

21. Laats, M. K. "Experimental Study of the Dynamics of an Air-Dust Jet," Inzhenerno-Fizicheskii Zhurnal, V. 10, N. 1, 1966, pp. 11-15.

22. Kusui, T. "Liquid Jet Flow Into Still Gas," Bulletin of JSME, V. 12, 1969, p. 1062.

23. Bryant, L. W., and Cowdrey, C. F. "Effects of Velocity and Temperature of Discharge on the Shape of Smoke Plumes From a Chimney; Experiments and Wind Tunnel," Instn. of Mech. Engr., Proceedings, Vol. 169, 1955, pp. 371-399.

24. Bosanquet, C. H. "The Rise of a Hot Waste Gas Plume," J. Inst. of Fuel, V. 30, No. 197, 1957, p. 322.

25. Ahmadi, G. "Analytical Predictions of Turbulent Dispersion of Finite Size Particles," Ph.D. Thesis, 1970, Purdue.

26. Soo, S. L. "Statistical Properties of Momentum Transfer in a Two-Phase Flow," J. of Chem. Engr. Science, V. 5, 1956, pp. 57-67.

27. Householder, M. K., and Goldschmidt, V. W. "Turbulent Diffusion and Schmidt Number of Particles," J. of Engr. Mech. Div., Vol. 95, December 1969, pp. 1345-1367.

28. Friedlander, S. K., and Topper, L. (Editors). Turbulence, Classic Papers on Statistical Theory, Interscience Publishers, 1961,

29. Tchen, C. M. "Mean Value and Correlation Problems Connected with the Motion of Small Particles Suspended in a Turbulent Fluid," The Hague, M. Nishoff, 1947.

30. Friedlander, S. K. "Behavior of Suspended Particles in a Turbulent Fluid," A.I.Ch.E.J., V. 3, September 1957, pp. 381-385.

31. Liu, V. C. "Turbulent Dispersion of Dynamic Particles," Journal of Meteorology, V. 13, August 1956, pp. 399-405.

32. Soo, S. L., Ihrig, H. K., and El Kouh, A. F. "Experimental Determination of Statistical Properties of Two-Phase Turbulent Motions," J. of Basic Engr., September 1960, pp. 609-621.

APPENDIX B - BIBLIOGRAPHY

1. Injection of a Gas Jet into a Transverse Stream

Abromovich, G. N. The Theory of Turbulent Jets, MIT Press, 1963.

Analysis of a Jet in a Subsonic Crosswind NASA Sp-218, Proceedings of a Symposium at Langley Research Center, September 9 and 10, 1969.

Callaghan, E., and Ruggeri, R. S. "A General Correlation of Temperature Profiles Downstream of a Heated-Air Jet Directed Perpendicularly to an Air Stream," NACA Tech. Note 2466.

Carlson, C. W., Hsu, J. J., and Meyers, C. A. "The Penetration and Mixing of Air Jets Directed Perpendicular to a Stream," ASME Paper 68-WA/GT-6.

Keffer, J. F., and Baines, W. D. "The Round Turbulent Jet in a Crosswind," J. Fluid Mech., 1963, V. 8, p. 481.

Krzywoblocki, M. Z. "Jets-Review of Literature," Jet Propulsion, Sept. 1956, pp. 760-779.

Patrick, M. A. "Experimental Investigation of the Mixing and Penetration of a Round Turbulent Jet Injected Perpendicularly into a Transverse Stream," Trans. Instn. Chem. Engrs., Vol. 45, 1967, pp. T-16-T31.

Platten, J. L., and Keffer, J. F. "Deflected Turbulent Jet Flows," ASME Paper 71-APM-SS.

Pratte, B. D., and Baines, W. D. "Profiles of the Round Turbulent Jet in a Cross Flow," Journal of the Hydraulics Division, V. 92, 1967, p. 53.

Weiland, R. H., and Trass, O. "Jet Penetration in Turbulent Streams," Canadian J. of Chem. Engr., V. 47, August 1969, Technical Note, pp. 443-444.

Wooler, P. T. "Flow of a Circular Jet into a Cross Flow," J. of Aircraft, V. 6, N. 3, 1969, pp. 283-284.

2. Injection of a Liquid Jet into a Transverse Gas Stream

Adelberg, M. "Breakup Rate and Penetration of a Liquid Jet in a Gas Stream," AIAA J., V. 5, N. 8, August 1967, pp. 1408-1415.

Catton, I., Hill, D. E., and McRae, R. P. "Study of Liquid Jet Penetration in a Hypersonic Stream," AIAA Journal, V 6, 1968, p. 2084.

Clark, B. J. "Breakup of a Liquid Jet in a Transverse Flow of Gas," NASA TN D-2424.

Norgren, C. T., and Humenik, F. M. "Dilution-Jet Mixing Study for Gas-Turbine Combustors," NASA TN D-4695.

Povinelli, F. P. "Displacement of Disintegrating Liquid Jets in Crossflow," NASA TN D-4334.

3. Free and Coflowing Jet (Single and Two-Phase)

Abromovich, G. N. (Already cited).

Braun, W., and Goldstein, M. E. "Analysis of the Mixing Region for a Two Dimensional Jet Injected at an Angle to a Moving Stream," NASA TN D-5531, 1969.

Forstall, W., Jr., and Shapiro, A. H. "Momentum and Mass Transfer in Coaxial Gas Jets," J. Applied Mech., 1950, V. 72, p. 339.

Goldschmidt, V., and Eskinazi, S. "Two-Phase Turbulent Flow in a Plane Jet," J. Applied Mech., December 1966, pp. 735-747.

Kusui, T. "Liquid Jet Flow Into Still Gas," Bulletin of JSME, V. 12, 1969, p. 1062.

Latts, M. K. "Experimental Study of the Dynamics of an Air-Dust Jet," Inzhenerno-Fizicheskii Zhurnal, V. 10, N. 1, 1966, pp. 11-15.

Lee, Y. N., and Soo, S. L. "Effects of Electrostatic Charges on Dust Particles in a Jet," Presented at Air Pollution Control Association Meeting, 1970.

Maczyski, J. F. "A Round Jet in an Ambient Coaxial Stream," J. of Fluid Mech., V. 13, 1962, pp. 597-608.

Mikhail, S. "Mixing of Coaxial Streams in a Closed Conduit," J. of Mech. Engr. Sci., V. 2, N. 1, p. 59.

Pai, S. I. Fluid Dynamics of Jets, Van Nostrand Co. Inc., 1954.

Pai, S. I. "Unsteady Three-Dimensional Laminar Jet Mixing of a Compressible Fluid," AIAA J., V. 3, N. 4, April 1965.

Schetz, J. A. "Unified Analysis of Turbulent Jet Mixing," NASA CR-1382.

Singer, H. A. "Jet Mixing of a Two-Phase Stream with a Surrounding Fluid Stream," Ph.D. Thesis, U.S.C., 1970.

Soo, S. L. "Electrohydrodynamic Jets," Proceedings of the 11th Midwestern Mechanics Conf., 1969.

4. Stack Emission

Bosanquet, C. H. "The Rise of a Hot Waste Gas Plume," J. Inst. of Fuel, V. 30, No. 197, 1957, p. 322.

Bosanquet, C. H., Carey, W. V., and Halton, E. M. "Dust Deposition From Chimney Stacks," I. Mech. Engr., 1950, p. 355.

Bryant, L. W., and Cowdrey, C. F. "Effects of Velocity and Temperature of Discharge on the Shape of Smoke Plumes From a Funnel or Chimney; Experiments in a Wind Tunnel," Instn. of Mech. Engr., Proceedings, Vol. 169, 1955, pp. 371-399.

Minutes of the Symposium on Plume Behavior, Air and Water Pollut. Int. J., 1966, Vol. 10, p. 393.

Moore, D. J. "Physical Aspects of Plume Models," Air and Water Pollut. Int. J., 1960, Vol. 10, p. 411.

Pasquill, F. *Atmospheric Diffusion*, Van Nostrand, 1962.

Priestley, C. H. B. "A Working Theory of the Bent Over Plume of Hot Gas," Q. J. R. Met. Soc., V. 82, p. 165.

Scorer, R. S. "The Behavior of Chimney Plumes," Int. J. Air Poll., 1959, V. 1, p. 198.

Soo, S. L. "Effect of Simultaneous Diffusion and Fallout from Plumes of Stack and Jet Engines," Presented at Air Pollution Control Association Meeting, 1970.

Sutton, O. G. "The Dispersion of Hot Gases in the Atmosphere," J. of Meteorology, V. 7, N. 5, 10/50, p. 307.

5. Two-Phase Turbulent Motion

Ahmadi, G. "Analytical Predictions of Turbulent Dispersion of Finite Size Particles, Ph.D. Thesis, 1970, Purdue.

Baw, P. S. H., and Peskin, R. L. "Some Aspects of Gas-Solid Suspension Turbulence," ASME Paper No. 71-FE-15.

Boothroyd, R. G. "Turbulence Characteristics of Gaseous Phase in a Duct Flow of a Suspension of Fine Particles," Trans. Inst. Chem. Engr., V. 45, 1967, pp. T297-T310.

Brodkey, R. S. The Phenomena of Fluid Motions, Addison Wesley, 1967.

Friedlander, S. K. "Behavior of Suspended Particles in a Turbulent Fluid," A.I.Ch.E.J., V. 3, September 1957, pp. 381-385.

Hinze, J. O. "Momentum and Mechanical Energy Balance Equation for a Flowing Homogeneous Suspension with Slip Between the Two Phases," Applied Science Res., V. 11, pp. 33-46.

Hinze, J. O. Turbulence, McGraw-Hill, 1959.

Hjelmfelt, A. T., and Mockros, L. F. "Motion of Discrete Particles in a Turbulent Fluid," Applied Science Res., V. 16, p. 149.

Householder, M. K., and Goldschmidt, V. W. "Turbulent Diffusion and Schmidt Number of Particles," J. of Engr. Mech. Div., Vol. 95, December 1969, pp. 1345-1366.

Liu, V. C. "Turbulent Dispersion of Dynamic Particles," Journal of Meteorology, V. 13, August 1956, pp. 399-405.

Peskin, R. L. "Statistical Effects Resulting from the Presence of Many Particles in Motion in an Ideal Fluid," Heat Trans. & Fl. Mech. Inst., 1960.

Shirazi, A. A. "On the Motion of Small Particles in a Turbulent Fluid Field," Ph.D. Thesis, Univ. of Illinois, 1967.

Soo, S. L. Fluid Dynamics of Multiphase Systems, Ginn Blaisdell, 1967.

Soo, S. L. "Fully Developed Turbulent Pipe Flow of a Gas-Solid Suspension," I & EC Fundamentals, Vol. 1, 1962, p. 33.

Soo, S. L. "Statistical Properties of Momentum Transfer in a Two-Phase Flow," J. of Chem. Engr. Science, V. 5, 1956.

Soo, S. L., Ihrig, H. K., and El Kouh, A. F. "Experimental Determination of Statistical Properties of Two-Phase Turbulent Motions," J. of Basic Engr., September 1960, pp. 609-621.

Stukel, J. J., and Soo, S. L. "Turbulent Flow of a Suspension into a Channel," Power Technology, Vol. 2, No. 5, June 1969, pp. 278-289.

Tchen, C. M. "Mean Value and Correlation Problems Connected with the Motion of Small Particles Suspended in a Turbulent Fluid," The Hague, M. Nishoff, 1947.

Wallace, J. P. "A Study of the Fluid Turbulence Energy Spectrum in a Gas Solid Suspension," Ph.D. Thesis, Rutgers, 1966.

6. Flame Studies

Chigier, N. A. "Pressure, Velocity, and Turbulence Measurements in Flames," Presented at the ASME Fluids Engr. Div. Conf., Pgh., Pa., May 1971.

Gunther, R., and Simon, H. 12th Symp. on Comb., 1969, p. 1069.

Gross, R. A. "Flame Generated Turbulence," Jet Propulsion, V. 26, 1956, p. 716.

Putnam, A. A. "Swirl Burning," Presented to American Flame Research Committee, Jan. 1967.

Karlovitz, B., Denniston, D. W., and Wells, F. E. "Investigation of Turbulent Flames," The Journal of Chemical Physics, V. 19, 1951, p. 541-547.

7. Additional Bibliography

Batchelor, G. K., and Townsend, A. A. "Decay of Isotropic Turbulence in the Initial Period," Proc. Roy. Soc. London, Series A, Vol. 193, 1948, p. 539.

Batchelor, G. K., and Townsend, A. A. "Decay of Turbulence in the Final Period," Proc. Roy. Soc. London, Series A, Vol. 194, 1949, p. 527.

Boothroyd, R. G. "Similarity in Gas-Borne Flowing Particle Suspensions," Journal of Engineering for Industry, No. 68-MH-11, May 1969, pp. 303-313.

Cheng, L., and Soo, S. L. J. Applied Physics, V. 41, N. 2, 1970.

Csanady, G. T. "Dispersal of Effluents in the Great Lakes," Water Research, V. 4, Pergamon Press, 1970, pp. 79-114.

Doughman, E., and Lewis, C. H. "Radial Lag of Solid Particles in Delaval Nozzles," AIAA Journal, V. 3, 1965, p. 169.

Dryden, H. L., Schubauer, G. B., Mock, W. C., and Skramstad, H. K. "Measurements of Intensity and Scale of Wind-Tunnel Turbulence and Their Relation to the Critical Reynolds Number of Spheres," NBS Report No. 581, 1937, p. 109.

Friedlander, S. K., and Topper, L. (Editors). Turbulence, Classic Papers on Statistical Theory, Intersicence Publishers, 1961.

Hinze, J. O. Turbulence, McGraw-Hill Publishing Company, 1959.

Klein, S. J. Similitude and Approximation Theory, McGraw-Hill, 1965.

Oldshue, J. Y. "Mixing," Indust. Engr. Chem., V. 60, N. 11, November 1968, pp. 24-35.

Peskin, R. L. "Some Effects of Particle-Particle and Particle-Fluid Interaction in a Two-Phase Flow System," Ph.D. Thesis, Princeton Univ., 1959.

Pfeifer, W. A. "Jet Penetration and Dispersion Study," Babcock & Wilcox Co., Research Center, Alliance, Ohio, October 1968.

Rose, H. E., and Barnacle, H. E. "Flow of Suspensions of Non-Cohesive Spherical Particles in Pipes - No. I," The Engineer, Vol. 203, June 14, 1957, pp. 898-901.

Rose, H. E., and Barnacle, H. E "Flow of Suspensions of Non-Cohesive Spherical Particles in Pipes - No. II," The Engineer, Vol. 203, June 21, 1957, pp. 939-941.

Rudinger, G. "Addition of Heated Solid Particles to a Gas Flowing in a Pipe," ASME Paper No. 71-FE-22.

Soo, S. L., Trejek, G. J., Dimick, R. C., and Hohnstrither, G. F. "Concentration and Mass Flow Distribution in a Gas Solid Suspension," Ind. Engr. Chem. Qtrly., V. 3, 1964.

Soo, S. L., and Tung, S. K. "Gravity Effect in Pipe Flow Suspensions," Presented at the Symposium on Flow, Pittsburgh, May 1971.

Thring, M. W. The Science of Flames and Furnaces, Wiley & Sons, 1962.

Vogt, E. G., and White, R. R. "Friction in the Flow of Suspensions," Industrial and Engineering Chemistry, Vol. 40, No. 9, September 1948, pp. 1731-1738.

APPENDIX C

C.0 FRACTIONAL ANALYSIS

C.1 Introduction

The solid-gas jet penetration and dispersion phenomenon is quite complex and a relatively new area of study, thus, it was felt that the most reasonable approach was to combine a theoretical and an experimental program. The first step was to develop a partial or fractional analysis of the governing equations for a solid-gas suspension. This analysis includes the nondimensionalization of the conservation of mass and momentum equations which yield a set of dimensionless parameters which characterize the physical phenomena. These parameters are then used to provide the rationale for an experimental program. The jet experiments and modeling of the Shawnee boiler were based on a set of dimensionless parameters obtained in this manner.

The term fractional analysis encompasses three basic techniques, which are 1) dimensional analysis, 2) similitude, and 3) nondimensionalization of the governing equations. All three have been employed at one time or another in solid-gas suspension studies. Although no such study reported in the literature was found to be directly applicable to this investigation, there was some overlap. Most of the studies surveyed fell into either a dimensional analysis category or one where the governing equations were nondimensionalized.

C.2 Previous Work

The following discussion covers some solid-gas flow studies where a dependent variable such as pressure drop or eddy diffusivity are correlated to a set of dimensionless groups. Table C.1 summarizes the results of a selected group of investigations. As can be seen, these studies were primarily concerned with frictional losses in flows through tubes and ducts. Although none included jet injection, it is felt that at some point downstream of the injection point, the flow characteristics will not differ appreciably from the solid-gas suspension studies listed in Table C.1. This table indicates that although the important variables are common to all of the studies, there are some differences in the resulting sets of dimensionless parameters. Thus, one given study may consider the Reynolds number as an independent dimensionless parameter whereas another indicates that Reynolds number by itself does not adequately correlate the data. This discussion is not intended to explain the individual differences in frictional loss studies of two-phase suspensions, but to point out these differences in order to illustrate the general form of the results which have been obtained with fractional analysis.

It is interesting to note that only Soo (1) and Soo, et al. (2) include both the scale and intensity of turbulence as characteristic values in the analyses. However, in some flows these turbulence values are dependent upon the geometry and mean velocity and therefore do not appear as independent variables. Stuckel and Soo (3) as well as Boothroyd (4) include a dimensionless group which is related to the electrostatic charge of the particulate phase. The importance of this term will vary with experimental conditions and is generally neglected as a first order approximation.

In summary, Table C.1 lists the various dimensionless parameters

References	Dimensionless Parameters	Comments
Vogt, E. G., and White, R. R. (5)	Press. Drop $= F\left(\frac{D}{a}, \frac{\rho_g}{\rho_p}, \frac{\dot{m}_s/\dot{m}_g}{Re}, \sqrt{\frac{(\rho_p-\rho)\rho g a^3}{\mu}}\right)$ $= F\left(\frac{D}{a}, \frac{\rho_g}{\rho_p}, \Pi_6/\Pi_1, \sqrt{\frac{(\rho_p-\rho)\rho g a^3}{\mu}}\right)$	Pipe Flow
Soo, S. L. (1)	$\Delta P = F\left(\frac{a v' \rho_0}{\mu}, \frac{a}{\lambda}, \frac{\hat{\rho}_p}{\rho_0}\right)$ Momentum Transfer $= F\left(\Pi_1 \Pi_2 \frac{a}{D}, \frac{a}{D}\frac{1}{\Pi_3}, \frac{\hat{\rho}_p}{\rho_0}\right)$	Stream Flow
Soo, S. L., Ihrig, H. K., and El Kouh, A. F. (2)	$\frac{\hat{D}_p}{D_p} = F\left(\frac{a^2 v'}{\mu} \frac{\hat{\rho}_p}{\lambda}\right)$ $= F\left(\frac{\Pi_1 \Pi_2}{\Pi_3 \Pi_5}\right)$	Pipe Flow
Stuckel, J. J. and Soo, S. L. (3)	$\frac{\hat{D}_p}{U_0 D} = F\left(\frac{FD}{U_0}, \left(\frac{q}{m_p}\right)^2 \frac{\rho_{pe} a^4}{\epsilon_0 D_p^2}\right)$ $= F\left(\frac{\Pi_5}{\Pi_1}, \left(\frac{q}{m_p}\right)^2 \frac{\rho_{pe} a^4}{\epsilon_0 D_p^2}\right)$	Inlet of Channel
Boothroyd, R. G. (4)	$\frac{\Delta P_t}{\Delta P_0} = \frac{f}{f_0} = F\left(\frac{U_0 D}{\nu}, \frac{\dot{m}_s}{\dot{m}_g}, \frac{\rho D^2}{\rho_p a^2 Re}, \frac{2/m\, a\, \hat{\rho}_{pe}^{1/2}}{\square\, \epsilon_0^{1/2}}\right)$ $= F\left(\Pi_1, \Pi_0, \frac{\Pi_5}{\Pi_1}, \left(\frac{q}{m_p}\right)^2 \left(\frac{a^2 \hat{\rho}_{pe}}{\epsilon_0 \square^2}\right)\right)$	Pipe Flow
Boothroyd, R. G. (6)	$\frac{\Delta P_t}{\Delta P_0} = F\left(\frac{\rho D^2}{\rho_p Re}, Re, \frac{\dot{m}_s}{\dot{m}_g}\right)$ $= F\left(\frac{\Pi_5}{\Pi_1}, \Pi_1, \Pi_6\right)$	Pipe Flow
Rose, H. E., and Barnacle, H. E. (7, 8)	$\frac{\Delta P}{\rho U_0^2} = F\left(\frac{L}{D}, \frac{\hat{\rho}_p}{\rho_0}, \frac{\dot{m}_s}{\dot{m}_g}, Re\right)$ $= F\left(\Pi_0, \frac{\hat{\rho}_p}{\rho_0}, \Pi_6, \Pi_1\right)$	Pipe Flow

Table C.1. Dimensionless Parameters Obtained in Solid-Gas Suspension Studies

obtained by a number of different analyses. All were concerned with solid-gas suspensions and none include jet injection. Nevertheless, it is to be expected that similar parameters would be found in the solid-gas jet injection study in addition to those parameters which specifically characterize the jet.

C.3 Fractional Analysis of Solid-Gas Jet Injection

Several goals of this study dictated the need for a fractional analysis of a solid-gas jet. As stated earlier the complexity of this problem in addition to a lack of prior work strongly suggested an experimental program to provide insight into the basic fluid mechanics of the solid-gas jet interaction. Furthermore, by merely listing the variables which could influence both the jet penetration and the concentration of particulate downstream from the injection point, it appears that a "brute force" experimental approach of systematically changing these variables would be difficult. The dependent variables, e.g., penetration or concentration of the solid phase, labeled ϕ for simplicity will be influenced by the following independent variables.

$$\phi = \phi(P, \rho_a, \rho_j, \hat{\rho}_P, U_o, V_j, v', L, D, d, a, \Lambda, \mu) \qquad \text{C-1}$$

In order to reduce the experimental effort, it was decided to utilize some aspect of fractional analysis. Kline (9) cites the three possible approaches listed above and discusses the advantages and disadvantages of each. Table C.2 summarizes the rationale of this discussion.

In agreement with Table C.2, the next step was to make a choice between the differential formulation and the integral formulation of the governing equations. In either case, it was felt that the overall system

Method	Power	Rigor	Accuracy	Simplicity	Input
Dimensional Analysis	Least	Least	Least	Intermediate	Least
Method of Similitude	Intermediate	Intermediate	Intermediate	Greatest	Intermediate
Systematic Use of Differential Equations	Far Greater Than Others	Much Better Than Others	Greatest	Most Complicated	Greatest

POWER - The amount of output information achievable

RIGOR - The accuracy inherent in the method

ACCURACY - The percentage of correct answers achieved in practice

SIMPLICITY - The effort and knowledge required for use

INPUT - The amount of information required to utilize the method

Table C.2. (Reference Kline (9)). A Comparison of Scaling Techniques boundaries should include both the solid-gas jet and the solid-gas suspension within the duct downstream of the nozzle. As was mentioned above, this was one of the major points of departure from existing studies which either consider a jet alone or a solid-gas suspension by itself. Since the literature generally indicated that the differential formulation was more widely used, it was selected for the first approach. The resulting dimensionless parameters agreed well with those from the solid-gas suspension analyses. However, the basic dimensionless parameter of a jet, the dynamic pressure ratio of the jet to the duct, was missing. At this point, the uncertainty in the analyses coupled with what appeared to be the omission of this experimentally proven parameter, motivated the integral approach. This technique did produce the dynamic pressure ratio as well as all of the other dimensionless parameters found by the differential equation approach. Because of the good agreement between the two approaches, it is felt that all of the dimensionless parameters were identified. The fact that the integral technique produced a dynamic pressure ratio while the other did not only lies in the more complete description of the boundary conditions with the integral approach.

C.3.1 Nondimensionalization of the Governing Differential Equations for Multiphase Flow

To properly describe a flow problem, one must write both the conservation equations and the boundary conditions. Thus, it is necessary to define the domain of interest. For this approach, the overall system includes a plane perpendicular to duct axis upstream of the injection point to a parallel plane a sufficient distance L from the injection point. The duct walls provide the remaining surfaces for this system. Figure C.1

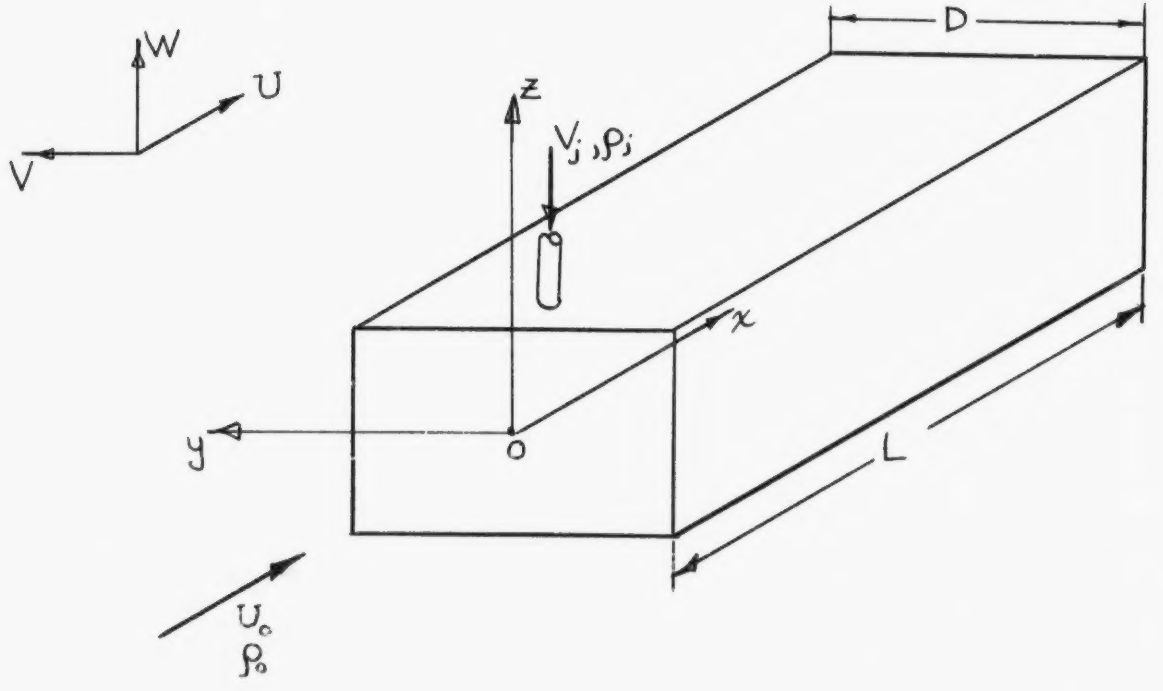
W
U
V
z
V_j, ρ_j
x
y
o
D
L
U_o
ρ_o

Figure C.1. Coordinate System - Fractional Analysis

illustrates this domain. The conservation equations are written in the differential form for an arbitrary location within the system. Thus, the jet itself now is treated as a boundary condition where the mass crosses the system boundary at the injection point. Then once the jet has spread across the entire duct cross section, the flow could be treated as a conventional two-phase suspension. It should be noted that another technique for analyzing a jet is to treat it separately, writing the conservation equation specifically for the jet. However, for this technique defining both the boundaries and the boundary conditions would be quite difficult. It is anticipated that both of these approaches should yield the same dimensionless groups.

For this portion of the study the particle motion is represented by a particle cloud having the properties of a continuum. The governing equations therefore include the conservation of mass and momentum for both the gas and the particle cloud and are treated in a manner outlined by Soo (10). As a first approximation for analysis of this problem the energy equation has been omitted. This seems to be a reasonable assumption since the dispersion phenomenon is dominated by the inertial effects of the mainstream and jet fluid motion. That is, the heat transfer and related energy phenomena will be controlled by the various velocities where the effects of these processes on the velocity are negligible except through the dependence of ρ upon temperature. Therefore, it is necessary to use mean values of the properties for the modeling process which would account for thermal gradients without explicitly treating the energy equation.

A number of simplifying assumptions are made in the analysis of four mass and momentum equations. The first is that all time variations in velocity are associated with the turbulence conditions and that the mean velocities are time independent. In addition, the fluid can be treated as incompressible. The instantaneous component of velocity at any point can be written

$$U(\vec{r},t) = \overline{U}(\vec{r}) + u(\vec{r},t) \tag{C-2}$$

A reference velocity is chosen to be the time averaged (mean) velocity at a reference x = 0 and is written as U_o.

Conservation Equations

Since the momentum equations for all three directions would yield the same dimensionless groups, only the momentum equations will be written for the x direction. The continuity equations in orthogonal Cartesian coordinates for the gaseous phase and the particle cloud are, respectively,

$$\frac{\partial \rho U}{\partial x} + \frac{\partial \rho V}{\partial y} + \frac{\partial \rho W}{\partial z} = 0 \tag{C-3}$$

and

$$\frac{\partial \rho_p}{\partial t} + \frac{\partial \rho_p U_p}{\partial x} + \frac{\partial \rho_p V_p}{\partial y} + \frac{\partial \rho_p W_p}{\partial z} = 0 \tag{C-4}$$

The momentum equations in the x direction for the gas phase and the particle cloud, respectively, are

$$\begin{aligned} \rho \frac{\partial U}{\partial t} + \rho U \frac{\partial U}{\partial x} + \rho V \frac{\partial U}{\partial y} + \rho W \frac{\partial U}{\partial z} &= -\frac{\partial p}{\partial x} \\ &+ \mu\left(\frac{\partial^2 U}{\partial x^2} + \frac{\partial^2 U}{\partial y^2} + \frac{\partial^2 U}{\partial z^2}\right) - K_m F \rho_p (U - U_p) \end{aligned} \tag{C-5}$$

$$\frac{\partial U_p}{\partial t} + U_p \frac{\partial U_p}{\partial x} + V_p \frac{\partial U_p}{\partial y} + W_p \frac{\partial U_p}{\partial z} = F(U - U_p) \tag{C-6}$$

Soo (10) labels the term K_m as the effectiveness which is a measure of the transfer of momentum of the mass motion of the particle cloud to the gas. In a dilute suspension K_m tends towards zero. When the interparticle spacing is of the order of ten times the particle diameter, the value of K_m is close to zero, (see Soo (6)). In the most closely packed region of flow in this problem, i.e., the nozzle exit, the density is still small enough to neglect K_m.

The body force term shown in equation C-6 includes the assumption that the particle Reynolds number $(\rho_o a(U - U_p)/\mu)$ is small enough that the force on a particle can be described by Stokes drag law. This is described in detail in references (7) and (10).

Nondimensionalization of the Equations

The equations are nondimensionalized by transforming the variables to dimensionless variables. The transformation is accomplished by dividing each variable by some value of that variable which characterizes that particular aspect of the problem. The following transformations are used in this study.

$$
\begin{aligned}
&x^* = \frac{x}{L}, \qquad && y^* = \frac{y}{D}, \qquad && z^* = \frac{z}{D} \\
&u^* = \frac{u}{u_o}, && v^* = \frac{v}{u_o}, && w^* = \frac{w}{u_o} \\
&u_p^* = \frac{u_p}{u_o}, && v_p^* = \frac{v_p}{u_o}, && w_p^* = \frac{w_p}{u_o} \qquad \text{C-7} \\
&\rho_p^* = \frac{\rho_p}{\rho_o}, && P^* = \frac{P}{\rho_o u_o^2}, && t^* = \frac{t}{\Lambda / v'}
\end{aligned}
$$

Figure C.2 shows the coordinate system and the duct dimensions. Replacing the variables with the transformed quantities in equation C-7 results in the following dimensionless conservation equations.

Conservation of mass-gas

$$\frac{\partial \rho^* U^*}{\partial x^*} + \frac{L}{D}\left(\frac{\partial \rho^* V^*}{\partial y^*} + \frac{\partial \rho^* W^*}{\partial z^*}\right) = 0 \qquad \text{C-8}$$

Conservation of mass-cloud

$$\left(\frac{v'}{U_o}\right)\left(\frac{L}{\Lambda}\right)\frac{\partial \rho_p^*}{\partial t^*} + \frac{\partial \rho_p^* U_p^*}{\partial x^*} + \frac{L}{D}\left(\frac{\partial \rho_p^* V_p^*}{\partial y^*} + \frac{\partial \rho_p^* W_p^*}{\partial z^*}\right) = 0 \qquad \text{C-9}$$

Conservation of momentum-gas (x direction)

$$\left(\frac{v'}{U_o}\right)\left(\frac{L}{\Lambda}\right)\frac{\partial U^*}{\partial t^*} + U^*\frac{\partial U^*}{\partial x^*} + \frac{L}{D}\left(V^*\frac{\partial U^*}{\partial y^*} + W\frac{\partial U^*}{\partial z^*}\right) = -\frac{\partial P}{\partial x}$$

$$+ \frac{D}{L}\left(\frac{\mu}{\rho_o U_o D}\right)\frac{\partial^2 U^*}{\partial x^{*2}} + \left(\frac{\mu}{\rho_o U_o D}\right)\left(\frac{L}{D}\right)\left(\frac{\partial^2 U^*}{\partial y^{*2}}\right.$$

$$\left. + \frac{\partial^2 U^*}{\partial z^{*2}}\right) - K_m\left(\frac{L}{D}\right)\left(\frac{FD}{U_o}\right)\left(U^* - U_p^*\right) \qquad \text{C-10}$$

Conservation of momentum-cloud (x direction)

$$\left(\frac{v'}{U_o}\right)\left(\frac{L}{\Lambda}\right)\frac{\partial U_p^*}{\partial t^*} + U_p^*\frac{\partial U_p^*}{\partial x^*} + \frac{L}{D}\left(V_p^*\frac{\partial U_p^*}{\partial y^*} + W_p^*\frac{\partial U_p^*}{\partial z^*}\right)$$

$$= \left(\frac{L}{D}\right)\left(\frac{FD}{U_o}\right)\left(U^* - U_p^*\right) \qquad \text{C-11}$$

Thus, the dimensionless variables obtained from the conservation equations are

$$(U^*, V^*, W^*, U_p^*, V_p^*, W_p^*, P^*, \rho_p^*)$$

and the dimensionless parameters are

$$(L/D, \rho_o U_o D/\mu, FD/U_o, v'/U_o, \Lambda/L)$$

where the term F (Soo (10)) is

$$F = \frac{9}{2} \frac{\mu}{\rho_p a^2} \qquad \text{C-12}$$

As can be seen, there are eight equations (six momentum and two continuity equations) and eight dimensionless variables so that the number of equations is sufficient. Finally, the application of the boundary conditions is required to complete the solution.

Boundary Conditions

In considering the boundary conditions for the gas, the usual no-slip condition at the walls is assumed as well as assuming the normal components of the velocity at the walls to be zero. However, at the y-z plane for x = 0, the mean velocity is U_o and the density is ρ_o with the turbulence associated with this flow characterized by v' and Λ, the root mean square of the fluctuating velocity and the scale of turbulence, respectively. The velocity components normal to the walls are considered to be zero with the exception of the injection point where the velocity is V_j. The cloud density at this location is $\rho_p = \rho_{p,\ jet}$.

Because of the geometry of the problem, it is not expected that the boundary layer effects would be significant. Even if considered, the boundary layer thickness would be negligibly small compared to the duct dimensions so that potential flow boundary conditions are applicable for both the gas and the cloud (i.e., velocity at wall is tangent to same).

At this point it is necessary to obtain the boundary conditions for the conservation of mass and momentum equations. The momentum equations are examined first and here

$$U = U_o \quad \text{at } x = 0 \ \text{ in the y-z plane}$$

and

$$V = W = 0 \ \text{at } x = 0 \ \text{ in the y-z plane} \qquad \text{C-13}$$

In addition for the particle phase

$U_p = V_p = W_p = 0$ at $x = 0$ in the y-z plane

but $V_p = V = V_j$ at the nozzle exit where it is assumed that the gas and particulate velocities of the jet are the same.

In the dimensionless form these boundary conditions are

$U_p^* = V_p^* = W_p^* = 0$ at $x = 0$ in the y-z plane C-14

$V^* = W^* = 0$ at $x = 0$ in the y-z plane

and

$V^* = V_j/U_o$ at nozzle exit

$V_p^* = V_j/U_o$ at nozzle exit.

It is convenient to add the two conservation of mass equations which gives

$$\left(\frac{V'}{U_o}\right)\left(\frac{L}{\Lambda}\right)\frac{\partial(\rho_p^* + \rho^*)}{\partial t^*} + \frac{\partial}{\partial x^*}(\rho_p^* U_p^* + \rho^* U^*)$$

$$+ \frac{L}{D}\left(\frac{\partial}{\partial y^*}(\rho_p^* V_p^* + \rho^* V^*) + \frac{\partial}{\partial z^*}(\rho_p^* W_p^* + \rho^* W^*)\right) = 0$$

Here, the dimensionless boundary conditions for $(\rho_p^* + \rho^*)$ are

$\rho_p^* + \rho^* = \rho^* = 1$ at $x = 0$ in the y-z plane C-15

and $\rho_p^* + \rho^* = \rho_{p,j}^* + \rho_{a,j}^* = \dfrac{\rho_{p,j} + \rho_{a,j}}{\rho_o} = \dfrac{\rho_j}{\rho_o}$ at nozzle exit

Dimensionless Parameters

Hence, the two additional dimensionless parameters V_j/U_o and ρ_j/ρ_o result from the application of the boundary conditions.

It should be noted here that isotropic turbulence has been assumed as a first approximation where u' = v' = w'.

In summary then, one can express the dimensionless density at a fixed point, i, in space as

$$\rho_i^* = \rho_{p_i}^* + \rho_i^* = f\left(L/D,\ v'/U_o,\ \Lambda/L,\ \rho_o U_o D/\mu,\ FD/U_o,\ \rho_j/\rho_o,\ V_j/U_o\right) \qquad \text{C-16}$$

The term FD/U_o in equation C-16 can be rewritten as

$$\frac{FD}{U_o} = \left(\frac{F\Lambda}{v'}\right)\left(\frac{v'}{U_o}\frac{D}{\Lambda}\right)$$

which upon multiplying and dividing by like terms can be again rewritten

$$\left(\frac{F\Lambda}{v'}\right)\left(\frac{v'}{U_o}\frac{D}{\Lambda}\right) = \left(\frac{C_1 \mu \Lambda}{\rho_p\, a^2}\right)\left(\frac{v'}{U_o}\frac{D}{\Lambda}\right)$$

$$= C_1\left(\frac{\mu}{\rho_o a}\right)\left(\frac{\Lambda}{a}\right)\left(\frac{\rho_o}{\rho_p}\right)\left(\frac{v'}{U_o}\frac{D}{\Lambda}\right) \qquad \text{C-17}$$

In summary, equation C-16 gives the dimensionless parameters which can affect the cloud density. For a comprehensive understanding of the solid-gas jet into a turbulent crosswind, the effect of each group on the particle cloud at a point must be known. However, in a model study such as the scale model of the Shawnee boiler, it is not necessary to ascertain the effect of each of the dimensionless parameters but only to assure that they are the same for both the model and full-scale systems.

C.3.2 Nondimensionalization of the Governing Integral Equations

As an independent check, another approach was utilized to obtain the applicable dimensionless parameters. For this approach the analysis is divided into three parts. First, the continuity and momentum equations are expressed in integral form and integrated over the entire control volume. The final part of this approach is the analysis of a single particle in a turbulent flow field. In this manner the parameters related to interaction of the solid phase and the ambient turbulence are obtained.

The integral approach outlined in the following pages is significantly different from that outlined in section C.3.1. However, more significant than the differences between the two approaches to obtain the applicable dimensionless parameters, is the similarity of the results obtained. The results of these two approaches complement one another but in no way are contradictory.

The system being analyzed is shown in Figure C.2. The appropriate inlet and outlet parameters are also shown on the figure.

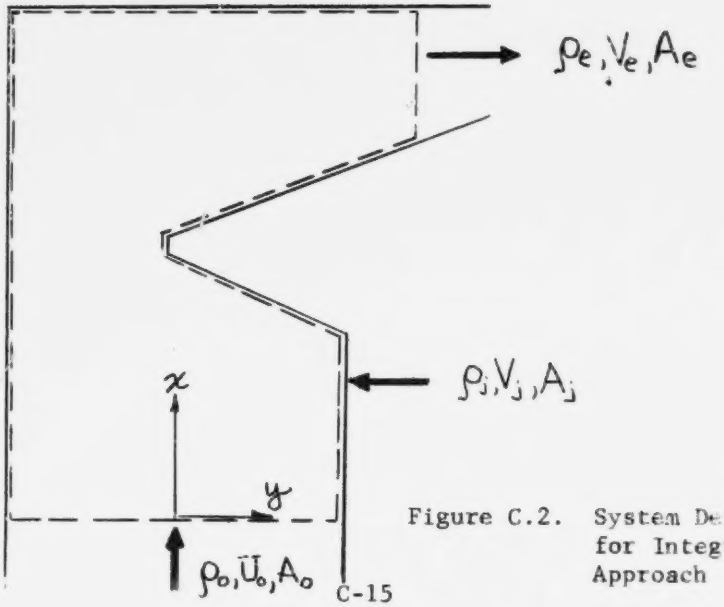

Figure C.2. System Definition for Integral Approach

Continuity Equation

The continuity equation for the entire control volume is obtained from the Lagrangian integral formulation.

$$M = \iiint_{V_{ol}(t)} \rho \, dV_{ol} \qquad \text{C-18}$$

The time rate of change

$$\frac{d}{dt} M = \frac{d}{dt} \iiint_{V_{ol}(t)} \rho \, dV_{ol} = 0 \qquad \text{C-19}$$

where $V_{ol}(t)$ defines the volume boundary of the closed system and can be related to V_{ol_o} by the Jacobian of the transformation

$$dV_{ol}(t) = J(t) \, dV_{ol_o}$$

$$\frac{d}{dt} \iiint_{V_{ol}(t)} \rho \, dV_{ol} = \frac{d}{dt} \iiint_{V_{ol_o}} \rho J(t) \, dV_{ol_o} = \iiint_{V_{ol_o}} \left[J \frac{d}{dt} \rho + \rho \frac{d}{dt} J \right] dV_{ol_o}$$

$$\frac{d}{dt} J(t) = \nabla \cdot \vec{V} \, J(t)$$

$$\frac{d}{dt} M = \iiint_{V_{ol}(t)} \left[\frac{d}{dt} \rho + \rho \nabla \cdot \vec{V} \right] dV_{ol} \qquad \text{C-20}$$

The intergrand can be written

$$\frac{d}{dt} \rho + \rho \nabla \cdot \vec{V} = \frac{\partial}{\partial t} \rho + \nabla \cdot (\rho \vec{V})$$

Integrating over the control volume and using the divergence theorem

$$\iiint_{V_{C.V.}} \frac{\partial}{\partial t} \rho + \oiint_{S_{CV}} \rho \vec{V} \cdot n \, ds = 0 \qquad \text{C-21}$$

Assuming a steady state operating condition the first term is zero. The second term integrated over the closed surface of the control volume is zero except at the inlets and outlet where

$$\rho_o U_o A_o + \rho_j V_j A_j - \rho_e V_e A_e = 0 . \qquad \text{C-22}$$

Factoring out $\rho_o U_o A_o$ and equating the model to the full sized system, the dimensionless terms are

$$\frac{\rho_j V_j A_j}{\rho_o U_o A_o}, \quad \text{and} \quad \frac{\rho_e V_e A_e}{\rho_o U_o A_o} \; .$$

Momentum Equation

A twofold procedure will be used for examining the momentum equation. The momentum equation will be expressed in integral form without utilizing the identity obtained from the continuity equation. This is necessary in order to maintain the independence of the two equations, since it may not be possible to satisfy the constraints of both the continuity and momentum equations. The second aspect of the analysis of the momentum equation is the nondimensionalization of the integrand. The parameters obtained from this procedure are required in order to obtain similarity of the interior flow patterns between the model and the actual system.

The momentum of a closed system is

$$M_{om} = \iiint\limits_{V_{ol}(t)} \rho \vec{V} \, dV_{ol} \; . \qquad \text{C-23}$$

The rate of change of this property is directly proportional to the sum of all forces acting on the system

$$\frac{d}{dt} \iiint\limits_{V_{ol}(t)} \rho \vec{V} \, dV_{ol} = \Sigma \vec{F} \; . \qquad \text{C-24}$$

The term on the left is operated on in exactly the same manner (equation C-20)) as was done for the continuity equation. The argument $\rho \vec{V}$ is substituted for ρ of the previous case yielding

$$\frac{d}{dt} \iiint\limits_{V_{ol}(t)} \rho \vec{V} \, dV_{ol} = \iiint\limits_{V_{ol}(t)} \left[\frac{d}{dt} (\rho \vec{V}) + \rho \vec{V} \; \nabla \cdot \vec{V} \right] dV_{ol} \qquad \text{C-25}$$

or in terms of the partial derivative with respect to time the integrand can be rewritten

$$\frac{\partial}{\partial t}\rho\vec{V} + \nabla\cdot(\rho\vec{V}:\vec{V}) \qquad \text{C-25a}$$

where $\vec{V}:\vec{V}$ is a tensor product.

The summation over all forces include both body and surface forces acting on the system. Body forces include those resulting from magnetic fields (on ferrous materials), electric fields (on charged particles and ions) and gravitational fields. The most important is the last and so the other body forces will be neglected

$$\vec{F}_B = -\iiint_{V_{oL}(t)} \rho g \mathbb{i}\, dV_{oL} \qquad \text{C-26}$$

The combined surface forces, normal and shear, are expressed in terms of the gradient of the stress tensor

$$\vec{F}_S = \iiint_{V_{oL}(t)} \nabla\cdot\mathbb{P}\, dV_{oL} \qquad \text{C-27}$$

The stress tensor $\mathbb{P}$ can be obtained from numerous sources and will be given here for completeness with one limiting assumption. For this analysis it will be assumed that, μ, the viscosity is constant throughout the control volume. In the real system this is not the case since μ is temperature dependent. However, by choosing a representative value for viscosity this variation is taken into account. Using this assumption the stress tensor can be written

$$\mathbb{P} = \mathbb{i}\vec{P}_x + \mathbb{j}\vec{P}_y + \mathbb{k}\vec{P}_z$$

$$\vec{P}_x = \mathbb{i}\left[-P - \frac{2}{3}\mu\nabla\cdot\vec{V} + 2\mu\frac{\partial}{\partial x}U\right] + \mathbb{j}\tau_{yx} + \mathbb{k}\tau_{zx}$$

$$\vec{P}_y = \mathbb{i}\tau_{yx} + \mathbb{j}\left[-P - \frac{2}{3}\mu\nabla\cdot\vec{V} + 2\mu\frac{\partial}{\partial y}V\right] + \mathbb{k}\tau_{yz}$$

$$\vec{P}_z = \mathbb{i}\tau_{zx} + \mathbb{j}\tau_{yz} + \mathbb{k}\left[-P - \frac{2}{3}\mu\nabla\cdot\vec{V} + 2\mu\frac{\partial}{\partial z}W\right]$$

where P = static pressure

$$\tau_{xy} = \mu\left[\frac{\partial}{\partial y}U + \frac{\partial}{\partial x}V\right]$$

$$\tau_{xz} = \mu\left[\frac{\partial}{\partial z}U + \frac{\partial}{\partial x}W\right]$$

$$\tau_{zy} = \mu\left[\frac{\partial}{\partial z}V + \frac{\partial}{\partial y}W\right]$$

Using these relations (equations C-25, C-26 and C-27) momentum equation C-24 can be written for the control volume as

$$\iiint_{V_{C.V.}}\left[\frac{\partial}{\partial t}\rho\vec{V} + \nabla\cdot(\rho\vec{V}:\vec{V}) + \rho g\mathbb{i} - \frac{\partial}{\partial x}\vec{P}_x - \frac{\partial}{\partial y}\vec{P}_y - \frac{\partial}{\partial z}\vec{P}_z\right]dV_{oL} = 0 \qquad \text{C-28}$$

For an infinitesmal volume the integrand of the equation above must be equal to zero. In treating this integrand the equation is separated into its steady state and turbulent components. Each of these components is nondimensionalized in order to obtain the scaling parameters associated with each. For this process the X component of the momentum equation will be used. This component will give the same dimensionless groups as the other two components, but will have an additional group which is associated with the gravitational effects.

The $\mathbb{i}$ component of the momentum integrand is

$$\frac{\partial}{\partial t}\rho U + \nabla\cdot(\rho\nabla U) + \rho g + \frac{\partial}{\partial y}P - \frac{1}{3}\mu\frac{\partial}{\partial y}\nabla\cdot\vec{V} + \mu\nabla^2 U = 0$$

The turbulent and steady state components of the velocity vector are

$$\vec{V} = \bar{\vec{V}} + \vec{v}$$

$$= \bar{U}i + \bar{V}j + \bar{W}k + ui + vj + wk \qquad \text{C-29}$$

Density and viscosity are assumed not to have variations related to turbulence. The momentum equation can now be written

$$\begin{aligned}&\frac{\partial}{\partial t}(\rho\bar{U}) + \nabla\cdot(\rho\bar{\vec{V}}\bar{U}) + \rho g + \frac{\partial}{\partial x}\bar{P} - \frac{1}{3}\mu\frac{\partial}{\partial x}(\nabla\cdot\bar{\vec{V}})\\ &+\mu\nabla^2\bar{U} + \frac{\partial}{\partial t}\rho u + \nabla\cdot(\rho\bar{\vec{V}}u) + \nabla\cdot(\rho\vec{v}\bar{U}) \qquad \text{C-30}\\ &+\nabla\cdot(\rho\vec{v}u) + \frac{\partial}{\partial x}p - \frac{1}{3}\mu\frac{\partial}{\partial x}(\nabla\cdot\vec{v}) + \mu\nabla^2 u = 0\end{aligned}$$

By performing a time averaging procedure on this equation we obtain the steady state momentum equation.

$$\begin{aligned}&\frac{\partial}{\partial t}(\rho\bar{U}) + \nabla\cdot(\rho\bar{\vec{V}}\bar{U}) + \rho g + \frac{\partial}{\partial x}\bar{P} - \frac{1}{3}\mu\frac{\partial}{\partial x}(\nabla\cdot\bar{\vec{V}})\\ &+\mu\nabla^2\bar{U} + \nabla\cdot(\overline{\rho\vec{v}u}) = 0 \qquad \text{C-31}\end{aligned}$$

This last term is usually referred to as the Reynolds stress. It is the interaction term between the steady state and turbulent components of the momentum equation. In other words the steady state flow is not completely independent of the ambient turbulence condition.

Subtracting C-31 from C-30 the turbulent component is

$$\begin{aligned}&\frac{\partial}{\partial t}(\rho u) + \nabla\cdot(\rho\bar{\vec{V}}u) + \nabla\cdot(\rho\vec{v}\bar{U}) + \nabla\cdot(\rho\vec{v}u) - \nabla\cdot(\overline{\rho\vec{v}u}) \qquad \text{C-32}\\ &+ \frac{\partial}{\partial x}p - \frac{1}{3}\mu\frac{\partial}{\partial x}(\nabla\cdot\vec{v}) + \mu\nabla^2 u = 0\end{aligned}$$

Nondimensionalization

Separate scale components are used for nondimensionalizing equations C-31 and C-32. The characteristic scales for C-31 are the dimensions related to duct size. The characteristic length for equation C-32 is the size of the turbulent eddies, Λ .

For equation C-31 the following nondimensionalization groups are used

$$t = \frac{L}{U_o}\tau \qquad \bar{P} = \rho_o U_o^2 \bar{P}^+ \qquad \nabla = \frac{1}{L}\nabla^+$$

$$x = L x^+ \qquad \bar{\bar{V}} = U_o \bar{\bar{V}}^+ \qquad \nabla^+ = \mathbb{i}\frac{\partial}{\partial x^+} + \mathbb{j}\frac{L}{D}\frac{\partial}{\partial y^+} + \mathbb{k}\frac{L}{D}\frac{\partial}{\partial z^+}$$

$$y = D y^+ \qquad \vec{v} = v'\vec{v}^+ \tag{C-33}$$

$$z = D z^+ \qquad u = v' u^+$$

$$\rho = \rho_o \rho^+ \qquad v' = \sqrt{\overline{v^2}}$$

Substituting these terms into C-31

$$\frac{\partial}{\partial \tau}(\rho^+ \bar{U}^+) + \nabla^+ \circ (\rho^+ \bar{\bar{V}}^+ \bar{U}^+) + \frac{gL}{U_o^2}\rho^+ + \frac{\partial}{\partial x^+}\bar{P}^+$$

$$- \frac{1}{3}\frac{\mu}{\rho_o L U_o}\frac{\partial}{\partial x}(\nabla^+ \cdot \vec{V}^+) \tag{C-34}$$

$$\frac{\mu}{\rho_o L U_o}\nabla^{+2}\bar{U}^+ + \left(\frac{v'}{U_o}\right)^2 \nabla^+ (\rho^+ \vec{v}^+ u^+) = 0$$

By examining the nondimensional coefficients we obtain four groups. These are

$$\frac{L}{D}, \quad \frac{gL}{U_o^2}, \quad \frac{\mu}{\rho_o L U_o}, \quad \text{and} \quad \frac{v'}{U_o}$$

Performing a similar analysis of the turbulent portion of the momentum equation different scale factors are used for time, length and velocity. These scale factors are the ones most closely associated with the turbulent condition

Λ - scale of turbulence $\qquad \nabla = \frac{1}{\Lambda}\nabla^+$

$v' = \sqrt{\overline{v^2}}$ - R.M.S. turbulent velocity $\qquad \nabla^+ = \mathbb{i}\frac{\partial}{\partial x^+} + \mathbb{j}\frac{\partial}{\partial y^+} + \mathbb{k}\frac{\partial}{\partial z^+}$

$$t = \frac{\Lambda}{v'}\tau \qquad z = \Lambda z^+ \qquad P = \rho_o v'^2 P^+$$

$$x = \Lambda x^+ \qquad \vec{v} = v'\vec{v}^+$$

$$y = \Lambda y^+ \qquad u = v' u^+$$

Substituting into C-32 one finds that

$$\frac{\partial}{\partial \tau}(\rho^+ u^+) + \frac{U_0}{v'} \nabla^+ \cdot \left(\rho^+ \vec{\bar{V}}^+ u^+\right) + \frac{\bar{U}_0}{v'} \nabla^+ \cdot \left(\rho^+ \vec{v}^+ \bar{U}^+\right)$$
$$+ \nabla^+ \cdot (\rho^+ \vec{v}^+ u^+) - \nabla^+ \cdot \left(\overline{\rho^+ \vec{v}^+ u^+}\right) + \frac{\partial}{\partial x^+} p^+$$
$$- \frac{1}{3} \frac{\mu}{\rho_0 v' \Lambda} \frac{\partial}{\partial x^+}(\nabla^+ \cdot \vec{v}^+) + \frac{\mu}{\rho_0 v' \Lambda} \nabla^{+2} u^+ = 0$$

There are two dimensionless groups associated with this differential equation

$$\frac{U_0}{v'} \quad \text{and} \quad \frac{\rho_0 v' \Lambda}{\mu}$$

The first was obtained previously. The second term can be rewritten in terms of the main duct Reynolds number and intensity of turbulence

$$\frac{\rho_0 v' \Lambda}{\mu} = \frac{\rho_0 \bar{U}_0 L}{\mu} \left(\frac{v'}{U_0}\right)\left(\frac{\Lambda}{L}\right)$$

In summary nondimensionalizing the integrand of the control volume momentum equation results in five dimensionless groups. These groups can be reduced to five independent parameters

$$\frac{L}{D}, \ \frac{\rho_0 L U_0}{\mu}, \ \frac{v'}{U_0}, \ \frac{\Lambda}{L}, \ \text{and} \ \frac{gL}{U_0^2}$$

By scaling these five parameters or the most significant of the five original groups will result in the successful momentum scaling of the system. This scaling includes both steady state and turbulence considerations and is therefore a completely general statement.

Boundary Conditions

The boundary conditions are included by integrating over the entire control volume. Applying the divergence theorem to equation C-28

$$\iiint\limits_{V_{c.v}} \left[\frac{\partial}{\partial t}(\rho \vec{V}) + \rho g \mathbf{i} - \nabla \cdot \mathbb{P} \right] d\mathcal{V}_{cv} + \oiint\limits_{S_{c.v}} \rho \vec{V}(\vec{V} \cdot \mathbf{n})\, dS = 0 \qquad \text{C-35}$$

The second term is identically zero except at the inlets and outlet. Assuming constant properties across these areas the second term is

$$\oiint\limits_{S_{c.v.}} \rho \vec{V}(\vec{V} \cdot \mathbf{n})\, dS = \rho_e V_e^2 A_e \mathbf{j} + \rho_j V_j^2 A_j \mathbf{j} - \rho_o U_o^2 A_o \mathbf{i}$$

The first term of equation C-35 may be written

$$\rho_o U_o^2 L^2 \left\{ \iiint\limits_{V^+_{c.v}} \left[\frac{\partial}{\partial \tau}(\rho^+ \vec{V}^+) + \frac{gL}{U_o^2} \rho^+ \mathbf{i} + \cdots \right] dV^+_{cv} \right\}$$

where the large scale nondimensionalization procedure is utilized. This term maintains a similarity condition between the model and the full sized system as long as the five parameters are satisfied. Substituting these last two relationships into equation C-35

$$\rho_o U_o^2 L^2 \left\{ \iiint\limits_{V_{c.v}} \left[\frac{\partial}{\partial \tau}(\rho^+ \vec{V}^+) + \frac{gL}{U_o^2} \rho^+ \mathbf{i} + \cdots \right] dV^+_{cv} + \frac{\rho_e V_e^2 A_e}{\rho_o U_o^2 L^2} \mathbf{j} + \frac{\rho_j V_j^2 A_j}{\rho_o U_o^2 L^2} \mathbf{j} - \frac{A_o}{L^2} \mathbf{i} \right\} = 0$$

The term inside the large brackets must be zero. More exactly, each component of the vector within the bracket must be zero. Since the integral term has already been scaled then the remaining groups are those necessary to scale the boundary conditions.

$$\frac{\rho_j V_j^2 A_j}{\rho_o U_o^2 L^2}, \quad \frac{\rho_e V_e^2 A_e}{\rho_o U_o^2 L^2}, \quad \text{and} \quad \frac{A_o}{L^2}$$

C.3.2.1 Motion of a Single Particle in a Turbulent Stream

To determine the interaction of turbulence and particle motion associated with this problem, a single particle in a turbulent field will be rigorously analyzed. A number of authors point out that for certain limiting conditions the turbulent dispersion of a dilute solid phase is very closely related to the dynamics of a single particle in an accelerating flow field. The flow about such a particle has been obtained analytically through the work of Oseen, Basset, and Boussinesq. These equations were later modified by Tchen (11) in order to obtain a form applicable to a particle caught up in a turbulent eddy. The limitations on the applicability of this equation to turbulent dispersion are

1. Particle spherical and so small that its relative motion gives rise to resistance according to Stokes' law.
2. Particle small when compared with smallest wavelength of turbulence.
3. Dispersion effect of shear flow is negligible.

These limitations are taken directly from Soo (10). There are additional implied constraints which are considered (and discussed at some length) by Hinze (12).

The equation for an accelerating particle in an infinite accelerating fluid is determined to be

$$\frac{4}{3}\pi a^3\left(\hat{\rho}_p + \frac{\rho_0}{2}\right)\frac{d}{dt}\vec{V}_p = 6\pi a\mu(\vec{V}-\vec{V}_p) + 2\pi a^3\rho_0\frac{d}{dt}\vec{V} + 6a^2\rho_0\sqrt{\pi\nu}\int_{-\infty}^{t}\frac{\frac{d}{d\xi}\left[\vec{V}(\xi)-\vec{V}_p(\xi)\right]}{\sqrt{t-\xi}}\,d\xi \qquad \text{C-36}$$

A good deal of insight may be gained from this equation with just a general acknowledgment of the turbulent field in which it is flowing. It is possible to nondimensionalize the turbulent portion of this equation using R.M.S. turbulent velocity and a representative length scale. This nondimensionalization gives certain relevant information when the various dimensionless coefficients are sized and compared.

First, equation C-36 is written in terms of the mean and turbulence terms. The turbulent portion of the equation is:

$$\frac{d}{dt}\vec{v}_p = \frac{9}{2}\frac{\nu}{a^2}\left(\frac{\hat{\rho}_p}{\rho_0}+\frac{1}{2}\right)^{-1}(\vec{v}-\vec{v}_p) + \frac{3}{2}\left(\frac{\hat{\rho}_p}{\rho_0}+\frac{1}{2}\right)^{-1}\frac{d}{dt}\vec{v} + \frac{9}{2}\frac{1}{a}\frac{\hat{\rho}_p}{\rho_0}\sqrt{\frac{\nu}{\pi}}\int_{-\infty}^{t}\frac{\frac{d}{d\xi}\left[\vec{v}(\xi)-\vec{v}_p(\xi)\right]}{\sqrt{t-\xi}}\,d\xi \qquad \text{C-37}$$

Using the nondimensionalization procedure as outlined previously, equation C-37 is transformed to obtain

$$\frac{d}{d\tau}(\vec{v}_p^{\,+}) = \frac{9}{2}\left[\frac{\nu\Delta}{a^2 v'}\right]\left(\frac{\hat{\rho}_p}{\rho_0}+\frac{1}{2}\right)^{-1}(\vec{v}^{\,+}-\vec{v}_p^{\,+}) + \frac{3}{2}\left(\frac{\hat{\rho}_p}{\rho_0}+\frac{1}{2}\right)^{-1}\frac{d}{d\tau}(\vec{v}^{\,+}) + \frac{9}{2}\left[\frac{\nu\Delta}{a^2 v'}\right]^{\frac{1}{2}}\frac{1}{\sqrt{\pi}}\left(\frac{\hat{\rho}_p}{\rho_0}+\frac{1}{2}\right)^{-1}\int_{-\infty}^{\tau}\frac{\frac{d}{d\eta}\left[\vec{v}^{\,+}(\eta)-\vec{v}_p^{\,+}(\eta)\right]}{\sqrt{\tau-\eta}}\,d\eta \qquad \text{C-38}$$

A number of authors have disregarded this last term and this can be shown to be reasonable by sizing the various coefficients of equation C-38.

For a solid particle (sp gr ≃ 2.5) in air

$$\frac{\hat{\rho}_p}{\rho_0} = O(10^3), \text{ so that } \frac{\hat{\rho}_p}{\rho_0}+\frac{1}{2} \simeq \frac{\hat{\rho}_p}{\rho_0}$$

By the constraint on the relative size of the particle compared with that of the turbulence scale

$$\frac{\Lambda}{a} \gg 1.0$$

Finally, in order to satisfy the Stokes' flow constraint

$$\frac{\nu}{a v'} \geq O(1.0)$$

Now we can compare the first term with the second and it is apparent that the first term is larger by a factor of

$$\frac{\nu}{a v'} \frac{\Lambda}{a} \gg 1.0$$

The first term is larger than the third by a factor of this term to the one-half power.

Now the dynamic equation for the particle flow subject to the constraints outlined earlier can be written as

$$\frac{d}{d\tau}(\vec{v}_p^{\,+}) = \frac{9}{2} \frac{\nu}{a v'} \frac{\Lambda}{a} \frac{\rho_0}{\rho_p} (\vec{v}^{\,+} - \vec{v}_p^{\,+}) \qquad \text{C-39}$$

This dimensionless group is exactly the same as was obtained from the previous analysis (equation C-35) using a gas and particle cloud approximation. As was stated earlier, the same results should be obtained irrespective of the approach used. Of course, these results are not new or unique, and a number of authors have used this term in correlating turbulent dispersion data. The results of these correlations can be seen in papers by Householder and Goldschmidt (13), Ahmadi (14), and Soo (15).

C.3.3 Summary of the Dimensional Analysis

It has been found that the nondimensionalization of the governing equations in the differential form (section C.3.1) or in the integral form coupled with the equation of motion for a single particle in a turbulent field (section C.3.2) yield results which are nearly the same. A discussion of these results follows along with Table C.3 which summarizes the dimensionless groups obtained with each approach.

The first four dimensionless groups in Table C.3 have the same form for each approach but differ in the characteristic value for length that is used. Since geometric similarity is to be maintained, i.e., L/D is constant, it is arbitrary as to which length is selected. The fifth group, with both techniques, is obtained from the equation of motion of the particles. The resulting group in the left-hand column includes in it the term on the right-hand side. The additional terms in the left-hand column arise from the use of different characteristic values in nondimensionalization. However, since these additional terms are the third and fourth dimensionless groups, the final term in each column will be the same.

The sixth term was included in the integral approach and relates the gravity to inertia forces, i.e., the Froude number. It is expected that this number would have also been obtained with differential equation approach if the body force term were not assumed to be negligible. However, when the effect of gravity is evaluated by determining the slip velocity of a particle as a result of the gravitational forces, the assumption of the first analysis is shown to be reasonable. Therefore, this term was not retained for further design considerations.

Group 7, which only appears in the second column, is a reiteration of Group 1 since A_o is proportional to D^2. Group 7 therefore is equal to Group 1 squared.

Groups 8 and 9 at first glance might appear to indicate a significant

	Section C.3.1	Section C.3.2
1	$\frac{L}{D}$	$\frac{L}{D}$
2	$\frac{\rho U_o D}{\mu}$	$\frac{\rho U_o L}{\mu}$
3	$\frac{v'}{U_o}$	$\frac{v'}{U_o}$
4	$\frac{\Lambda}{L}$	$\frac{\Lambda}{L}$
5	$\frac{FD}{U_o}=\frac{\nu}{aU_o}\frac{\rho_o}{\rho_p}\frac{D}{a}$	$\frac{\nu}{v'a}\frac{\Lambda}{a}\frac{\rho_o}{\rho_p}$
6	——	$\frac{gL}{U_o^2}$
7	——	$\frac{A_o}{L^2}$
8	$\frac{\rho_j}{\rho}$	$\frac{\rho_j V_j A_j}{\rho U_o L^2}$
9	$\frac{V_j}{U_o}$	$\frac{\rho_j V_j^2 A_j}{\rho U_o^2 L^2}$

Table C.3. Summary of Dimensionless Groups Obtained by Two Techniques

difference between the two approaches, but further analysis shows that this is not the case. In the first approach when the term L/D was obtained it was assumed that this also applied to scaling the jet nozzle. For the second approach this was not assumed, and hence A_j/L^2 appears in lines 8 and 9. However, when complete geometric scaling is satisfied (including the nozzle size) the last two lines become

$$\frac{\rho_j}{\rho_o} \qquad \frac{\rho_j V_j}{\rho_o U_o}$$

and

$$\frac{V_j}{U_o} \qquad \frac{\rho_j V_j^2}{\rho_o U_o^2}$$

The two groups in the second column are combinations of the two groups in the first column. From both analyses there are two groups obtained which relate with the boundary conditions at the jet inlet to those at the main duct inlet (see Figure C.2). The difference is that terms of the second column combine the density and velocity ratios into the dynamic pressure ratio and a mass flow ratio. The dynamic pressure ratio has been shown to be a significant parameter in papers reviewed in the literature of jet injection. Therefore, it is concluded that the dimensionless groups of the second analysis provide a more physically significant way of nondimensionalizing the boundary conditions. Nevertheless, from the standpoint of scaling both techniques lead to the same set of experimental parameters for modeling the Shawnee boiler system.

C.4 Shawnee Model

In scaling the Shawnee boiler, it is desirable to satisfy as many of the dimensionless terms contained in Table C.3 as is possible. Prior to constructing the model, these dimensionless parameters were rewritten. Table C.4 summarizes the dimensionless ratios from Table C.3 and the rewritten set of independent dimensionless parameters. Here the original parameters are listed along with the independent parameters within each group. The following discussion outlines the steps in doing so term by term.

C.4.1 Geometric Scale

The term L/D is maintained by preserving the geometric similarity between the Shawnee system and the model. Hence, all dimensions were scaled linearly. In addition, the term d/D which appears within several of the dimensionless groups was also selected to preserve geometric scale. Thus, the nozzle diameter is also scaled linearly.

C.4.2 Reynolds Number

The flow Reynolds number was used for determining the scale factor for sizing the model with respect to the Shawnee system. The limit for sizing the duct was based upon the output characteristics of the existing blower system and filter. This led to the selection of 12.5 as the value for scaling the Shawnee system.

C.4.3 Turbulence Intensity Parameter, Π_2, and Turbulence Scale Parameter, Π_3

It has not been possible to obtain turbulence information for the Shawnee system. It was therefore necessary to operate the model under as wide a range of the turbulence parameters, Π_2 and Π_3, as is possible. In this way it was hoped that the scaled turbulence conditions of the

From Equation (19)	Independent Dimensionless Terms	Descriptive Term
$\frac{L}{D}$ & $\frac{d}{D}$	same: $\Pi_0 = \frac{L}{D}$ & $\Pi_0' = \frac{d}{D}$	Geometric Scale
$\frac{\rho_o U_o D}{\mu}$	same: $\Pi_1 = \frac{\rho_o U_o D}{\mu}$	Reynolds Number
$\frac{v'}{U_o}$	same: $\Pi_2 = \frac{v'}{U_o}$	Turbulence Parameter
$\frac{\Delta}{D}$	same: $\Pi_3 = \frac{\Delta}{D}$	Turbulence Parameter
$\frac{\rho_j V_j^2 d^2}{\rho_o U_o^2 D^2}$	rewritten: $\Pi_4 \times (\Pi_0')^2$ $\Pi_4 = \frac{\rho_j V_j^2}{\rho_o U_o^2}$	Dynamic Pressure Ratio
$\frac{FD}{U_o} \sim \left[\frac{v}{aU_d}\right]\left(\frac{\rho_o}{\rho_p}\right)\left(\frac{D}{a}\right)$	rewritten: Π_5 / Π_1 $\Pi_5 = \frac{\rho_o}{\rho_p}\left(\frac{D}{a}\right)^2$	Particle Interaction Parameter
$\frac{\rho_j V_j d^2}{\rho_o U_o D^2}$	(not scaled) $\Pi_6 = \frac{\rho_j V_j}{\rho_o U_o}$	Mass Flux Ratio

Table C.4 Independent Dimensionless Parameters

Shawnee boiler would be bracketed by those of the model.

C.4.4 Dynamic Pressure Ratio

In order to satisfy both the dynamic pressure ratio and mass flow ratio scaling factors, it would be necessary to scale ρ_j/ρ_o and V_j/U_o (same as dynamic pressure ratio and mass ratio). This would have required the jet dust loading to be a factor of five greater than the model feed system was capable of attaining. Therefore, it was necessary to choose between modeling to dynamic pressure ratio or the mass ratio. Based upon the results of previous authors in the field of jet trajectory studies (Table A.1), the dynamic pressure ratio was chosen as the preferable scaling term. As shown in Table C.4, the dynamic pressure ratio when separated into independent dimensionless groups results in an independent parameter, Π_4.

C.4.5 FD/U_o

The dimensionless term, FD/U_o, includes the Reynolds number, Π_1. No generality is lost in factoring out Π_1 since the overall functional dependence on this term is maintained. The grouping that is left is a term which scales the particle size and density of the two systems, Π_5.

C.5 Summary

With the guidelines stated above the model was scaled to five of the six dimensionless parameters obtained through the dimensional analysis of Section C.3. Since two of these five dimensionless groups are dependent upon the others, the groups were first separated into independent dimensionless groups. As was stated previously, the geometric scale factor of

12.5 was selected for modeling the Shawnee system. It was not possible to hold all the variables constant during operation for both the Shawnee system and the model. Table C.5 either lists the values or range of values for the independent variables shown in Table C.6 for both the Shawnee boiler and the scale model. These were the values used for sizing the nondimensional parameters.

The range of values obtained for three of the five independent pi's for both the Shawnee system and model are shown in Table C.6. The values in this table show that Π_1 and Π_4 for the model are within the operational range of the Shawnee system. The term Π_5, a single valued function, was matched as closely as was possible. Finally, the turbulence parameters, Π_2 and Π_3, for the model will hopefully bracket the values for the Shawnee system.

Shawnee	Model
$T = 2110^\circ$ F	$T = 76^\circ$ F
$\rho_o = 0.01435$ #m/ft^3	$\rho_o = .0752$ #m/ft^3
$\mu = .1245$ #m/ft-hr	$\mu = .0406$ #m/ft-hr
$\nu = 2.41 \times 10^{-3}$ ft^2/sec	$\nu = 1.5 \times 10^{-4}$ ft^2/sec
43 ft/sec $\leq U_o \leq$ 68 ft/sec	42.5 ft/sec $\leq U_o \leq$ 46 ft/sec
$\hat{\rho}_p = 150$ #m/ft^3	$\hat{\rho}_p = 167$ #m/ft^3
.53 #m/ft^3 $\leq \rho_j \leq$ .73 #m/ft^3	.663 #m/ft^3 $\leq \rho_j \leq$ .782 #m/ft^3
$V_j = 130$ ft/sec	224 ft/sec $\leq V_j \leq$ 245 ft/sec
$a \simeq 16$ microns	$a = 5$ microns
D	D/12.5

Table C.5. Independent Variables

Shawnee	Group	Model
$4.1 \times 10^5 \leq \Pi_1 \leq 6.5 \times 10^5$	$\Pi_1 = R_e = \frac{U_0 D}{\nu}$	$5.21 \times 10^5 \leq \Pi_1 \leq 5.69 \times 10^5$
$135 \leq \Pi_4 \leq 465$	$\Pi_4 = \frac{\rho_i V_j^2}{\rho_0 U_0^2}$	$209 \leq \Pi_4 \leq 331$
$\Pi_5 = 2.18 \times 10^7$	$\Pi_5 = \frac{\rho_0}{\rho_p}\left(\frac{D}{a}\right)^2$	$\Pi_5 = 6.7 \times 10^6$

Table C.6. Range of Parameters

C.6 References

1. Soo, S. L. "Fully Developed Turbulent Pipe Flow of a Gas-Solid Suspension," I & EC Fundamentals, Vol. 1, 1962, p. 33.

2. Soo, S. L., Ihrig, H. K., and El Kouh, A. F. "Experimental Determination of Statistical Properties of Two-Phase Turbulent Motions," J. of Basic Engr., September 1960, pp. 609-621.

3. Stukel, J. J., and Soo, S. L. "Turbulent Flow of a Suspension into a Channel," *Power Technology*, Vol. 2, No. 5, June 1969, pp. 278-289.

4. Boothroyd, R. G., "Similarity in Gas-Borne Flowing Particle Suspensions," *Journal of Engineering for Industry*, No. 68-MH-11, May 1969, pp. 303-313.

5. Vogt, E. G., and White, R. R. "Friction in the Flow of Suspensions," *Industrial and Engineering Chemistry*, Vol. 40, No. 9, September 1948, pp. 1731-1738.

6. Boothroyd, R. G. "Turbulence Characteristics of the Gaseous Phase in Duct Flow of a Suspension of Fine Particles," Trans. Instn. Chem. Engrs., Vol. 45, 1967, pp. T297-T310.

7. Rose, H. E., and Barnacle, H. E. "Flow of Suspensions of Non-Cohesive Spherical Particles in Pipes - No. I," *The Engineer*, Vol. 203, June 14, 1957, pp. 898-901.

8. Rose, H. E., and Barnacle, H. E. "Flow of Suspensions of Non-Cohesive Spherical Particles in Pipes - No. II," *The Engineer*, Vol. 203, June 21, 1957, pp. 939-941.

9. Kline, S. J. *Similitude and Approximation Theory*, McGraw-Hill, 1965.

10. Soo, S. L. *Fluid Dynamics of Multiphase Systems*, Blaisdell Publishing Company, 1967.

11. Tchen, C. M. "Mean Value and Correlation Problems Connected with the Motion of Small Particles Suspended in a Turbulent Fluid," The Hauge, M. Nishoff, 1947.

12. Hinze, J. O. *Turbulence*, McGraw-Hill Publishing Company, 1959.

13. Householder, M. K., and Goldschmidt, V. W. "Turbulent Diffusion and Schmidt Number of Particles," J. of Engr. Mech. Div., Vol. 95, December 1969, pp. 1345-1367.

14. Ahmadi, G. "Analytical Predictions of Turbulent Dispersion of Finite Size Particles," Ph.D. Thesis, 1970, Purdue.

15. Soo, S. L. "Statistical Properties of Momentum Transfer in a Two-Phase Flow," J. of Chem. Engr. Science, V. 5, 1956.

APPENDIX D

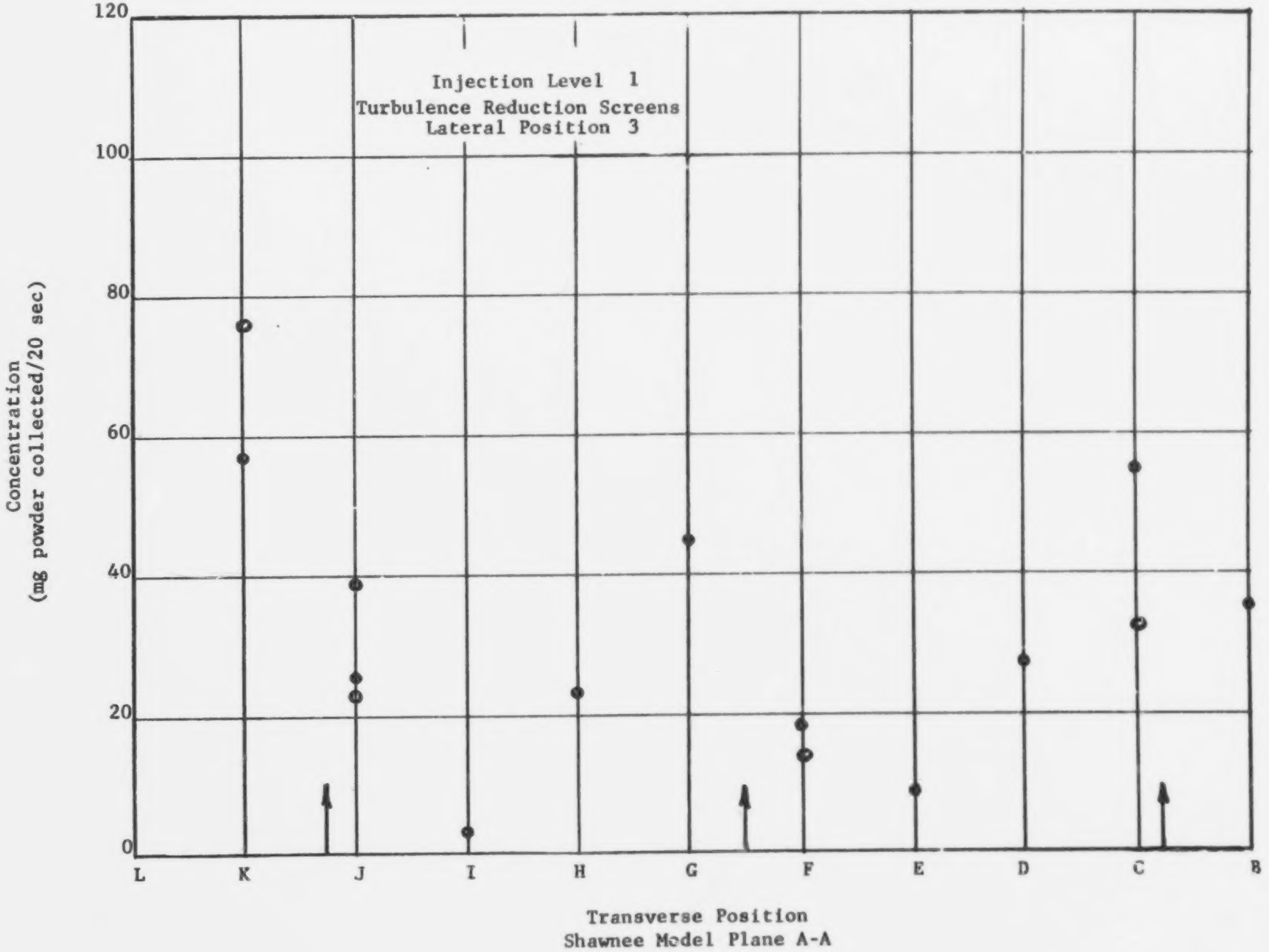

CONCENTRATION PROFILE

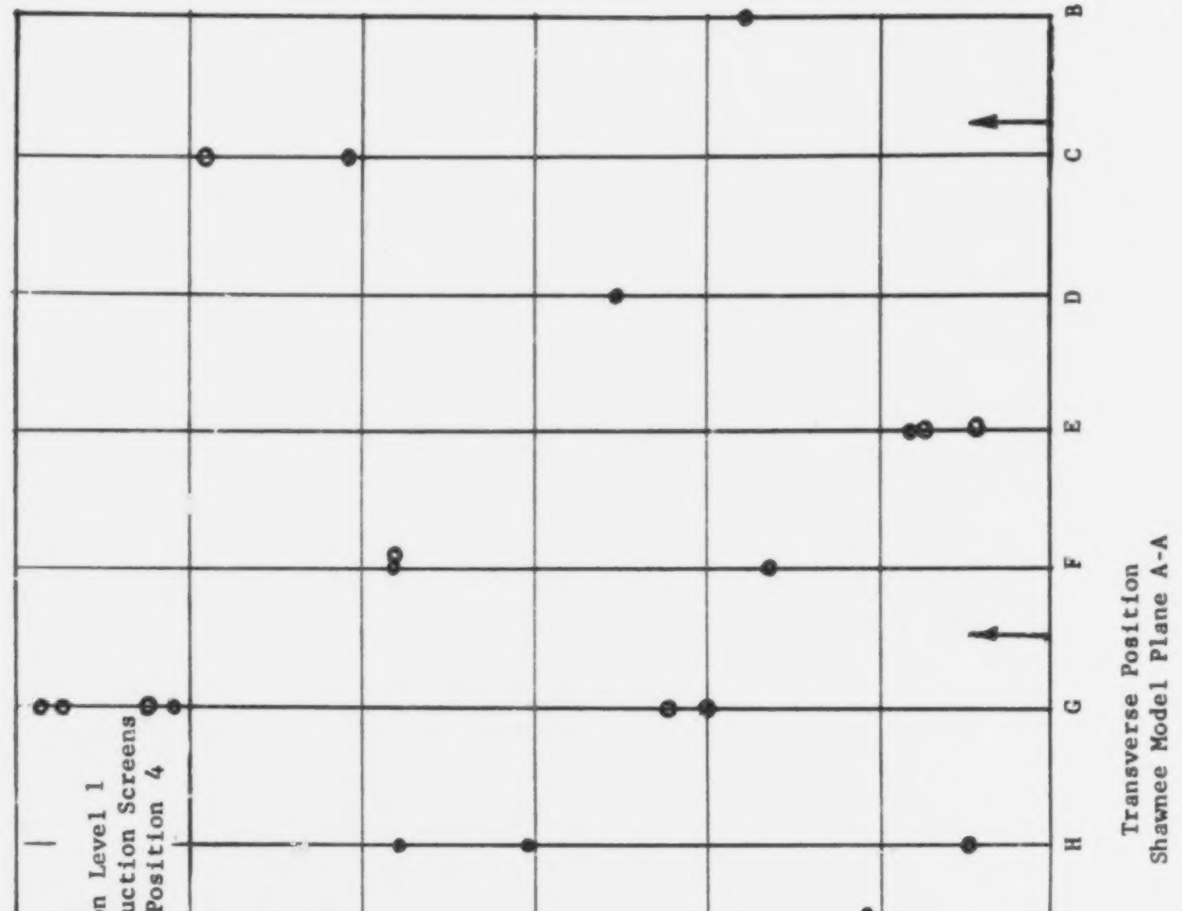

Injection Level 1
Turbulence Reduction Screens
Lateral Position 4

CONCENTRATION PROFILE

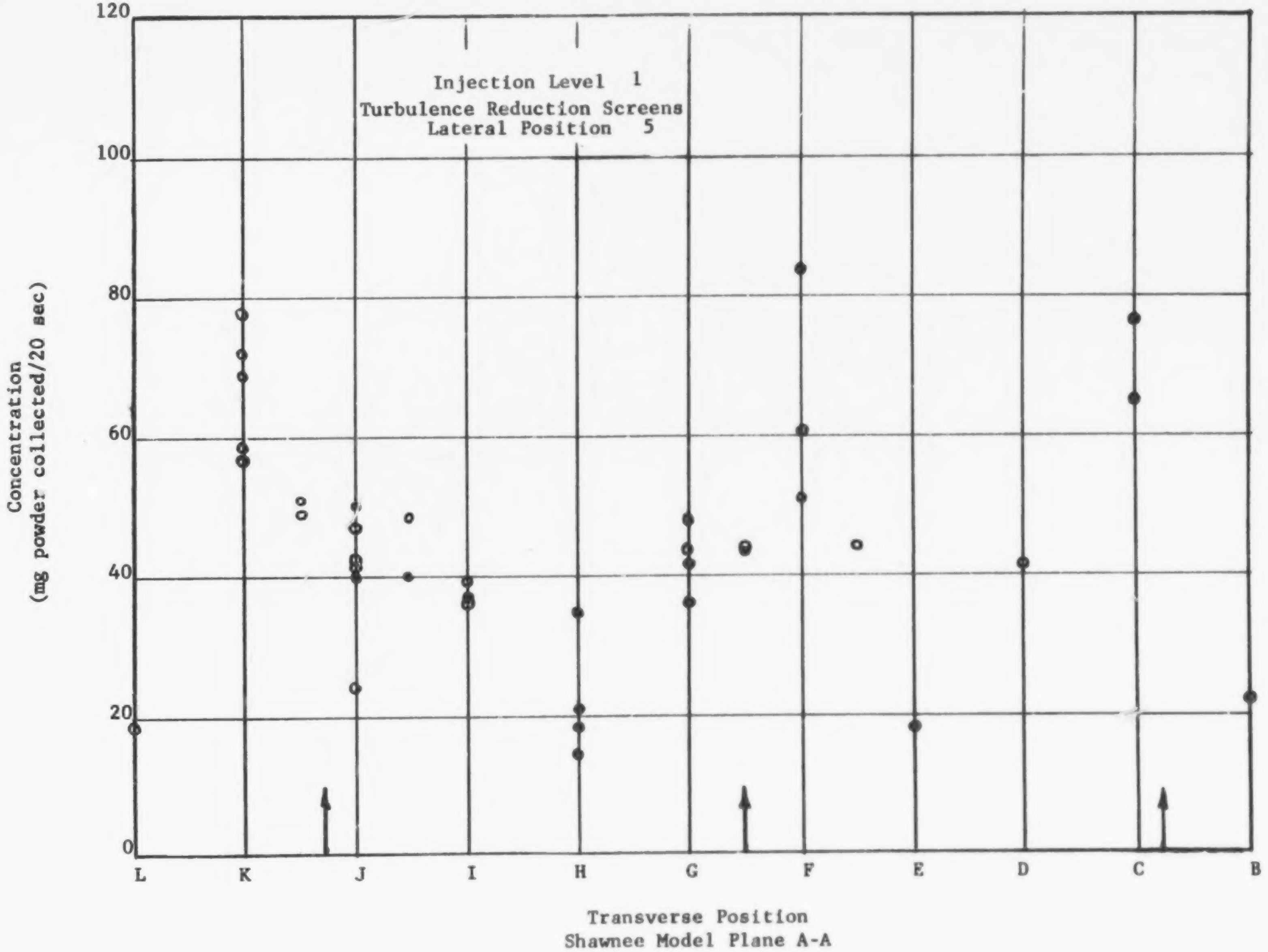

CONCENTRATION PROFILE

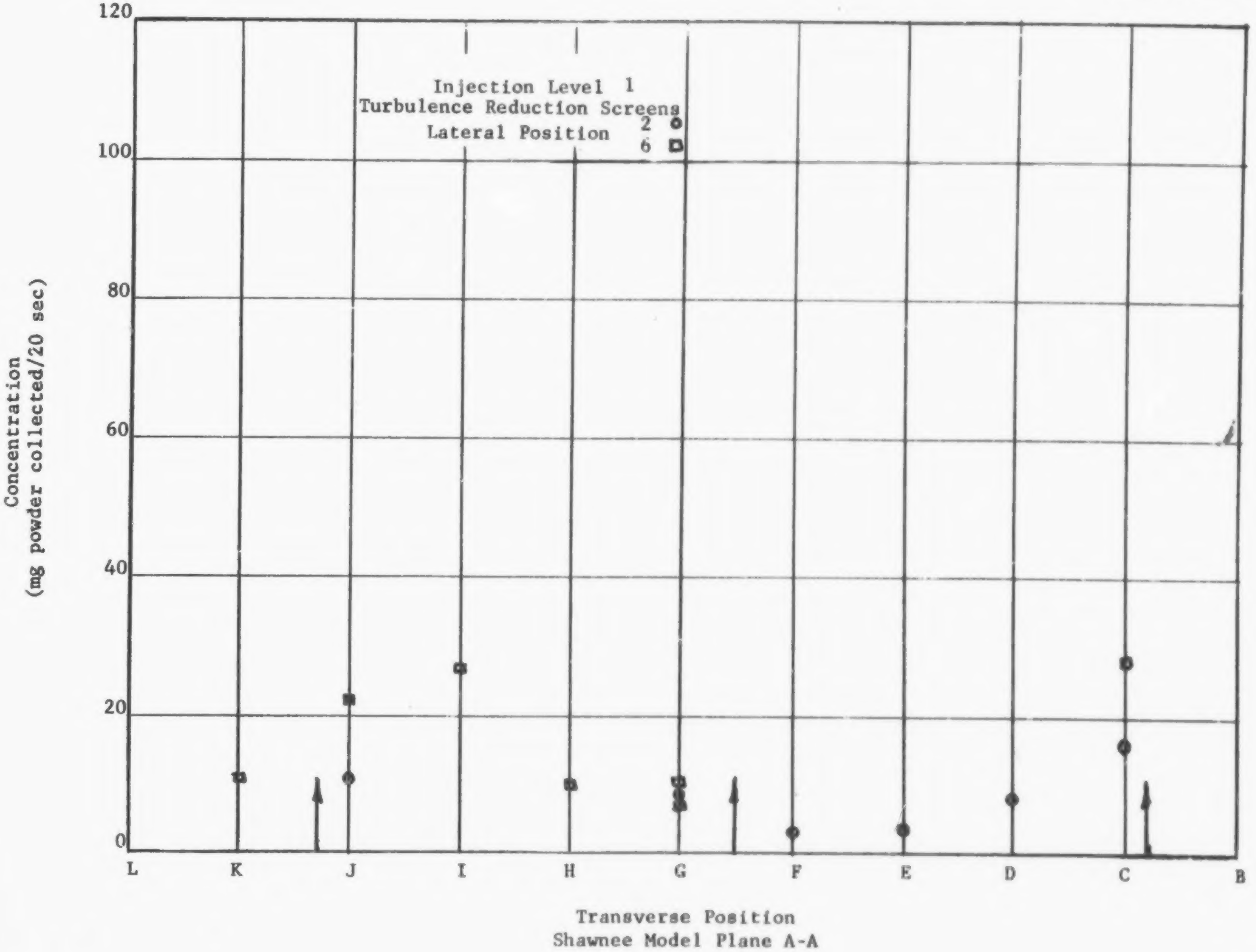

CONCENTRATION PROFILE

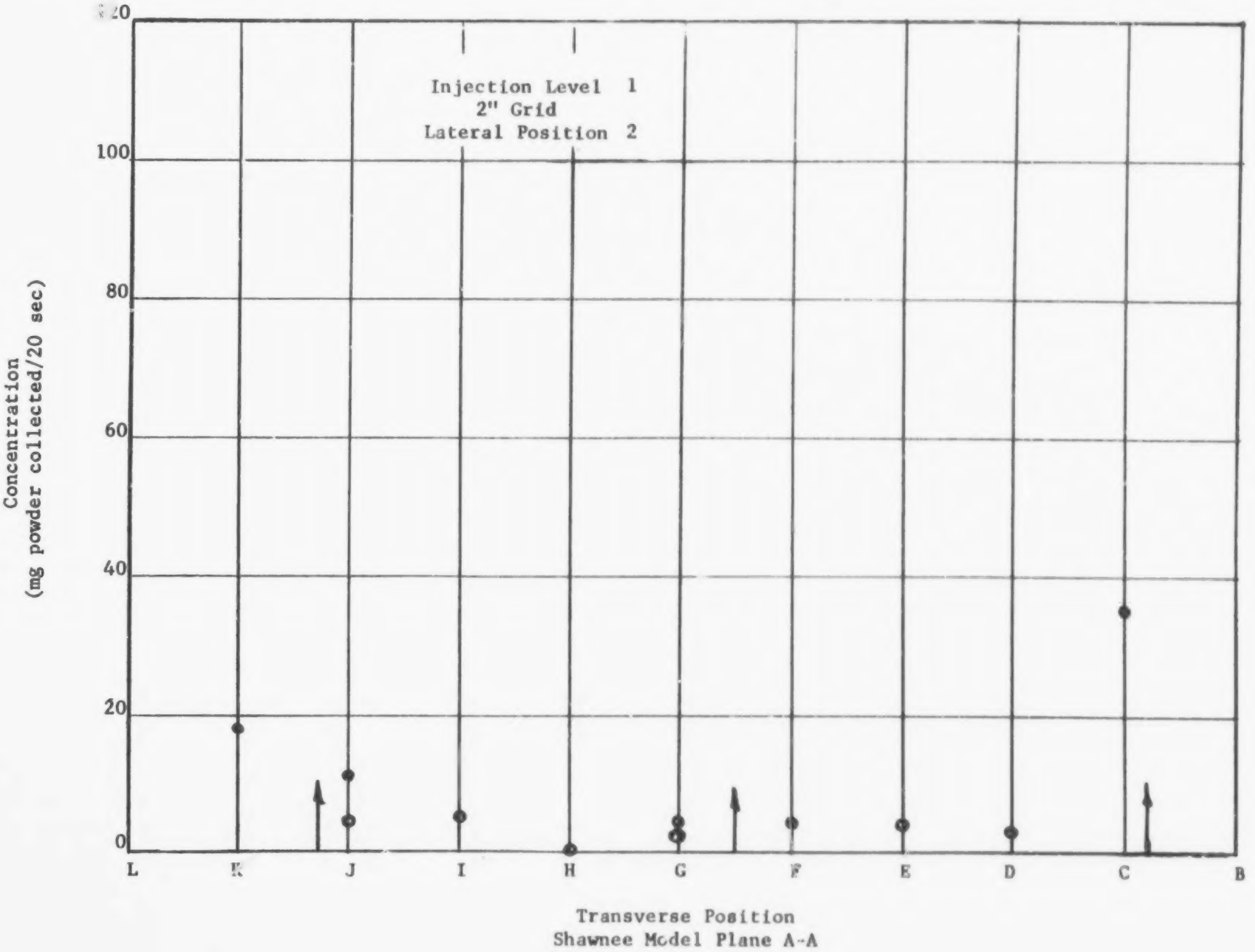

CONCENTRATION PROFILE

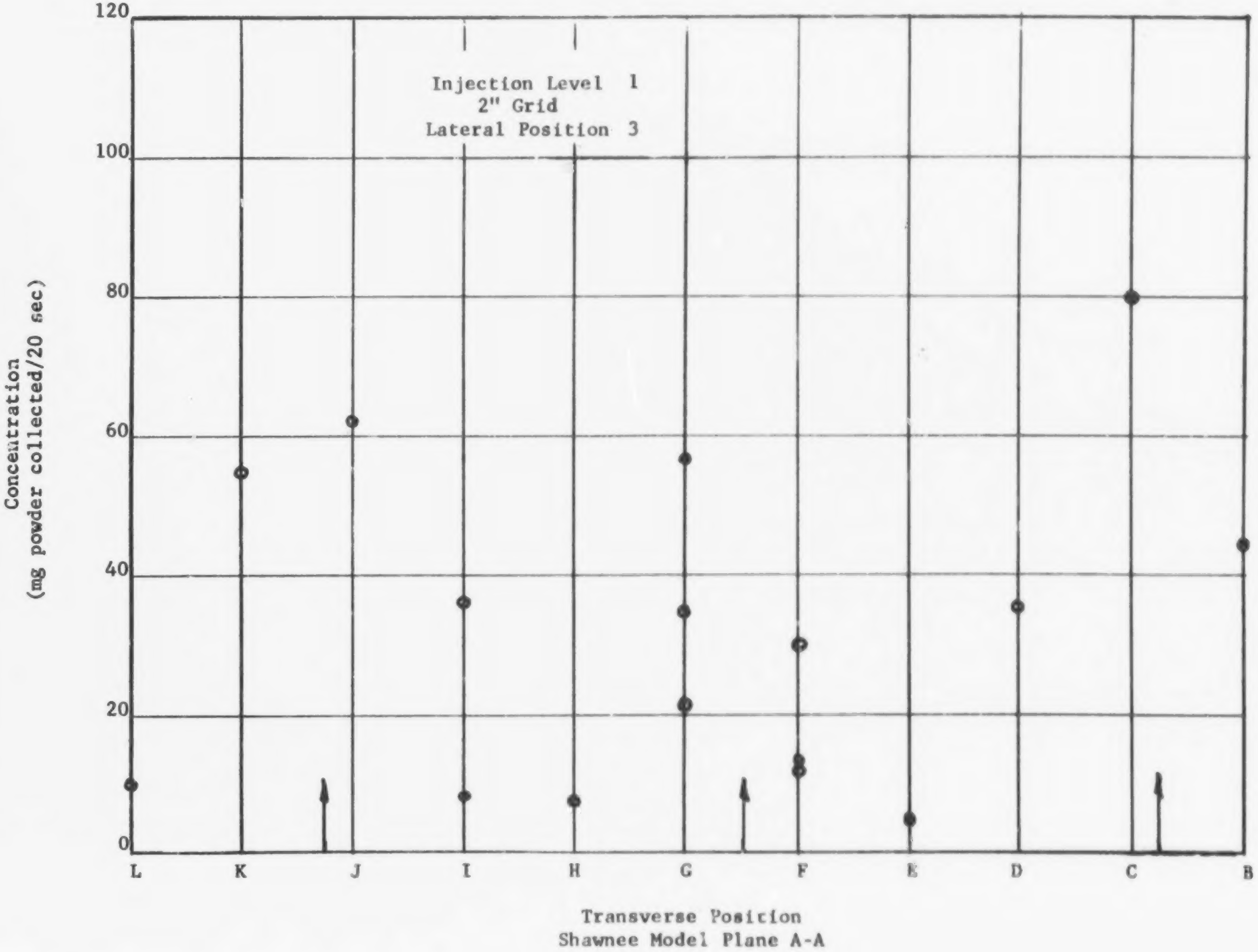

CONCENTRATION PROFILE

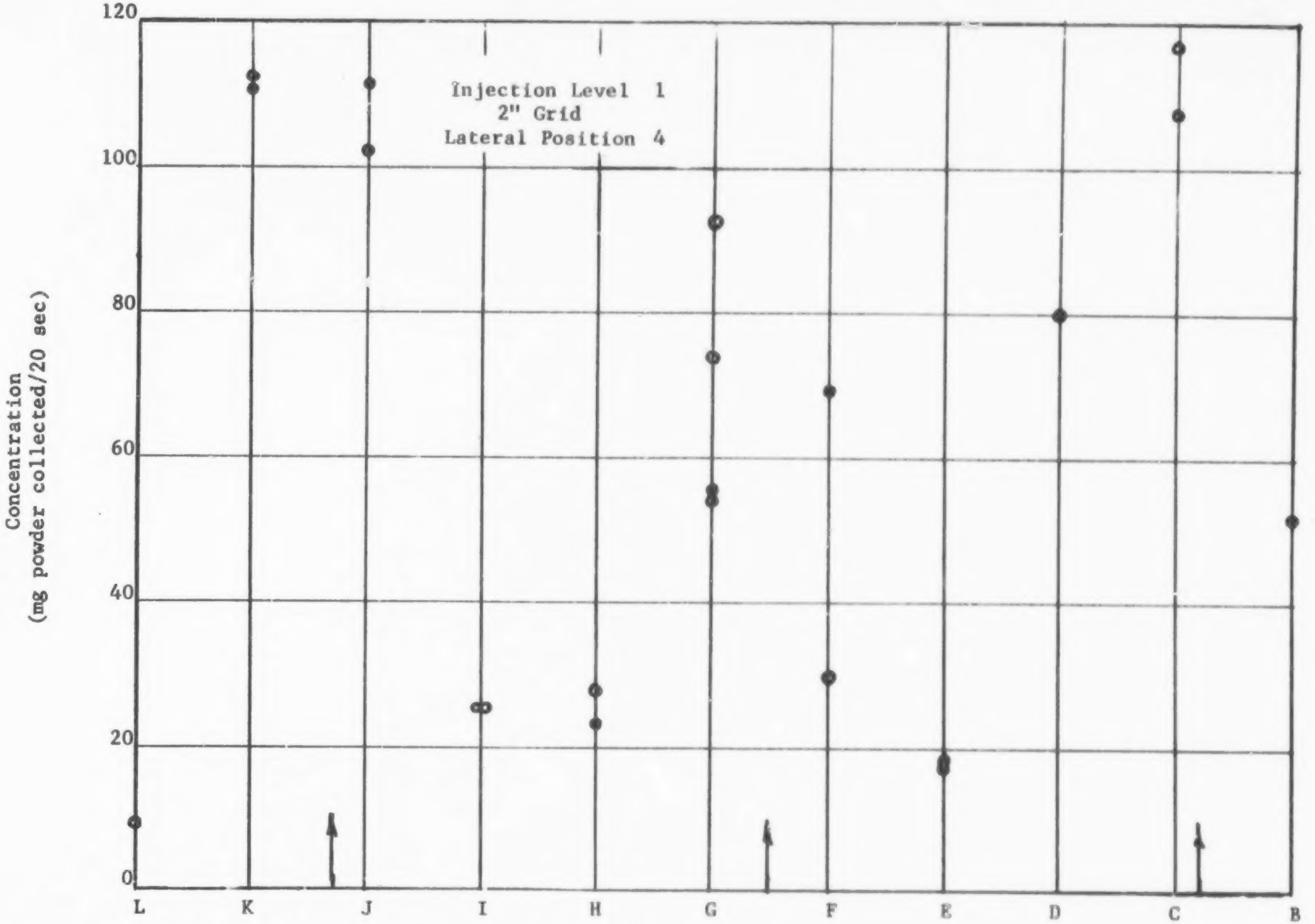

Transverse Position
Shawnee Model Plane A-A

CONCENTRATION PROFILE

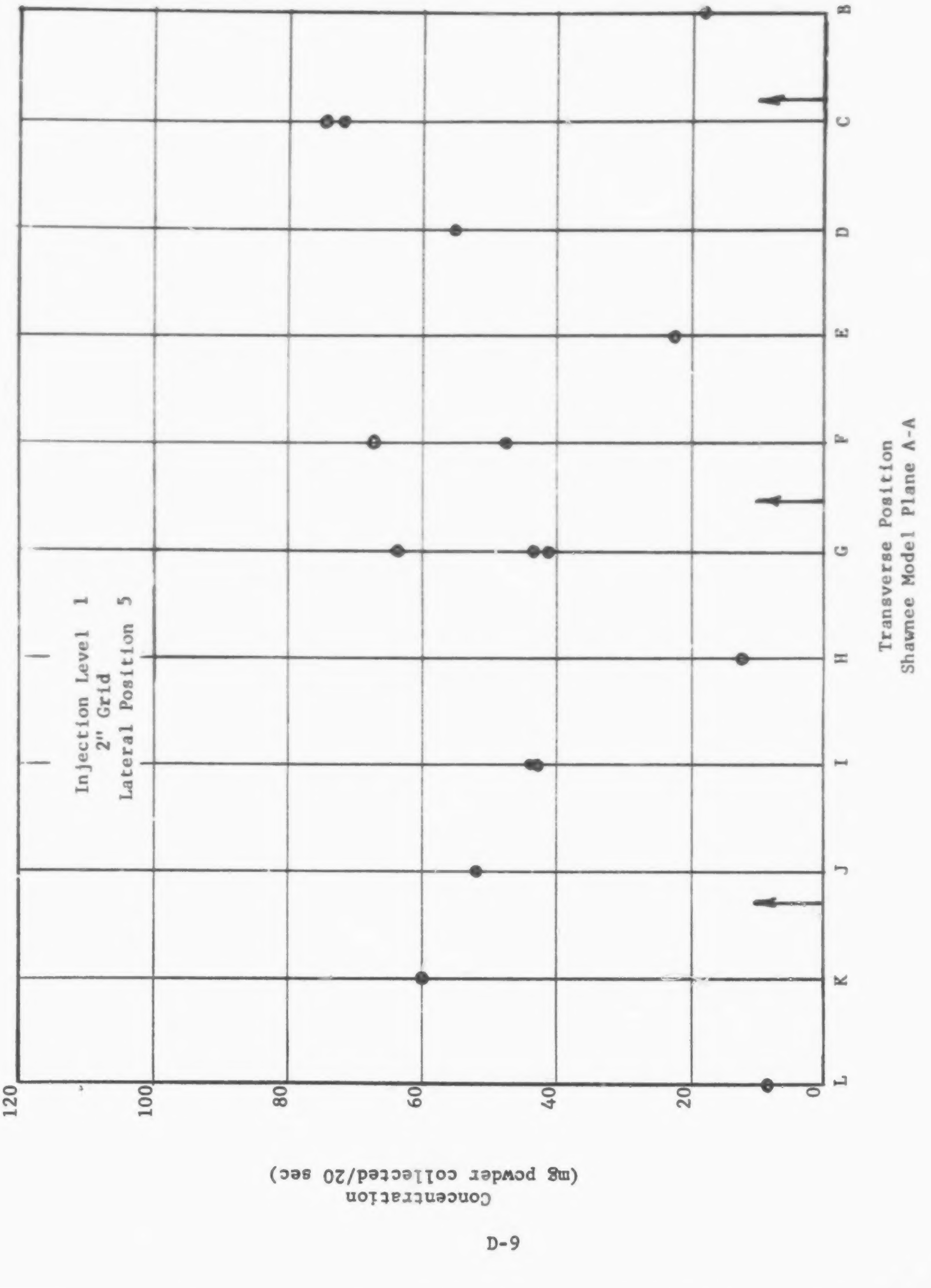

CONCENTRATION PROFILE

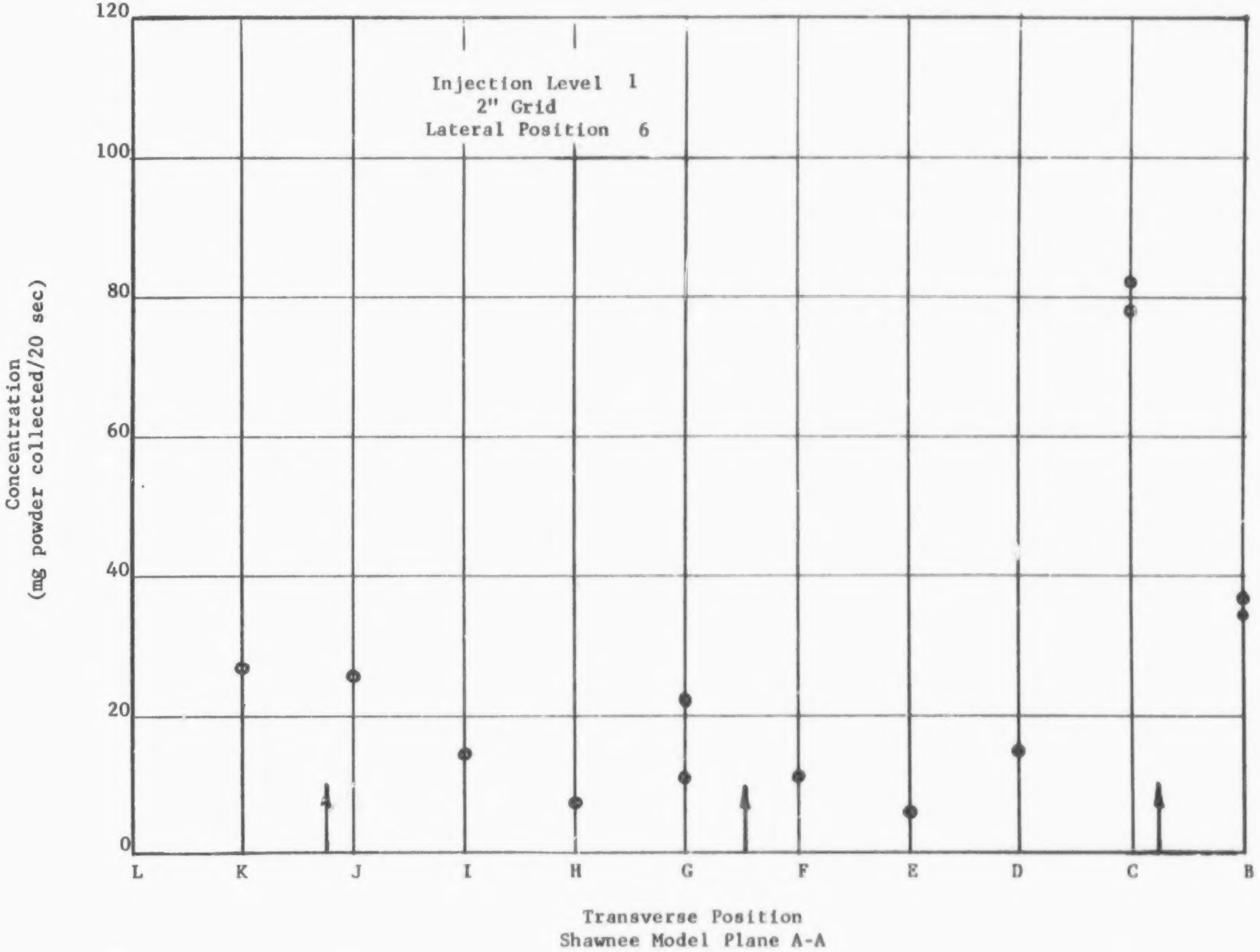

CONCENTRATION PROFILE

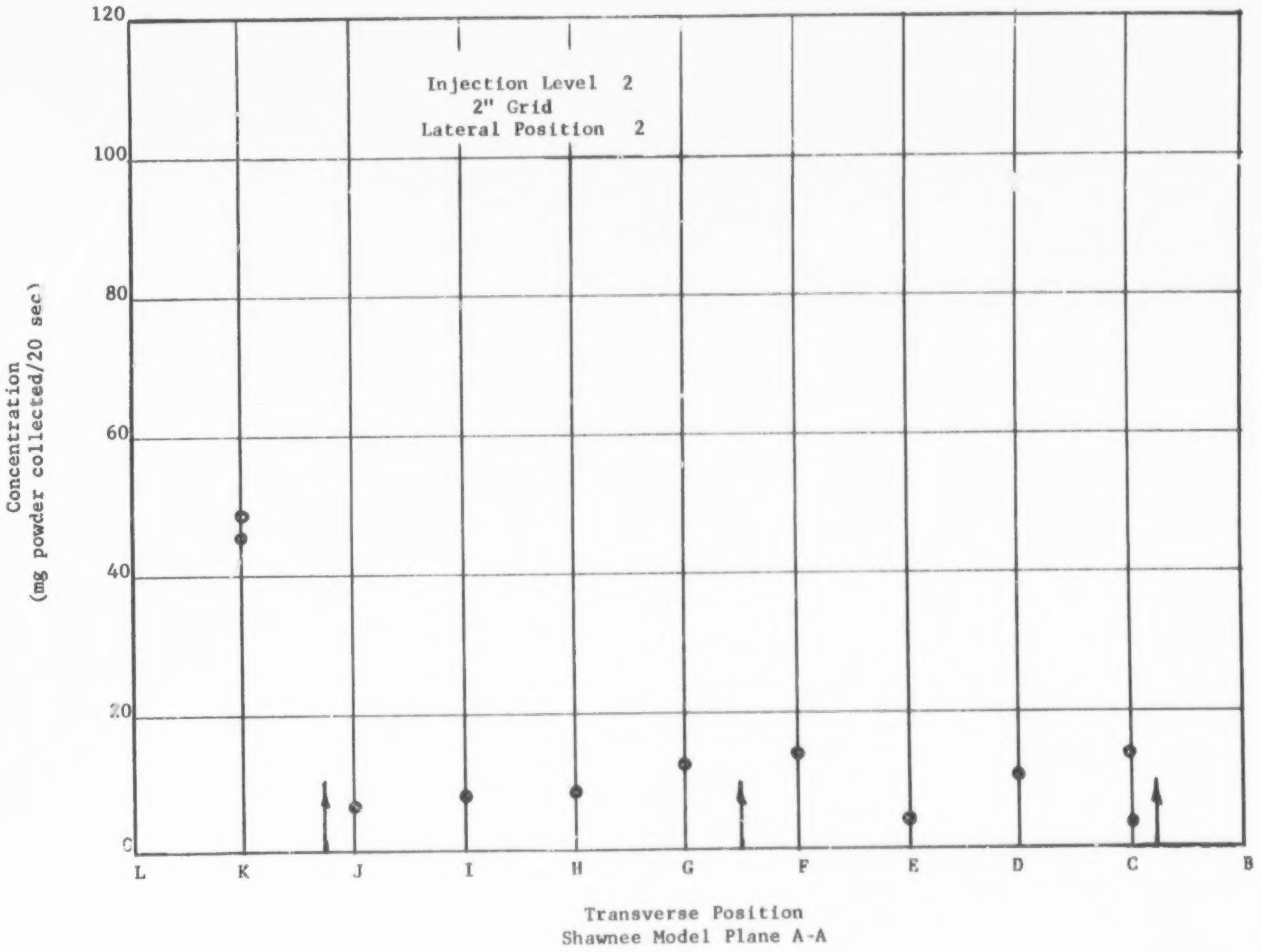

CONCENTRATION PROFILE

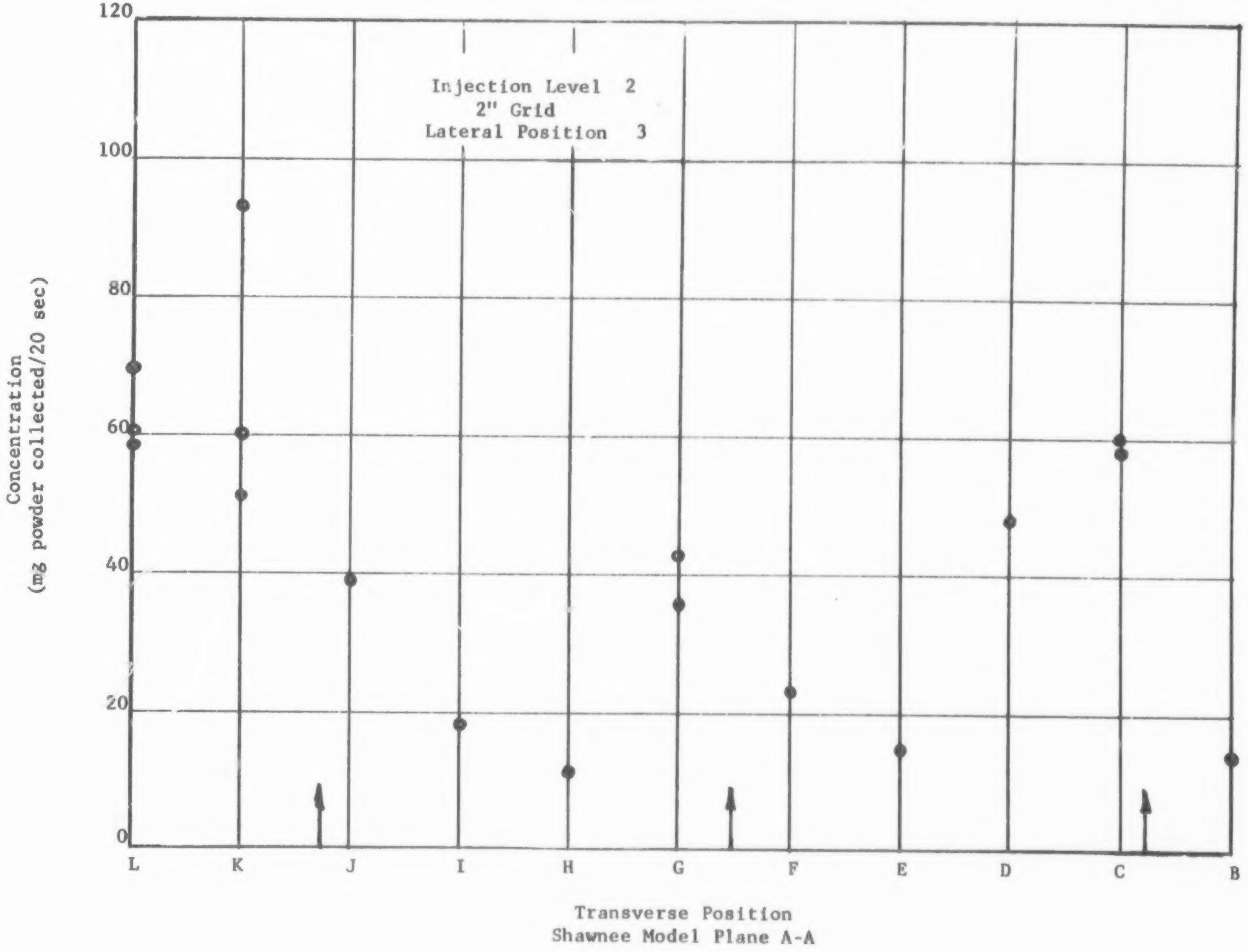

CONCENTRATION PROFILE

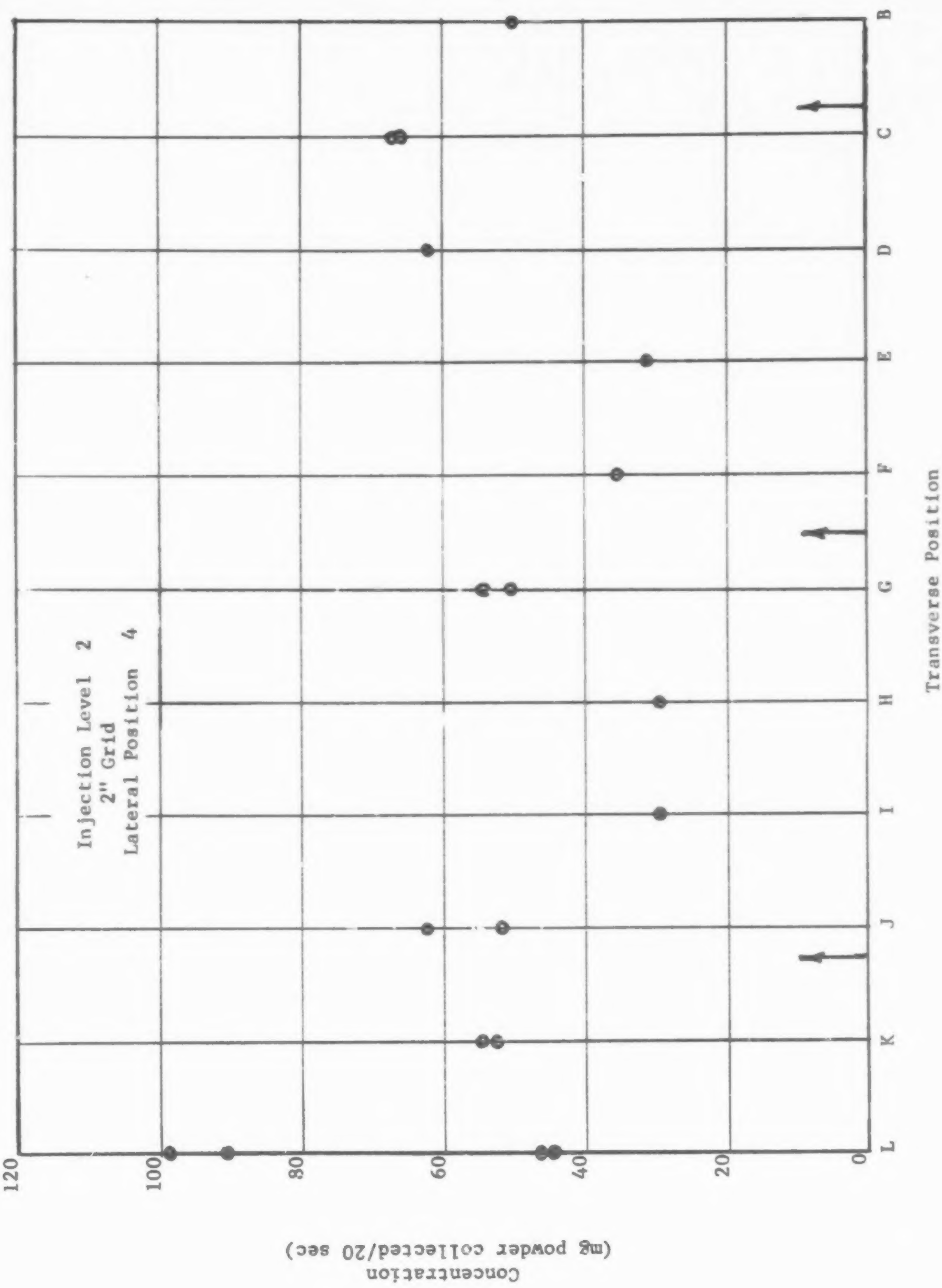

Shawnee Model Plane A-A

CONCENTRATION PROFILE

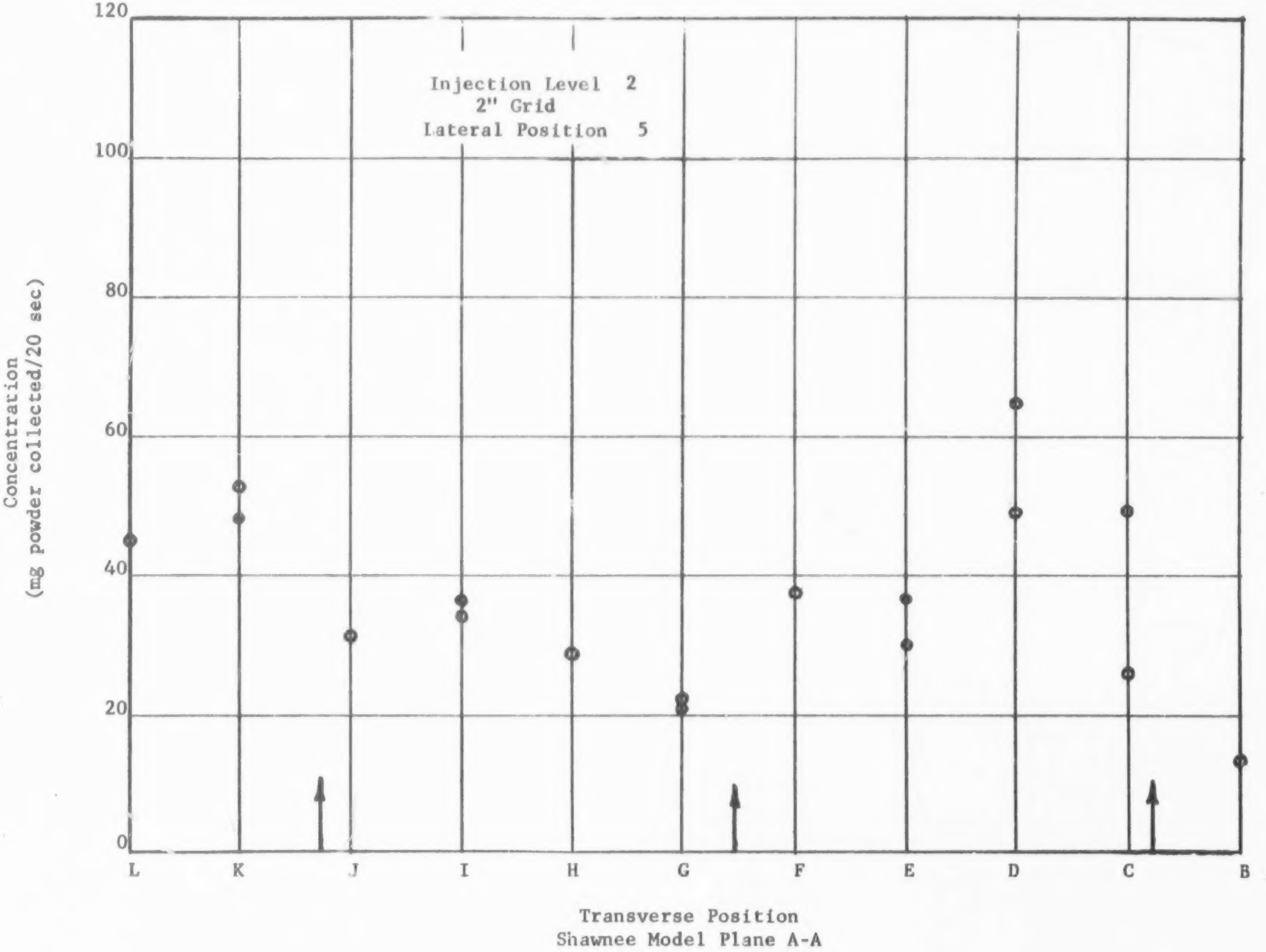

CONCENTRATION PROFILE

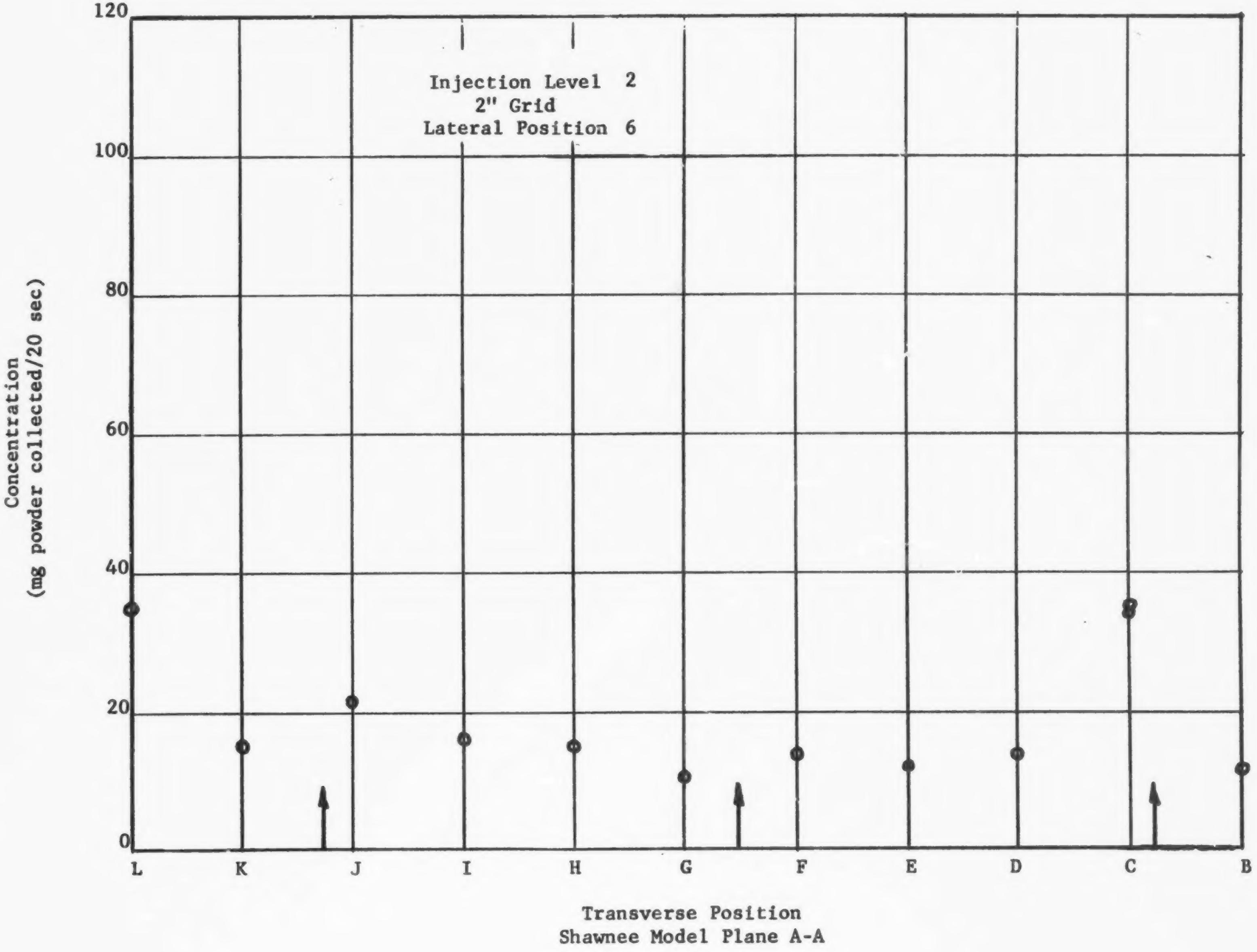

CONCENTRATION PROFILE

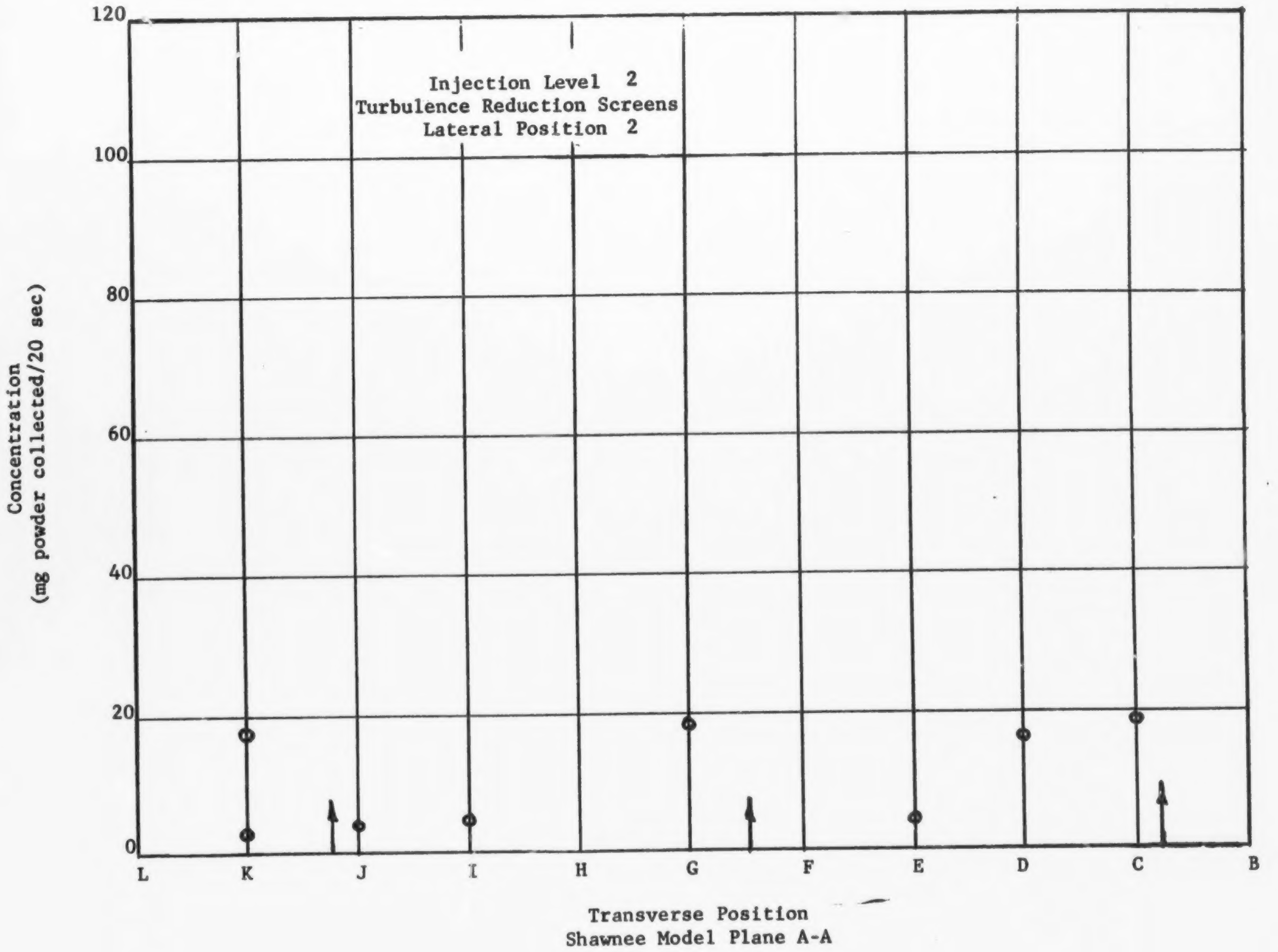

CONCENTRATION PROFILE

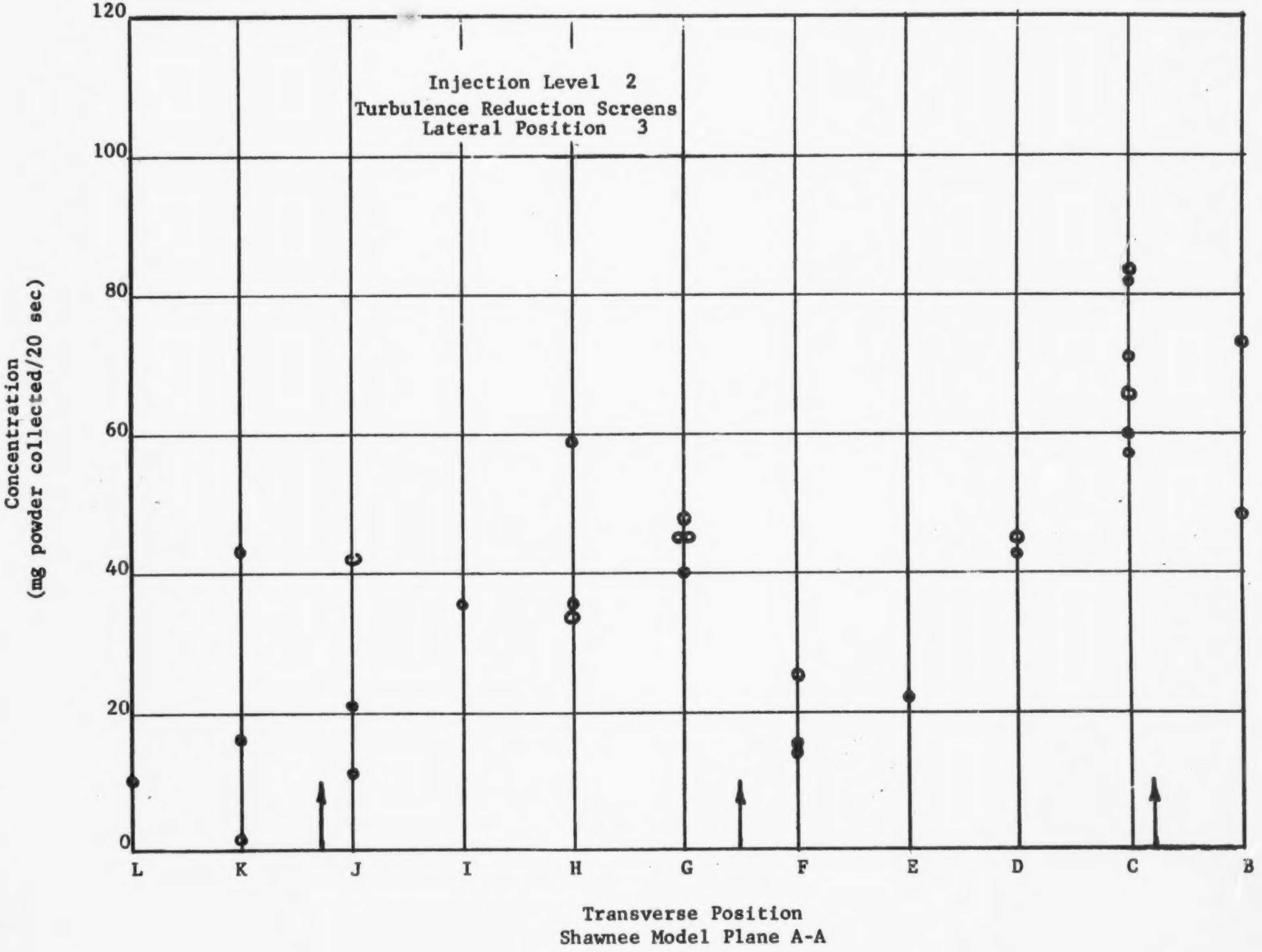

CONCENTRATION PROFILE

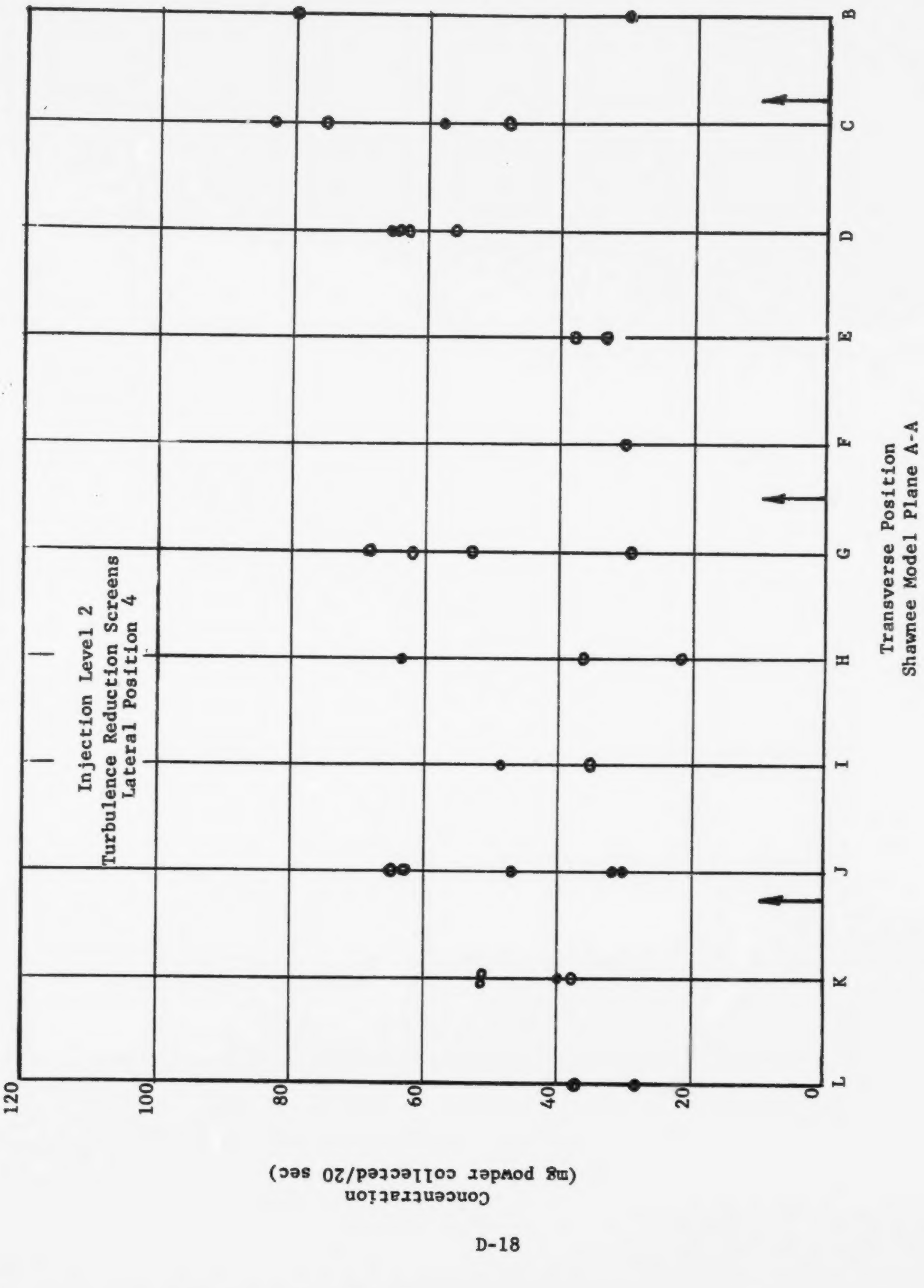

CONCENTRATION PROFILE

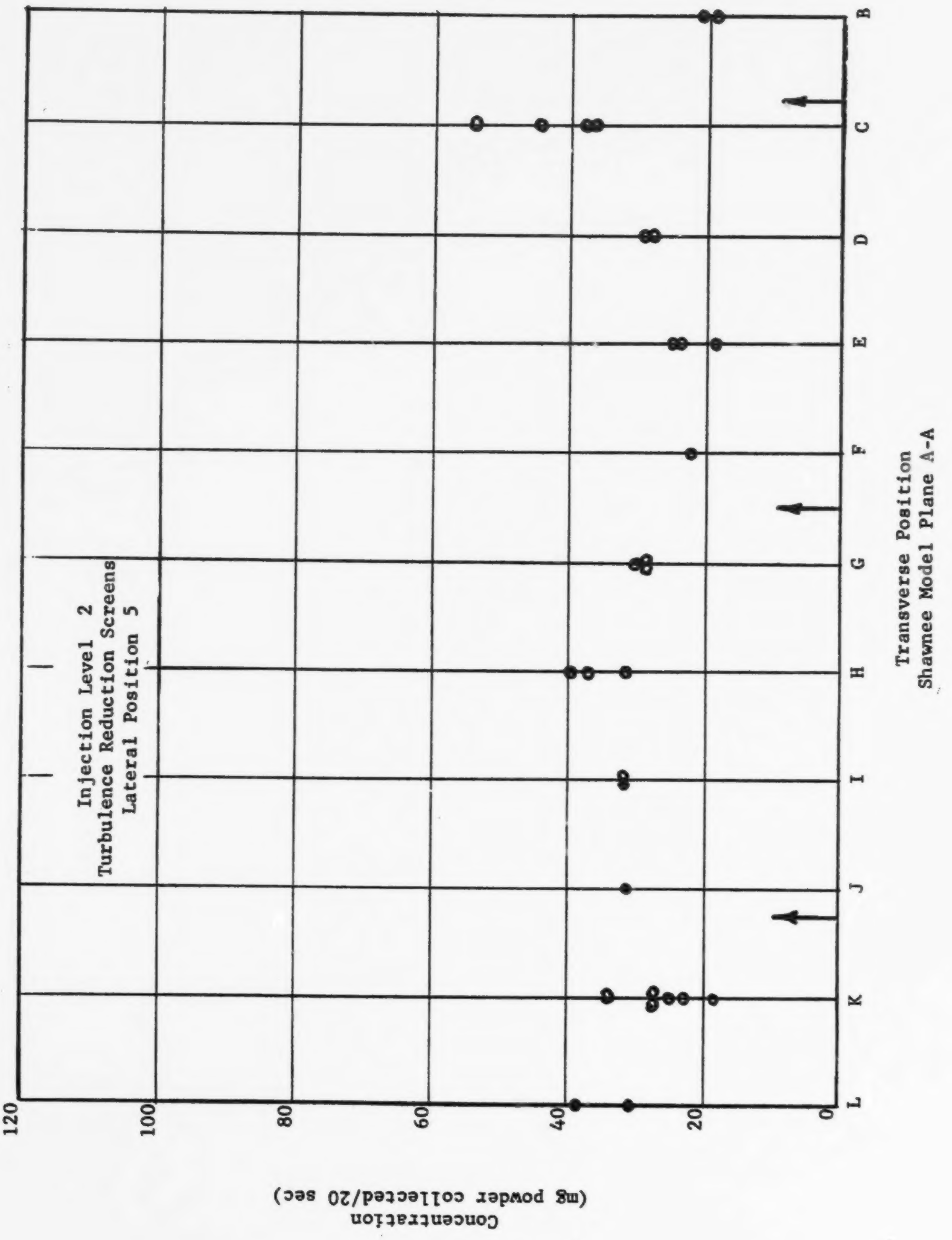

CONCENTRATION PROFILE

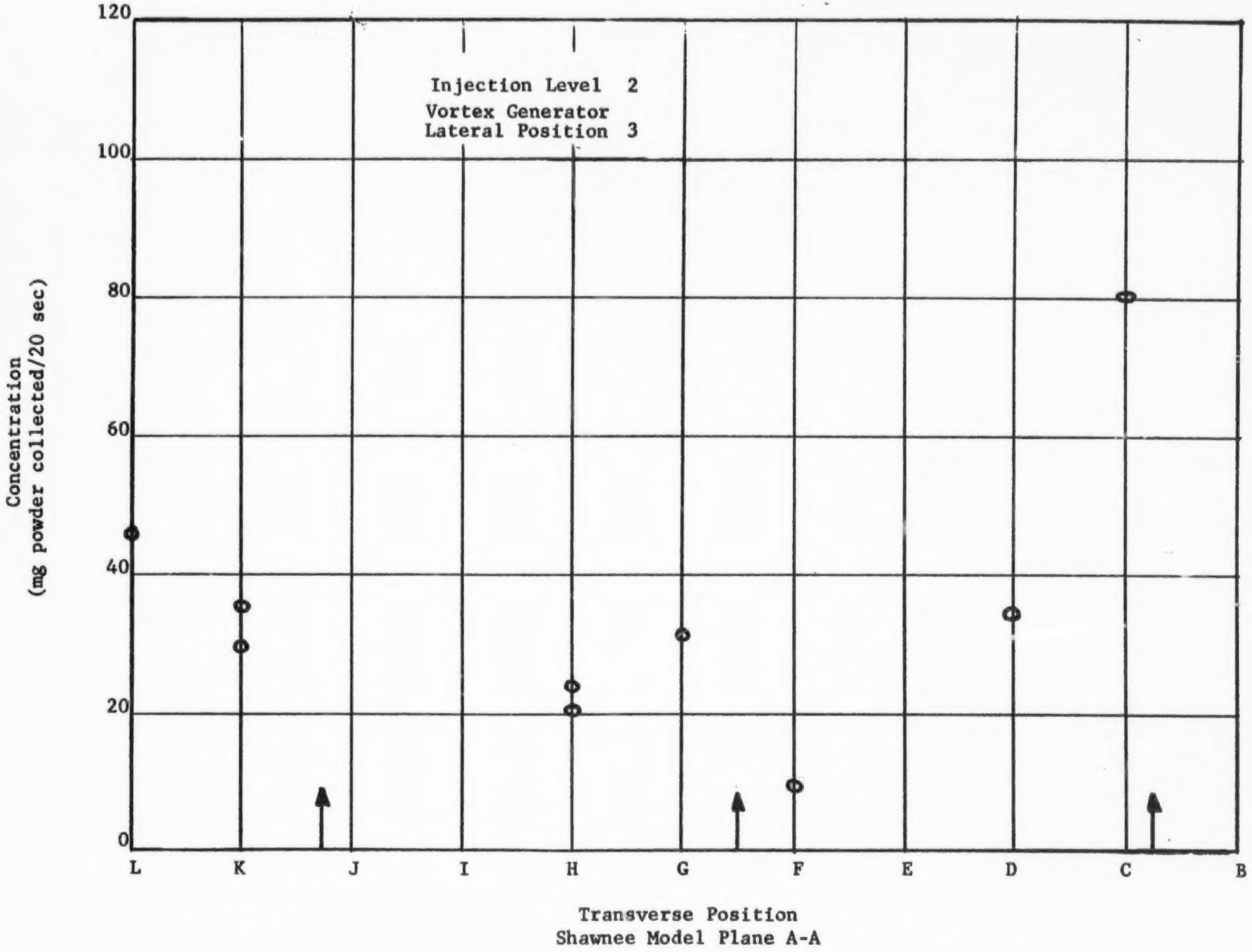

CONCENTRATION PROFILE

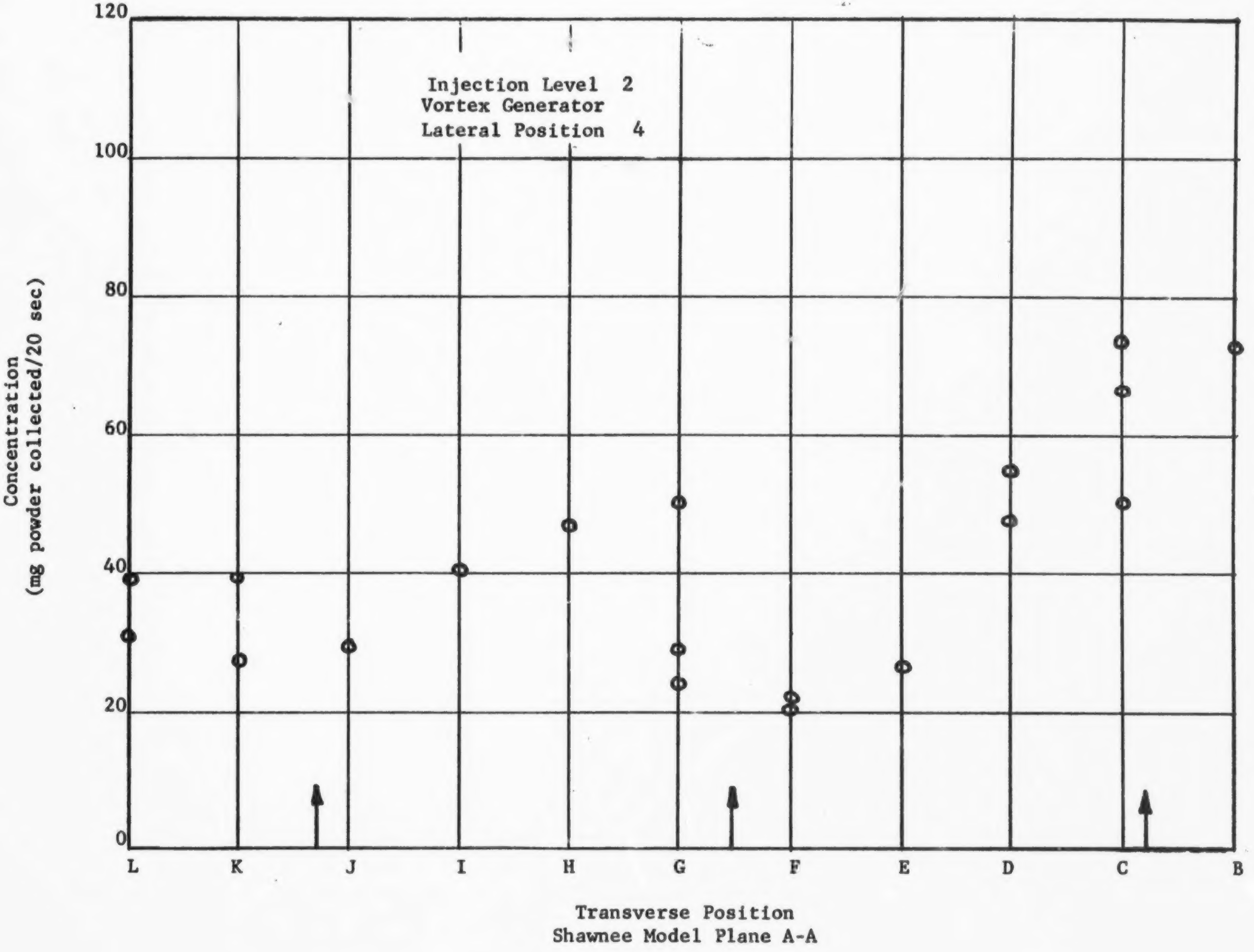

CONCENTRATION PROFILE

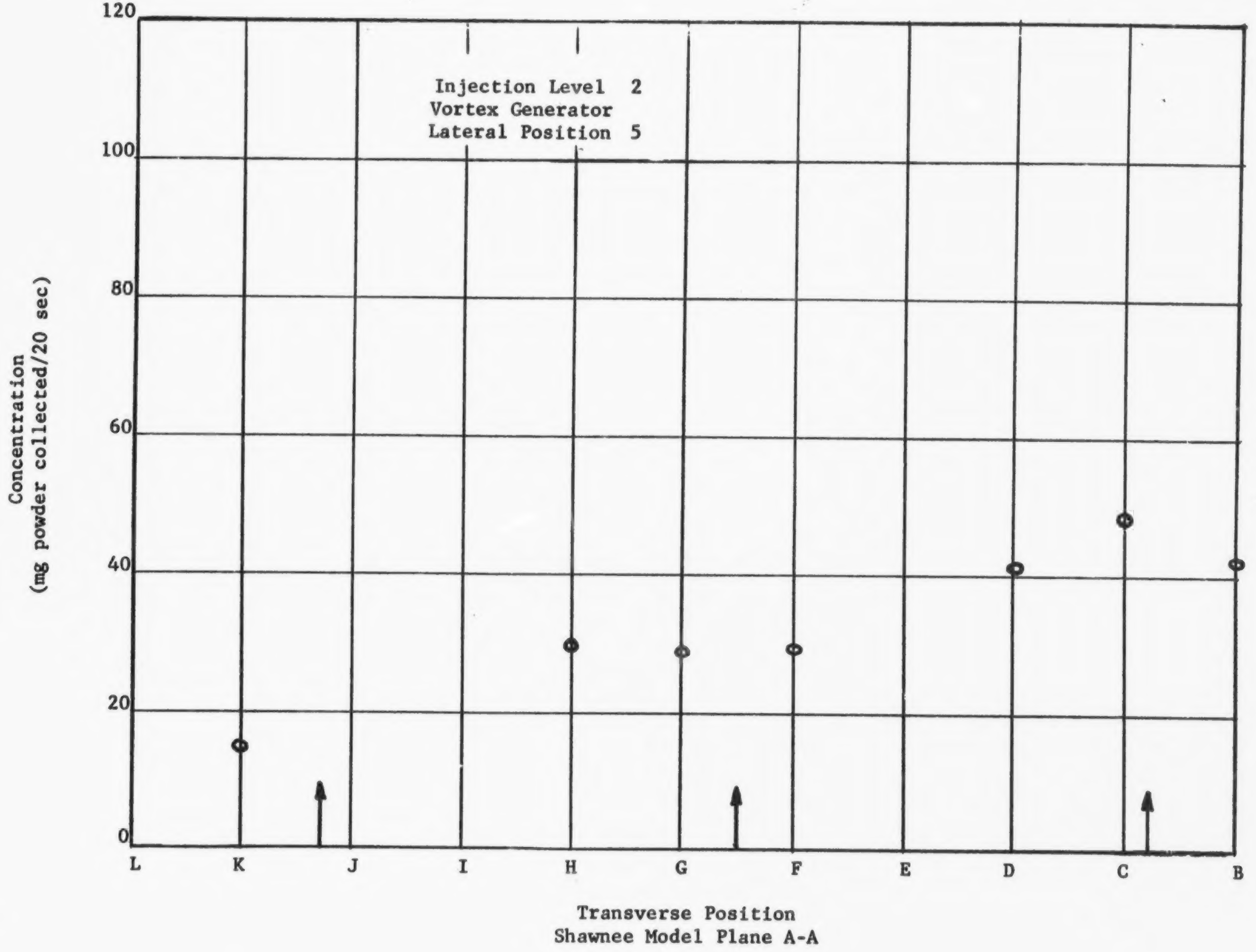

CONCENTRATION PROFILE

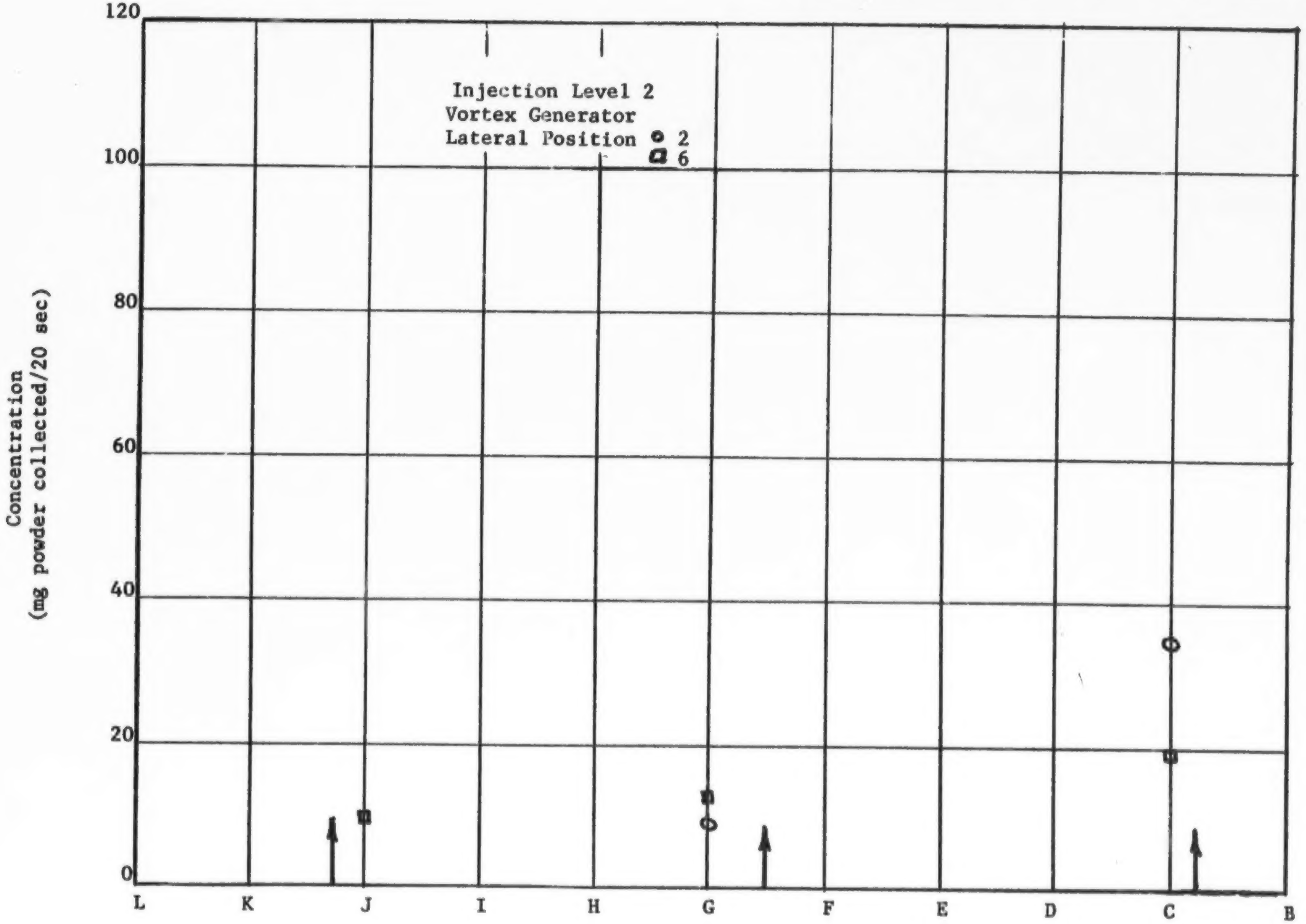

Transverse Position
Shawnee Model Plane A-A

CONCENTRATION PROFILE

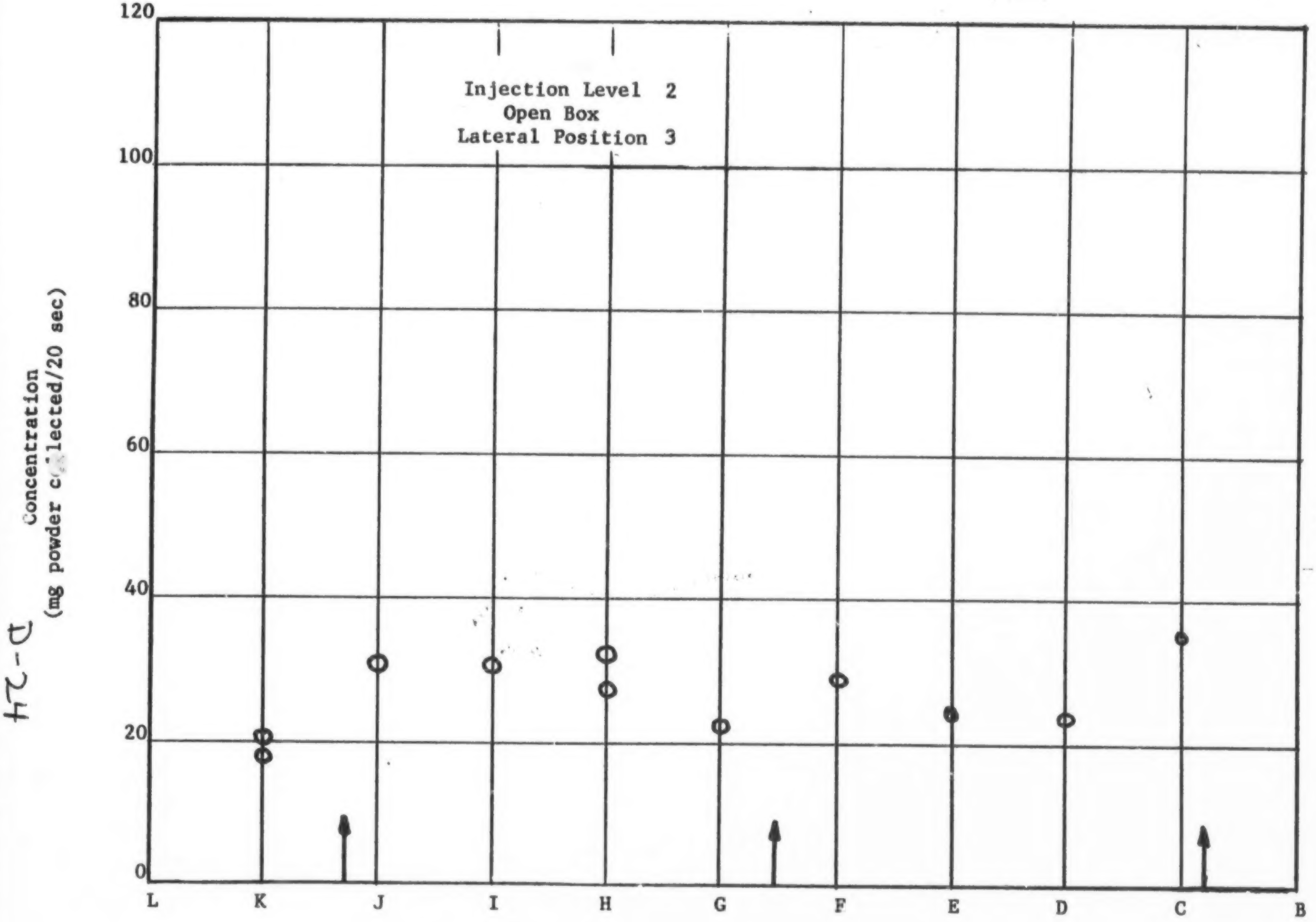

Transverse Position
Shawnee Model Plane A-A

CONCENTRATION PROFILE

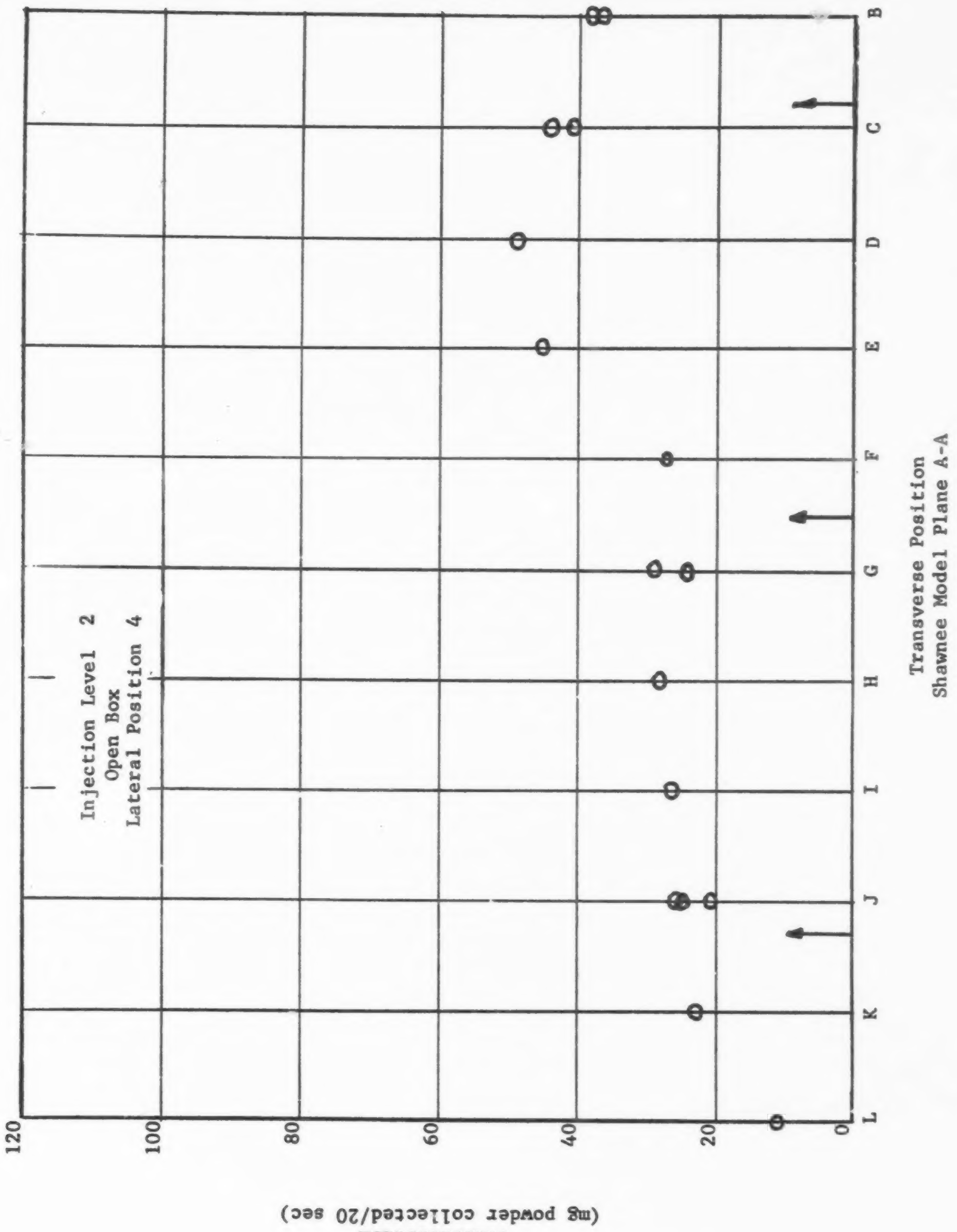

CONCENTRATION PROFILE

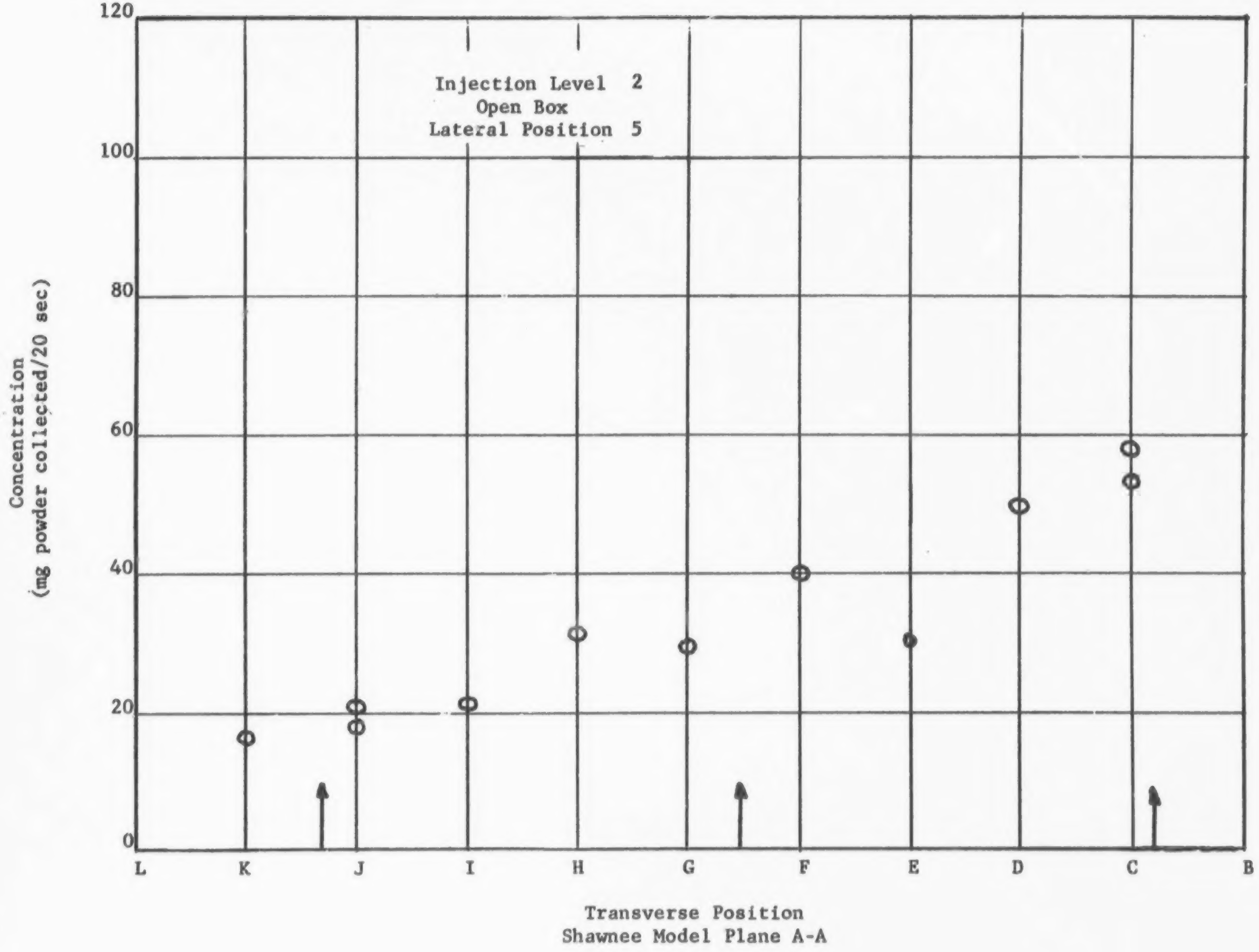

CONCENTRATION PROFILE

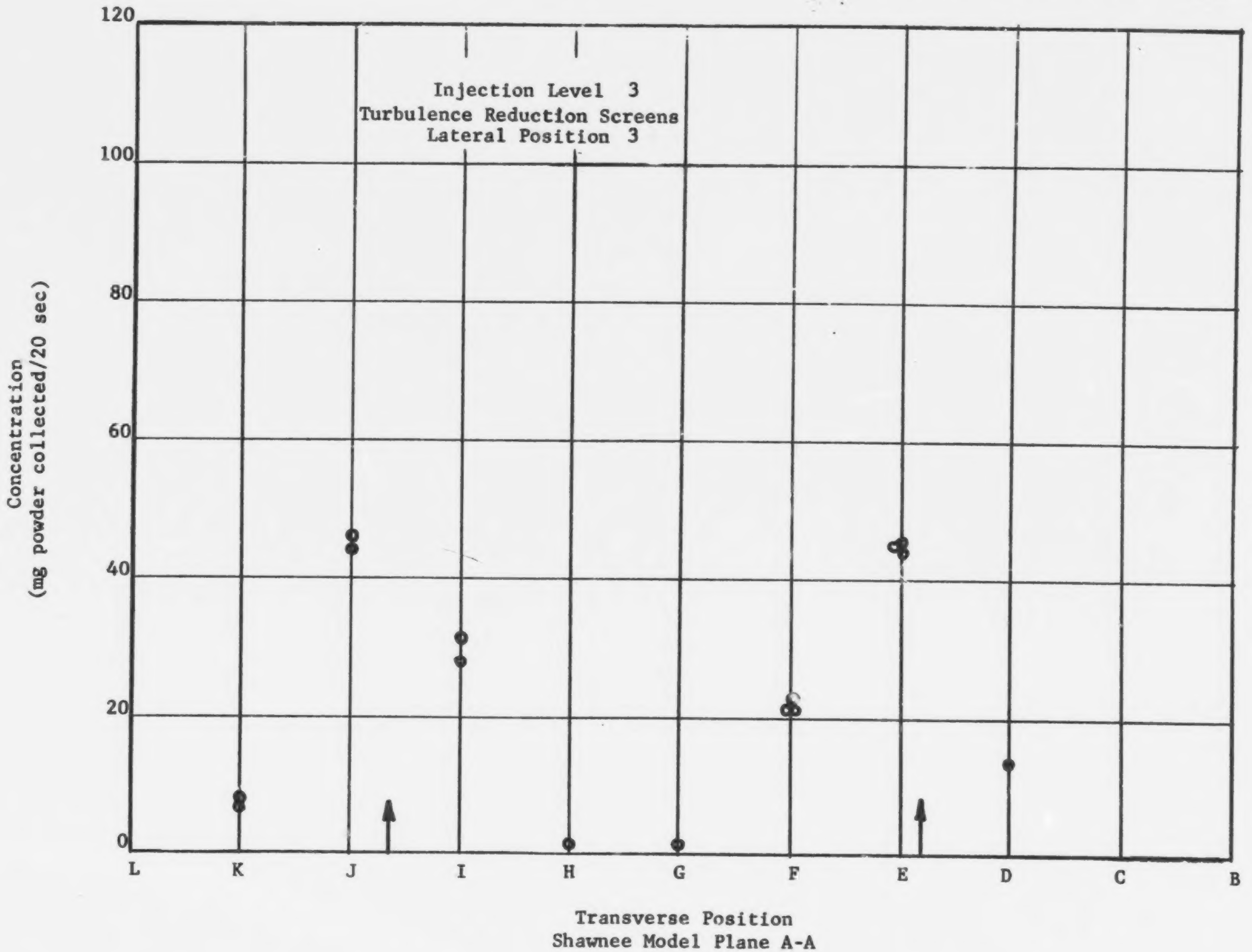

CONCENTRATION PROFILE

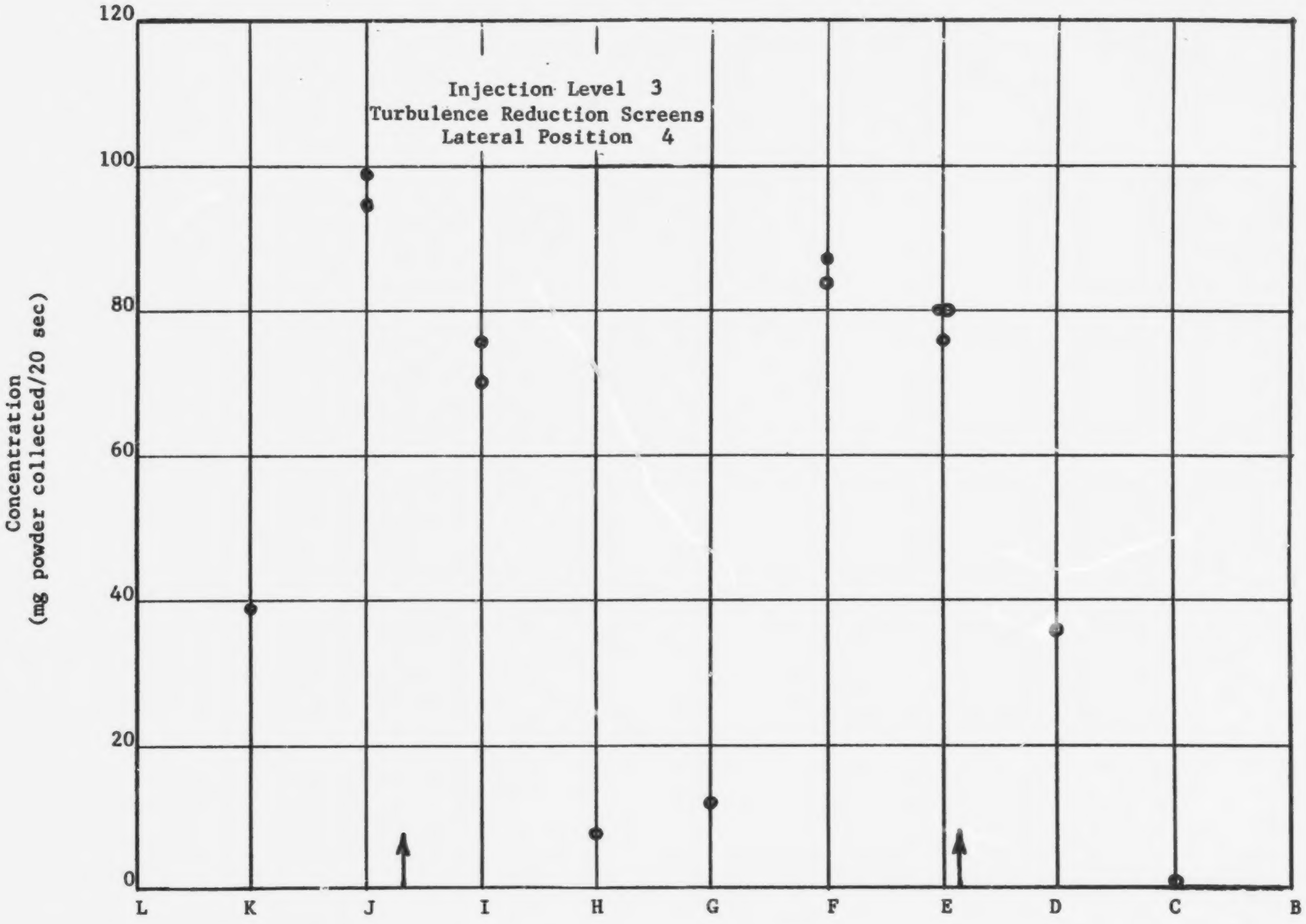

Transverse Position
Shawnee Model Plane A-A

CONCENTRATION PROFILE

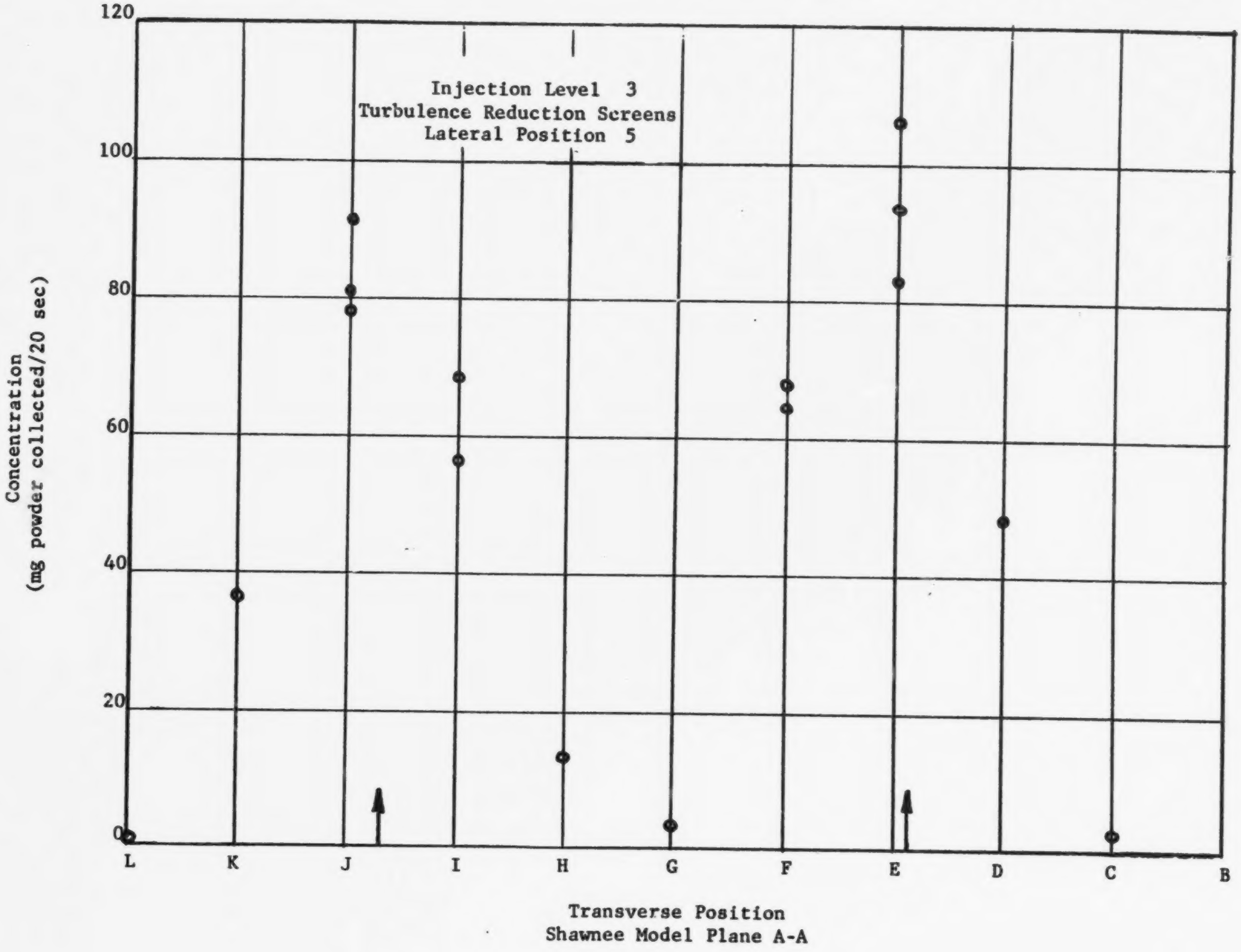

CONCENTRATION PROFILE

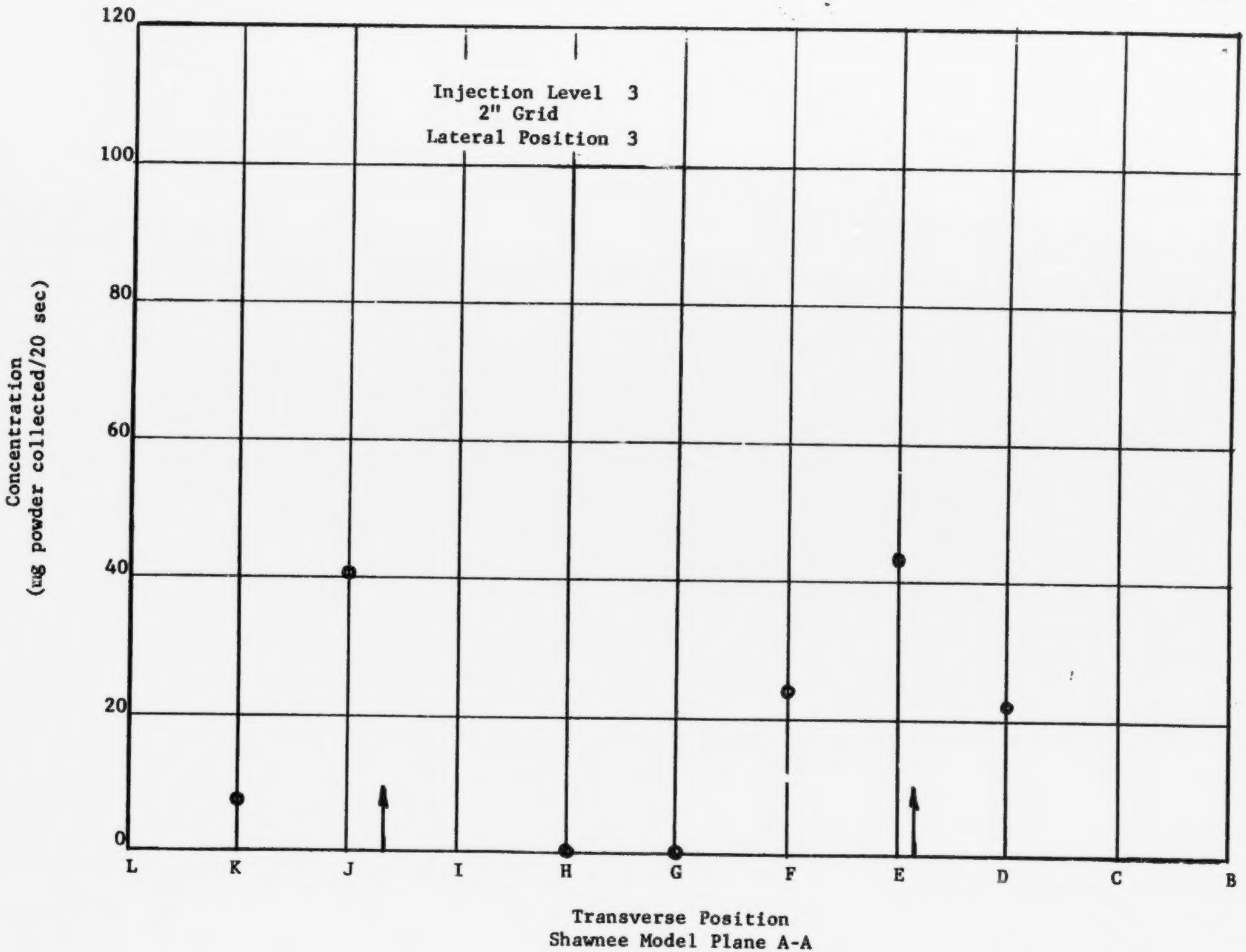

CONCENTRATION PROFILE

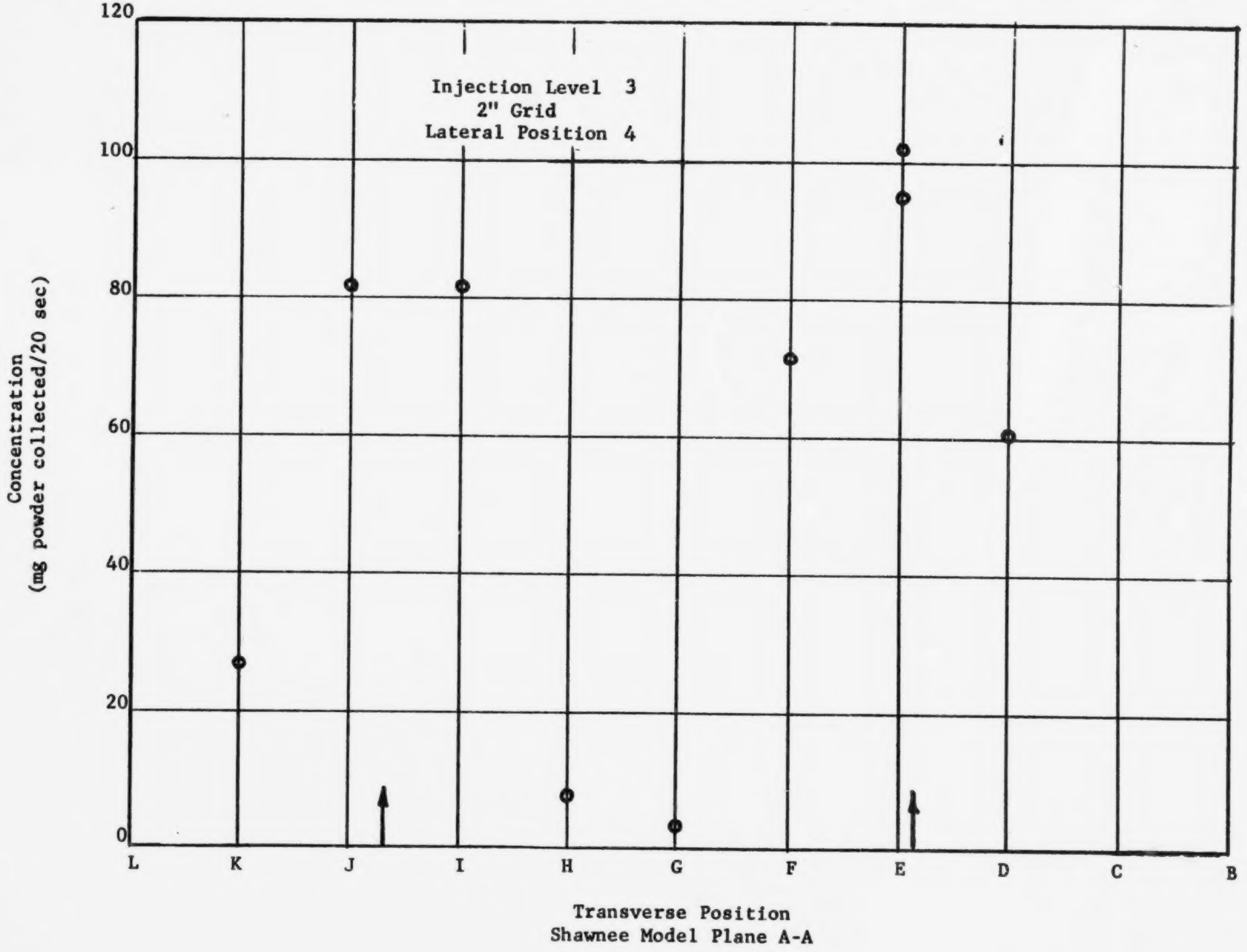

CONCENTRATION PROFILE

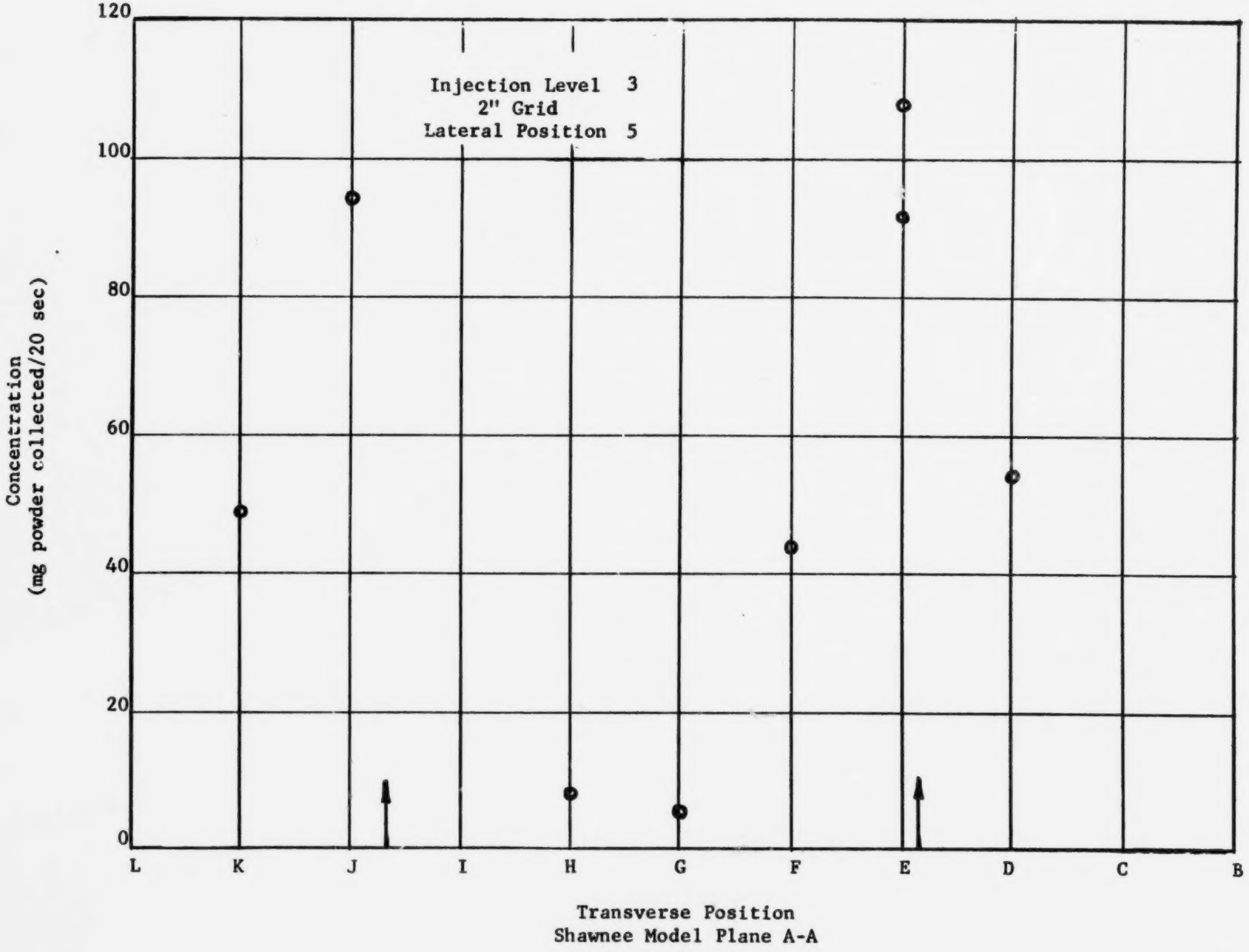

CONCENTRATION PROFILE

WEST VIRGINIA BOARD OF REGENTS FOR HIGHER EDUCATION, 1969/70

John E. Amos, *President*, Charleston
Earle T. Andrews, *Vice-president*
Berkeley Springs
Amos A. Bolen, *Secretary*, Huntington
Dr. Forrest L. Blair, Walker
David L. Dalzell, Moundsville
Mrs. Elizabeth H. Gilmore, Charleston
Edward H. Greene, Huntington
Albert M. Morgan, Morgantown
Okey L. Patteson, Mount Hope
Rex M. Smith, *ex officio*, Charleston
Dr. Prince B. Woodard, *Chancellor*, Charleston